

Chemical mutagenesis screen identifies AMDHD2 as a critical regulator of the hexosamine biosynthetic pathway

Inaugural-Dissertation
zur
Erlangung des Doktorgrades
der Mathematisch-Naturwissenschaftlichen Fakultät
der Universität zu Köln



vorgelegt von
Virginia Kroef
aus Köln

Köln, Juli 2021

Gutachter: Dr. Martin Denzel
Prof. Dr. Jürgen Dohmen

Tag der mündlichen Prüfung: 01.09.2021

Table of content

Acknowledgements	1
List of abbreviations	4
Abstract	8
Zusammenfassung	9
1 Introduction	11
1.1 The aging process	11
1.1.1 The aging population: An age-old problem needs new insight.....	11
1.1.2 Universal hallmarks of aging	12
1.2 The hexosamine biosynthetic pathway	13
1.2.1 Regulation of the HBP	15
1.2.1.1 Glutamine fructose-6-phosphate amidotransferase 1 and 2	16
1.2.1.2 N-acetylglucosamine-6-phosphate deacetylase.....	17
1.2.2 Physiological relevance of the HBP	19
1.2.2.1 N-linked glycosylation.....	19
1.2.2.2 O-GlcNAcylation.....	21
1.2.2.3 Other functional outputs of the HBP	24
1.2.3 Crosstalk of the HBP and other metabolic pathways	26
1.2.4 The role of the HBP in the metabolic control of pluripotency	29
1.2.4.1 The metabolic rewiring of pluripotent ESCs	29
1.2.4.2 The role of the HBP in pluripotent ESCs.....	31
1.2.5 The role of the HBP in aging	35
1.3 Functional genetic screening approaches	38
1.3.1 The evolution of genetic screening strategies.....	38
1.3.2 Haploid mESCs as a novel screening tool.....	40
1.4 Aim of the project	43
2 Results	45
2.1 Identification of AMDHD2	45
2.1.1 Chemical mutagenesis screen for tunicamycin resistance in mESCs identifies AMDHD2.....	45
2.1.2 Confirmation of <i>Amdhd2</i> as tunicamycin resistance-conferring gene	47
2.1.3 Loss of AMDHD2 leads to HBP activation	47
2.1.4 Insertional mutagenesis screen confirms the loss of AMDHD2 as HBP activator	48
2.2 Characterization of AMDHD2	50
2.2.1 Biochemical characterization of AMDHD2	50
2.2.1.1 Structural properties of human AMDHD2.....	50

2.2.1.2	<i>In vitro</i> characterization of identified loss-of-function mutations in AMDHD2	52
2.2.2	Biological/physiological characterization of AMDHD2.....	54
2.2.2.1	Loss of the <i>C. elegans</i> AMDHD2 homolog F59B2.3 has no effect on HBP activity	54
2.2.2.2	Loss of AMDHD2 in <i>M. musculus</i> leads to embryonic lethality	55
2.2.2.3	Loss of AMDHD2 in N2a cells leads to HBP activation	57
2.3	Cell type-specific regulation of the HBP	58
2.3.1	GFAT2 controls metabolite entry into the HBP in mESCs	59
2.3.2	GFAT2 has a lower sensitivity to UDP-GlcNAc feedback inhibition compared to GFAT1	61
2.3.3	AMDHD2 in tandem with GFAT2 result in elevated HBP flux in mESCs.....	62
2.3.4	Differentiation of human ESCs reduces the GFAT2:GFAT1 ratio	63
2.3.5	Partial differentiation of AN3-12 cells by LIF removal reduces GFAT2 abundance	64
2.3.6	Differentiation of AN3-12 cells into neural progenitor cells (NPCs) is delayed upon AMDHD2 K.O.....	66
2.3.7	Loss of AMDHD2 increases mESCs maintenance under basal conditions..	67
3	Discussion	70
3.1	Identification of AMDHD2.....	70
3.1.1	Identification of AMDHD2 demonstrates the power of drug resistance screens in haploid mESCs	71
3.1.2	Loss of AMDHD2 is a novel mechanism to mediate tunicamycin resistance by HBP activation	72
3.2	<i>In vivo</i> characterization of AMDHD2.....	74
3.2.1	Loss of the <i>C. elegans</i> AMDHD2 homolog <i>F59B2.3</i> has no effect on HBP activity.....	74
3.2.2	AMDHD2 is essential for embryonic development in <i>M. musculus</i>	75
3.3	Cell type-specific regulation of the HBP	76
3.3.1	GFAT2 controls metabolite entry into the HBP in mESCs	76
3.3.2	AMDHD2 in tandem with GFAT2 results in elevated HBP flux in mESCs....	78
3.3.3	Differentiation of ESCs reduces the GFAT2:GFAT1 ratio	78
3.3.4	Loss of AMDHD2 delays differentiation and increases ESC maintenance... 80	
3.3.5	GFAT2 and GFAT1 differ in their substrate affinity and susceptibility for feedback inhibition	82
3.3.6	Enzymatic reconfiguration of the HBP as an adaptation to ESC metabolism	83
3.4	AMDHD2 as a novel target for multifunctional applications.....	84
3.4.1	The HBP as therapeutic target in aging and disease	85
3.4.2	AMDHD2 as a promising druggable target for manipulation of the HBP flux	87
4	Future perspective	89
4.1	What is the role of the HBP in ESC fate decisions?.....	89

4.2	What is the role of AMDHD2 in embryonic development?.....	91
5	Material and methods.....	92
5.1	Mouse handling	92
5.1.1	<i>M. musculus</i> maintenance.....	92
5.1.2	Generation of transgenic mice.....	92
5.1.2.1	CRISPR/Cas9-mediated generation of transgenic mice	92
5.1.2.2	Microinjections of mouse zygotes.....	93
5.2	<i>C. elegans</i> handling.....	93
5.2.1	<i>C. elegans</i> maintenance.....	93
5.2.2	Generation of transgenic worms.....	93
5.2.2.1	CRISPR/Cas9-mediated generation of transgenic worms	93
5.2.2.2	Microinjections of <i>C. elegans</i>	94
5.2.3	Developmental tunicamycin resistance assay	94
5.3	Cell biological methods.....	94
5.3.1	Cell maintenance.....	94
5.3.2	Cell sorting	95
5.3.3	Cell viability assay (XTT).....	95
5.3.4	Insertional mutagenesis screening	95
5.3.4.1	Retroviral-based insertional mutagenesis and drug selection	95
5.3.4.2	Inverse PCR	96
5.3.5	Chemical mutagenesis screening.....	97
5.3.5.1	Chemical-based mutagenesis and drug selection.....	97
5.3.5.2	Exome sequencing and analysis	97
5.3.6	Differentiation into neural progenitor cells (NPCs).....	97
5.3.7	Colony formation assay (CFA).....	98
5.4	Molecular biological methods.....	98
5.4.1	Mouse genotyping.....	98
5.4.1.1	Isolation of mouse genomic DNA from ear clips	98
5.4.1.2	Genotyping PCR for the <i>Amdhd2</i> locus.....	99
5.4.2	Worm genotyping.....	99
5.4.2.1	Single worm lysis.....	99
5.4.2.2	Genotyping PCR for the F59B2.3 locus.....	99
5.4.3	Gel electrophoresis	100
5.4.4	Gene editing and genotyping by Sanger sequencing	100
5.4.5	RNA isolation	101
5.4.6	Quantitative PCR (qPCR).....	102
5.5	Biochemical methods.....	103
5.5.1	Immunoblot analysis.....	103

5.5.2 LC-MS/MS and IC-MS/MS analysis.....	103
5.5.2.1 Determination of UDP-HexNAc levels	103
5.5.2.2 Determination of UDP-GlcNAc and UDP-GalNAc levels.....	104
5.5.3 Protein expression and purification.....	105
5.5.3.1 Expression and purification of human AMDHD2.....	105
5.5.3.2 Expression and purification of human GFAT1 and GFAT2	105
5.5.3.3 Expression and purification of human GNA1	106
5.5.4 Site-directed mutagenesis.....	106
5.5.5 Enzyme activity assays	108
5.5.5.1 GlcN6P production of AMDHD2.....	108
5.5.5.2 GNA1 and GNA1-coupled activity assays.....	108
5.5.5.3 GDH-coupled activity assay and UDP-GlcNAc inhibition	109
5.5.6 Generation of anti-AMDHD2 antibody	109
5.5.7 Human AMDHD2 crystallization and crystal soaking	110
5.6 Data collection and refinement.....	110
5.7 Data availability.....	110
5.8 Alignments	111
5.9 Statistical analysis.....	111
5.10 Software	111
References	112
Appendix	133
Supplementary data	133
List of figures.....	135
List of tables	136
Work contributions.....	137
Curriculum Vitae.....	138
Erklärung zur Dissertation	140

Acknowledgements

I started working in the Denzel lab by doing a 6-week internship but I quickly felt confident and recognized how special and deep the connections within the lab are. Therefore, I did not only decide to continue with my master thesis but also stayed for my PhD in this incredible friendly atmosphere and I can proudly say that I do not regret this decision! Along the journey of my PhD I meet so many incredible and outstanding personalities that I could fill up additional 100 pages. However, I try to narrow it down and I hope I even roughly find some word which can express my endless gratefulness.

First of all, I want to address special thanks to my supervisor Dr. Martin S. Denzel for believing in me and my potential and giving me the opportunity to perform my PhD in his laboratory. I am really glad that you consistently trusted in me and the project and helped me to develop personally and professionally. Your motivation was always contagious!

I want to express my thanks to my advisory committee for taking the time to discuss my project during TAC meetings and for their helpful input. I am grateful to Prof. Dr. Jürgen Dohmen who supported me during my complete scientific career. I also want to thank Dr. David Vilchez for his feedback and the support to develop this project. Moreover, I like to thank Prof. Dr. Ulrich Baumann for agreeing to be part of my thesis committee. I thank all of my thesis committee members for spending their time on reading and evaluating my thesis as well as for joining the defense!

In particular, I want to thank Dr. Sabine Ruegenberg who performed the whole biochemical analysis of this thesis. Your contribution was essential for the project and I am really thankful for all your helpful comments and proofreading of my thesis. Thank you for investing so much time!

I am immensely grateful to Dr. Kira Allmeroth, who helped me on a daily basis not only on a scientific but also on a personal level. Although we were often mistaken for being twins, I rather consider you as my big sister! You were always there for me when I needed help or just some nice words to calm down and I learned so much from your (endless) expertise. Thanks for spending so much time on encouraging me anytime and for proofreading this apparently endless thesis.

I gratefully acknowledge the Metabolomics Core Facility, including Patrick Giavalisco, Yvonne Hinze, and Silvina Perin. Thank you for spending hours on measuring UDP-HexNAc levels of actually every existing cell line and model organism!

Moreover, I gratefully acknowledge the FACS & Imaging Core Facility, by name Kat Folz-Donahue and Lena Schumacher. I want to thank you for the countless hours you spend with me in front of the FACS, hoping to have enough GFP-positive cells.

Special thanks go also to the Bioinformatics Core Facility and the Comparative Biology Facility, which were indispensable for this project.

I want to express my special gratitude to all former and current members of the Denzel lab and the Antebi lab. I enjoyed the friendly atmosphere you spread and it is really hard to distinguish between colleagues and friends! Thank you for the plenty of time you spend with me during the “Scientific discussion forum” to discuss (of course scientific) but also any other issue. It is a pleasure to be surrounded by so many great personalities. Thanks to Dr. Kira Allmeroth, Laura Wester, Miriam Popkes, and Dr. Isabelle Schiffer for consuming an infinite amount of coffee/beer and always cheering me up when I needed some emotional support. Spending time with you guys was/is always a highlight! I owe special thanks to Dr. Moritz Horn for the supervision and sharing this project with me. I enjoyed all the scientific and the more often occurring “less serious” conversations. Moreover, I want to thank Dr. Matías Hartmann for his great input and his consistently positive attitude. I am really impressed by all the warmth you are spreading and being your neighbor was always a pleasure (although we sometimes needed Kira’s translation abilities). In addition, I want to thank Dr. Matheus Dyczynski for all the helpful discussions and for being the incredible person you are. Special thanks also to the remaining members of the Denzel lab: Dr. Maxime Derisbourg, Felix A.M.C. Mayr, Dr. Gabriel Guerrero, and Marco Giorda. Lab Meeting with you guys was always fun and all of you contributed to the success of this project! Sincere thanks are extended to my lunch crew: Kira Allmeroth, Ruth Baddi, Stephan Miethe, Laura Wester, and Eike Dinort. No matter how bad days have been, every lunch was pure entertainment with you and you definitely made this place feel like a second home. I received so much support from all of you and I am really happy that our journeys crossed!

My sincere thanks go to all my long-time friends in Cologne, who accompanied me on my way for the last years and hopefully will continue for the upcoming ones. An immense thank you to Carolin Schog, who consistently supported me and shared all my ups and down during the last 14 years of my life! You are truly my anchor and I am endless grateful

for this unique friendship! Moreover, I owe endless gratitude to Lennard-Maximilian Döring and his exceptional patience. I am eternally grateful that you believed in me and motivated me even when I was full of doubts. You consistently helped me to calm down whenever I was stressed (which was actually on a daily basis). Thank you!

Zum Schluss möchte ich mich bei meiner Familie für ihre unendliche Unterstützung und den grenzenlosen Rückhalt bedanken. Ich finde keine Worte, die ausdrücken könnten wie dankbar ich für eure bedingungslose Liebe und Hilfe bin. Ohne euch wäre ich nicht an dem Punkt, an dem ich jetzt bin! Danke für die unzähligen Momente, in denen ihr mich beruhigt, mir gut zugeredet und mich wieder aufgebaut habt. Besonders während des letzten Jahres! Ihr hattet recht: ich bin stärker als ich es mir selbst je zugetraut hätte und ich habe es geschafft! Dank euch!

Thanks to all of you! I owe you an endless amount of coffee/ chocolate/ beer!

List of abbreviations

%	percent
°C	degree Celsius
α-KG	α-ketoglutarate
acetyl-CoA/ac-CoA	acetyl-coenzyme A
AD	Alzheimer's disease
ADP	adenosine 5'-diphosphate
AMDHD2	N-acetylglucosamine-6-phosphate deacetylase
AMPK	AMP-activated protein kinase
Asn	asparagine
ATP	adenosine 5'-triphosphate
ACLY	ATP-citrate lyase
bp	base pair
BSA	bovine serum albumin
<i>B. subtilis</i>	<i>Bacillus subtilis</i>
<i>C. elegans</i>	<i>Caenorhabditis elegans</i>
CaCl ₂	calcium chloride
CaMKII	calcium/calmodulin-dependent protein kinase II
CFA	colony formation assay
CO ₂	carbon dioxide
CSC	cancer stem cell
ctrl	control
Da	dalton
ddH ₂ O	deionized water
DMEM	Dulbecco's Modified Eagle's <i>Medium</i>
DNA	deoxyribonucleic acid
dNTPs	deoxynucleosidetriphosphate
Dol-P	dolichol-phosphate
DON	6-diazo-5-oxo-L-norleucine
DUF	domain of unknown function
EB	embryoid body
<i>E. coli</i>	<i>Escherichia coli</i>
ECL	enhanced luminol-based chemiluminescent substrate
ECM	extracellular matrix
EDTA	ethylenediaminetetraacetic acid
EGFR	EGF receptor
ENU	N-ethyl-N-nitrosourea
ER	endoplasmic reticulum
ERAD	ER-associated degradation
ESC	embryonic stem cell
ESCM	embryonic stem cell medium
ETC	electron transport chain
FACS	fluorescence-activated cell sorting
FADH ₂	reduced flavin adenine dinucleotide
FBS	fetal bovine serum
FC	fold change
FoxO	Fork head box O
Frc6P	fructose-6-phosphate
fwd	forward
g	gram

GAG	glycosaminoglycan
GALE	UDP-galactose-4'-epimerase
GAPDH	glyceraldehyde 3-phosphate dehydrogenase
GDP	guanosine 5'-diphosphate
GFAT	glutamine fructose-6-phosphate amidotransferase
GFP	green fluorescent protein
Glc	D-glucose
Glc6P	D-glucose-6-phosphate
GlcN	D-glucosamine
GlcN6P	D-glucosamine-6-phosphate
GlcNAc	N-acetyl-D-glucosamine
GlcNAc1P	N-acetyl-D-glucosamine-1-phosphate
GlcNAc6P	N-acetyl-D-glucosamine-6-phosphate
Gln	L-glutamine
GLS	glutaminase
Glu	L-glutamate
GLUT	glucose transporters
GNA1	D-glucosamine-6-phosphate N-acetyltransferase
GNPDA1/2	D-glucosamine-6-phosphate deaminase 1/2
GOF	gain-of-function
GPI	glycophosphatidylinositol
GST	glutathione-S-transferase
GSL	glycosphingolipids
GTP	guanosine 5'-triphosphate
h	hour
HA	hemagglutinin
HA	hyaluronic acid
hESC	human embryonic stem cell
HDAC	histone deacetylase
HK	hexokinase
HBP	hexosamine biosynthetic pathway
HRP	horseradish peroxidase
hu	human
IC	ion chromatography
IIS	insulin/IGF-1 signaling
iPSC	induced pluripotent stem cell
ISC	intestinal stem cell
ISR	integrated stress response
K	lysine
kDa	kilodalton
K.O.	knock-out
l	liter
LC	liquid chromatography
LDH	lactate dehydrogenase
LIF	leukemia inhibitory factor
LOF	loss-of-function
mESC	mouse embryonic stem cell
mFAO	mitochondrial fatty acid oxidation
min	minute
ml	milliliter
mM	millimolar
<i>M. musculus</i>	<i>Mus musculus</i>

mRNA	messenger RNA
MS	mass spectrometry
ms	mouse
mTOR	mammalian target of rapamycin
N2a	Neuro-2a
N	asparagine
NAD ⁺	oxidized nicotinamide adenine dinucleotide
NADH	reduced nicotinamide adenine dinucleotide
NagA	N-acetylglucosamine-6-phosphate deacetylase
NAGK	N-acetyl-D-glucosamine kinase
Neu5Gc	N-glycolylneuraminic acid
ng	nanogram
nm	nanomolar
NPC	neural progenitor cell
nt	nucleotide
OCT4	octamer-binding protein 4
OE	overexpression
OGA	O-GlcNAcase
OGT	O-GlcNAc transferase
ORF	open reading frame
OST	oligosaccharyltransferase
OXPPOS	oxidative phosphorylation
PAGE	polyacrylamidegelelectrophoresis
PBS	phosphate-buffered saline
PCR	polymerase chain reaction
PD	Parkinson's disease
PDK	pyruvate dehydrogenase kinase
PFA	paraformaldehyde
PFK	phosphofructokinase
PGI	phosphoglucose isomerase
PGM3	phosphoglucomutase 3
PI	propidium iodide
PKA	cAMP-dependent protein kinase A
PQC	protein quality control
PPP	pentose phosphate pathway
PTM	post-translational modification
qPCR	real-time quantitative PCR
rev	reverse
R5P	ribose-5-phosphate
ROS	reactive oxygen species
RNA	ribonucleic acid
RNAi	RNA interference
rpm	rounds per minute
RT	room temperature
s	second
SAM	S-adenosylmethionine
<i>S. cerevisiae</i>	<i>Saccharomyces cerevisiae</i>
SD	standard deviation
SDS	sodium dodecyl sulfate
SEM	standard error of the mean
Ser	serine
sgRNA	single guide RNA

siRNA	small interfering RNA
SNV	single nucleotide variant
SOX2	sex determining region Y-box 2
T _A	annealing temperature
TBS	Tris-buffered saline
TCA	tricarboxylic acid
TET1	ten-eleven translocation 1
TF	transcription factor
Thr	threonine
TM	tunicamycin
TPR	tetratricopeptide repeats
tRNA	transfer RNA
U	units
UAP1	UDP- <i>N</i> -acetylglucosamine pyrophosphorylase
UDP	uridine 5'-diphosphate
UDP-GalNAc	uridine 5'-diphospho- <i>N</i> -acetyl-D-galactosamine
UDP-GlcNAc	uridine 5'-diphospho- <i>N</i> -acetyl-D-glucosamine
UDP-HexNAc	uridine 5'-diphospho- <i>N</i> -acetyl-D-hexosamine
UPR	unfolded protein response
UPS	ubiquitin-proteasome system
UTP	uridine-5'-triphosphate
V	volt
v/v	volume/volume
WB	Western blot
w/v	weight/volume
WT	wildtype
μg	microgram
μl	microliter

Abstract

Aging is associated with a variety of common disorders such as cancer, diabetes, neurodegenerative, or cardiovascular diseases. Consequently, the steady expansion of the older population raises a dramatic global concern regarding health issues. The aging process is accompanied by multiple metabolic changes which contribute to the physiological decline and manipulation of relevant pathways is sufficient to extend lifespan. Therefore, it is critical to further elucidate how nutrient signaling is interconnected to the metabolic regulation of aging and thereby identify novel druggable targets.

The hexosamine biosynthetic pathway (HBP) is a nutrient-sensing pathway that consumes fructose, glutamine, acetyl-CoA, and UTP to generate UDP-GlcNAc, an essential precursor for post-translational protein glycosylation. Thus, the HBP is optimally positioned to integrate signals from diverse metabolic pathways and its manipulation is likely to influence the overall metabolic state. The HBP is controlled by its rate-limiting enzyme glutamine fructose-6-phosphate amidotransferase (GFAT) that is feedback inhibited by UDP-GlcNAc. While HBP regulation by GFAT is well-studied, other HBP regulators remain obscure. Elevated UDP-GlcNAc levels can counteract toxicity induced by tunicamycin (TM), a potent glycosylation inhibitor. Therefore, TM resistance is a suitable proxy for elevated UDP-GlcNAc levels and thus, HBP activity. In order to identify novel regulators of the HBP, we performed an unbiased TM resistance screen in haploid mouse embryonic stem cells (mESCs) using random chemical mutagenesis. We identified multiple loss-of-function mutations in the enzyme N-acetylglucosamine deacetylase (AMDHD2) that catalyzes a reverse reaction in the HBP. By solving the crystal structure of human AMDHD2, we found that loss-of-function is caused by impaired protein stability and catalytic activity. Finally, we showed that AN3-12 mESCs express AMDHD2 together with GFAT2 instead of the more common GFAT1. GFAT2 is less susceptible to UDP-GlcNAc inhibition compared to GFAT1, explaining how loss of AMDHD2 elevates HBP flux. This specialized HBP configuration, characterized by co-expression of AMDHD2 and GFAT2, was also observed in other mESCs. Consistently, we confirmed a decreased GFAT2:GFAT1 ratio upon differentiation of mouse and human ESCs. The relevance of this specific HBP regulation for ESC fate decisions was reinforced by embryonic lethality of homozygous AMDHD2 K.O. mice. Together, this work reveals a critical function of AMDHD2 in balancing UDP-GlcNAc levels in cells that use GFAT2 for metabolite entry into the HBP, which potentially serves as a metabolic adaptation for distinct nutrient-requirements. Overall, the crucial role for AMDHD2 in HBP regulation offers novel approaches for the development of therapeutic agents to tackle age-related diseases.

Zusammenfassung

Das Altern ist mit einer Vielzahl von Volkskrankheiten verbunden wie Krebs, Diabetes, neurodegenerativen oder kardiovaskulären Erkrankungen. Folglich stellt der stetig zunehmende Anteil an älteren Menschen ein dramatisches weltweites Gesundheitsproblem dar. Der Alterungsprozess wird von zahlreichen metabolischen Veränderungen begleitet, die zum physiologischen Verfall beitragen und eine Manipulation der relevanten Stoffwechselwege reicht aus, um die Lebensspanne zu verlängern. Daher ist es von entscheidender Bedeutung, tiefgehender aufzuklären, wie die Nährstoffsignalübertragung mit der metabolischen Regulation des Alterns zusammenhängt, um dadurch neue Angriffspunkte für die Entwicklung von Medikamenten zu identifizieren.

Der Hexosamin-Biosyntheseweg (HBW) ist ein nährstoffsensitiver Stoffwechselweg, der Fruktose, Glutamin, Acetyl-CoA und UTP verbraucht, um UDP-GlcNAc zu erzeugen, ein essentielles Vorprodukt für die posttranslationale Proteinglykosylierung. Somit ist der HBW optimal positioniert, um Signale aus verschiedenen Stoffwechselwegen zu vernetzen und seine Manipulation kann wahrscheinlich den gesamten Stoffwechselzustand beeinflussen. Der HBW wird durch sein Reaktionsgeschwindigkeit-bestimmende Enzym Glutamin-Fruktose-6-Phosphat-Amidotransferase (GFAT) kontrolliert, das durch UDP-GlcNAc rückkoppelnd gehemmt wird. Während die HBW-Regulation durch GFAT gut untersucht ist, bleiben andere HBW-Regulatoren unerforscht. Erhöhte UDP-GlcNAc-Spiegel können der durch Tunicamycin (TM), einem potenten Glykosylierungsinhibitor, ausgelösten Toxizität entgegenwirken. Daher ist eine TM-Resistenz ein geeigneter Indikator für erhöhte UDP-GlcNAc-Spiegel und damit für die HBW-Aktivität. Um neue Regulatoren des HBW zu identifizieren, haben wir einen unvoreingenommenen TM-Resistenz-Screen in haploiden murinen embryonalen Stammzellen (mES-Zellen) mittels chemischer Zufallsmutagenese durchgeführt. Wir konnten mehrere Mutationen identifizieren, die zu einem Funktionsverlust in dem Enzym N-Acetylglukosamin-Deazetylase (AMDHD2) führen, welches eine Rückreaktion im HBW katalysiert. Durch die Auflösung der Kristallstruktur des humanen AMDHD2 fanden wir heraus, dass der Funktionsverlust durch eine beeinträchtigte Proteinstabilität und reduzierte katalytische Aktivität verursacht wird. Schließlich konnten wir zeigen, dass AN3-12 mES-Zellen AMDHD2 zusammen mit GFAT2 anstelle des häufiger vorkommenden GFAT1 exprimieren. GFAT2 ist im Vergleich zu GFAT1 weniger anfällig für eine UDP-GlcNAc-Inhibition, was erklärt, wie der Verlust von AMDHD2 die HBW-Aktivität erhöht. Diese spezialisierte HBW-Konfiguration, charakterisiert durch die Koexpression von AMDHD2 und GFAT2, wurde auch in anderen mES-Zellen beobachtet. Übereinstimmend konnten wir ein vermindertes GFAT2:GFAT1-Verhältnis während der Differenzierung von

murinen und humanen ES-Zellen zeigen. Die Relevanz dieser spezifischen HBW-Regulation für die Schicksalsentscheidungen von ES-Zellen wurde durch die embryonale Letalität von homozygoten AMDHD2 K.O.-Mäusen verstärkt. Zusammenfassend verdeutlicht diese Arbeit eine kritische Funktion von AMDHD2 beim Aufrechterhalten der UDP-GlcNAc-Spiegel in Zellen, die GFAT2 für den Metabolit-Eintritt in die HBW verwenden, was möglicherweise als metabolische Anpassung an unterschiedliche Nährstoffanforderungen dient. Insgesamt bietet die wesentliche Rolle von AMDHD2 bei der HBW-Regulation neue Ansätze für die Entwicklung von Therapeutika zur Bekämpfung altersbedingter Krankheiten.

1 Introduction

1.1 The aging process

Aging is a complex phenotype which can be defined as the inevitable and time-dependent functional impairment of tissues and organs (López-Otín et al. 2013). This not only leads to a decline in the ability to manage daily life, but also builds the major risk for a wide variety of common disorders as cancer, diabetes, neurodegenerative, or cardiovascular diseases (Kaeberlein 2013). It is supposed that the aging mechanism is driven by dysfunctions on a cellular level, which result in the accumulation of damage with age. Besides environmental influences, recent publications provide evidence that aging is also modulated by genetic factors. For example, longevity as an inherited trait is of growing interest and many human studies could already estimate heritability of longevity based on pedigree data (van den Berg et al. 2017; Kaplanis et al. 2018; Partridge, Deelen, and Slagboom 2018). Additionally, single-gene mutations in highly conserved pathways regulating nutrient sensing, energy metabolism, or reproduction can affect lifespan in different model organisms (Vijg and Campisi 2008; Kenyon 2005). In line with that, mutations in single genes can also result in premature aging phenotypes, manifesting already early in life (Burla et al. 2018; Martin and Oshima 2000). However, the deep understanding of aging and its underlying molecular mechanisms is still incomplete and a currently emerging field in science.

1.1.1 The aging population: An age-old problem needs new insight

Although aging is a phenomenon that has fascinated people already since beginning of humankind, unraveling the aging process in a molecular context just started approximately 30 years ago with the identification of the first long-lived *Caenorhabditis elegans* (*C. elegans*) strain (Klass 1983). The increase in life expectancy in parallel to decreasing fertility rates accelerated the speed of population aging globally (Harper and Leeson 2008). In most developed countries, life expectancy has doubled within the last two centuries (Oeppen and Vaupel 2002). Not only better living conditions, but also the improved healthcare system could reduce early mortality and therefore extend longevity (Vaupel et al. 1998). Along with this, also the overall body function with older ages, including cognitive and physical aspects, has improved (Christensen et al. 2013; Zeng et al. 2017). However, the onset of morbidity and most health issues has not

extended to the same degree as lifespan (Crimmins 2015). Due to this discrepancy, on average people have to suffer 16-20% of their life from age-related morbidity (Jagger et al. 2008). This state includes the impairment of motor and cognitive functions as well as the accumulation of age-related disease conditions like cancer, neurodegenerative diseases, diabetes type II, and cardiovascular disorders (Niccoli and Partridge 2012). Moreover, it is predicted that the extension in longevity will continue. It is expected that the population above 60 years (current fraction 17%) will double within the next thirty years, resulting in every third person falling into this category (Mitrečić et al. 2020). This aging of the population is a dramatic global challenge in economic, social, and especially medical regard. Therefore, it is of fundamental importance to also increase the disease-free lifespan (health span) and delay the onset of dysfunctional conditions and disabilities. In order to extend healthy life years, however, the understanding of the cellular mechanisms of aging requires further investigation.

1.1.2 Universal hallmarks of aging

In the fundamental work from López-Otín et al. (2013) nine different molecular mechanisms of the aging process were outlined and defined as the hallmarks of aging. All of them share the manifestation during normal aging and their experimental manipulation can alter the onset as well as the progress of aging. These nine hallmarks, that together modulate and define the aging phenotype, are: genomic instability, telomere attrition, epigenetic alterations, loss of protein homeostasis, deregulated nutrient-sensing, mitochondrial dysfunction, cellular senescence, stem cell exhaustion, and altered intercellular communication (Figure 1A). Furthermore, these hallmarks can be categorized into three layers, according to their time of onset. While the primary hallmarks are the cause for cellular damage, the antagonistic hallmarks react to this first impulse and aim to prevent further impairment. Therefore, these responding hallmarks are protective at low levels but an excess and chronic activity can be deleterious for health. Ultimately, the persistent accumulation of damage can induce the integrative hallmarks that contribute to the aging phenotype directly by provoking tissue dysfunctionality (Figure 1B). Notably, the hallmarks cannot be strictly separated, but can be interconnected and co-occur in some diseases like cancer. Taken together, all these cellular processes can influence the onset as well as the severeness of the age-related morbidity in elderly. Therefore, understanding the detailed molecular mechanism of the aging hallmarks is essential and can help to

identify potential drug targets that may delay aging and improve health span of the steadily growing aging population.

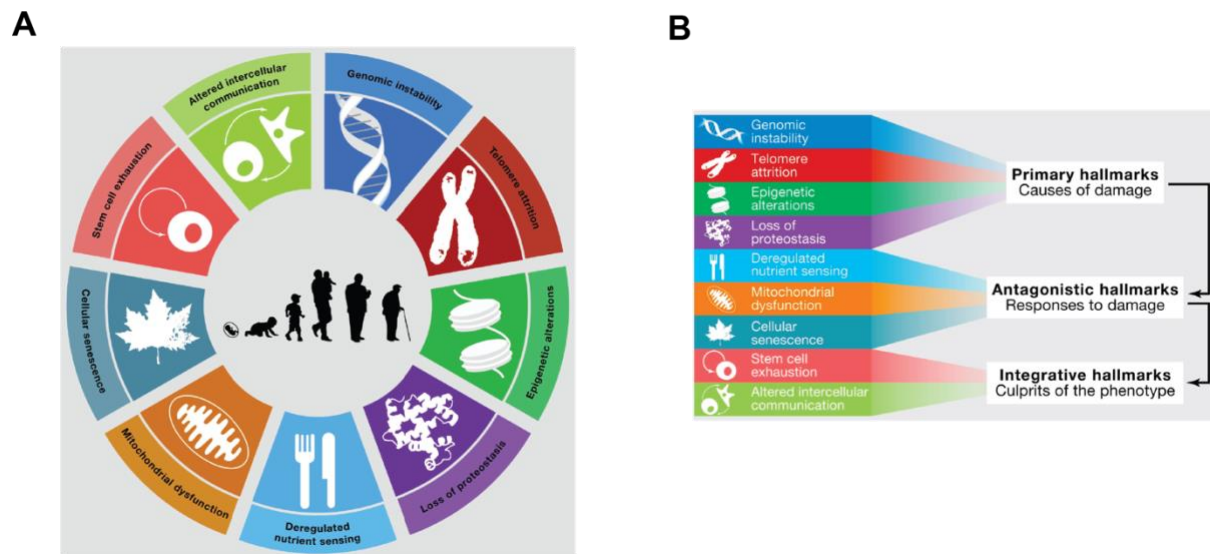


Figure 1: The universal hallmarks of aging. (A) Schematic representation of the nine hallmarks of aging: genomic instability, telomere attrition, epigenetic alterations, loss of proteostasis, deregulated nutrient sensing, mitochondrial dysfunction, cellular senescence, stem cell exhaustion, and altered intercellular communication. (B) The nine hallmarks can be clustered in three categories, which are functionally interconnected: primary hallmarks, antagonistic hallmarks, and integrative hallmarks (modified from López-Otín et al., 2013).

1.2 The hexosamine biosynthetic pathway

Previously, it was shown that activation of the hexosamine biosynthetic pathway (HBP) is able to improve protein homeostasis and thereby can extend lifespan in *C. elegans* (Denzel et al. 2014). The HBP is an anabolic sub-branch of glycolysis, consuming about 2-3% of cellular glucose in order to produce uridine 5'-diphosphate-N-acetyl-D-glucosamine (UDP-GlcNAc) (Marshall, Bacote, and Traxinger 1991; Ghosh et al. 1960). Synthesis of this amino sugar occurs in four consecutive enzymatic reactions (Figure 2). In the first and rate-limiting step of the HBP, glutamine fructose-6-phosphate amidotransferase (GFAT) catalyses the conversion of fructose-6-phosphate (Frc6P) and L-glutamine (L-Gln) to D-glucosamine-6-phosphate (GlcN6P) (Ghosh et al. 1960). In mammals two GFAT paralogs (GFAT1 and GFAT2) exist which share 75-80% amino acid sequence identity (Oki et al. 1999). Notably, GlcN6P can be reversed to Frc6P by the counteracting enzymes glucosamine-6-phosphate deaminase 1 and 2 (GNPDA1/2), thereby shunting metabolites back into glycolysis (Arreola et al. 2003). In the second step of the HBP, glucosamine-6-phosphate N-acetyltransferase (GNA1) produces N-acetylglucosamine-6-phosphate (GlcNAc6P) using GlcN6P and acetyl-CoA as the

acetyl donor (Wang et al. 2008). This reaction is also assumed to be reversible due to deacetylation of GlcNAc6P by the hitherto uncharacterized enzyme N-acetylglucosamine-6-phosphate deacetylase (AMDHD2) (Bergfeld et al. 2012; Weidanz et al. 1996). Of note, following catabolism of existing glycoconjugates or N-acetylglucosamine (GlcNAc) supplementation, GlcNAc can enter the HBP upon phosphorylation by GlcNAc kinase (NAGK) at this stage, and can thereby bypass GFAT (salvage pathway) (Schachter 1978). The followed isomerization into GlcNAc-1-phosphate (GlcNAc1P) is mediated by the enzyme phosphoglucomutase 3 (PGM3) (Ricciardiello et al. 2018). In a final step, UDP-N-acetylglucosamine pyrophosphorylase (UAP1) consumes UTP to ultimately synthesize the end product UDP-GlcNAc (Mio et al. 1998).

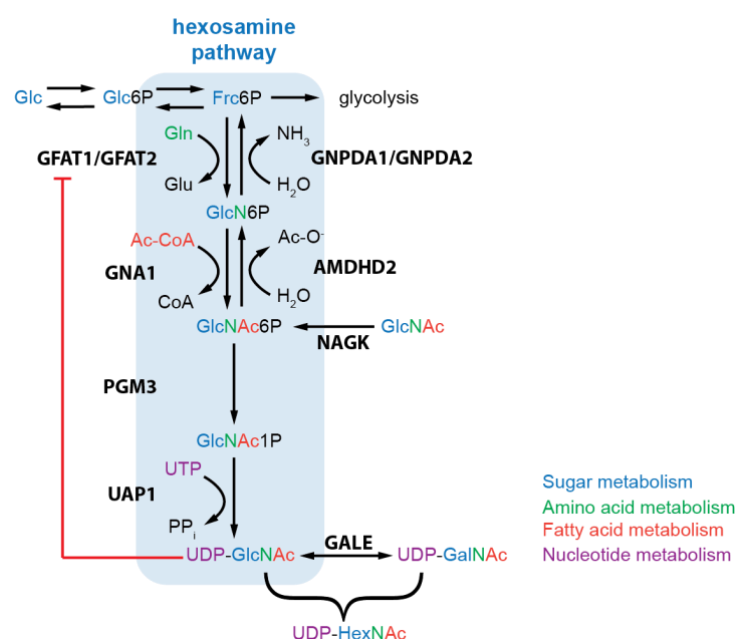


Figure 2: The hexosamine biosynthetic pathway. The HBP (blue box) generates UDP-GlcNAc and UDP-GalNAc (combination of both products is termed UDP-HexNAc) in multiple enzymatic steps. For the synthesis carbohydrates (blue), amino acids (green), fatty acids (red) and nucleotides (purple) are required. GFAT can be feedback inhibited by UDP-GlcNAc and to a minor extend by UDP-GalNAc (red arrow). GFAT: glutamine fructose-6-phosphate amidotransferase, GNPDA: glucosamine-6-phosphate deaminase, GNA1: glucosamine-6-phosphate N-acetyltransferase, AMDHD2: N-acetylglucosamine-6-phosphate deacetylase, NAGK: N-acetyl-D-glucosamine kinase, PGM3: phosphoglucomutase 3, UAP1: UDP-N-acetylglucosamine pyrophosphorylase, GALE: UDP-galactose-4'-epimerase.

Worth mentioning, UDP-GlcNAc can be reversibly interconverted to its epimer uridine 5'-diphosphate-N-acetyl-D-galactosamine (UDP-GalNAc) by the enzyme UDP-galactose-4'-epimerase (GALE) and the combination of both products is termed UDP-HexNAc (Thoden et al. 2001). Concentrations of UDP-GlcNAc (and to a lesser extend UDP-GalNAc) can inhibit enzyme activity of the rate-limiting enzyme GFAT1,

consequently, building a feedback loop that controls HBP activity (Ruegenberg et al. 2020b). This feedback inhibition seems to differ in GFAT2, since N-terminally tagged protein can only be moderately inhibited by 15% compared to GFAT1 (Hu et al. 2004). The HBP is the only source to produce the high energy molecule UDP-GlcNAc and relies on substrates from all big metabolic hubs: carbon-, nitrogen-, fatty acid-, and nucleotide metabolism. Therefore, the HBP is optimally positioned as a metabolic sensor that can transmit downstream cellular signalling through UDP-GlcNAc-dependent post-translational modifications (PTMs).

1.2.1 Regulation of the HBP

Regulation of HBP activity can occur on different levels. As already mentioned above, *de novo* synthesis of UDP-GlcNAc depends on glucose, glutamine, acetyl-CoA, and UTP levels; thus, the availability of those substrates can impact HBP flux. For instance, intracellular glucose levels, altered by glucose excess or deprivation in the media, was reported to have a positive correlation with UDP-GlcNAc levels (Nakajima et al. 2010; Abdel Rahman et al. 2013). Besides glucose availability, also D-glucosamine (GlcN) supplementation was sufficient to increase HBP flux (Marshall, Nadeau, and Yamasaki 2004). GlcN is converted to GlcN6P by hexokinase (HK) and can enter the HBP downstream of its rate-limiting enzyme GFAT1. However, it was shown that GlcN6P can also act as a moderate inhibitor of GFAT1, limiting GlcN's activating function (Grigorian et al. 2007). Additionally, GlcNAc can enter the HBP downstream of GFAT1 upon phosphorylation to GlcNAc6P by GlcNAc kinase (NAGK). Thereby, entry of GlcNAc into the HBP can circumvent UDP-GlcNAc inhibition of GFAT1, resulting in a more potent activation than Glc or GlcN (Grigorian et al. 2007; Broschat et al. 2002). In contrast to GlcN, GlcNAc treatment does not influence cellular acetyl-CoA levels, therefore better representing physiological conditions.

Since GFAT1 is the rate-limiting enzyme of the HBP, it is conceivable that its protein abundance as well as mutations affecting its activity can also alter HBP flux. Indeed, overexpression (OE) of GFAT1 is sufficient to increase UDP-GlcNAc levels in *C. elegans* and cell culture models like primary murine keratinocytes (Horn et al. 2020; Denzel et al. 2014; Weigert et al. 2001). Comparably, also specific gain-of-function (GOF) mutations in *Gfat1*, that were identified in a forward genetic screen in *C. elegans*, can elevate HBP flux (Denzel et al. 2014). Of note, introducing the same G451E (*dh785* in *C. elegans*) substitution into the highly conserved GFAT1 of murine neuro-2a (N2a) cells, is also

sufficient to boost HBP flux, indicating a similar mechanism in mammals (Horn et al. 2020; Ruegenberg et al. 2020b).

In sum, HBP activity can be enhanced by substrate availability as well as protein abundance and activity of its rate-limiting enzyme GFAT1 in different model organisms, ultimately resulting in increased UDP-GlcNAc levels.

1.2.1.1 Glutamine fructose-6-phosphate amidotransferase 1 and 2

As described in detail above, the first and rate-limiting step of the HBP is catalyzed by GFAT. Besides the HBP's key enzyme GFAT1, another cell type-specific paralog exists, which is called GFAT2. *Gfat2* is reported to be mainly expressed in the central nervous system, whereas *Gfat1* is ubiquitously expressed with particularly high mRNA abundance in pancreas, placenta, and testis (Oki et al. 1999). Although, GFAT1 and GFAT2 share 75% amino acid identity, they are clearly separable genes, localized on different chromosomes (Sayeski, Paterson, and Kudlow 1994; Oki et al. 1999).

Apart from differences in tissue distribution, GFAT1 and GFAT2 can be differentially regulated by PTMs. GFAT1 contains three known independent phosphorylation sites: S205, S235, and S243. While S205 and S235 are target sites of cAMP-dependent protein kinase A (PKA), S243 is phosphorylated by AMP-activated protein kinase (AMPK). Only S205 (S202 in hGFAT2) and S243 (S244 in hGFAT2) are conserved in GFAT2, whereas S235 is missing. However, for S235 no impact on enzyme activity was shown to date (Chang et al. 2000). In contrast, only recently it was discovered that S205 phosphorylation by PKA can either have an activating or inhibiting impact on human GFAT1 activity, depending on intracellular UDP-GlcNAc concentrations (Ruegenberg et al. 2021). For the AMPK phosphorylation site at S243 the current literature is controversial, since activating and inhibitory affects were reported (Li, Roux, et al. 2007; Zibrova et al. 2017; Eguchi et al. 2009). In addition, solely GFAT1 contains a putative ubiquitination site at the Lys48 residue, which is not preserved in GFAT2 and may pinpoint to a different mechanism with regard to their degradation (Wagner et al. 2011; Akimov et al. 2018). In accordance, GFAT1 was shown to interact with different E3 ligases and proteasomal components, further strengthening the hypothesis of an UPS-driven degradation (Kristensen, Gsponer, and Foster 2012; Wan et al. 2015).

In addition, the sensitivity of GFAT1 and GFAT2 towards UDP-GlcNAc feedback inhibition seems to differ. One publication claimed that GFAT2, carrying an N-terminal GST-tag, can

only be moderately inhibited by 15% compared to GFAT1 (Hu et al. 2004). If the tag can disturb enzyme activity, however, was not excluded.

To summarize, growing evidence indicates that GFAT1 and GFAT2 underly different regulatory mechanism, including their expression pattern, activity, and stability. However, whether these two paralogs indeed display differential roles in HBP regulation remains elusive.

1.2.1.2 N-acetylglucosamine-6-phosphate deacetylase

AMDHD2 (EC 3.5.1.25) was identified as N-acetylglucosamine-6-phosphatideacetylase (NagA) in *E. coli* due to its hydrolyzing activity of GlcNAc6P, ultimately producing GlcN6P and acetate (White and Pasternak 1967). Although this reaction also occurs in the “reverse” step of the HBP, AMDHD2 is often not integrated into this pathway. Instead, most knowledge is based on its bacterial and fungal homologs, where it is essential for the catabolism of cell wall components as peptidoglycans or chitin (Plumbridge 2009; Park 2001; Uehara et al. 2005). Therefore, it was already discussed to be a suitable target for development of anti-fungal or antibiotic agents (Choi et al. 2013; Swiatek et al. 2012; Ahangar et al. 2018). In mammals, AMDHD2 was shown to be implicated in generation of ECM components, potentially affecting melanoma metastasis (Campbell et al. 1990; Qiu et al. 2015; Oikari et al. 2016). Moreover, mammalian AMDHD2 was described as a crucial factor for degradation of N-glycolylneuraminic acid (Neu5Gc). Neu5Gc is one of the most common sialic acid in mammals that often occurs at the terminal position of glycoconjugates (Bergfeld et al. 2012). Humans are unable to synthesize Neu5Gc *de novo*, but can receive and incorporate the molecule upon uptake from dietary sources (Bardor et al. 2005). Since Neu5Gc is sensed as a “foreign” epitope by the human immune system, an excess uptake or failure in turnover can result in inflammation-based health issues (Bergfeld et al. 2012; Dhar, Sasmal, and Varki 2019).

Regardless of these facts, mammalian AMDHD2 is a rather unstudied protein and the knowledge about it is restricted, lacking detailed information about its structure, expression, localization, or regulation. Amino acid alignments between AMDHD2 homologs revealed a moderate conservation (Supplementary Figure 1). More precisely, AMDHD2 (isoform 1) exhibits 91% sequence homology with *M. musculus*, 50% with *C. elegans*, 36% with *C. albicans*, 33% with *E. coli*, and 33% with *B. subtilis*.

The first protein structure of bacterial AMDHD2 (NagA) was solved in 2004, using bacterial protein from *B. subtilis* (Vincent et al. 2004). Later, also the NagA structure of *E. coli* was

reported (Ferreira et al. 2006). In general, the enzyme consists of 2 domains: a deacetylase domain and a second smaller domain with unknown function (DUF). For bacterial NagA it is assumed that the DUF is required for protein oligomerization (Ferreira et al. 2006). Despite a high degree of conservation, the active sites of NagA from *E. coli* and *B. subtilis* differ. While the enzyme activity of *E. coli* relies on a single Zn ion, *B. subtilis* protein requires two Fe ions as co-factor (Hall, Brown, et al. 2007). Moreover, NagA of *B. subtilis* seem to act as a dimer, while the enzyme in *E. coli* rather forms a tetramer. Structural analysis of eukaryotic AMDHD2 is still missing, although some studies indicate the importance of a single divalent cation for proper activity based on the primary amino acid sequence (Hall, Xiang, et al. 2007). Given the information of bacterial NagA structures, the Asp273 (Asp294 in human AMDHD2, isoform 1) as well as the His143 residue (His155 in human AMDHD2, isoform 1) are assumed to be important for catalytic activity (Hall, Xiang, et al. 2007).

Interestingly, substrate binding in the bacterial homologs requires residues of two monomers, indicating that the oligomerization state can impact affinity and thereby turnover (Vincent et al. 2004). Moreover, in bacteria, *nagA* is regulated by an operon system and co-expressed with *nagB*, a gene that encodes the enzyme glucosamine-6-phosphate deaminase (in mammals: GNPDA) (Arreola et al. 2003; Ferreira et al. 2006). GNPDA mediates the catalysis from GlcN6P to Frc6P, another reaction of the reverse flux in the HBP. Not only the transcription of this operon but also the enzymatic activity can be enhanced by the presence of GlcNAc6P, indicating a tightly regulated program for catabolism of HBP metabolites (Álvarez-Añorve et al. 2011). In addition, independent interactome studies revealed a putative interaction of AMDHD2 and GNPDA1/GNDPA2 in humans (Rolland et al. 2014; Huttlin et al. 2015). Moreover, there is evidence that AMDHD2 activity underlies product inhibition by GlcN6P (Campbell, Laurent, and Roden 1987; Weidanz et al. 1996).

Taking together, AMDHD2 is a fundamental enzyme for the reverse flux of the HBP, which seems to be involved in a tightly regulated process of metabolite catabolism, and therefore, enables metabolite entry into other pathways like glycolysis. However, there is still information lacking about eukaryotic AMDHD2 and how it regulates the HBP, potentially affecting whole cell metabolism.

1.2.2 Physiological relevance of the HBP

The HBP products UDP-GlcNAc and UDP-GalNAc are the precursor molecules for the synthesis of various biopolymers like chitin, peptidoglycans, and glycosaminoglycans as well as for several glycosylation events. Glycosylation of proteins is one of the most common co- or post-translational modification and occurs at around 50% of the eukaryotic proteome (Apweiler, Hermjakob, and Sharon 1999). Besides influencing protein folding and turnover, glycans also play a functional role in cell-cell communication and the modulation of immune responses (Lis and Sharon 1993; Dwek 1996). Additionally, since UDP-GlcNAc production can reflect the energetic status of a cell by interconnecting multiple metabolic pathways, it plays a major role in cell signaling in order to respond to stress and environmental conditions (Figure 2). Therefore, UDP-GlcNAc is involved in the regulation of many biological processes, impacting a broad spectrum of downstream physiological consequences.

1.2.2.1 N-linked glycosylation

Besides calcium storage and lipid biosynthesis, the endoplasmic reticulum (ER) is the compartment where folding and PTM of all secreted and membrane-bound proteins occurs (Hetz 2012). Asparagine-linked (N-linked) protein glycosylation is one of these PTMs, which is required for proper protein maturation, quality control as well as mediating a wide variety of signaling pathways (Parodi 2000). Due to this essential role N-linked glycosylation evolved in all domains of life. During N-linked glycosylation a pre-assembled oligosaccharide precursor is transferred to the amide group of an asparagine residue in the consensus sequence (Asn-X-Ser/Thr) of a target protein (Helenius and Aebi 2004) (Figure 3A). The assembly of the glycan precursor partially takes place in the cytosol, while some reactions occur within the ER lumen (Figure 3B). In this process, dolichol-phosphate (Dol-P), an ER membrane-bound polyisoprenoid lipid, is required for anchoring and translocation of the sugar complex across the ER membrane by flipping between the cytosol and the ER lumen (Behrens and Leloir 1970). In a first cytosolic assembly step, the enzyme UDP-GlcNAc:dolichol-P GlcNAc-1P transferase (GPT) transfers GlcNAc1P derived from UDP-GlcNAc to Dol-P. This reaction is essential for N-glycosylation and can be inhibited by the toxin tunicamycin (TM) (Takatsuki, Arima, and Tamura 1971). TM is a mixture of homologous nucleoside antibiotics with structural similarity to UDP-GlcNAc, resulting in a competitive inhibition of GPT (Tkacz and Lampen

1975). During the second step of the oligosaccharide assembly, another GlcNAc and five mannose residues are added to GlcNAc1P. The whole construct is flipped from the cytosolic to the ER luminal face, where the final addition of four mannoses and three glucose molecules takes place. The completed 14 residue oligosaccharide donor (Glc₃Man₉(GlcNAc)₂) is transferred *en bloc* to an asparagine residue of nascent polypeptide chains, catalyzed by the key enzyme oligosaccharyltransferase (OST) (Silberstein and Gilmore 1996). This transmission of the polysaccharide-complex to the target protein can either occur co-translationally or post-translationally. The glucose molecules play a pivotal role in quality control of newly synthesized glycoproteins within the ER, in a lectin-dependent manner (Helenius, Aebi, and Markus 2001). Upon removal of the two outermost glucose residues by glucosidases I/II, the mono-glucosylated proteins are substrates for the ER-specific chaperones calnexin and calreticulin (Vembar and Brodsky 2008). Binding of these chaperones assists efficient protein folding in two ways: on the one hand they prevent aggregation of unfolded proteins and on the other hand un- or misfolded proteins are retained within the ER to increase their chance of proper folding (Hebert, Foellmer, and Helenius 1996; Rajagopalan, Xu, and Brenner 1994). Upon removal of the final glucose and a mannose molecule, the native protein can be exported to the cytosol or to the Golgi apparatus for further processing (Helenius, Aebi, and Markus 2001). In case un- or misfolded proteins are released from the calnexin/calreticulin cycle, such proteins can either undergo an additional cycle of lectin binding or they can be targeted for ER-associated degradation (ERAD) in the cytosol (Hosokawa et al. 2001). Moreover, N-glycosylation can enhance thermodynamic stability and increases stability of target proteins (Schroder and Kaufman 2005; Wyss et al. 1995). Since N-linked glycosylation can influence protein homeostasis on many different levels, perturbation of this PTM, as induced for example by TM treatment, causes protein misfolding within the ER (ER stress). In order to cope with ER stress and to re-maintain protein homeostasis, as a response a subset of specific target genes is expressed by the ER unfolded protein response (UPR^{ER}) (Kozutsumi et al. 1988). Summarizing, N-linked glycosylation is an essential and UDP-GlcNAc-dependent protein modification, which is not only required for proper protein folding, but also contributes to protein stability and localization, thereby playing a significant role in protein homeostasis.

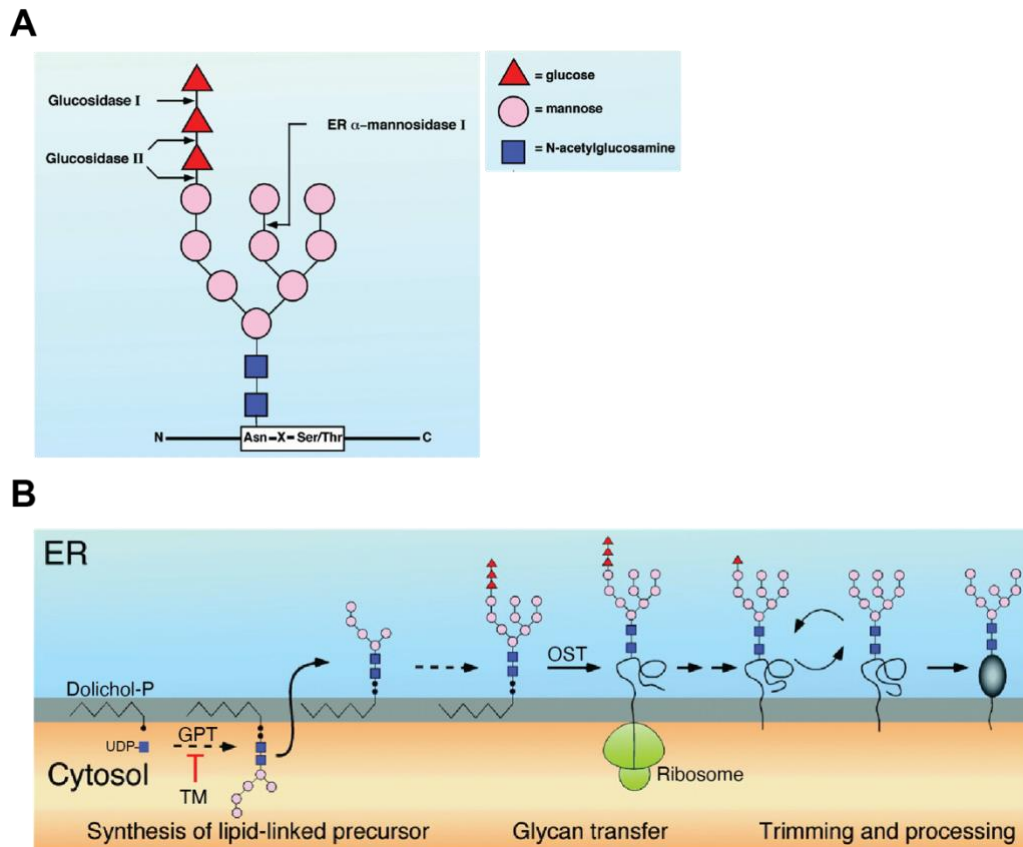


Figure 3: Schematic representation of N-linked glycosylation. (A) The precursor oligosaccharide consists of 2x N-acetylglucosamine (GlcNAc), 9x mannose and 3x glucose molecules. The complex is transferred to the consensus sequence Asn-X-Ser/Thr of target peptides. Terminal glucose and a mannose molecule can be removed by glucosidase I/II and ER α -mannosidase I. **(B)** Oligosaccharide synthesis starts in the cytosol by addition of GlcNAc-1P derived from UDP-GlcNAc to the Dolichol-P anchor. This initial step is catalyzed by UDP-GlcNAc:dolichol-P GlcNAc1P transferase (GPT), which can be inhibited by tunicamycin (TM). In a second step another GlcNAc and 5 mannose molecules are added. After the whole construct is flipped to the ER lumen, further addition of 4x mannose and 3x glucose molecules occurs before the whole construct is transferred to the nascent polypeptide chain, which is catalyzed by oligosaccharyltransferase (OST). Upon transfer, the glycan is trimmed and processed. Properly folded proteins can be exported to the cytosol or transported to the Golgi apparatus for further processing (modified from Helenius et al., 2001).

1.2.2.2 O-GlcNAcylation

O-GlcNAcylation is another dynamic type of PTM that includes the attachment of a single GlcNAc moiety to the hydroxyl group of a serine (Ser) or threonine (Thr) residue of cytoplasmic, nuclear or mitochondrial target proteins (Hart 1997) (Figure 4). Since the high energetic molecule UDP-GlcNAc serves as a donor, O-GlcNAcylation acts as a perfect molecular sensor that can transmit downstream signaling according to the cellular nutrient status or upon different stressors. Thus, the abundance of O-GlcNAcylation can reflect metabolic dynamics within a cell and rapidly adjusts cellular processes according to the

metabolic status. In contrast to phosphorylation, where several kinases catalyze the addition of a phosphate group, the transfer of the GlcNAc moiety is transferred by only one enzyme called O-GlcNAc transferase (OGT) (Haltiwanger, Holt, and Hart 1990) (Figure 4). In addition, the hydrolysis-driven removal of GlcNAc is catalyzed by a single enzyme, O-GlcNAcase (OGA) (Braidman et al. 1974). Thus, this highly important protein modification is regulated by only two enzymes, which are essential and highly conserved among different species (Lubas et al. 1997; Gao et al. 2001).

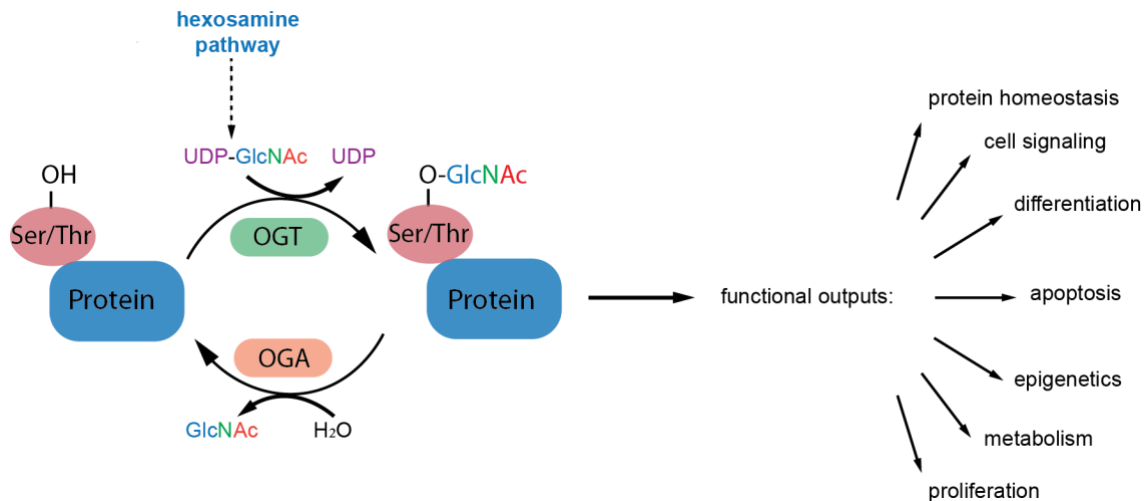


Figure 4: Schematic representation of O-GlcNAcylation and its functional outputs. The HBP product UDP-GlcNAc serves as the substrate for O-GlcNAc modifications. The transfer of a single GlcNAc moiety to the hydroxyl group (OH) of a Ser/Thr residue of the target protein is catalyzed by O-GlcNAc transferase (OGT), while the cleavage is mediated by O-GlcNAcase (OGA). O-GlcNAcylation of target proteins can regulate diverse functional downstream processes.

The exact mechanisms how OGT and OGA alone are able to recognize specifically the complete O-GlcNAc proteome is still under investigation. For OGT, it was shown that it does not rely on a specific consensus sequence for target recognition, but rather uses active site contacts with the backbone of its substrates (Lazarus et al. 2011). Moreover, it is assumed that the amino acid context surrounding the target Ser/Thr residue can influence OGT substrate selection (Pathak et al. 2015). Additionally, the N-terminal tetratricopeptide repeats (TPR) domain of OGT potentially contributes to target recognition by unveiling access to the active site upon a conformational change, when interacting with target proteins (Yang, Zhang, and Kudlow 2002; Lazarus et al. 2013). Another possibility could be the usage of adaptor proteins which specifically recruit and mediate the interaction of OGT with its target substrates in a context-specific manner (Cheung and Hart 2008; Ruan et al. 2012). Additionally, there is growing evidence that OGT prefers substrates with flexible regions that occur in unstructured regions of un- or misfolded

proteins. Consistently, O-GlcNAcylation seems to be involved in the response to proteotoxic stress (Yang and Qian 2017). OGA, in contrast, most likely interacts directly with the GlcNAc moiety and not with the substrate protein, although the peptide sequence around the glycosylation site can influence OGA efficiency (Schimpl et al. 2012). Similarly, as for phosphorylation, OGT rather confers the substrate specificity while OGA seems to show substrate promiscuity analog to phosphatases.

In general, it is well-described that a crosstalk of O-GlcNAcylation and other PTMs exists. For example, O-GlcNAc and phosphorylation can occur mutually exclusive at the same Ser/Thr residue of target proteins, like it is known for Tau (Yuzwa et al. 2008). In addition, O-GlcNAc modifications can influence phosphorylation events in their close proximity and *vice versa* (van der Laarse, Leney, and Heck 2018). Besides the interplay with phosphorylation, O-GlcNAcylation can also influence other PTMs like ubiquitination, acetylation, or methylation (Ruan, Nie, and Yang 2013; Dehennaut, Leprince, and Lefebvre 2014). Comparable to other PTMs, O-GlcNAcylation can impact several cellular downstream pathways and interconnection with other PTMs can even broaden the repertoire of target processes. As a matter of fact, O-GlcNAcylation was shown to be involved in chromatin remodeling, regulation of gene transcription, translation, protein solubility, stability, activity, and localization (Bond and Hanover 2015). Therefore, it plays a major role in plenty of cellular functions like epigenetics, cell metabolism, proliferation, differentiation, signaling, apoptosis, and protein homeostasis, among others (Ong, Han, and Yang 2018) (Figure 4). Since O-GlcNAc modifications and the corresponding downstream pathways are of essential importance and have to be adjusted rapidly according to external signals, the O-GlcNAcylation cycle has to be tightly regulated. Therefore, a multilayered regulatory mechanism has evolved to maintain O-GlcNAc homeostasis in an optimal range. UDP-GlcNAc serves as a direct precursor for O-GlcNAcylation. Consequently, altered substrate concentrations due to changes in nutrient availability and HBP activity can influence O-GlcNAcylation, resulting in hypo- or hyper-O-GlcNAcylation (Shen et al. 2012; Taylor et al. 2008). However, substrate concentrations are not always in a linear relationship with O-GlcNAcylation, indicating additional regulatory mechanisms (Ruan et al. 2012; Taylor et al. 2009). Consistently, it is well-studied that OGT and OGA expression are mutually linked and show compensatory modulation. Upon OGT knockdown or inhibition, also OGA levels are reduced to maintain O-GlcNAc homeostasis (Kazemi et al. 2010). This compensatory downregulation of OGA seems to be regulated mainly on a transcriptional level. A recent publication raises the possibility of an additional regulation driven by an epigenetic mechanism (Lin et al. 2021).

Conversely, compound-based inhibition of OGA results in reduced OGT expression in parallel to increased OGA levels (Zhang et al. 2014). In contrast to OGA regulation, OGT regulation rather seems to occur in a post-transcriptional manner. A recent study could show enhanced translation of OGT upon OGA inhibition using the potent inhibitor Thiamet G (Lin et al. 2021). Discordantly, however, also transcriptional regulation of OGT was reported, indicating different mechanisms depending on the cellular context (Qian et al. 2018). In addition, OGA and OGT can be O-GlcNAcylated themselves which can alter their stability, assuming a regulatory feedback loop (Khidekel et al. 2007). Latest studies identified intron-retention, induced upon alterations in O-GlcNAc levels, which can impact OGT and OGA availability (Park et al. 2017; Tan et al. 2020). Altogether, O-GlcNAcylation is a stress- and nutrient-responsive PTM, which is important to coordinate vital cellular processes such as epigenetics, protein homeostasis, cell survival and cell signaling. Therefore, a complex and fine-tuned regulatory mechanism, including mutual regulation of OGA and OGT, has evolved to preserve O-GlcNAc levels in an optimal zone and prevent cellular dysfunction.

1.2.2.3 Other functional outputs of the HBP

UDP-GlcNAc is not only the precursor for O-GlcNAcylation and N-linked glycosylation, but also for a third type of PTM called O-linked glycosylation. In contrast to N-linked glycosylation, in this case the polysaccharide is linked to the hydroxyl group of a Ser/Thr residue (Hounsell, Davies, and Renouf 1996). Mucin-type O-glycosylation is a subtype of O-linked glycosylation, which consists of glycans attached to the target protein linked by a GalNAc molecule (Bennett et al. 2012). This type of glycosylation mainly occurs in the Golgi apparatus, after the mature proteins have left the ER (Gill, Clausen, and Bard 2011). In an initial reaction UDP-GalNAc serves as a donor for GalNAc, which is transferred to the target protein (Weissmann and Hinrichsen 1969). Transmitting of this first GalNAc moiety is the pre-requirement for further addition of multiple carbohydrates, which results in very complex and versatile branched polysaccharide structures. Upon completion of O-glycosylation, the target protein is protected from proteolytic degradation and consequently stabilized (Kozarsky, Kingsley, and Krieger 1988). Moreover, O-linked glycosylation plays a significant role in recognition, adhesion, and communication between cells, as well as with their surrounding environment. Thus, alterations in O-glycosylation levels were previously connected with different types of cancer development like colon or breast cancer (Brockhausen 2006). In addition, there is

evidence that O-glycans have a pivotal function during embryogenesis in different organisms like *Drosophila melanogaster* (*D. melanogaster*) and mammals (Zhang, Tran, and Ten Hagen 2010; Tian, Hoffman, and Ten Hagen 2012). Finally, besides N-glycans, also O-glycans have crucial importance in immunity by being involved in antigen-presenting and thus, mediating inflammation (Petersen, Purcell, and Rossjohn 2009; Werdelin, Meldal, and Jensen 2002; Larsson et al. 2011).

Apart from the different glycosylation events, UDP-GlcNAc/UDP-GalNAc are important molecules for the synthesis of diverse essential polymers (Figure 5). The extracellular matrix (ECM) is a non-cellular component that surrounds all cells, composed of different macromolecules including proteins like collagen, proteoglycans, and cell-binding glycoproteins (Hynes and Naba 2012). Together, these components build a mechanical scaffold, and in parallel can influence cell physiology by controlling cell migration, adhesion, proliferation, differentiation, and apoptosis (Lu et al. 2011). Proteoglycans are proteins with attached glycosaminoglycan (GAG) chains, which in turn are polysaccharides composed of repetitive disaccharide units (Lindahl 2014). Since, UDP-GlcNAc and UDP-GalNAc belong to the main components of GAGs, their abundance does also influence ECM composition and its downstream functional consequences.

Another polysaccharide that requires HBP metabolites for its synthesis is chitin, which is the second most abundant biopolymer in nature (Tharanathan and Kittur 2003). It is a homopolymer solely consisting of GlcNAc, that is essential for cell walls of fungi and arthropods. Additionally, GlcNAc together with N-acetylmuramic acid (MurNAc) are the precursor molecules for peptidoglycan synthesis, which is the key component in the cell wall of nearly all bacteria. Therefore, the HBP is of especial importance in fungi and bacteria and it is considered as target for many antifungal agents and antibiotics (Munro and Gow 2001; Swiatek et al. 2012; Yamada-Okabe et al. 2001).

Apart from proteins and polysaccharide structures, also lipids can be glycosylated. For example, glycosphingolipids (GSLs) are composed of a ceramide lipophilic backbone with complex glycans, including GlcNAc and GalNAc, attached to it (Merrill 2011). They are located in the plasma membrane and are required to transmit extracellular signals by inducing intracellular cascades. One of the most prominent processes regulated by GSLs is the epidermal growth factor receptor (EGFR) signaling pathway, which is important for the regulation of cell growth (Coskun et al. 2011; Hanai et al. 1988). Additionally, previous reports have already outlined the central role of GSLs in developmental processes in

different model organisms, and alterations in GSL compositions can promote developmental disorders in human (Sheikh et al. 1999; Yamashita et al. 1999).

In sum, the HBP generates precursors for versatile PTMs and for the synthesis of plenty polysaccharide-containing structures (Figure 5). Thus, it is plausible that alterations of HBP flux can influence multiple downstream processes and have an impact on physiological consequences on many different levels.

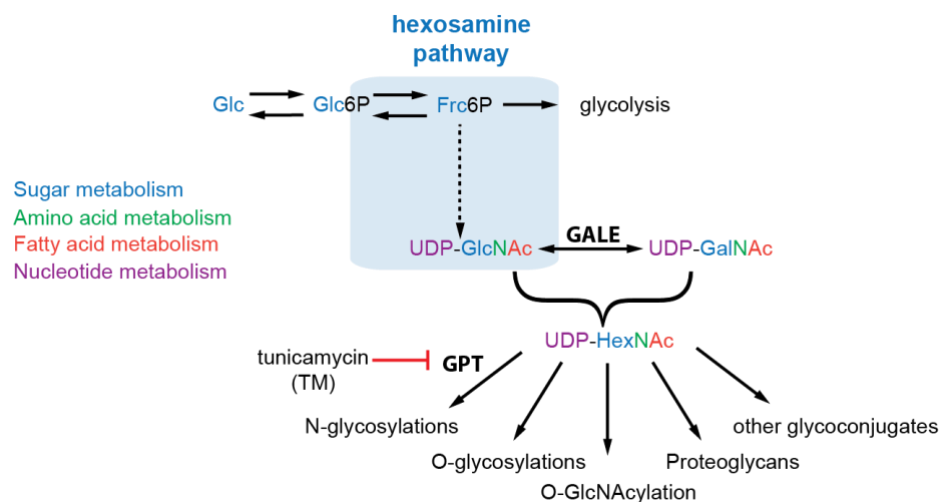


Figure 5: The hexosamine biosynthetic pathway and its multiple functional outputs. UDP-HexNAc can be used as a precursor for different glycosylation reactions including N-glycosylation, O-glycosylation, and O-GlcNAcylation. UDP-GlcNAc:dolichol-P GlcNAc-1-P transferase (GPT, N-glycosylation) can be inhibited by TM treatment (red arrow). Moreover, UDP-HexNAc is required for synthesis of proteoglycans and other glycoconjugates. TM: tunicamycin, GPT: UDP-GlcNAc:dolichol-P GlcNAc-1P transferase, GALE: UDP-galactose-4'-epimerase.

1.2.3 Crosstalk of the HBP and other metabolic pathways

As the HBP is a nutrient-responsive pathway that depends on the consumption of carbohydrates, amino acids, lipids, and nucleotides it is not surprising that it serves as an integrator of diverse fundamental metabolic pathways. Since it metabolizes about 2-3% of intracellular glucose, it is directly linked to glycolysis (Marshall, Bacote, and Traxinger 1991). Glycolysis is a linear cytoplasmic pathway that is essential for catabolism of glucose, in order to generate reduced nicotinamide adenine dinucleotide (NADH) and energy in form of adenosine 5'-triphosphate (ATP) (Lunt and Vander Heiden 2011). Upon entry of glucose into the cell via specific glucose transporters (GLUT1,3,4), it is trapped by phosphorylation catalyzed by hexokinase (HK) in an ATP-dependent manner (Figure 6). The enzyme phosphoglucose isomerase (PGI) converts Glc6P in a second step into fructose-6-phosphate (Frc6P), which is either further metabolized in several steps into

pyruvate during glycolysis or can enter the HBP at this stage. Under aerobic conditions pyruvate and NADH are transported into mitochondria, where the tricarboxylic acid (TCA) cycle takes place. Pyruvate dehydrogenase (PDH) is required for oxidative decarboxylation of pyruvate, resulting in acetyl coenzyme A (acetyl-CoA) production which subsequently can enter the TCA cycle to generate more NADH and reduced flavin adenine dinucleotide (FADH₂). During the electron transport chain (ETC) these reducing equivalents are essential to establish a proton gradient across the inner mitochondrial membrane. Of note, oxygen is used as the terminal electron acceptor for the ETC. The proton gradient is ultimately utilized by ATP-synthase to generate ATP. Since this process, also known as oxidative phosphorylation (OXPHOS), relies on oxygen availability, under anaerobic conditions lactate dehydrogenase (LDH) is used to metabolize pyruvate into lactate and NAD⁺ from NADH (Goldblatt and Cameron 1953). This alternative pathway ensures energy production under hypoxic conditions and is called anaerobic glycolysis.

Apart from that, glucose is not only catabolized during glycolysis but can also enter the pentose phosphate pathway (PPP) as Glc6P (Wamelink, Struys, and Jakobs 2008) (Figure 6). The pathway can be splitted into two steps: in the first oxidative and irreversible part, more NADPH and pentose phosphate are produced. During the second non-oxidative and reversible step, ribose-5-phosphate (R5P) is generated, which serves together with glutamine as a precursor for nucleic acid and nucleotide synthesis. Therefore, Glc6P fuels three major catabolic pathways for glucose: glycolysis, the PPP and the HBP, which have to be tightly regulated. Besides competing for Glc6P, the PPP is additionally connected with the HBP by providing UTP, which in turn is required for UDP-GlcNAc synthesis.

As already mentioned, the HBP's end product UDP-GlcNAc is the precursor for O-GlcNAcylation: a PTM which can regulate protein turnover, localization and function. Interestingly, almost all glycolytic enzymes are themselves O-GlcNAcylated, indicating a regulatory feedback loop (Bacigalupa, Bhadiadra, and Reginato 2018). For example, glucose uptake can be regulated by altered availability of the glucose transporters (GLUT1,4) in an O-GlcNAc-dependent manner (Park, Ryu, and Lee 2005; Ferrer et al. 2014). Besides essential enzymes of glycolysis, PPP and TCA cycle were described to be regulated by O-GlcNAc levels (Yi et al. 2012; Chaiyawat et al. 2015; Rao et al. 2015; Tan et al. 2014).

As both, the TCA cycle and the HBP, depend on acetyl-CoA these two pathways have to be properly coordinated. The acetyl-CoA pool is not only provided by glycolysis but also by the catabolism of fatty acids during mitochondrial fatty acid oxidation (mFAO). During

this process, also the reduced products NADH and FADH₂ are generated, which can be shunted directly into OXPHOS or are used to maintain cellular redox levels. Moreover, breakdown of glutamine, also known as glutaminolysis, can contribute to acetyl-CoA production (Metallo et al. 2012). During this process, glutamine is converted to glutamate via glutaminase (GLS), shunted into the mitochondria, and subsequently further metabolized to α -ketoglutarate, which can enter the TCA cycle (Figure 6).

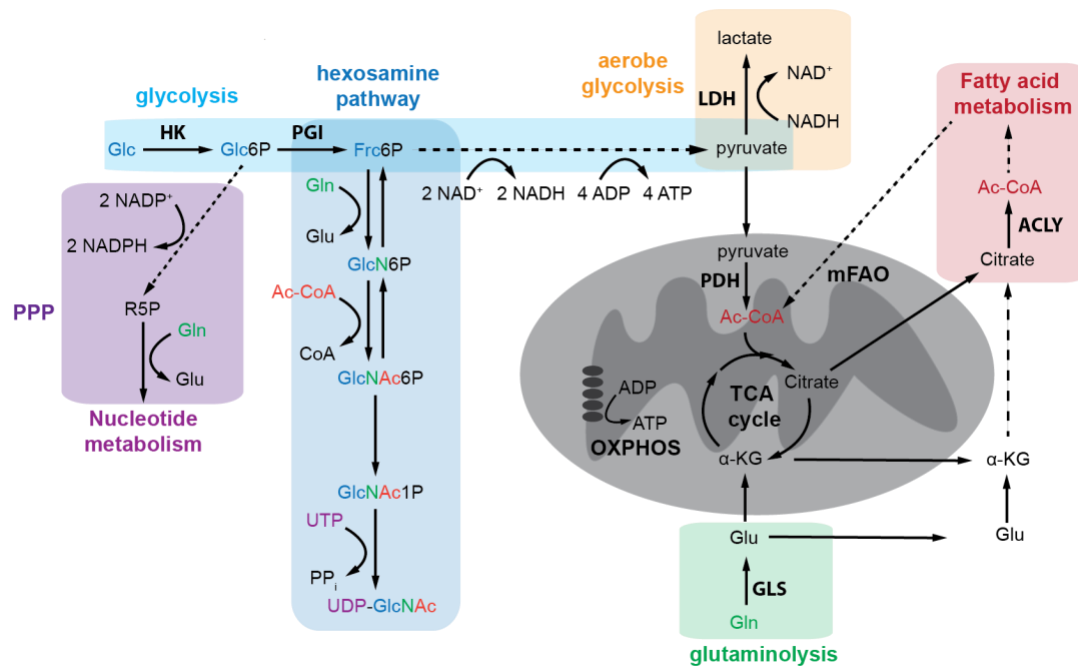


Figure 6: The HBP and its interconnection with other metabolic pathways. During glycolysis (light blue box) glucose (Glc) is phosphorylated by hexokinase (HK) to form glucose-6-phosphate (Glc6P) which can be shunted into the pentose phosphate pathway (PPP, purple box) for generation of nucleotides. Glc6P can also be processed to fructose-6-phosphate (Frc6P) which can either enter the HBP (dark blue box) or can be further metabolized to pyruvate. Pyruvate is converted to lactate during aerobic glycolysis (orange box) or can enter the tricarboxylic acid (TCA) cycle after breakdown to acetyl-CoA (Ac-CoA). The TCA generates citrate for fatty acid metabolism while mitochondrial fatty acid oxidation (mFAO) can degrade lipids again to form Ac-CoA. Reducing equivalents generated by PPP, glycolysis, and TCA cycle can be used for ATP generation during oxidative phosphorylation (OXPHOS) or for lactate synthesis. Glutaminolysis (green box) uses glutamine (Gln) to form glutamate (Glu), which is further catabolized to α -ketoglutarate (α -KG), a metabolite of the TCA cycle. α -KG can also be converted to citrate and acetyl-CoA in the cytosol, to feed lipid synthesis. All metabolites that are required for HBP and involved in other pathways are depicted according to a color code. PGI: phosphoglucose isomerase, LDH: lactate dehydrogenase, PDH: pyruvate dehydrogenase, GLS: glutaminase, ACLY: ATP-citrate lyase

Besides entering the TCA cycle, α -ketoglutarate can also be exported to the cytosol where it is carboxylated into citrate that serves as substrate for ATP-citrate lyase (ACLY) forming acetyl-CoA, mainly used for *de novo* lipid synthesis. Since the HBP requires glutamine as well as acetyl-CoA, glutaminolysis can be connected to HBP flux. Indeed, it was shown

that glutaminolysis and the HBP are competing for glutamine and blockage of glutaminolysis can enhance HBP flux (Araujo et al. 2017). Additionally, glutamine is used for nucleotide biosynthesis, which in turn is required for UDP-GlcNAc production, creating another level of interplay with the HBP.

To summarize, the HBP utilizes macromolecules of all major metabolic pathways, thereby serving as sensor of energy and nutrient availability and a central node that interconnects diverse metabolic pathways. Together, this complex network can transmit external signals and allows to rewire cellular metabolism rapidly according to metabolic changes and stress.

1.2.4 The role of the HBP in the metabolic control of pluripotency

Embryonic stem cells (ESCs) are defined as cells capable of self-renewal, a high proliferation rate, and the ability to differentiate into all three germ layers (Blair, Wray, and Smith 2011). These specific functional properties are accompanied with a metabolic rewiring that greatly differs from the metabolic state of somatic cells. Like described in detail in the previous paragraph (see paragraph 1.2.3), the HBP is tightly interconnected with other metabolic pathways as glycolysis, the TCA cycle, the PPP, and glutaminolysis which are all part of the metabolic reprogramming in pluripotent ESCs. Thereby, HBP flux can influence ESC maintenance on many different levels: either directly by its downstream PTMs or indirectly by modulating other metabolic pathways, required for pluripotency and self-renewal (Figure 7).

1.2.4.1 The metabolic rewiring of pluripotent ESCs

Nearly a century ago, Otto Warburg already recognized that fast proliferating cancer cells metabolize far more glucose than their normal counterparts and mainly rely on glycolysis for energy consumption even in oxygen-rich conditions (Warburg, Wind, and Negelein 1927). This metabolic switch is called the “Warburg effect” or “aerobic glycolysis” since despite sufficient oxygen availability for complete oxidation during OXPHOS, these cells utilize glycolysis resulting in the production of lactate. Apparently, this adaptation of fast proliferating cells seems discordant since aerobic glycolysis only generates 2 ATPs per one glucose molecule, while up to 36-38 ATP molecules can be achieved by complete oxidation during OXPHOS. Despite this reduced efficiency, in the presence of abundant glucose, aerobic glycolysis is much faster, results in lower reactive oxygen species (ROS)

levels, and ensures the production of important molecules for rapid cell proliferation like nucleotides, amino acids, or lipids (Vander Heiden, Cantley, and Thompson 2009). Interestingly, it was shown that not only cancer cells but also other fast proliferating cells display the “Warburg effect”, including pluripotent stem cells (Shyh-Chang and Ng 2017). Not only mESC and hESC but also reprogrammed induced pluripotent stem cells (iPSCs) were described to have an elevated dependence on glycolysis compared to differentiated cells (Kondoh et al. 2007; Varum et al. 2011; Panopoulos et al. 2012). Inhibition of glycolysis results in reduced reprogramming capacity, while induced glycolytic levels could improve the same, indicating high glycolytic levels as a requirement for stem cell function (Folmes et al. 2011; Zhu et al. 2010). Additionally, reprogrammed cells displayed a drastic upregulation of glycolytic genes, along with downregulation of TCA genes compared to somatic cells (Prigione et al. 2014; Folmes et al. 2011) (Figure 7). Not only alterations in glycolytic levels, but also in mitochondrial organization build a hallmark of stem cells, in line with the reduced requirement of the TCA cycle. Many studies demonstrated that mitochondrial dynamics are connected to pluripotency and that ESCs rather contain small and functionally immature mitochondria compared to differentiated cells (Zhang, Khvorostov, et al. 2011). In accordance, blocking of enzymes important for mitochondrial fusion results in decreased differentiation into OXPHOS-dependent cells (Kasahara et al. 2013; Zhong et al. 2019), while mitochondrial fission is required for reprogramming into iPSCs (Vazquez-Martin et al. 2012).

Although the TCA cycle is downregulated in ESCs, high levels of acetyl-CoA were described to be essential for pluripotency. Under normal conditions, acetyl-CoA is mainly generated by breakdown of pyruvate during the TCA cycle. However, like described above during aerobic glycolysis, glucose is converted to lactate instead of pyruvate and enzymes of the TCA cycle are downregulated, reducing TCA cycle activity. Contradictive, especially rapidly proliferating cells show a high demand for acetyl-CoA for lipid synthesis. Indeed, upon reprogramming into iPSCs, gene expression for *de novo* fatty acid synthesis is upregulated and pharmacological inhibition of required enzymes causes defects in reprogramming capacity (Vazquez-Martin et al. 2013).

Besides being shunted into the TCA cycle, acetyl-CoA is also highly important for epigenetic events such as acetylation of histones (Figure 7). Histone H3 acetylation was described to change chromatin accessibility and thereby expression of genes involved in pluripotency and self-renewal (Azuara et al. 2006; Gaspar-Maia et al. 2011). A recent study confirmed a positive correlation of glycolysis-mediated acetyl-CoA availability and ESC maintenance (Moussaieff et al. 2015). In line, failure in histone deacetylation

improved reprogramming into iPSCs (Mali et al. 2010). *Vice versa*, supplementation of ESCs with acetate as a precursor for acetyl-CoA could disturb differentiation in a dose-dependent manner (Moussaieff et al. 2015).

In addition to the TCA cycle, glutaminolysis can be used to provide acetyl-CoA. Therefore, besides the “Warburg effect” another metabolic feature of rapid proliferating cells is the high dependency on glutamine as carbon source, to compensate the reduced TCA cycle activity (Vander Heiden, Cantley, and Thompson 2009) (Figure 7). Consequently, glutamine-derived α -ketoglutarate is used to enter the TCA cycle in order to maintain fatty acid synthesis. In line with these findings, glutamine catabolism was shown to be essential for hESCs survival (Tohyama et al. 2016). Increased α -ketoglutarate levels due to elevated glutaminolysis, moreover, were shown to be essential for histone demethylation, thereby required to maintain pluripotency in mESCs (Carey et al. 2015) (Figure 7).

Additionally, glutamate is important for generation of the antioxidant glutathione (GSH) (Figure 7). Plenty of studies could show that pluripotent ESCs are highly dependent on low ROS levels in order to reduce DNA damage during their rapid proliferation (Song et al. 2014; Cho et al. 2006). A recent publication unraveled that glutamine consumption in hESC is required to maintain high GSH levels, which in turn is important to regulate Octamer-binding protein 4 (OCT4) stability (Marsboom et al. 2016).

To summarize, most major metabolic pathways are known to be rewired in ESCs compared to their derivative cells in order to adapt to their specific metabolic needs. Impairment of these metabolic transitions can impact epigenetic changes and thereby cell fate, by either disturbing pluripotency or differentiation.

1.2.4.2 The role of the HBP in pluripotent ESCs

Given the interconnected and complex coordinated metabolic network and its rewiring in ESCs, it is not surprising that alterations in HBP flux can also disturb other pathways and cellular metabolism, thereby affecting cell identity indirectly.

However, key transcription factors that are essential for ESC pluripotency can be regulated by O-GlcNAcylation, and thereby HBP activity, directly (Constable et al. 2017a; Jang et al. 2012) (Figure 7). OCT4, for instance, is a transcription factor which is required for early embryo development and pluripotency in mammalian ESCs (Nichols et al. 1998; Loh et al. 2006; Hay et al. 2004). Multiple studies could demonstrate that OCT4 is O-GlcNAcylated, which in turn is required for its activity and the expression of stem cell factors (Jang et al. 2012; Constable et al. 2017b). Additionally, other crucial stem

cell-specific transcription factors including sex determining region Y-box 2 (SOX2) were shown to be positively regulated by O-GlcNAcylation (Myers et al. 2016; Jang et al. 2012). In line with these results, reducing overall O-GlcNAc levels by OGT knockdown disturbs ESC self-maintenance and is sufficient to reduce reprogramming into iPSCs (Jang et al. 2012). *Vice versa*, the same study showed that increased O-GlcNAcylation by GlcN treatment or OGA inhibition disturb ESC differentiation. These data indicate that high O-GlcNAcylation levels promote ESC maintenance and pluripotency, while decreased levels are required for proper differentiation.

Intriguingly, changes in O-GlcNAc levels do not only modulate gene expression patterns by activity of transcription factors, but also by altering chromatin structure and therefore DNA accessibility (Figure 7). Several studies could show that all four core histones can directly O-GlcNAcylation, which affects the chromatin compaction status (Fujiki et al. 2011; Sakabe, Wang, and Hart 2010; Fong et al. 2012; Zhang, Roche, et al. 2011). Moreover, it was shown that O-GlcNAcylation can positively regulate the activity of the DNA demethylation enzyme ten-eleven translocation 1 (TET1), which increases demethylation of specific promoter regions and therefore induces transcriptional reprogramming (Vella et al. 2013; Shi et al. 2013). Indeed, knock down studies confirmed that both OGT and TET1 are required to maintain ESC pluripotency since their loss was sufficient to increase differentiation. *Vice versa*, compound-based inhibition of OGA resulted in increased O-GlcNAc levels and delayed differentiation of mESCs by activation of epigenetically regulated genes (Speakman et al. 2014). Loss of OGT not only results in reduced pluripotency of ESCs but also in defective embryogenesis in diverse species like the fly, zebrafish, and in mice (Shafi et al. 2000; Webster et al. 2009; O'Donnell et al. 2004; Mariappa et al. 2015). In addition, the complete knockout as well as catalytical inactive OGA was shown to be lethal in mice, supporting the essential role of proper O-GlcNAc cycling in a developmental context (Yang et al. 2012; Keembiyehetty 2015; Muha et al. 2021).

Interestingly, a balanced O-GlcNAc cycle also seems to be of special importance for differentiation into the neuronal and cardiac lineage. Chemical inhibition of OGA as well as GlcN treatment impaired differentiation of mESCs and hESCs into neural progenitor cells and of hESCs into cardiomyocyte precursors, respectively (Speakman et al. 2014; Kim et al. 2009; Parween et al. 2017). On the other hand, inhibition of OGT or GFAT1 had the opposite effect, resulting in an elevated potential for differentiation of hESCs into the neuronal or cardiac lineage (Andres et al. 2017; Kim et al. 2009). Consistently, *in vivo* experiments confirmed the vital importance of HBP activity on normal myogenesis and

neurogenesis. A conditional cardiomyocyte-specific OGT knockout induced severe cardiomyopathy, resulting in heart failure and high mortality rates (95% with 12 weeks) (Watson et al. 2014). Additionally, N-linked glycosylation is essential for proper muscular function since diverse mutations disturbing the glycosylation, including mutations in GFAT1, impair acetylcholine receptor maturation and transport to the plasma membrane (Senderek et al. 2011; Zoltowska et al. 2013). Consequently, neuromuscular signal transmission is altered, resulting in limb-girdle myasthenia, a specific subtype of myasthenic disorders (O'Connor et al. 2018). Moreover, current research demonstrated that severe neurodevelopmental disorders are accompanied by disturbed O-GlcNAc cycling *in vivo* (Olivier-Van Stichelen et al. 2017; Chen, Dong, et al. 2021; White et al. 2020).

The HBP is not only important to generate precursor molecules for O-GlcNAcylation, but also for synthesis of macromolecules as GAGs, which are highly important for the composition of the ECM (Figure 7). The ECM is part of the microenvironmental cell niche and was shown to affect stem cell homeostasis by different means, *inter alia* supporting cell attachment, proliferation, signaling, and differentiation (Discher, Mooney, and Zandstra 2009). Primary, the biochemical stiffness of the ECM has a pivotal role for pluripotency and differentiation (Nallanthighal, Heiserman, and Cheon 2019; Engler et al. 2006; Wen et al. 2014). Of note, increased HBP flux by GlcN supplementation was shown to positively affect hyaluronan (HA) levels, a GlcNAc containing polysaccharide and one of the main GAGs in the ECM (Jokela et al. 2011). Interestingly, the HBP can regulate HA concentrations not only by substrate availability, but it can also promote stability and activity of the HA producing enzyme hyaluronan synthase 2 (HAS2) by O-GlcNAcylation (Vigetti et al. 2012). Indeed, inhibition of GFAT1 as well as OGT were shown to reduce HA synthesis and thereby stem cell properties in cancer stem cells (Chokchaitaweasuk et al. 2019).

Like discussed in detail in the following section, HBP activity was reported to affect a broad range of protein quality control (PQC) mechanisms including the UPR, autophagy, the UPS and chaperone recruitment (see paragraph 1.2.5) (Figure 7). Since ESCs have a high rate of proliferation and protein synthesis, a properly coordinated PQC is indispensable for stem cell function and maintenance (Yan et al. 2020; Vilchez, Simic, and Dillin 2014).

Collectively, HBP activity has a broad impact on ESC pluripotency and maintenance: 1) alterations in HBP flux can manipulate substrate availability of other interconnected metabolic pathways, which is required to for stem cell properties; 2) HBP products can

directly influence stem cell identity by changed levels of PTMs (affecting TFs, chromatin remodeling, PQC) or glycoconjugate production, essential for ECM compounds. Therefore, a tightly controlled HBP is not only essential for ESC maintenance but ultimately also for embryonic development.

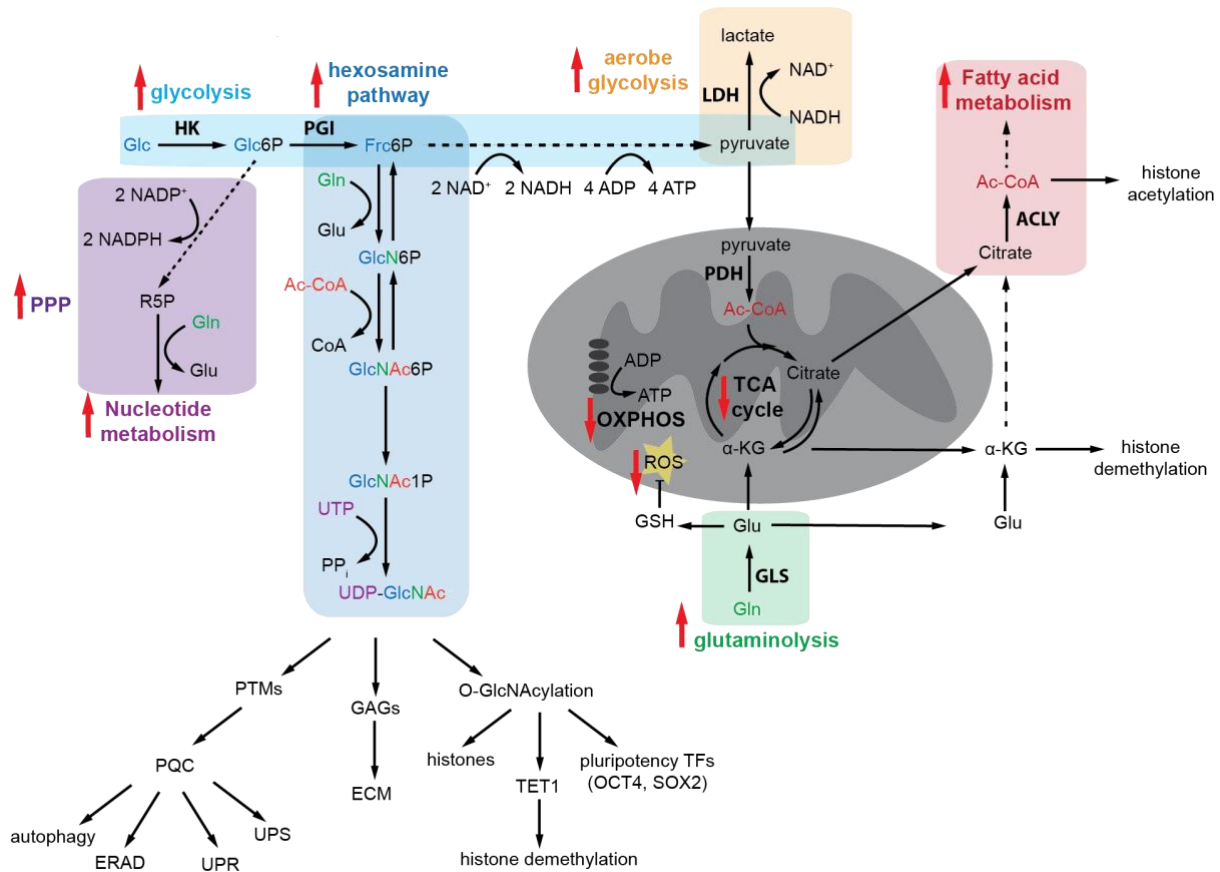


Figure 7: Stem cell maintenance requires metabolic rewiring and the accompanying HBP outputs. Stem cell metabolism is characterized by increased glycolysis (light blue box) with increased lactate production during aerobic glycolysis (orange box). Thus, shunt of metabolites into the pentose phosphate pathway (PPP, purple box) and the hexosamine pathway (dark blue box) is increased. In contrast, pyruvate entry into tricarboxylic acid (TCA) cycle and consequently oxidative phosphorylation (OXPHOS) levels are decreased. Instead, elevated glutaminolysis (green box) can serve as carbon source for the TCA cycle and thus citrate production for the increased demand of fatty acid metabolism (red box). Alterations in HBP flux can also change activity of interconnected pathways. Increased Ac-CoA production can increase histone acetylation. Reduced OXPHOS in combination with increased glutathione (GSH) production reduces reactive oxygen species (ROS) levels. Increased α-ketoglutarate (α-KG) levels can promote histone demethylation. Elevated UDP-HexNAc levels serves as precursor for O-GlcNAcylation of histones and transcription factors (TFs), other posttranslational modifications (PTMs) which can influence protein quality control (PQC) and synthesis of glycosaminoglycans (GAGs), required for the extracellular matrix (ECM). HK: hexokinase, PGI: phosphoglucose isomerase, LDH: lactate dehydrogenase, PDH: pyruvate dehydrogenase, GLS: glutaminase, ERAD: ER-associated degradation, UPR: unfolded protein response, UPS: ubiquitin-proteasome system, TET1: ten-eleven translocation 1, OCT4: octamer-binding protein 4, SOX2: sex determining region Y-box 2

1.2.5 The role of the HBP in aging

As described in the previous paragraphs, the HBP's products are essential precursors for several glycosylation events as well as for the synthesis of a broad range of macromolecules, which can interfere with highly important downstream signaling pathways. Therefore, it is not unexpected that disturbances of the HBP activity can result in pathological conditions that are often associated with aging. Remarkably, almost all of the hallmarks of aging (Figure 1) are described to be affected by alterations of the HBP flux. First of all, variations in UDP-GlcNAc levels can influence protein homeostasis on many different levels. For example, disturbances in N-linked glycosylation can induce ER stress which leads to the activation of the UPR in order to restore ER protein homeostasis (see paragraph 1.2.2.1) (Wang et al. 2014). However, PQC mechanisms as the UPR, ERAD, proteasomal activity, and autophagy can decline during aging (Hipp, Kasturi, and Hartl 2019). Activation of the HBP in *C. elegans* was previously shown to counteract this phenomenon by elevation of ERAD, proteasomal activity, and autophagy, thereby improving protein homeostasis and extending lifespan (Denzel et al. 2014). This protective effect of HBP activation against proteotoxic stress was also shown to be conserved in a mammalian system (Horn et al. 2020). In addition, the accumulation of metastable aggregation-prone proteins associated with age-related neurodegenerative diseases (Tau, α -synuclein, Ataxin-3) could be prevented by HBP activation in *C. elegans* as well as in a neuronal cell model (Denzel et al. 2014; Horn et al. 2020). Consistently, it is well-described that increased O-GlcNAcylation can counteract abnormal hyperphosphorylation of Tau, which causes protein aggregation and ultimately lead to Alzheimer's disease (Arnold et al. 1996; Liu et al. 2004). Moreover, recent publications described that the ubiquitin-proteasome system (UPS) can be regulated by O-GlcNAcylation, in a direct, as well as in an indirect manner (Sekine et al. 2018; Zhang et al. 2003). Additionally, it has been hypothesized that O-GlcNAcylation mainly occurs in unstructured regions, which seems to block aggregation and facilitate refolding (Zhu et al. 2015). At the same time, O-GlcNAcylation can enhance the recruitment of chaperons in a lectin-dependent manner, thereby assisting proper protein folding (Guinez et al. 2004). Thus, based on the literature, HBP activation is likely counteracting proteotoxic stress and important for maintaining protein homeostasis by increased O-GlcNAcylation.

Besides protein homeostasis, mounting evidence indicates that UDP-GlcNAc concentrations can affect epigenetic regulation of transcription, which is also altered during the aging process. For instance, it was shown that all four core histones can be

modified by O-GlcNAc, which results in changed chromatin structure and accessibility of the DNA (Sakabe, Wang, and Hart 2010). Besides this direct manipulation, O-GlcNAcylation can also alter histone acetylation and methylation indirectly by modification of epigenetic modifiers (Lewis and Hanover 2014). Love et al. were able to delineate that manipulation of the O-GlcNAcylation cycle could modulate promoter regions of nutrient-responsive pathways, impacting longevity and stress responses in *C. elegans* (Love et al. 2010). Additionally, the activity of RNA polymerase II and several transcription factors rely on this PTM, thereby affecting transcription (Ranuncolo et al. 2012; Lewis and Hanover 2014).

Moreover, DNA damage-responses were shown to rely on O-GlcNAcylation, therefore building a connection to age-dependent increases in genome instability (Zachara et al. 2011; Chen and Yu 2016). Independent publications confirmed that altered OGT expression correlates with impaired DNA-repair mechanisms and changes in cell senescence (Efimova et al. 2019; Lee and Zhang 2016).

Since the HBP serves as a metabolic hub by connecting different metabolic pathways, its role in maintaining nutrient sensing and induction of adaptive pathways is obvious. For example, a cross-regulation between the HBP and the nutrient-dependent mammalian target of rapamycin (mTOR) and AMPK signaling exists, thereby allowing rewiring of a cell's metabolic program (Cork, Thompson, and Slawson 2018; Bullen et al. 2014). Sustained elevation of O-GlcNAc levels is also known to reprogram energy metabolism by impacting the mitochondrial proteome and its function (Love et al. 2003; Tan et al. 2014; Tan et al. 2017). Not only the intracellular signaling, but also intercellular communication and regulation of energy homeostasis can be affected by impaired HBP activity, for example by altered hormone signaling via insulin as well as leptin (Wang et al. 1998; McClain and Crook 1996; Marshall, Bacote, and Traxinger 1991). Additionally, cell-cell communication is disturbed by aberrant glycosylation patterns on the cell surface (Saxon and Bertozzi 2001). Apart from that, HBP activation can reduce stem cell exhaustion. It was shown that activity of important pluripotency factors like OCT4 and SOX2 can directly be regulated by O-GlcNAcylation (Jang et al. 2012). The importance of the HBP for stem cell self-renewal was furthermore emphasized by its essential role in mESCs as well as embryonic lethality in mice, induced by OGA or OGT knock outs (for detailed information see paragraph 1.2.4.2) (O'Donnell et al. 2004; Yang et al. 2012). Moreover, cell identity properties can be impacted by changes in extracellular matrix (ECM) composition, which can be influenced by UDP-GlcNAc levels (Jokela et al. 2011; Vigetti et al. 2012).

Taken together, the HBP's activity can be associated with most of the nine hallmarks of aging (Figure 8). Thereby, changes in its activity can induce different human pathologies and common age-related diseases like cancer, diabetes, neurodegenerative diseases, cardiovascular diseases, and defects in immunity, which highlights the importance of the HBP in the context of aging. Thus, further understanding of the HBP and its regulation could provide novel targets for anti-aging drugs and could aid to develop novel therapies. For identification of putative druggable targets, we made use of genetic screens which are introduced in the section below.

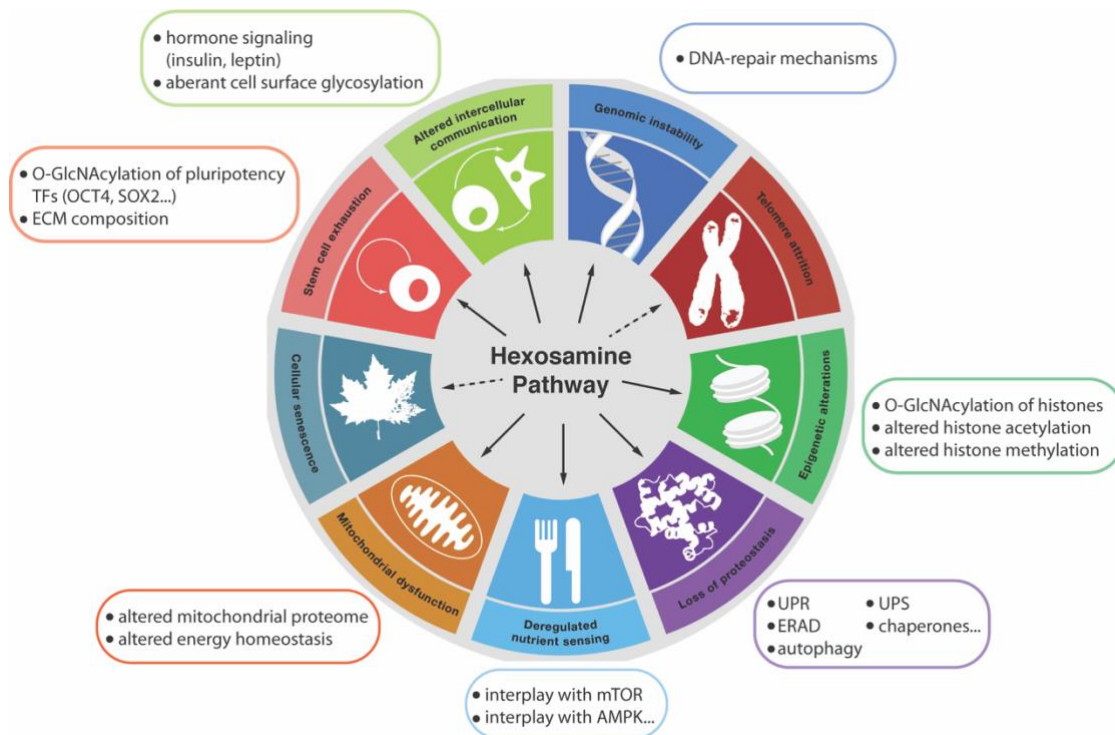


Figure 8: The HBP has a putative central role for the manifestation of the hallmarks of aging. Depicted are the nine hallmarks of aging which can be influenced by the products of the HBP. Dotted arrows indicate a putative connection (modified from López-Otín et al., 2013). UPR: unfolded protein response, UPS: ubiquitin-proteasome system, ERAD: ER-associated degradation, mTOR: mammalian target of rapamycin, AMPK: AMP-activated protein kinase, TF: transcription factor, OCT4: octamer-binding protein 4, SOX2: sex determining region Y-box 2.

1.3 Functional genetic screening approaches

1.3.1 The evolution of genetic screening strategies

One of the most powerful techniques for the discovery of novel biological processes is genetic screening. Overall, two variants of genetic screening can be distinguished: forward and reverse genetics. For reverse genetic screens, meaning a genome-to-phenotype approach, already existing knowledge is required, which complicates the identification of unknown genes. In contrast, forward genetic screens are phenotype-to-genome approaches, seeking for the identification of crucial genes based on a selected phenotype. This technique enables a systematic and genome-wide screen

for discovery of novel genes involved in a specific pathway. In spite of this, deciphering of recessive mutations is challenging, since in a diploid system the presence of a second chromosome set potentially masks phenotypes. Therefore, many fundamental mechanisms were uncovered by performing forward genetics using the haploid model organism *Saccharomyces cerevisiae* (*S. cerevisiae*) (Hartwell et al. 1974). Almost 20 years ago a yeast collection containing null mutants of almost the complete set of ORFs was established, allowing a comprehensive genome-wide forward genetic screen for the first time in eukaryotic cells (Winzeler et al. 1999; Giaever et al. 2002).

In higher eukaryotes however, all somatic cells are diploid, which limits their potential for forward genetic screening approaches. Therefore, typically inbreeding of heterozygous mutants was used in order to generate homozygous genomes for example in *C. elegans*. For forward genetic screen in mammalian cells, however, libraries of RNA interference (RNAi) were used in order to generate gene knockdowns (Sharp 1999). Since RNAi only induces a knockdown, remaining gene activity is might be not sufficient to mediate a phenotype, although on the other hand an incomplete inactivation of essential genes can be beneficial. Moreover, a high rate of off-targets and false positive hits for RNAi screens has been reported (Echeverri et al. 2006; Kaelin 2012). Luckily, the development of the CRISPR/Cas9 method revolutionized genome editing and opened a completely new field for screening technologies within the last decade (Doudna and Charpentier 2014). Libraries of small guide RNAs (sgRNA), which recruit the endonuclease Cas9 to the corresponding target site to generate a DNA double strand break, were established to facilitate homozygous knockouts in mammalian cells (Shalem, Sanjana, and Zhang 2015). Another fundamental progress for screens was the establishment of haploid mammalian cells, thus overcoming the problem of diploidy and providing a novel powerful tool for

genetic screens (see paragraph 1.3.2). A haploid mESC line was generated by two independent labs and was already successfully used for insertional-based mutagenesis (Elling et al. 2011; Leeb and Wutz 2011). Similarly, insertional mutagenesis screens were already performed in a near-haploid human leukemia cell line, containing a haploid chromosome set except for chromosome 8 (Carette et al. 2009; Kotecki, Reddy, and Cochran 1999). Emerging from this cell line, the fully haploid human cell line HAP1 was generated and used for insertional mutagenesis screens (Essletzbichler et al. 2014; Wijdeven et al. 2015). In contrast to the CRISPR/Cas9 system, which requires a sgRNA library, insertional mutagenesis has the advantage to generate mutations randomly across the genome with only negligible integration bias (Schnütgen et al. 2008). Moreover, the genomic integration site can be determined easily, due to transposon- or retroviral gene-trapping, which relies on a viral-specific molecular marker (Carette et al. 2009; Elling and Penninger 2014). This high efficiency for insertion site-mapping permits genome-wide and high-throughput screening.

Nevertheless, all of these approaches are limited since they cause knockout mutations and therefore, only gene loss-of-function (LOF) but no gain-of-function (GOF) mutations can be identified. Further development of the CRISPR/Cas9 technology though, allows additional identification of hypomorph mutations by partial gene repression (CRISPRi) and gain-of-function (GOF) mutations by gene activation and overexpression (CRISPRa) (Gilbert et al. 2014). Another mechanism to also obtain GOF mutations is the introduction of single nucleotide variants (SNVs) that can be introduced into the genome by usage of alkylating reagents like N-ethyl-N-nitrosourea (ENU). The ethyl group of ENU can be transferred to nucleotides, mainly inducing A-T to T-A transversions and A-T to G-C transitions and thereby mediating nonsynonymous amino acid alterations in approximately 70% of mutations (Arnold et al. 2012). Besides being capable to also induce GOF mutations, chemical-based mutagenesis has the advantage to cover the whole genome in an unbiased manner since mutations are introduced randomly, including non-coding regions. Most importantly, SNV-based screening has the unique feature to enable the functional analysis of proteins on a single amino acid resolution, which is not possible with approaches like RNAi, insertional mutagenesis or the CRISPR/Cas9 system. Due to these benefits, the combination of haploid mESC and SNV integration by usage of alkylating agents is a powerful state-of-the-art genetic screening tool, which was already successfully demonstrated in recent studies (Horn et al. 2018; Allmeroth et al. 2020). Thus, this unique combination allows not only the identification of recessive mutations in

a mammalian system but also in parallel permits to uncover the whole range of mutations including hypomorph, hypermorph, neomorph, or null mutations.

1.3.2 Haploid mESCs as a novel screening tool

As mentioned above, haploidy is a beneficial trait with regard to genetic screens, since also recessive mutations can be identified due to the lack of a second gene copy, which could otherwise mask a phenotype. Thus, haploid organisms like yeast were favored for screening assays in the past and have been extensively used to elucidate many pivotal biological processes (Hartwell et al. 1974). Since haploidy is incompatible with mammalian development however, all somatic cells of higher eukaryotes are diploid (Latham et al. 2002). Thus, hitherto mammalian cells were neglected for forward and reverse genetic screens. Previously, haploidy was only achieved in fish ESCs and a human near-haploid leukemia cell line KBM7, which has a haploid set of chromosomes except for chromosome 8 (Kotecki, Reddy, and Cochran 1999; Yi, Hong, and Hong 2009). Further engineering of this cell line enabled cultivation of the first completely haploid human cell line HAP1 (Essletzbichler et al. 2014). However, HAP1 cells still contain various genomic alterations and cancer properties, limiting their use for deciphering physiological genetic pathways. Two independent groups established a method that enables the generation and cultivation of haploid mESCs (Elling et al. 2011; Leeb and Wutz 2011). Using these haploid mESCs for forward genetic screens can overcome the problems of diploidy in mammalian cells, transferring the benefits from lower eukaryotes like yeast to a mammalian system.

Already 1983 Kaufman and colleagues attempted to generate haploid mESCs from parthenogenetic embryos, meaning developed from an unfertilized oocyte (Kaufman et al. 1983). For development of parthenogenetic embryos, murine oocytes were isolated and activated without fertilization by exposure to 5% ethanol or SrCl₂ for 5 min (Figure 9A). The activated oocytes were transferred into a pseudo-pregnant foster mother and after 3.5 days of development, blastocysts were isolated and cultivated under conditions used to derive mESCs from the inner cell mass. However, all parthenogenetically derived mESC lines remained diploid (Kaufman et al. 1983). Just recently the protocol of Kaufman et. al was extended by a series of FACS sorts, which revealed that indeed a minor subpopulation of the cells derived from parthenogenetic blastocysts was haploid (Elling et al. 2011; Leeb and Wutz 2011). In order to enrich for haploidy, cells were stained with Hoechst33342, a fluorescent dye that incorporates into the DNA, and sorted according to their DNA content. While haploid cells show a peak in the FACS histogram corresponding

to 1n and only a smaller peak for 2n representing the cells in the cell cycle, the histogram of diploid cells displays shifted peaks that correspond to 2n or 4n, respectively (Figure 9B).

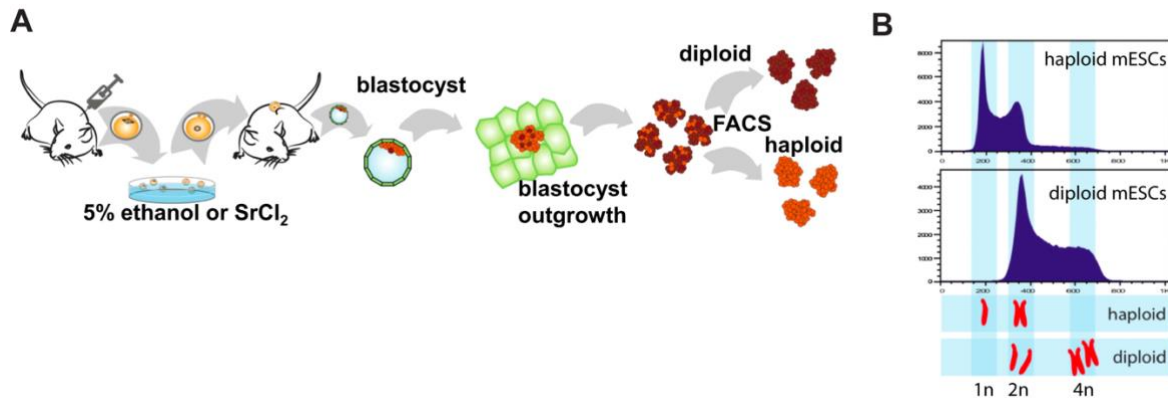


Figure 9: Schematic workflow of haploid mESC generation. (A) Isolated mouse oocytes are activated without fertilization by incubation with 5% ethanol or SrCl_2 before implanted into pseudo-pregnant foster mice. Upon 3.5 days of development, blastocysts are isolated and used for outgrowth of mESCs. Cells are sorted according to their ploidy by FACS analysis. **(B)** Schematic histogram of FACS sorting upon Hoechst33324 staining. Depicted is the DNA content of haploid and diploid mESCs. 1n and 2n chromosome sets correspond to haploid while 2n and 4n chromosome sets correspond to diploid cells (modified from Elling et al., 2011).

For functional characterization of haploid mESCs, chromosome spreads were performed which confirmed that indeed the complete chromosome set is haploid (Elling et al. 2011). Further analysis of chromosomes excluded aberrant rearrangements including deletions or duplications of individual chromosomes. The parthenogenic AN3-12 cell line we used in this work, only contains minor genomic alterations that possibly affect the genes *Cdh4*, *Taf4*, *Agmo*, and *Cox7c* (Elling et al. 2017). Moreover, pluripotency of haploid mESCs was verified since all typical stem cell markers (*Oct4*, *Nanog* or *Sox2*) could be detected and cells were able to differentiate into all three germline layers *in vitro* as well as *in vivo*. Since the capacity for growth and the maintenance of stem cell function was not changed although passaged for more than 50 times, cells could be used for genome-wide saturating forward genetic screens. For example, haploid mESCs were already successfully used to identify targets for several compounds including ricin, 3-bromopyruvate, 6-thioguanine, and bortezomib as well as thapsigargin (Elling et al. 2011; Birsoy et al. 2013; Forment et al. 2017; Horn et al. 2018; Allmeroth et al. 2020). In addition, a comprehensive biobank containing reversible insertions in haploid mESC was established (<https://www.haplobank.at>). This publicly available resource contains 16.970

independent clones that cover around 70% of the protein coding genes, thus enabling an easy and high-throughput screening method for functional genomics (Elling et al. 2017). Importantly, haploidy is not a stable genomic condition and 2-3% of haploid cells spontaneously diploidize per day in culture (Elling et al. 2011). Therefore, it is inevitable to sort cells regularly in order to enrich and maintain haploidy over time. Worth mentioning, spontaneous diploidization most likely is promoted by failed cytokinesis or endoreplication since introduced mutations remain homozygous. Additionally, differentiation of mESCs can only originate from diploid cells, indicating that a haploid state is not compatible with differentiated cell types in the murine system, potentially due to imbalanced expression of X-chromosomal genes (Marahrens et al. 1997). In contrast, haploid human ESCs are able to differentiate into haploid somatic cells (Sagi et al. 2016). This phenomenon suggests evolutionary differences between human and mouse with regard to tolerance of haploidy. Concluding, the generation of haploid mESCs revolutionized the field of functional genomics since their usage enables the possibility to perform genome-wide forward and reverse genetic screens in a mammalian system, thus allowing the identification of dominant and recessive mutations, which was hitherto limited to haploid organisms like yeast

1.4 Aim of the project

The sustaining aging process of the population implies a dramatic global challenge for economic, social, and especially medical aspects. Therefore, it is of utmost importance to deepen our understanding of the cellular mechanisms of aging in order to extend not only lifespan but also health span. Interestingly, aging is accompanied by diverse metabolic changes and dietary restriction is able to extend lifespan. Consequently, we aimed to gain new insight into the interconnection of nutrient signaling and the metabolic regulation of aging.

The HBP is a nutrient-responsive pathway, which serves as a metabolic hub and is pivotal to adapt cellular processes according to external signals. The high energy end product of the HBP, UDP-GlcNAc, is an essential precursor for different glycosylation types and for the synthesis of a broad range of glycoconjugates, which all can interfere with highly important downstream signaling pathways. Remarkably, almost all of the hallmarks of aging, can be connected to alterations in HBP flux. Therefore, disturbances in the HBP activity can result in pathological conditions and common age-related diseases like cancer, diabetes, neurodegenerative diseases, cardiovascular diseases, and defects in immunity, which highlights the importance of the HBP in an aging context. However, while the regulation of the HBP via feedback inhibition of the rate-limiting enzyme GFAT1 is well-studied, other regulators and how the HBP can adapt UDP-GlcNAc levels according to nutrient availability, remain uncharted. Toxicity induced by the glycosylation toxin tunicamycin (TM) can be counteracted by elevated UDP-GlcNAc levels, thus representing a suitable proxy for increased HBP flux. Therefore, in this study we performed a forward genetic screen for TM resistance in haploid mouse embryonic stem cells (mESCs) using chemical-based mutagenesis, in order to identify novel HBP regulators. This unique combination of using haploid cells together with chemical mutagenesis, does not only allow the identification of recessive mutations in a mammalian system, but additionally permits to uncover the whole range of mutations including hypomorph, hypermorph, neomorph, or null mutations. Using this state-of-the-art method, we aimed to deepen the knowledge about the HBP's regulation in a mammalian system, which could assist to uncover potential drug targets that may ultimately help to delay aging and improve health span of the steadily growing aging population.

Work contributions of results

I performed all experiments described in the next section independently, except for:

2.1 Identification of AMDHD2

2.1.1 Chemical mutagenesis screen for TM resistance in mESCs identifies AMDHD2
(with the help/ under supervision of Dr. Moritz Horn)

2.1.4 Insertional mutagenesis screen confirms the loss of AMDHD2 as HBP activator
(virus transfection for insertional mutagenesis was performed by Dr. Ulrich Elling)

2.2 Characterization of AMDHD2

2.2.1 Biochemical characterization of AMDHD2
(the complete biochemical characterization was performed by Dr. Sabine Ruegenberg)

2.2.2 Biological/physiological characterization of AMDHD2

2.2.2.1 Loss of the *C. elegans* homolog F59B2.3 has no effect on HBP activity
(injections of worms was performed by Dr. Maxime Derisbourg)

2.2.2.2 Loss of AMDHD2 in *M. musculus* leads to embryonic lethality
(design for gene editing was done by Dr. Kira Allmeroth, injections were performed by Ingo Voigt)

2.3 Cell type-specific regulation of the HBP

2.3.2 GFAT2 has a lower sensitivity to UDP-GlcNAc feedback inhibition than GFAT1
(measurements of kinetic properties and feedback inhibition was performed by Dr. Sabine Ruegenberg)

For detailed information of working contributions see p. 137

2 Results

The aging process is a complex phenotype, which occurs on multiple levels and affects all kind of tissues and organs. Therefore, many diverse age-related diseases as cancer, cardiovascular diseases, neurodegenerative diseases, or diabetes are common and affect the majority of the steadily increasing human population. Interestingly, as already discussed in detail in the introduction, the hexosamine biosynthetic pathway (HBP) is connected to the aging process on many different levels by impacting essential processes like proteostasis, epigenetics, and stem cell quiescence (Denzel et al. 2014; Sun et al. 2016). Thus, it is highly important to understand how the HBP is regulated in detail and how it can be modulated to delay the onset of age-related diseases. The HBP is the only source for UDP-GlcNAc and consumes metabolites involved in all key metabolic pathways as carbon-, nitrogen-, fatty-acid-, and energy-metabolism. It is therefore optimally positioned to act as a metabolic sensor that can modulate downstream cellular signaling through UDP-GlcNAc-dependent post-translational modifications (PTMs) (Marshall, Bacote, and Traxinger 1991). How the HBP is regulated to adapt UDP-GlcNAc levels and thus downstream PTMs according to nutrient availability however, remains an open question. Therefore, we made use of knowledge from previous studies in *C. elegans*, which could show that tunicamycin (TM) resistance can be used as a proxy for increased HBP activity (Denzel et al. 2014). Additionally, this mechanism is conserved in the murine N2a cell line suggests that screening for TM resistance is a suitable unbiased method to further explore the HBP through genetic approaches in a mammalian system (Horn et al. 2020; Ruegenberg et al. 2020b). Consequently, in this study we performed a TM resistance screen in the haploid AN3-12 cell line to extend the understanding of HBP regulation in mammals, which might help to delay age-related dysfunctions and ultimately prolong health span.

2.1 Identification of AMDHD2

2.1.1 Chemical mutagenesis screen for tunicamycin resistance in mESCs identifies AMDHD2

Elevated HBP flux and consequential high concentrations of its end product UDP-GlcNAc suppress TM toxicity, rendering TM resistance a suitable proxy for HBP activity in genetic

screens. Therefore, we performed an unbiased TM resistance screen in order to further investigate HBP regulation in mammalian cells. The highly potent mutagen N-ethyl-N-nitrosourea (ENU) induces mispairings and base-pair substitutions that allow screening at amino acid resolution (Russell et al. 1979). Thus, we used ENU-based chemical mutagenesis in haploid cells as a unique method for identification of recessive alleles (Elling et al. 2011; Horn et al. 2018; Allmeroth et al. 2020). To achieve a highly saturated screen, 27 million AN3-12 mouse embryonic stem cells (mESCs) were used for mutagenesis, followed by TM selection using a wild type (WT) lethal dose (0.5 $\mu\text{g}/\text{ml}$) for three weeks (Figure 10A). Emerging from this screen, 29 resistant clones were randomly selected and singled to grow isogenic mutant lines. Initial whole exome sequencing was done with four clones that showed strong TM resistance compared to control cells, which was confirmed in a cell viability assay (Figure 10B). In two clones, independent missense mutations in the *Amdhd2* coding sequence could be detected (Figure 10C). Whole exome sequencing of the remaining 25 clones revealed in total 11 independent amino acid substitutions at 10 distinct positions within the *Amdhd2* locus (38% of sequenced clones) (Figure 10C, D). Therefore, we conclude a high degree of saturation of our chemical mutagenesis screen, which allowed the discovery of *Amdhd2* as a novel candidate to confer TM resistance.

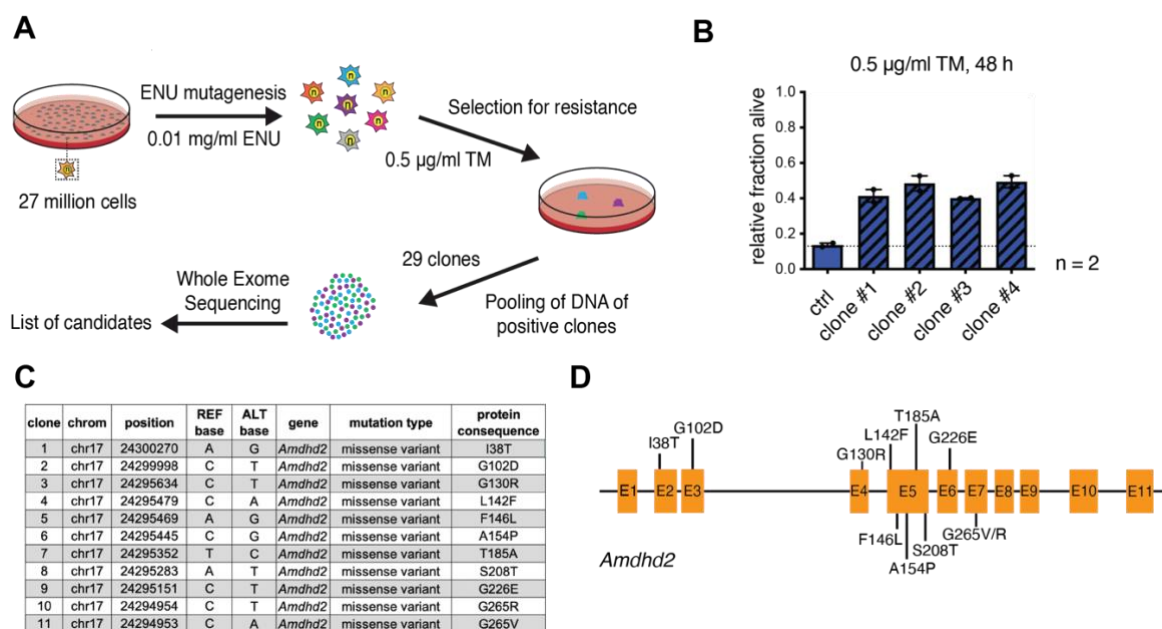


Figure 10: Chemical mutagenesis screen for tunicamycin resistance in mESCs identifies AMDHD2. (A) Schematic representation of experimental workflow for TM resistance screen using ENU mutagenesis in combination with whole exome sequencing. (B) Cell viability (XTT assay) of four TM resistant AN3-12 clones from mutagenesis screen that were used for WES upon treatment with 0.5 $\mu\text{g}/\text{ml}$ TM for 48h (mean \pm SEM, n=2). (C) Table listing all mutations in the *Amdhd2* locus identified in the TM resistance screen. (D) Schematic representation of the mouse *Amdhd2* locus. Amino acid substitutions identified in the screen are highlighted.

2.1.2 Confirmation of *Amdhd2* as tunicamycin resistance-conferring gene

To confirm *Amdhd2* as the TM resistance-mediating gene we generated *Amdhd2* K.O. mutants in WT AN3-12 cells using the CRISPR/Cas9 system. To prove the successful deletion, we generated and validated a specific AMDHD2 antibody. Indeed, we could confirm successful a loss of AMDHD2 by Western blot (WB) analysis (Figure 11A). In total, we tested three independent AMDHD2 K.O. clones, which were generated with different guide combinations in order to exclude that off-target effects contribute to the observed phenotype. In fact, all three AMDHD2 K.O. lines showed significant TM resistance compared to WT cells, proving AMDHD2 loss-of-function as causal for TM resistance (Figure 11B, C).

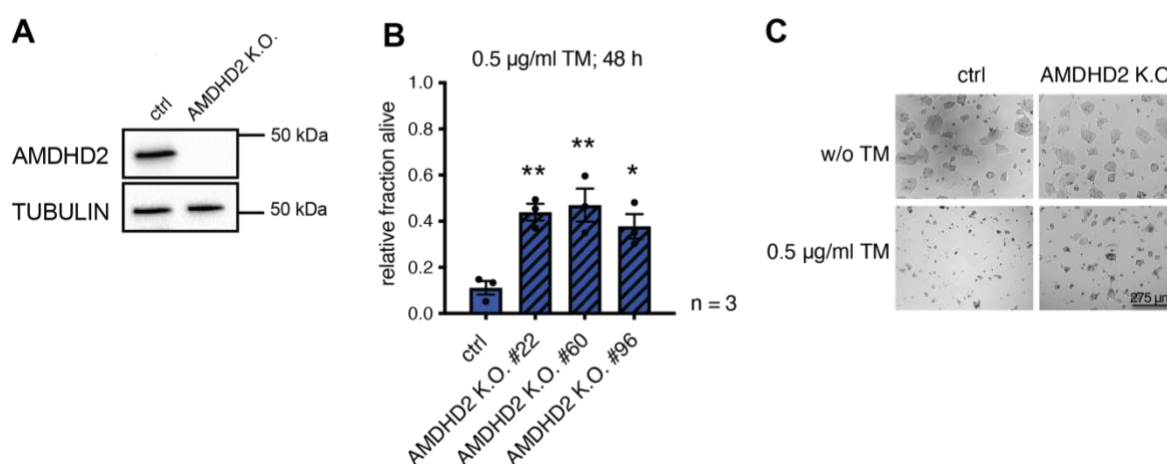


Figure 11: Confirmation of *Amdhd2* as tunicamycin resistance-conferring gene. (A) Western blot analysis of CRISPR/Cas9 generated AMDHD2 K.O. AN3-12 mESCs compared to wild type cells (ctrl). **(B)** Cell viability (XTT assay) of WT (ctrl) and AMDHD2 K.O. AN3-12 cells treated with 0.5 µg/ml TM for 48h (mean ± SEM, n=3, * p<0.05, ** p<0.01, One-way ANOVA Dunnett post-test). **(C)** Representative images of WT and AMDHD2 K.O. AN3-12 cells treated with 0.5 µg/ml TM for 48h or respective control. Scale bar, 275 µm.

2.1.3 Loss of AMDHD2 leads to HBP activation

AMDHD2 is an amidohydrolase that catalyzes the deacetylation of GlcNAc-6P to generate GlcN6P (White and Pasternak 1967). This reaction occurs in the “reverse” direction of HBP; however, the relevance of AMDHD2 in the context of adjusting cellular UDP-GlcNAc levels was not investigated before. We hypothesized that the loss of AMDHD2 function might increase HBP activity, thereby increasing UDP-GlcNAc levels, which in turn mediates TM resistance (Figure 12A). To test this hypothesis, we measured UDP-GlcNAc (or UDP-HexNAc) levels via ionic chromatography mass spectrometry

(IC-MS) (or LC-MS), which indeed corroborated significantly increased HBP product concentrations in the AMDHD2 K.O. mutants compared to control cells (Figure 12B, C). These results confirm that the observed TM resistance is conveyed by elevated HBP product availability due to reduced catabolism of GlcNAc-6P by AMDHD2.

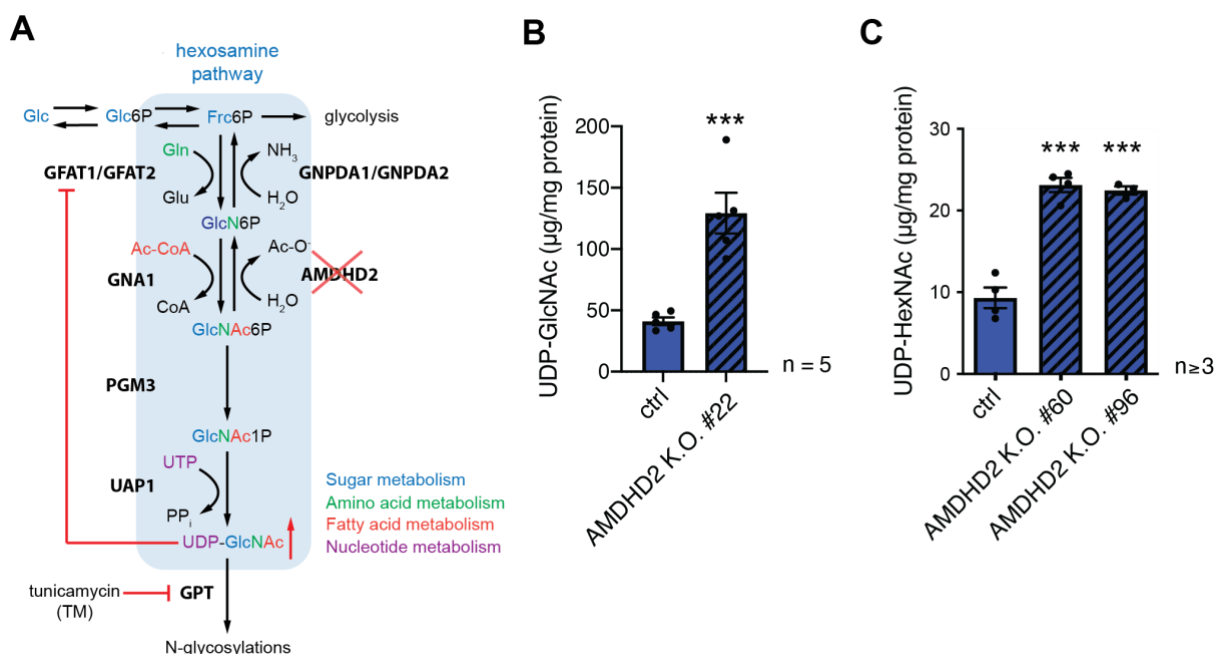


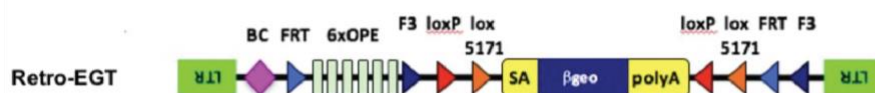
Figure 12: Loss of AMDHD2 leads to hexosamine pathway activation. (A) Schematic overview of the hexosamine pathway (blue box). The intermediate Frc6P from glycolysis is converted to UDP-GlcNAc, which is a precursor for glycosylation reactions. The enzymes are glutamine fructose-6-phosphate amidotransferase (GFAT1/2), glucosamine-6-phosphate N-acetyltransferase (GNA1), phosphoglucomutase (PGM3), UDP-N-acetylglucosamine pyrophosphorylase (UAP1), glucosamine-6-phosphate deaminase (GNPDA1/2), N-acetylglucosamine deacetylase (AMDHD2), and UDP-GlcNAc:dolichylphosphate GlcNAc-1-phosphotransferase (GPT). Red line indicates negative feedback inhibition of GFAT by UDP-GlcNAc. Formation of N-glycosylation is inhibited by tunicamycin (TM). **(B)** IC-MS analysis of UDP-GlcNAc levels of AMDHD2 K.O. compared to WT (ctrl) AN3-12 mESCs (mean ± SEM, n=5, *** p<0.001, unpaired t-test). **(C)** LC-MS analysis of UDP-HexNAc (combination of UDP-GlcNAc and UDP-GalNAc) levels of two more AMDHD2 K.O. clones compared to WT (ctrl) AN3-12 mESCs (mean ± SEM, n≥3, *** p<0.001, One-way ANOVA Dunnett post-test).

2.1.4 Insertional mutagenesis screen confirms the loss of AMDHD2 as HBP activator

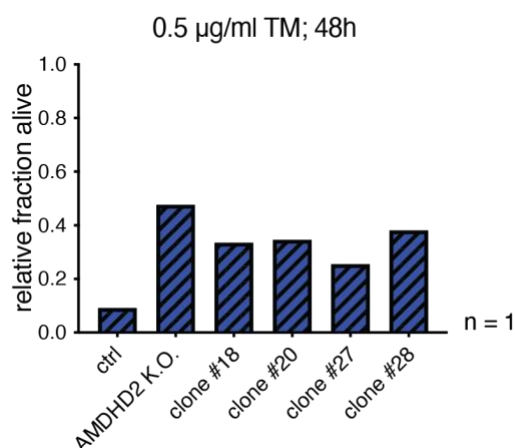
Besides the unbiased chemical-based mutagenesis, we performed an independent insertional mutagenesis screen to confirm the K.O. of AMDHD2 to be causative for TM resistance. For the genome-wide insertional mutagenesis we used a previously published retroviral-based system (Elling et al. 2017). The integrated transgene contains a splice acceptor site, which results in disruption of target gene expression (Figure 13A). The

invertible nature however, allows the reversion of the generated loss-of-function. Moreover, the introduced construct includes a barcode, which can be used for identification of the integration site by inverse PCR. Viral transfection as well as screening for TM resistance resulted in the identification of 20 isogenic clones. Indeed, further analysis of these clones by integration site mapping, revealed a disruption of the *Amdhd2* locus in 4 clones (20%). Using the XTT cell viability assay we could confirm TM resistance of these four clones, while WT cells served as negative and AMDHD2 K.O. cells as positive control (Figure 13B). Moreover, LC-MS measurements unveiled significantly elevated UDP-HexNAc (combination of UDP-GlcNAc and UDP-GalNAc) levels in all clones. Thereby, we confirmed hyperactivation of the HBP by loss of AMDHD2 in a completely independent screen.

A



B



C

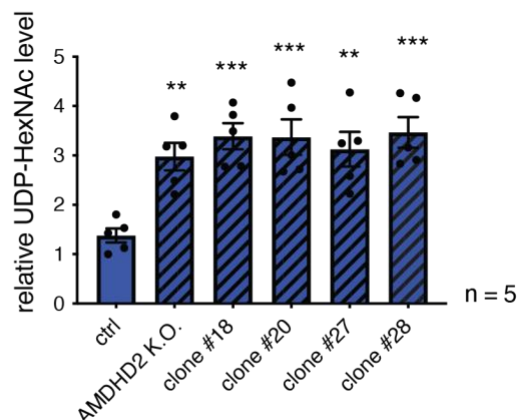


Figure 13: Insertional mutagenesis screen confirms the loss of AMDHD2 as hexosamine pathway activator. (A) Schematic representation of the enhanced gene trap (EGT) mutagenesis vector: Splice acceptor sites (SA) are revertible using non-compatible loxP/lox5171 and FRT/F3 sites (triangles). G418 resistance is mediated by expression of beta-Geo (bgeo). Six osteopontin enhancer (OPE) elements upstream of beta-Geo enhance the expression by Oct4/Pouf51 binding. The barcode (BC) is depicted by a purple diamond. LTR, long terminal repeats. (Elling et al. 2017) (www.haplobank.at). (B) Cell viability (XTT assay) of four TM resistant clones identified via insertional mutagenesis compared to control WT and AMDHD2 K.O. AN3-12 cells. Cells were treated with 0.5 µg/ml TM for 48h (n=1). (C) LC-MS analysis of UDP-HexNAc (combination of UDP-GlcNAc and UDP-GalNAc) levels of four TM resistant clones identified via insertional mutagenesis compared to control WT and AMDHD2 K.O. AN3-12 cells (mean ± SEM, n=5, ** p<0.01, *** p<0.001, One-way ANOVA Dunnett post-test).

2.2 Characterization of AMDHD2

2.2.1 Biochemical characterization of AMDHD2

After identifying AMDHD2 as a novel regulator for HBP activity, we aimed to deepen our understanding of the mechanism on a molecular level. However, mammalian AMDHD2 is a rather unstudied protein and hitherto there is no eukaryotic protein structure available. Instead, structural models are only predicted based on the bacterial homologue N-acetylglucosamine-6-phosphate deacetylase (NagA). As a result, biological and functional properties of mammalian AMDHD2 remain widely uncharted. Therefore, we performed the first structural and biochemical characterization of human AMDHD2.

2.2.1.1 Structural properties of human AMDHD2

To explore regulatory principles, we solved the first three-dimensional structure of human AMDHD2 by X-ray crystallography. Human AMDHD2 is composed of two domains: a deacetylase domain responsible for the conversion of GlcNAc-6P into GlcN6P and a second small domain with unknown function (DUF), consisting of residues from both N- and C-terminus (Figure 14A).

The structure of the deacetylase domain shows a TIM (triosephosphate isomerase) barrel-like fold (Figure 14A). A typical TIM-barrel scaffold comprises eight alternating β -strands forming a barrel shaped core, which is surrounded by eight α -helices (Banner et al. 1975). In AMDHD2 however, the eight alternating β -strands/ α -helices are interrupted by an insertion of three additional antiparallel β -strands (β 15- β 17) after eight β -strands and seven α -helices. The three antiparallel β -strands are organized in a β -sheet close to the active site. The smaller DUF-domain consists of two β -sheets, each composed of three or six antiparallel β -strands, and two small α -helices altogether forming a β -sandwich (Figure 14A). Furthermore, AMDHD2 occurs as a dimer through direct interactions of the two deacetylase domains (Figure 14B).

Interestingly, residues from both monomers participate in GlcN6P-binding (Figure 14C). Hydrogen bonds with Asn235 and Ala236 on the one hand as well as ionic interactions to His242* and Arg243* of the second monomer on the other hand, stabilize the phosphate group of the sugar. Additionally, hydrogen bonds are built between the hydroxyl groups of GlcN6P and Ala154 and His272. A Zn ion, which serves as potential cofactor, is coordinated via electrostatic interactions with Glu143, His211, His232, and two water

molecules. According to homology to bacterial NagA, Asp294 seems to be the catalytic residue (Hall, Xiang, et al. 2007) (Supplementary Fig. 1). In general, based on the high score of conservation of the structural features, a similar catalytic mechanism as it occurs in *E. coli* can be assumed (Hall, Xiang, et al. 2007).

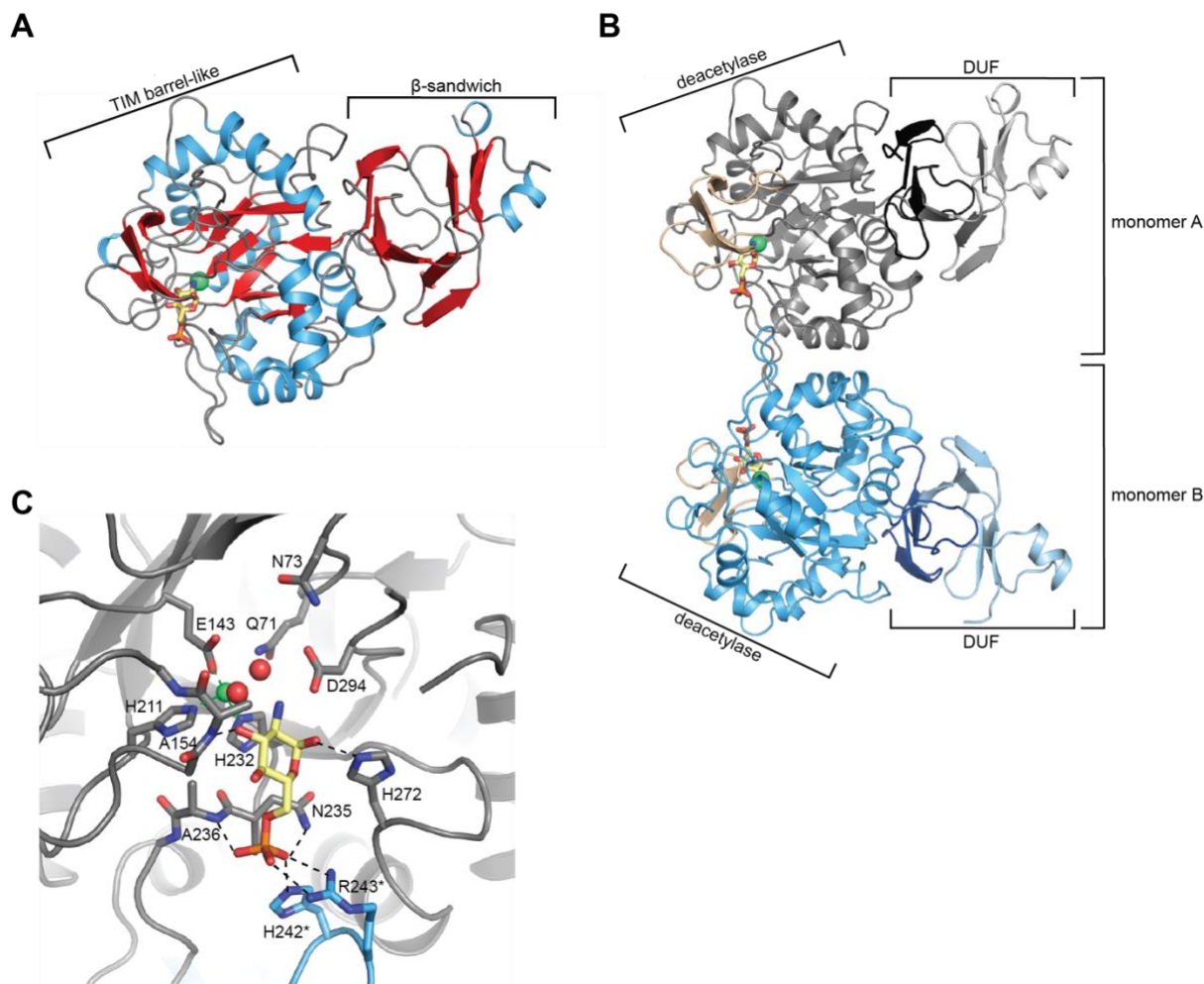


Figure 14: Structural analysis of human AMDHD2. (A) Domains and secondary structure elements within one AMDHD2 monomer. The deacetylase domain (left) shows a TIM barrel-like fold, while the small DUF domain (right) is composed of a β -sandwich fold. α -helices are colored in blue, β -strands in red, and loops in gray. GlcN6P (yellow sticks) and Zn^{2+} (green sphere) are highlighted. (B) Overview of the human AMDHD2 dimer in cartoon representation. Monomer A is colored in gray and monomer B in blue. The two deacetylase domains are interacting with each other. The DUF domain is formed by residues of the N-terminus (light gray, light blue) and residues of the C-terminus (black, dark blue). GlcN6P (yellow sticks), Zn^{2+} (green sphere), and the putative active site lid (wheat) are highlighted. (C) Close-up view of the active site in cartoon representation. Residues involved in ligand binding or catalysis are highlighted as sticks, as well as GlcN6P (yellow sticks), Zn^{2+} (green sphere) and two water molecules (red spheres). The GlcN6P binding site is formed by two deacetylase domains. Black dashed lines indicate key interactions to GlcN6P and green dashed lines the coordination of Zn^{2+} . Constructed with PyMOL using PDB ID 7NUT. (Data was already described in: Ruegenberg, 2020a).

2.2.1.2 *In vitro* characterization of identified loss-of-function mutations in AMDHD2

After identifying AMDHD2 as a novel regulator for HBP activity, we aimed to deepen our understanding of the mechanism on a molecular level. Given the knowledge from the AMDHD2 structure, we performed an *in vitro* characterization of the eleven AMDHD2 substitutions identified in the TM resistance screen to examine how they might affect enzymatic function. For this purpose, human WT and mutant AMDHD2 were expressed with an N-terminal His₆-tag in BL21 (DE3) *E. coli*. Protein expression was followed by a 2-step purification protocol consisting of immobilized metal affinity chromatography (IMAC) and size-exclusion chromatography (SEC) after thrombin-based cleavage of the His₆-tag. First, protein expressions of the recombinant mutant variants were tested to analyze their effect on protein solubility (Figure 15A). Additionally, based on bacterial homology the putative active site mutant D294A was generated as a control for activity assays (Hall, Xiang, et al. 2007). Many AMDHD2 variants were soluble upon bacterial expression, including F146L, A154P, T185A, S208T, and D294A (Figure 15A). These substitutions are located close to the active site of AMDHD2 (Figure 15C) and Ala154 is even directly involved in ligand binding (Figure 15D). In contrast, no protein could be detected in the soluble fraction of the mutants G102D, G130R, G226E, and G265V indicating a defect in protein folding. Furthermore, the I38T and G265R substitutions resulted in reduced solubility while the L142F mutation seemed to promote AMDHD2 fragmentation (Figure 15A). Next, the consequences of the I38T, T185A, G265R, and D294A substitutions were analyzed on AMDHD2 activity (Figure 15B). As expected, the D294A mutation impaired enzyme activity fully, supporting its functional role in mediating catalysis. Furthermore, the substitution G265R abolished enzyme activity completely whereas the T185A mutant showed reduced activity. Just the I38T mutation, the only mutation located in the DUF, did not have any influence on enzyme activity. To summarize, the AMDHD2 mutations identified in our screen can be divided into two groups either impairing protein folding or the catalytic activity (Figure 15D).

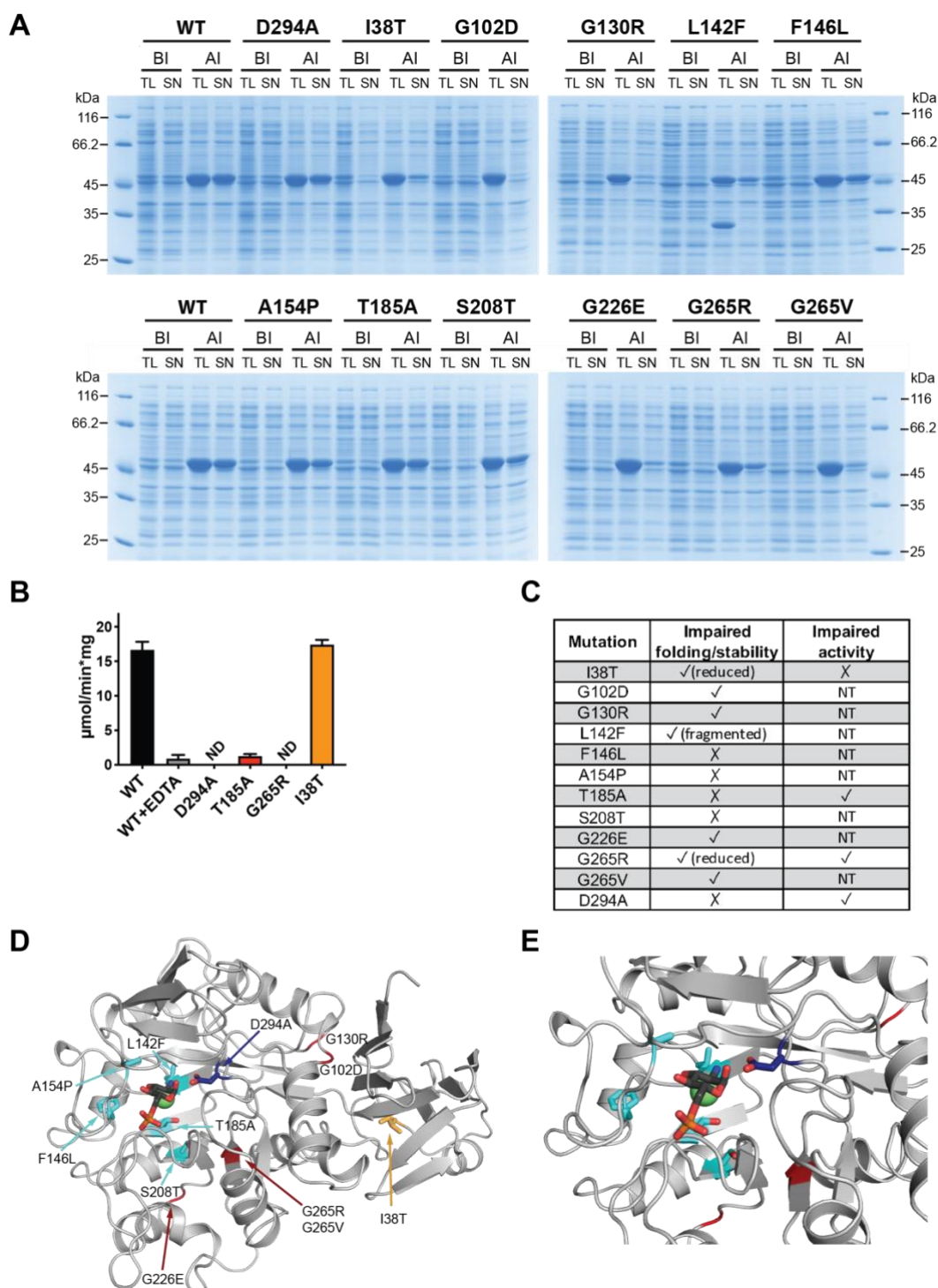


Figure 15: *In vitro* characterization of identified loss-of-function mutations in AMDHD2. (A) SDS-gels stained with Coomassie brilliant blue of a representative bacterial test expression of the human AMDHD2 variants. The experiment was repeated three times with similar results. BI: before induction, AI: after induction, TL: total lysate, SN: soluble fraction/ supernatant. A band corresponding to the molecular weight of human AMDHD2 with His₆-tag (46 kDa) was present in all total lysates after induction. **(B)** Activity of wild type (WT) and mutant human AMDHD2 (mean + SEM, n=6, ND=not detected). **(C)** Mutations can be classified into two groups either impairing protein folding/solubility or the catalytic activity. **(D)** Overview of the position of the potential loss-of-function mutations in human AMDHD2 in cartoon representation. GlcN6P (black sticks), the metal co-factor (green spheres) and the active site Asp294 (dark blue sticks) are highlighted. The eleven putative loss-of-function mutations are depicted in a color code: located in the domain

of unknown function (DUF) (orange), located in the active site (light blue) and that disturb protein folding/solubility (dark red). Constructed with PyMOL using PDB ID 7NUT. **(E)** Close-up view of **(D)** focusing on the active site. NT = not tested. (Data was already described in: Ruegenberg, 2020a).

2.2.2 Biological/physiological characterization of AMDHD2

Having characterized AMDHD2 on a biochemical level, we next aimed to further investigate the role of AMDHD2 in a more physiological context. To expand our understanding how the loss of AMDHD2 and the consequent elevated HBP activity can impact biological mechanisms, we generated and characterized different *in vivo* models lacking AMDHD2.

2.2.2.1 Loss of the *C. elegans* AMDHD2 homolog F59B2.3 has no effect on HBP activity

In previous studies it was already shown that not only GlcNAc supplementation but also gain-of-function (GOF) mutations as well as overexpression (OE) of the rate limiting HBP enzyme GFAT-1 and the accompanying increase of UDP-GlcNAc levels have a beneficial effect on protein homeostasis and lifespan in the nematode *C. elegans* (Horn et al. 2020; Denzel et al. 2014). Given this information, *C. elegans* presents a suitable *in vivo* model to manipulate and further characterize HBP function. To evaluate if also the newly identified AMDHD2 has physiological relevance in the nematode, a K.O. strain of the putative *C. elegans* homologue (*F59B2.3*) was generated using the CRISPR/Cas9 system. Two independent worm lines carrying different insertions/deletion leading to a frameshift in Exon 1 of *F59B2.3* and thereby to a premature stop codon, were analyzed (Figure 16A). Indeed, both K.O. lines showed a decreased expression of *F59B2.3* mRNA as measured by qPCR, indicating nonsense-mediated mRNA decay (Figure 16B). However, in contrast to the *gfat-1* (*dh784*) gain-of-function worm which shows highly elevated UDP-GlcNAc levels, the levels in the two *F59B2.3* K.O. strains were unchanged compared to WT animals (Figure 16C). In accordance with these data, the deletion of *F59B2.3* had no effect on TM resistance compared to the highly resistant GFAT-1 OE mutant (*gfat-1P::gfat1*) (Figure 16D). Taken together, the K.O. of the putative AMDHD2 homologue *F59B2.3* in *C. elegans* has no effect on HBP activation. This might be due to a different function of AMDHD2 in the nematode compared to the mammalian system.

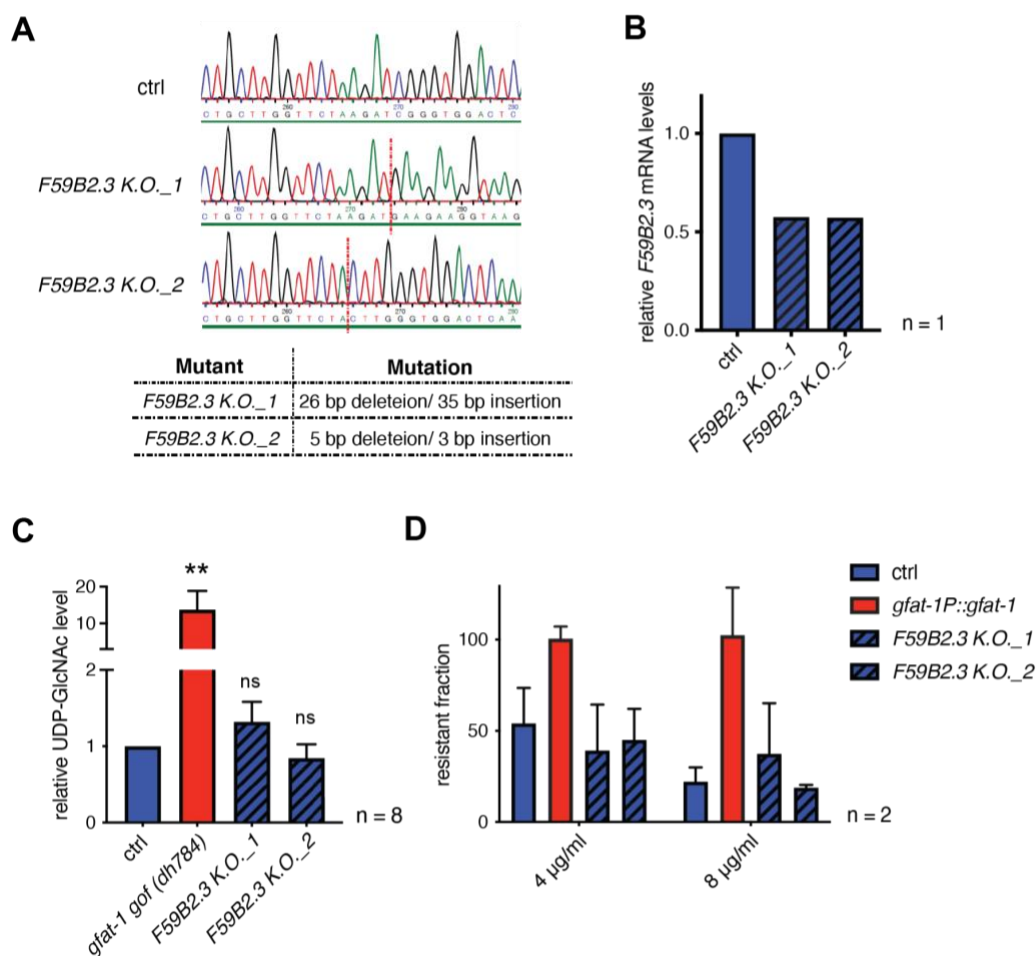


Figure 16: Loss of the *C. elegans* AMDHD2 homologue *F59B2.3* has no effect on HBP activity. (A) Sequencing results of the *F59B2.3* locus of control worms compared to two *F59B2.3* K.O. lines. Red dotted line indicates start of the frame shift. Exact details of the mutation in the respective K.O. line are described in the table below. (B) Relative *F59B2.3* mRNA levels in WT and *F59B2.3* K.O. worms measured by qPCR (n=1). (C) IC-MS analysis of relative UDP-GlcNAc levels of WT, *gfat-1* gain-of-function (GOF) (*dh784*), and *F59B2.3* K.O. worms (mean + SEM, n=8, ** p<0.01, One-way ANOVA Dunnett post-test). (D) Tunicamycin developmental assay with WT, GFAT-1 overexpressing (OE) line *gfat-1P::gfat1*, and *F59B2.3* K.O. animals. Relative fraction of eggs developed to L4 or adult stage after 4 days on plates containing 4 and 8 µg/ml tunicamycin (values were normalized to developed worms on control plates with DMSO) (mean + SD, n=2).

2.2.2.2 Loss of AMDHD2 in *M. musculus* leads to embryonic lethality

Since loss of the AMDHD2 homologue *F59B2.3* in *C. elegans* did not show any effect on HBP activity, in a next step we wanted to investigate the role of AMDHD2 in a higher organism. To better understand the physiological consequences of HBP activation through AMDHD2 disruption in a mammalian *in vivo* system, we targeted the *Amdhd2* locus by CRISPR/Cas9 to generate a K.O. mouse. Since our structural analysis of AMDHD2 showed that the identified mutations, which cluster in exon 4-5, are mainly located in the active site of the enzyme, we targeted this area to impair the enzyme's

function (Figure 10D, Figure 15C). In total we were able to generate four independent mouse founder lines (line 1-4) with different deletions in the *Amdhd2* locus (Figure 17A, B). Successful deletion within the *Amdhd2* gene could be confirmed by genotyping PCR (Figure 17C). The *Amdhd2* mutation was distributed in mendelian ratios in the offspring as we could show by prenatal dissection (E7-8) of embryos followed by genotyping PCR (Figure 17D). Despite this fact, no viable homozygous *Amdhd2* K.O. pups could be weaned, indicating an essential function of AMDHD2 during development (Figure 17D). In case of heterozygous animals however, no obvious phenotype could be observed up to the age of 1 year, which suggests that mutations in *Amdhd2* underly a recessive nature. Taken together, we demonstrated that homozygous mutations within *Amdhd2* most likely result in embryonic lethality, thus elucidating AMDHD2 as a novel regulator, essential for mammalian embryonic development. However, these are only preliminary data and further analysis needs to be done to investigate when exactly lethality occurs and which tissues are affected mostly.

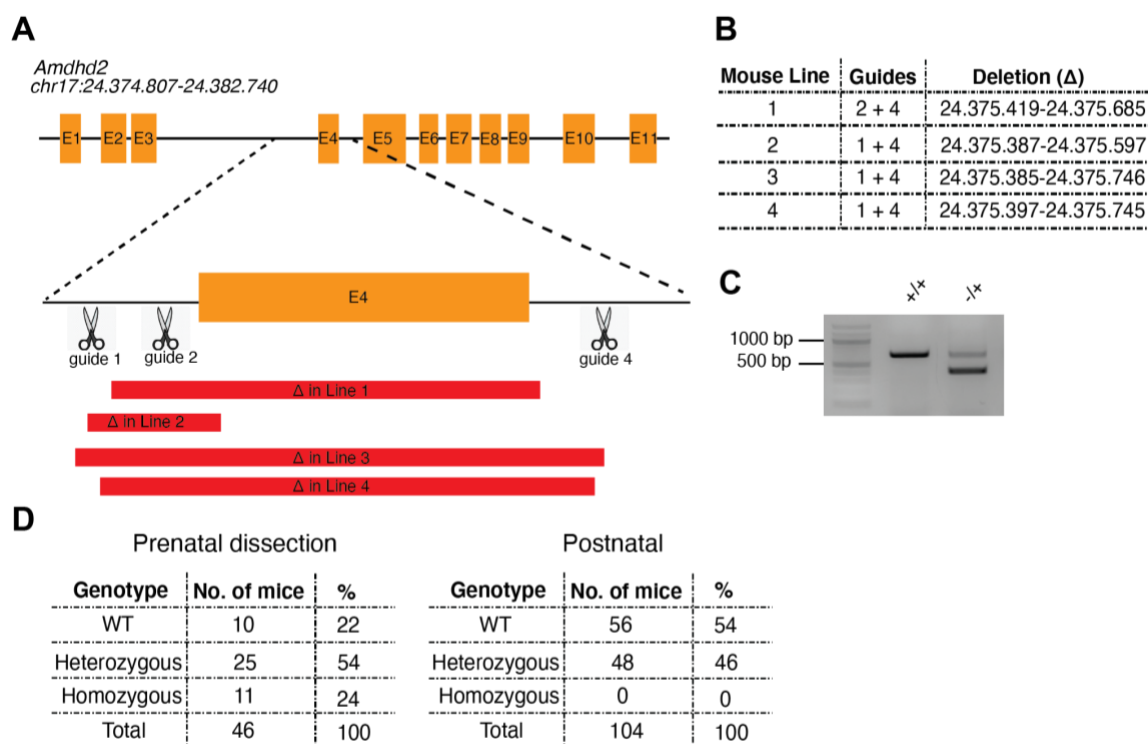


Figure 17: Loss of AMDHD2 in *M. musculus* leads to embryonic lethality. (A) Schematic representation of the CRISPR/Cas9-targeted exon 4 of the mouse *Amdhd2* locus. Deletions in founder lines 1-4 are indicated in red. (B) Table listing used guide combinations and deletion details of the respective AMDHD2 K.O. founder lines. (C) Representative genotyping results of heterozygous AMDHD2 K.O. mice. The WT PCR product is 675 bp and the *Amdhd2* K.O. allele shows a size of 300 bp (mouse line 1). (D) Genotyping results for the AMDHD2 deletion in dissected (E7-8) embryos and weaned mice.

2.2.2.3 Loss of AMDHD2 in N2a cells leads to HBP activation

Given the putative essential role in embryonic development and the relevance on HBP regulation in the AN3-12 mESC line used for the screen, we next wanted to further explore whether the loss of AMDHD2 can affect other murine cell lines. In a previous screen in the nematode *C. elegans*, it was shown that activation of the HBP through the G451E gain-of-function substitution in GFAT1 has beneficial effects on protein homeostasis (Denzel et al. 2014). In accordance, GlcNAc treatment as well as introducing the same mutation in the highly conserved GFAT1 of mouse neuroblastoma Neuro2a (N2a) cells, resulted in TM resistance and improved protein homeostasis mediated by elevation of UDP-GlcNAc levels (Ruegenberg et al. 2020b; Horn et al. 2020). Therefore, N2a cells are known to be a good cellular model with regard to manipulating and analyzing HBP activity. Based on this knowledge, we asked if the loss of AMDHD2 in the N2a cell line is also sufficient to increase HBP flux. To this end, we engineered an AMDHD2 K.O. in the N2a cell line using the CRISPR/Cas9 strategy. N2a cells have a complex karyotype varying between 59 and 193 chromosomes in isogenic clones, which requires the genomic editing of several *Amdhd2* copies (www.ATCC.org). Nevertheless, genotyping PCR as well as Sanger sequencing revealed a deletion within the *Amdhd2* locus, while no remaining WT allele could be observed (Figure 18A, B). Additional WB analysis confirmed the successful K.O. of AMDHD2 (Figure 18C). In line with previous findings, also in the N2a cell line the depletion of AMDHD2 resulted in significant TM resistance compared to WT cells (Figure 18D). In contrast to AN3-12 cells though, measurement of UDP-GlcNAc levels revealed only a mild but no significant elevation upon loss of AMDHD2 in N2a cells (Figure 18E). This suggests that AMDHD2 is constitutively active in AN3-12 cells, while catalysis of the reverse flux of the HBP by AMDHD2 seems to be negligible in N2a cells. In general, WT N2a cells showed 3,5-fold reduced basal UDP-GlcNAc levels compared to control AN3-12 mESCs (Figure 18E). In conclusion, the K.O. of AMDHD2 in N2a cells was sufficient to mediate TM resistance although UDP-GlcNAc levels were only slightly elevated. Together with the reduced basal UDP-GlcNAc levels in N2a cells compared to AN3-12 cells, these results suggest a different mechanism of HBP regulation in these two tested cell lines.

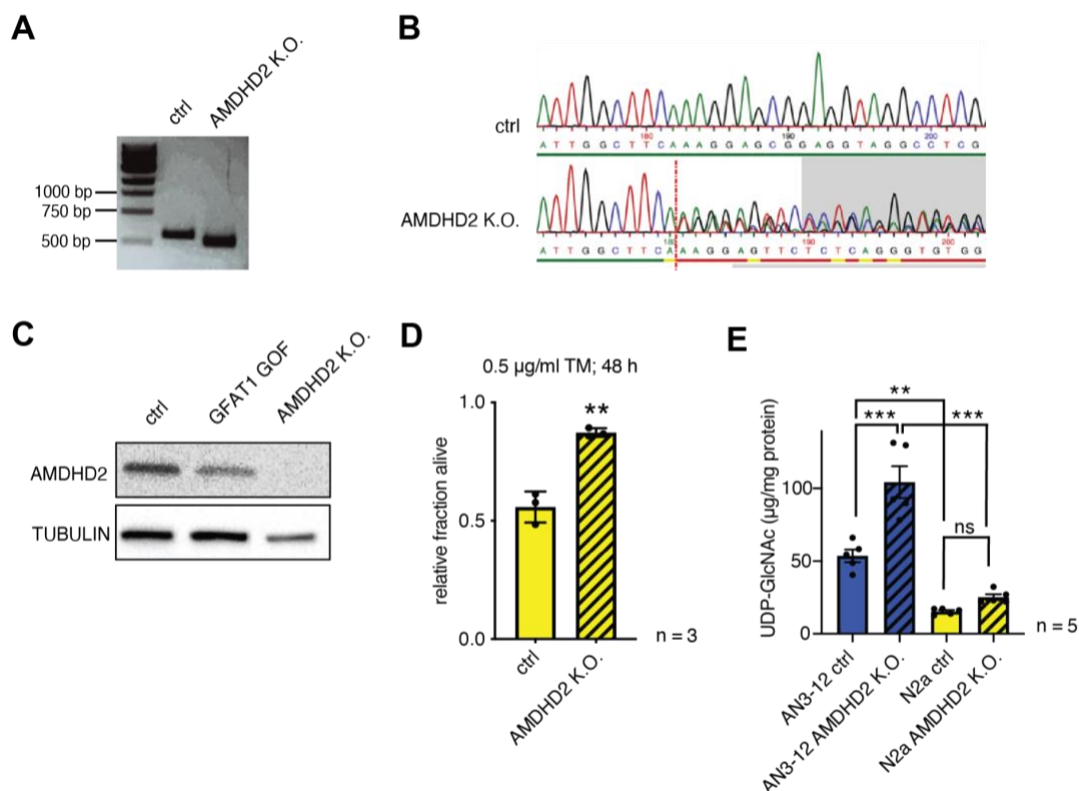


Figure 18: Loss of AMDHD2 in N2a cells leads to hexosamine pathway activation. (A) Representative genotyping results of AMDHD2 K.O. N2a cell line. The WT PCR product is 582 bp while the *Amdhd2* K.O. allele is around 500 bp. **(B)** Sequencing results of the *Amdhd2* locus of control N2a cells compared to the AMDHD2 K.O. line. Red dotted line indicates start region of the frame shift. **(C)** Representative Western blot analysis of CRISPR/Cas9-generated AMDHD2 K.O. N2a cells compared to WT (ctrl) and GFAT1 gain-of-function (GOF) cells. **(D)** Cell viability (XTT assay) of WT and AMDHD2 K.O. N2a cells treated with 0.5 µg/ml TM for 48h (mean ± SEM, n=3, ** p<0.01, unpaired t-test). **(E)** IC-MS analysis of UDP-GlcNAc levels in WT (ctrl) and AMDHD2 K.O. AN3-12 mESCs and N2a cells (mean ± SEM, n=5, ** p<0.01, *** p<0.001, ns = not significant, One-way ANOVA Tukey post-test).

2.3 Cell type-specific regulation of the HBP

Besides *Gfat1* also its paralog *Gfat2* can regulate metabolite entry into the HBP (Oki et al. 1999). The two paralogs exhibit 75% identity on an amino acid level and are located on different chromosomes (Zhou et al. 1995). While *Gfat1* shows ubiquitous expression, *Gfat2* is reported to be predominantly expressed in the central nervous system (Oki et al. 1999). Surprisingly, despite a high level of saturation we were not able to detect any mutation in one of the HBP's rate limiting enzymes GFAT1 or GFAT2 in the performed TM resistance screen (Figure 10C). This raises the question how the loss of AMDHD2 alone can lead to such drastic increases of UDP-GlcNAc levels although GFAT underlies a strict regulation via product feedback-inhibition (Ruegenberg et al. 2020b). Moreover, the AMDHD2 K.O. in AN3-12 cells showed a stronger impact on UDP-GlcNAc levels than in

N2a cells, which in general had lower HBP product concentrations (Figure 18E). Given the different gene expression of HBP enzymes together with a distinct functional importance of AMDHD2 across cell lines, this data prompted us to focus our efforts on the deeper analysis of HBP regulation in a cell type-specific manner.

2.3.1 GFAT2 controls metabolite entry into the HBP in mESCs

Since we assume the possibility of a cell type-specific HBP regulation, we compared different mechanism of HBP activation in AN3-12 cells and N2a cells. Supplementation of GlcNAc can elevate UDP-GlcNAc levels by entering the HBP downstream of GFAT upon NAGK-mediated phosphorylation (Weihofen et al. 2006). Thereby, GlcNAc treatment can bypass GFAT feedback regulation (Figure 2). Treatment of cells with 10 mM GlcNAc for 24h indeed resulted in a significant upregulation of UDP-GlcNAc levels in N2a cells, while in AN3-12 cells the treatment did not change HBP product levels compared to an untreated control (Figure 19A, B). In addition, we engineered AN3-12 cells carrying the previously identified GFAT1 G451E gain-of-function substitution. While we could reproduce the significantly elevated HBP flux in N2a cells with the G451E mutation (Ruegenberg et al. 2020b; Horn et al. 2020), the same mutation did not influence UDP-GlcNAc levels in AN3-12 cells. *Vice versa*, consistent with the data shown previously, the K.O. of AMDHD2 increased the HBP activity significantly only in AN3-12 cells but not in N2a cells (Figure 18E, Figure 19A, B).

Surprisingly, even the complete loss of GFAT1 in AN3-12 cells was not sufficient to alter UDP-GlcNAc levels (Figure 19C). It is known that *Gfat1* is ubiquitously expressed across cell types, while its paralog *Gfat2* is predominantly expressed in the central nervous system (Oki et al. 1999). Since even a full K.O. of GFAT1 in AN3-12 cells could not impact UDP-GlcNAc levels compared to control cells, we hypothesized that in this cell line GFAT2 may control the flux in the HBP. To test the possibility that in AN3-12 cells GFAT2 may be favored, we measured and compared mRNA levels of *Gfat1* and *Gfat2* in WT cells. In line with our hypothesis, *Gfat2* was 6-fold higher expressed than *Gfat1* (Figure 19D). In a next step, we performed WB analysis using defined amounts of pure purified human GFAT as standard to compare the absolute amount of intracellular GFAT levels. Besides N2a cells and AN3-12 mESCs, we tested E14 cells as a second mESC line as well as muscle precursor C2C12 cells (myoblasts). In AN3-12 mESCs GFAT2 was found abundantly expressed, while GFAT1 was hardly detected (Figure 19E). E14 mESCs showed a similar expression with predominant GFAT2 and low GFAT1 abundance, indicating a

mESC-specific expression pattern of GFAT1 and GFAT2. A contrary effect was observed in the more differentiated N2a and C2C12 cells. Both cell lines showed predominant GFAT1 expression while GFAT2 was virtually undetectable (Figure 19E). Concluding, these data suggest a specific HBP configuration in mESCs characterized by a high GFAT2:GFAT1 ratio, while more differentiated cells rather rely on GFAT1 than GFAT2. Moreover, AMDHD2 seems to have a specific role in cells with GFAT2 as main driver for metabolite entry into the HBP.

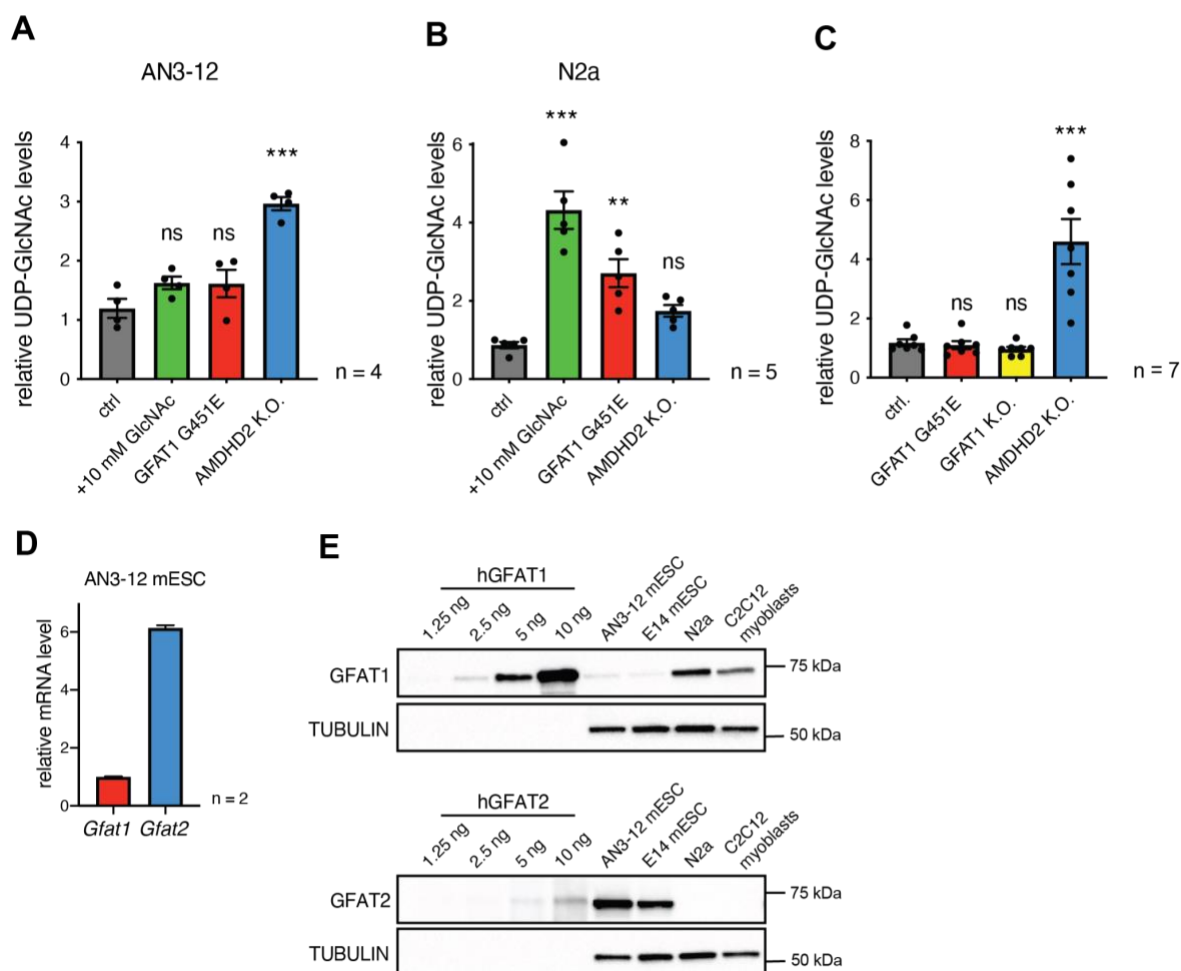


Figure 19: GFAT2 controls metabolite entry into the hexosamine pathway in mESCs. (A) IC-MS analysis of relative UDP-GlcNAc levels of WT (ctrl) cells, WT cells treated with 10 mM GlcNAc for 24h, GFAT1 G451E and AMDHD2 K.O. AN3-12 cells. (mean \pm SEM, n=4, *** p<0.001, ns = not significant, One-way ANOVA Dunnett post-test) **(B)** IC-MS analysis of relative UDP-GlcNAc levels of WT cells, WT (ctrl) cells treated with 10 mM GlcNAc for 24h, GFAT1 G451E and AMDHD2 K.O. N2a cells. (mean \pm SEM, n=5, ** p<0.01, *** p<0.001, ns = not significant, One-way ANOVA Dunnett post-test) **(C)** IC-MS analysis of relative UDP-GlcNAc levels of WT (ctrl), GFAT1 G451E, GFAT1 K.O. and AMDHD2 K.O. AN3-12 cells. (mean \pm SEM, n=7, *** p<0.001, ns = not significant, One-way ANOVA Dunnett post-test) **(D)** Relative *Gfat1* and *Gfat2* mRNA levels (qPCR) in WT AN3-12 cells (mean + SEM, n=2). **(E)** Representative Western blot analysis of indicated amounts of purified human GFAT1 and GFAT2 protein as standards to compare GFAT abundance in cell lysates of indicated cell lines.

2.3.2 GFAT2 has a lower sensitivity to UDP-GlcNAc feedback inhibition compared to GFAT1

To better understand why mESCs rather rely on GFAT2, while other cells predominantly use GFAT1, we next focused on the regulation of the two paralogs. Previously published data indicate that under basal conditions GFAT1 underlies constant UDP-GlcNAc inhibition, sufficient to fully suppress its activity (Ruegenberg et al. 2020b). Since mESCs mainly depend on GFAT2 and simultaneously show a specialized metabolic profile, we hypothesized that the kinetic properties and the feedback regulation differ in GFAT2. To this end, we generated recombinant human GFAT1 and GFAT2 tagged with an internal His₆ tag and characterized the two paralogs via activity assays. Kinetic measurements with either L-glutamine (L-Gln) or fructose-6-phosphate (Frc6P) as substrates revealed different affinities of GFAT2 compared to GFAT1. GFAT2 showed a significantly lower affinity for Frc6P, but higher affinity to L-Gln as substrate compared to GFAT1 (Figure 20A, B; Table 1). This opposite effect in substrate affinity of the two enzymes may hint to an adaptation for differences in metabolite availability. In addition, an UDP-GlcNAc dose-response assay unraveled a significant higher IC₅₀ value for GFAT2 (367.3 -43.6/+49,5 μ M) compared to GFAT1 (57.0 -8.3/+9.7 μ M) (Figure 20C, Table 2). Since higher product concentrations are required to inhibit GFAT2 to a similar extent as GFAT1, we conclude that UDP-GlcNAc inhibition is weaker in GFAT2 compared to GFAT1, allowing higher cellular UDP-GlcNAc levels in cells predominantly expressing GFAT2. This differences in feedback regulation as well as the distinct substrate affinities of the two enzymes may reflect adaptations to different cellular metabolite concentrations and therefore could explain different tissue distributions.

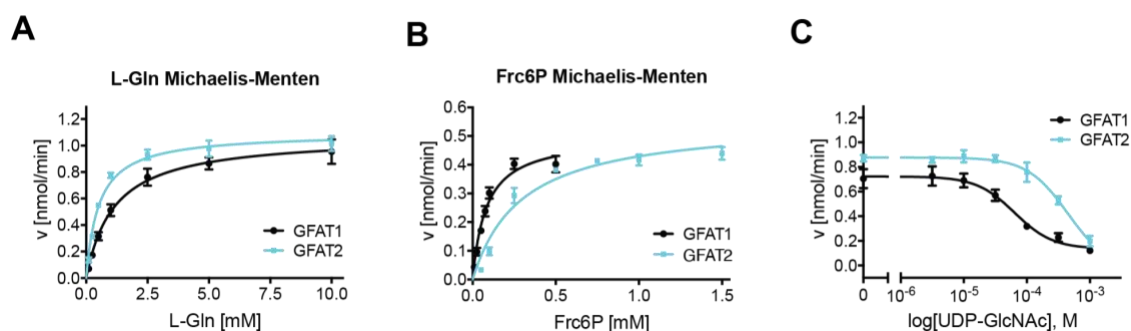


Figure 20: GFAT2 has a lower sensitivity to UDP-GlcNAc feedback inhibition than GFAT1. (A) L-Gln kinetic of WT human GFAT1 (black circle) and WT human GFAT2 (teal square) (mean \pm SEM, hGFAT1 n=5, hGFAT2 n=4). (B) Frc6P kinetic of WT hGFAT1 (black circle) and WT hGFAT2 (teal square) (mean \pm SEM, hGFAT1 n=5, hGFAT2 n=8). (C) Representative UDP-GlcNAc dose-response assay with hGFAT1 (black circle) and hGFAT2 (teal square) (mean \pm SD, n=3). (Data was already described in: Ruegenberg, 2020a).

Table 1: Kinetic measurements of human GFAT1 and GFAT2 enzyme.

	L-Gln production			D-GlcN6P production		
	K_m L-Gln [mM]	k_{cat} [s ⁻¹]	k_{cat}/K_m [mM]	K_m Frc6P [mM]	k_{cat} [s ⁻¹]	k_{cat}/K_m [mM]
GFAT1	1.1 ± 0.19	3.6 ± 0.18	3.3	0.08 ± 0.01	1.7 ± 0.09	21.3
GFAT2	0.5 ± 0.06	3.7 ± 0.10	7.4	0.29 ± 0.05	1.8 ± 0.09	6.2
Unpaired t-test	** p=0.005			** p=0.0027		

Table 2: UDP-GlcNAc inhibition of human GFAT1 and GFAT2 enzyme.

	UDP-GlcNAc inhibition
	IC ₅₀ [μM]
GFAT1	57.0 -8.3/+9.7
GFAT2	367.3 -43.6/+49.5
Unpaired t-test	*** p=0.0002

2.3.3 AMDHD2 in tandem with GFAT2 result in elevated HBP flux in mESCs

To further examine the existence of a potential ESC-specific HBP regulation, we next focused on AMDHD2 levels in mESCs and compared them to cells mainly expressing GFAT1. Preliminary qPCR data comparing *Amdhd2* mRNA levels in AN3-12, N2a, and C2C12 myoblasts did not show any differences on a transcriptional level (Figure 21A). However, similarly to the GFAT2 expression pattern, AMDHD2 protein abundance was higher in AN3-12 and E14 mESCs than in N2a and C2C12 cells (Figure 21B).

This result suggests that AMDHD2 plays a more substantial role for HBP regulation when GFAT2 controls the flux in the pathway instead of the more common GFAT1. Next, we were interested in how this putative specific configuration of enzymes is reflected in HBP's product levels. Comparing UDP-GlcNAc levels of the four different cell lines unraveled significantly higher concentrations in AN3-12 mESCs compared to N2a cells and C2C12 myoblasts (Figure 21C). E14 mESCs showed high UDP-GlcNAc levels comparable to those in AN3-12 mESCs, suggesting elevated HBP flux in mESCs. The elevated product levels in mESCs are in accordance with the weaker feedback inhibition of the predominantly expressed GFAT2 enzyme in these cells (Figure 20C). UDP-GlcNAc acts as the precursor for different types of glycosylation including O-GlcNAcylation, a post-translational-modification (PTM) where a single GlcNAc moiety is added to Thr/Ser residues (Hart 1997). To test if also downstream effects of the HBP are influenced by the differences in UDP-GlcNAc concentrations, we measured total O-GlcNAcylation levels in

the distinct cell lines by performing WB analysis with an antibody (RL2) specifically recognizing this PTM. Consistent with elevated UDP-GlcNAc levels, also the abundance of O-GlcNAc-modified proteins was higher in AN3-12 and E14 mESCs compared to the N2a and C2C12 cell line (Figure 21D). Overall, these data demonstrate, likewise as for GFAT2, a higher AMDHD2 abundance in the tested mESC lines compared to the more differentiated N2a and C2C12 cells. This mESC-specific co-expression of GFAT2 and AMDHD2 not only elevated HBP flux as reflected by increased UDP-GlcNAc levels, but is also sufficient to influence O-GlcNAcylation downstream of it.

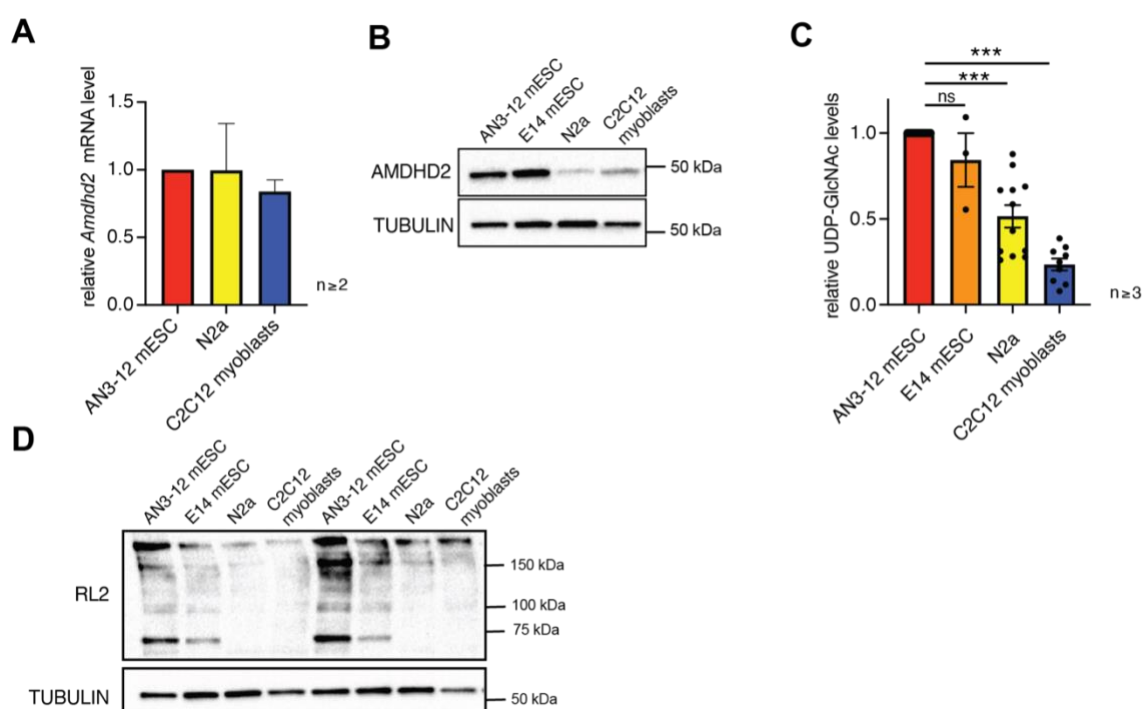


Figure 21: GFAT2 in tandem with AMDHD2 result in elevated hexosamine pathway flux in mESCs. (A) Relative *Amdhd2* mRNA level (qPCR) in indicated cell lines. Levels are normalized to those in AN3-12 mESCs (mean + SEM, n ≥ 2). (B) Representative Western blot analysis of AMDHD2 in indicated cell lines. (C) Relative UDP-GlcNAc levels in indicated cell lines measured by IC-MS. Levels are normalized to those in AN3-12 mESCs (mean ± SEM, n ≥ 3, *** p < 0.001, ns = not significant, One-way ANOVA Dunnett post-test) (D) Representative Western blot analysis of O-GlcNAc-modified proteins (RL2) in the indicated cell lines.

2.3.4 Differentiation of human ESCs reduces the GFAT2:GFAT1 ratio

Since our data indicated a mESC-specific expression of GFAT2 while more differentiated cells mainly rely on GFAT1, we were interested if differentiation of ESCs is sufficient to induce a switch in expression of the two paralogs. Indeed, multiple lines of evidence suggest a decreased GFAT2:GFAT1 ratio upon differentiation. By performing *in silico*

analysis of recently published datasets from collaborating laboratories (Laboratory of Dr. David Vilchez and Laboratory of Dr. Leo Kurian), we were able to observe a differentiation-induced exchange of GFAT2 by GFAT1 (Figure 22A, B). Relative GFAT2 mRNA and protein levels decreased during differentiation of human ESC into the cardiac lineage (Frank et al. 2019; Bartsch et al. 2021) and neuronal differentiation of human ESCs (Saez et al. 2018). Together, the results of these two independent studies not only strengthen our hypothesis of a switch in HBP's enzymatic configuration upon differentiation but also suggest a conserved mechanism in human ESCs.

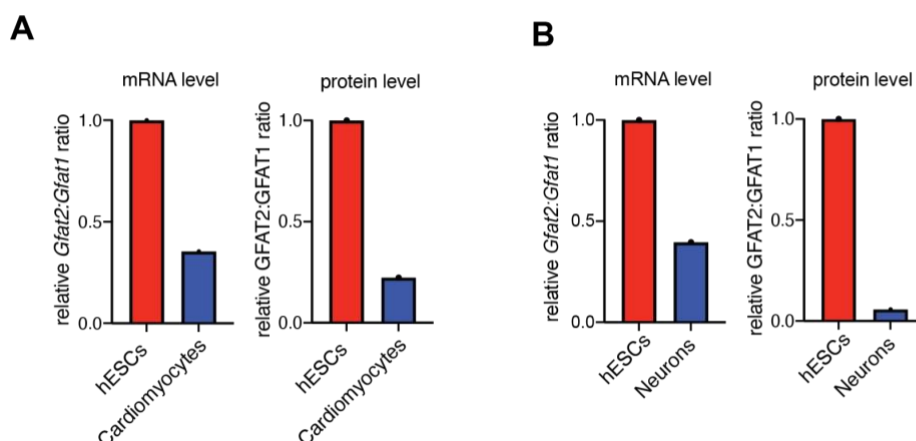


Figure 22: Differentiation of human ESCs results in a decreased GFAT2:GFAT1 ratio. (A) Relative *Gfat2:Gfat1* mRNA and GFAT2:GFAT1 protein ratios in human ESCs and upon differentiation into cardiomyocytes (data obtained from: Frank et al. 2019, Bartsch et al. 2021). **(B)** Relative *Gfat2:Gfat1* mRNA and GFAT2:GFAT1 protein ratios in human ESCs and upon differentiation into neurons (data obtained from: Saez et al. 2018).

2.3.5 Partial differentiation of AN3-12 cells by LIF removal reduces GFAT2 abundance

Given the published datasets confirming our hypothesis of an ESC-specific HBP regulation driven by GFAT2 and a differentiation-induced exchange by GFAT1, we next wanted to test AMDHD2 expression upon differentiation and if enzymatic rewiring can affect UDP-GlcNAc levels. Our previous data are based on the more differentiated N2a and C2C12 cell line as comparison to the mESCs, which do not serve as an optimal control. Therefore, we next aimed to perform partial differentiation of AN3-12 cells to have an appropriate cell model for comparison. For this purpose, we removed leukemia inhibitory factor (LIF) from the medium, which is known to initiate stem cell differentiation (Hocke, Cui, and Fey 1995). LIF depletion for five days resulted in partial differentiation of AN3-12 cells as indicated by a significant decrease of the stem cell markers *Nanog* and

Klf4 (Figure 23A). In fact, not only *Gfat2* mRNA but also GFAT2 protein levels decreased significantly upon LIF removal (Figure 23B, C). Partial differentiation by LIF removal however, was not sufficient to induce significant changes in GFAT1 and AMDHD2 mRNA levels or protein abundance (Figure 23D, E). Further analysis of the HBP activity by measuring UDP-GlcNAc levels also showed no alteration of LIF depleted cells compared to control cells cultured in LIF-containing medium (Figure 23F).

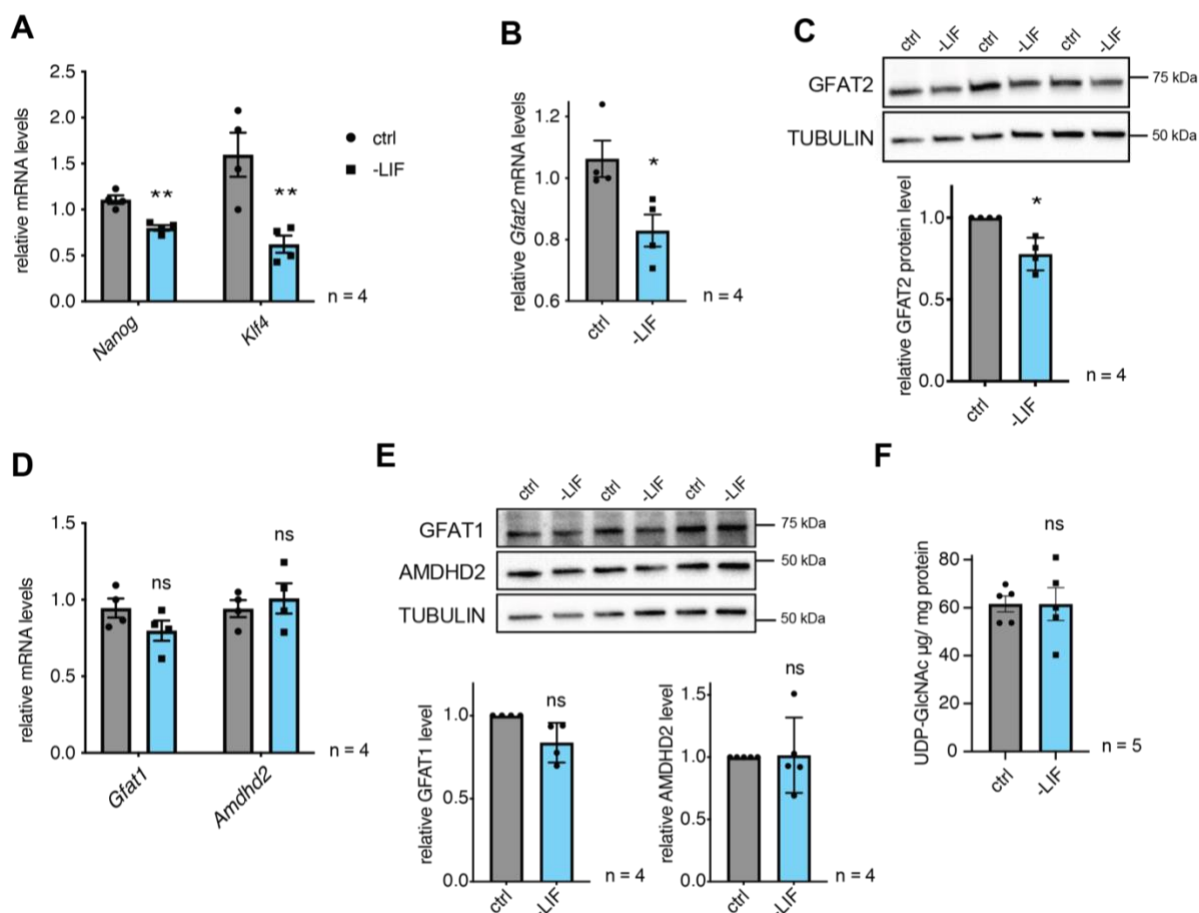


Figure 23: Partial differentiation of AN3-12 cells by LIF removal reduces GFAT2 abundance. (A) Relative *Nanog* and *Klf4* mRNA level (qPCR) of WT AN3-12 cells (ctrl) and upon partial differentiation by 5 days of LIF removal (-LIF) (SEM \pm n=4, ** p<0.01, ns = not significant, unpaired t-test). (B) Relative *Gfat2* mRNA level (qPCR) in WT AN3-12 cells (ctrl) and upon partial differentiation by 5 days of LIF removal (-LIF) (mean \pm SEM, n=4, * p<0.05, unpaired t-test). (C) Western blot analysis and quantification (mean \pm SD, n=4, * p<0.05, unpaired t-test) of GFAT2 in WT AN3-12 cells (ctrl) and upon partial differentiation by 5 days of LIF removal (-LIF). (D) Relative *Gfat1* and *Amdhd2* mRNA-level (qPCR) of WT AN3-12 cells (ctrl) and upon partial differentiation by 5 days of LIF removal (-LIF) (mean \pm SEM, n=4, ns = not significant, unpaired t-test). (E) Western blot analysis of GFAT1 and AMDHD2 in WT AN3-12 cells (ctrl) and upon partial differentiation by 5 days of LIF removal (-LIF), including quantification relative to tubulin and the WT cells (ctrl) (mean \pm SD, n=4, ns = not significant, unpaired t-test). (F) IC-MS analysis of UDP-GlcNAc levels in WT AN3-12 mESCs (ctrl) and upon partial differentiation by 5 days of LIF removal (-LIF) (mean \pm SEM, n=5, ns = not significant, unpaired t-test).

Considering all data, the removal of LIF for 5 days successfully initiates partial differentiation of AN3-12 cells resulting in a drop of GFAT2 levels. In contrast, this approach was not sufficient to affect GFAT1 and AMDHD2 levels or ultimately UDP-GlcNAc concentrations.

2.3.6 Differentiation of AN3-12 cells into neural progenitor cells (NPCs) is delayed upon AMDHD2 K.O.

Because the partial differentiation by LIF removal in AN3-12 cells was not sufficient to show an impact on AMDHD2 levels, in the next stage we performed further differentiation into neural progenitor cells (NPCs). NPCs were generated using the hanging drop method for embryoid body formation as described previously (Elling et al. 2017). In fact, qPCR analysis confirmed a decrease of the stem cell markers *Sox2*, *Oct4*, and *Nanog* in the generated NPCs compared to undifferentiated AN3-12 mESCs (Figure 24A). Upregulation of *Nestin*, a marker for early neural differentiation, in NPCs furthermore indicated a successful differentiation into the neural lineage. Since we assumed based on the previously shown data that AMDHD2 is of special importance in ESCs when co-expressed with GFAT2, next we compared the differentiation potential of WT and AMDHD2 K.O. AN3-12 cells. *Per se*, AMDHD2 K.O. cells were able to differentiate into NPCs as indicated by increased expression of *Nestin* mRNA although the mutant did not reach the same level of increase as in WT cells (Figure 24B).

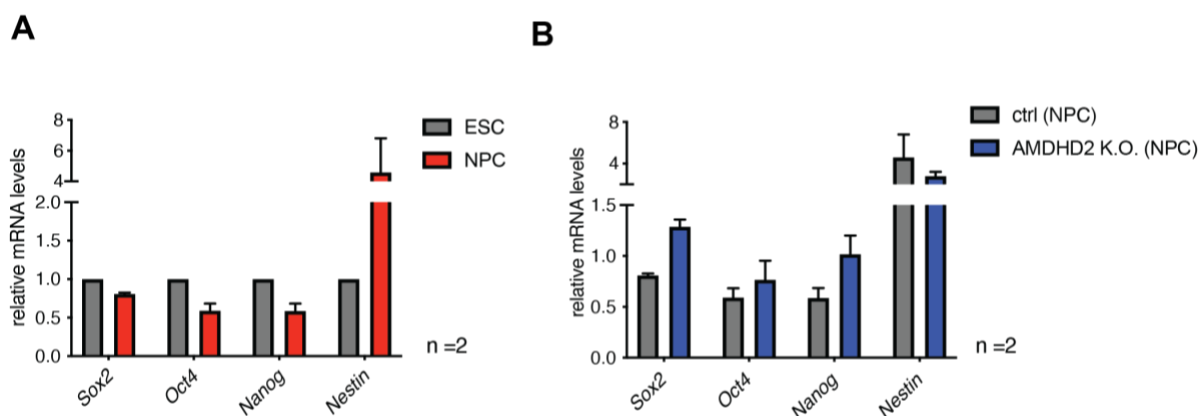


Figure 24: Differentiation of AN3-12 cells into NPCs is delayed upon AMDHD2 K.O. (A) Relative mRNA level of stem cell (*Sox2*, *Oct4*, *Nanog*) and neural (*Nestin*) marker genes in undifferentiated WT AN3-12 cells (ESCs) and upon differentiation into neural progenitor cells (NPCs) (mean + SEM, n=2). **(B)** Relative mRNA level of stem cell (*Sox2*, *Oct4*, *Nanog*) and neural (*Nestin*) marker genes in WT AN3-12 cells (ctrl) compared to AMDHD2 K.O. cells upon differentiation into neural progenitor cells (NPCs) (mean + SEM, n=2).

In addition, when we compared stem cell markers of WT and AMDHD2 K.O. NPCs upon differentiation, we observed that the levels remained higher in the mutant (Figure 24B). This delayed drop of stem cell markers in parallel to decreased *Nestin* levels could hint to a reduced differentiation potential upon AMDHD2 deletion. However, for statistical analysis further experiments have to be performed.

2.3.7 Loss of AMDHD2 increases mESCs maintenance under basal conditions

Due to the putative impaired differentiation capacity upon AMDHD2 deletion in AN3-12 mESCs (Figure 24B), we next focused on the investigation of the pluripotency potential in the same cell line. Ample evidence exists that increased levels of O-GlcNAc modifications (e.g., due to OGA inhibition or by GlcNAc supplementation) can reduce ESC differentiation (Parween et al. 2017; Speakman et al. 2014). *Vice versa*, it was previously shown that a decrease in O-GlcNAcylation upon an OGT knock down results in diminished self-renewal of ESCs and reduced reprogramming of somatic cells into iPSCs (Jang et al. 2012; Andres et al. 2017). Given the connection of O-GlcNAcylation and pluripotency in ESCs, and the observation of increased UDP-GlcNAc levels in the AMDHD2 K.O. cells, we hypothesized that the AMDHD2 absence may result in altered stem cell maintenance. To assess this assumption, we first measured if the elevated UDP-GlcNAc concentration in AMDHD2 K.O. AN3-12 cells is sufficient to upregulate levels of O-GlcNAc-modified proteins. By performing a WB analysis using the O-GlcNAc-specific RL2 antibody, we confirmed an increase of O-GlcNAc modifications in WT cells upon treatment with the potent OGA inhibitor GlcNAcstatin G (Dorfmueller et al. 2010), in a dose-dependent manner (Figure 25A). However, we were not able to measure significant differences with regard to O-GlcNAc levels upon loss of AMDHD2 compared to control WT cells (Figure 25B, C).

Nevertheless, in a next step, we performed a colony formation assay (CFA) using WT and AMDHD2 K.O. AN3-12 mESCs to assess differences in stem cell maintenance. Cells cultured in medium without LIF were forced to partially differentiate and served as a negative control for stem cell maintenance. Since we observed higher O-GlcNAc levels in the tested mESCs compared to more differentiated cells, we tested if differentiation is sufficient to alter O-GlcNAc levels (Figure 21D). WT cells were collected for WB analysis to measure differences in O-GlcNAc levels upon LIF removal. In line with an unchanged HBP configuration, LIF removal for 5 days was not sufficient to induce measurable differences in O-GlcNAcylation of proteins (Figure 23E; Figure 25D, E). Tracking of differences in stem cell self-renewal capacity between WT and AMDHD2 K.O. cells was

performed by determination of alkaline phosphatase activity, a universal pluripotency marker (Singh et al. 2012). Upon alkaline phosphatase staining, 100 randomly chosen colonies of each condition were analyzed and classified either into “stem cell”, “intermediate cell” or “differentiated cell” according to the staining intensity (Figure 25F, G). Since only a really small portion of cells showed complete differentiation even upon LIF removal (less than 10%), the latter group was neglected for further analysis. Despite the similar O-GlcNAc levels, alkaline phosphatase staining of colonies revealed a decrease in the stem cell fraction along with an increase in the number of intermediate cells upon LIF depletion in WT as well as AMDHD2 K.O. cells, although no statistical significance was reached (Figure 25H, I). From these data, a successful partial differentiation as well as specific staining of stem cells can be concluded. Interestingly, AMDHD2 K.O. cells showed a significantly higher percentage of stem cells and a reduced number of intermediate cells under basal conditions compared to control mESCs (Figure 25H, I). This finding, in line with the delayed differentiation into NPCs (Figure 24B), suggests that the deletion of AMDHD2 may lead to increased stem cell maintenance. However, the general size of colonies of AMDHD2 K.O. cells was smaller compared to those of WT cells, indicating reduced cell proliferation (Figure 25F). The reduced cell number should be taken into account in future experiments. Overall, these data suggest that loss of AMDHD2 can impact stem cell maintenance under basal conditions.

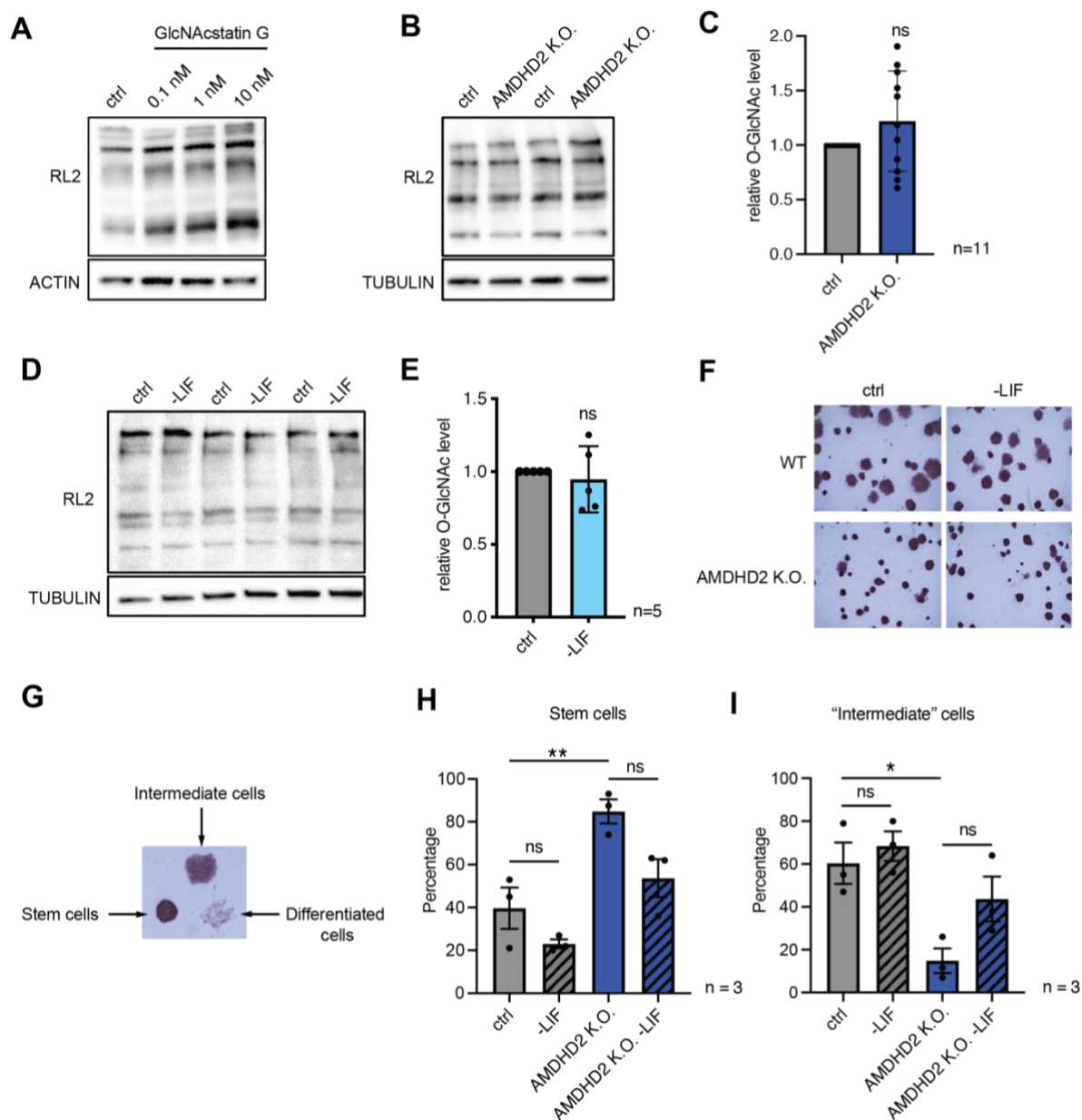


Figure 25: The loss of AMDHD2 increases stem cell maintenance under basal conditions. (A) Representative Western blot (WB) analysis of O-GlcNAcylated proteins (RL2) in WT AN3-12 cells treated with 0 (ctrl), 0.1, 1 and 10 nM GlcNAcstatin G for 24h. (B) Representative WB analysis of O-GlcNAcylated proteins (RL2) in WT AN3-12 (ctrl) compared to AMDHD2 K.O. cells. (C) Quantification of WB as shown in (B) (mean \pm SD, n=11, ns = not significant, unpaired t-test). (D) Representative WB analysis of O-GlcNAcylated proteins (RL2) in WT AN3-12 (ctrl) and upon partial differentiation by 5 days of LIF removal (-LIF). (E) Quantification of WB as shown in (D) (mean \pm SD, n=5, ns = not significant, unpaired t-test). (F) Representative colony formation assay (CFA) of WT and AMDHD2 K.O. AN3-12 cells followed by alkaline phosphatase staining after 5 days. Partial differentiation by 5 days of LIF removal (-LIF) served as positive control for differentiation. (G) Representative image of the different stages of differentiation upon CFA and alkaline phosphatase staining. (H) Relative fraction of colonies classified as "stem cells" in WT (ctrl) and AMDHD2 K.O. AN3-12 cells cultured in standard medium and upon 5 days of LIF removal (-LIF) (mean \pm SEM, n=3, ** p<0.01, ns = not significant, One-way ANOVA Tukey post-test). (I) Relative fraction of colonies classified as "intermediate cells" in WT (ctrl) and AMDHD2 K.O. AN3-12 cells cultured in standard medium and upon 5 days of LIF removal (-LIF) (mean \pm SEM, n=3, * p<0.05, ns = not significant, One-way ANOVA Tukey post-test).

3 Discussion

In this study we aimed to identify novel regulators of the hexosamine biosynthetic pathway (HBP) and thus, thereby new targets for manipulation of the concentration of its end products UDP-GlcNAc and UDP-GalNAc. These acetylated amino sugars serve as precursor molecules for a wide range of glycosylation events and PTMs. Given the importance of HBP flux on multiple downstream processes and its association with most of the nine hallmarks of aging, extending the understanding of its regulatory principles could provide novel approaches to slow down the aging process (Figure 8).

Although regulation of the rate-limiting enzyme glutamine fructose-6-phosphate amidotransferase (GFAT) by UDP-GlcNAc feedback inhibition is well-studied (Ruegenberg et al. 2020b), little data is available concerning other regulators. Therefore, in this study, we used tunicamycin (TM) resistance as a proxy for increased HBP activity and performed an unbiased forward genetic screen in haploid mouse embryonic stem cells (mESCs) in combination with chemical and insertional mutagenesis. We identified the N-acetylglucosamine deacetylase AMDHD2, which catalyzes a reverse reaction of the HBP. Further characterization of AMDHD2 unraveled that loss-of-function, caused by mutations interfering with protein folding or catalytic activity, ultimately elevate UDP-GlcNAc levels in mESCs. Finally, we showed that mESCs co-express AMDHD2 together with GFAT2 instead of the more common paralog GFAT1. Compared to GFAT1, GFAT2 has a decreased sensitivity to UDP-GlcNAc feedback inhibition, explaining how AMDHD2 loss-of-function results in HBP activation in AN3-12 cells. This HBP configuration, in which AMDHD2 serves to balance GFAT2 activity, was also observed in other mESCs and, consistently, the GFAT2:GFAT1 ratio decreased with differentiation of human ESCs into the neural or cardiac lineage. Together, we discovered a potential ESC-specific regulation of the HBP and a hitherto unexpected function of AMDHD2 in fine-tuning UDP-GlcNAc levels in cells that use GFAT2 for metabolite entry into the HBP.

3.1 Identification of AMDHD2

The HBP is a metabolic pathway, converting Frc6P into the high energy molecule UDP-GlcNAc and its epimer UDP-GalNAc. A previous chemical mutagenesis screen in *C. elegans* established resistance to the toxin tunicamycin (TM) as a proxy for elevated HBP activity (Denzel et al. 2014). TM acts as a competitive inhibitor of

UDP-GlcNAc:dolichylphosphate GlcNAc-1-phosphotransferase (GPT), which catalyzes the first step of N-glycan synthesis (Heifetz, Keenan, and Elbein 1979). Thus, increased UDP-GlcNAc concentrations, achieved by gain-of-function (GOF) mutations in the rate-limiting enzyme GFAT1, were shown to outcompete TM toxicity. Further, introducing the same GOF mutation into GFAT1 of mouse neuroblastoma Neuro2a (N2a) cells confirmed a conserved mechanism in mammalian cells (Horn et al. 2020; Ruegenberg et al. 2020b). Taken together, screening for TM resistance should also be a suitable approach in mammalian cells for identification of novel HBP regulators.

3.1.1 Identification of AMDHD2 demonstrates the power of drug resistance screens in haploid mESCs

In the first part, we performed an ENU-based DNA mutagenesis followed by forward genetic screening for TM resistance in the haploid mESC line AN3-12. This unique combination of a haploid system with chemical mutagenesis allows the identification of all types of mutations, including dominant and recessive, hypo-, hyper-, and neomorph mutations. Moreover, in contrast to RNAi or CRISPR-based screens, no guide library is required, ensuring an unbiased screening approach. The most powerful advantage, however, is the possibility to narrow down mutations to an amino acid resolution. Out of 29 TM resistant clones that were sent for whole exome sequencing only *Amdhd2* fulfilled all criteria of being a candidate gene, which includes the presence of at least two independent alleles. In total, 38% of all clones revealed a mutation in *Amdhd2* (11 independent alleles). This large number of allelism indicates a high degree of saturation of the screen, although no other candidates could be identified. The lack of other TM resistance-conferring genes could be due to the harsh screening conditions with a relatively high TM concentration (0.5 µg/mg TM). Repeating the screen with a lower TM concentration may allow identification of other genes, conferring a lower degree of resistance, but at the same time would also increase the probability of false positive candidates to grow. Interestingly, we were only able to identify missense mutations within *Amdhd2*. However, since we only performed whole exome sequencing other mutations in the remaining clones that may disturb the promoter region cannot be excluded. Moreover, no nonsense mutations were detected possibly due to the usage of the mutagen ENU, which induces nonsense mutations only in 10% of the cases (Takahasi, Sakuraba, and Gondo 2007). Chemical mutagenesis with reagents having other chemical properties may alter the spectrum of induced mutations.

In addition to the chemical mutagenesis, we made use of a comprehensive library of clones containing reversible insertions, which cover around 70% of the protein coding genes in AN3-12 cells. This library was established using an enhanced gene trapping system and was already successfully used for drug resistance screens (Elling et al. 2011; Elling et al. 2017; Horn et al. 2018). In contrast to the chemical-based screen, this insertional mutagenesis approach is restricted to identification of hyper- or hypomorph mutations. However, to identify mutation sites no whole exome sequencing is required. Instead, due to a viral-specific barcode within the insert, mutations can be determined easily by inverse PCR. Thus, besides the ENU-based screen, we performed a second completely independent insertional mutagenesis screen in the haploid AN3-12 cell line. Also in this screen, AMDHD2 was the only candidate gene and disruption of *Amdhd2* was verified in 20% of the tested clones. Combining two different approaches of forward genetic screens with the same result, reinforced the hypothesis of a novel and significant role of AMDHD2 in HBP regulation in mESCs. In addition, the K.O. of AMDHD2 in mice resulted in lethality of homozygous mutants, while heterozygous mice had no obvious phenotype, indicating that mutations within *Amdhd2* are recessive. Thus, identification of AMDHD2 as an uncharted and essential gene for mammalian development was only possible using haploid mESCs, emphasizing the power of this state-of-the-art tool. Consequently, we could demonstrate that forward genetic screening in haploid mESCs can push boundaries and is a promising novel technique, which can be applied to unravel diverse scientific questions in the future.

3.1.2 Loss of AMDHD2 is a novel mechanism to mediate tunicamycin resistance by HBP activation

Three independent AMDHD2 K.O. AN3-12 lines were generated and confirmed that AMDHD2 and no off-targets mediated TM resistance. Consistently, the initial clones that were sent for sequencing and the generated AMDHD2 K.O. cell lines showed very similar levels of TM resistance, up to 4-fold compared to control cells (Figure 10B, Figure 11B). We concluded that the identified mutations are LOF mutations, since the AMDHD2 K.O. cell lines phenocopied the initially identified mutants. The 11 mutations were mainly localized in exon 4 and 5, suggesting that this locus most likely encodes residues close to the active site of AMDHD2. Based on the first eukaryotic crystal structure of AMDHD2 we confirmed this assumption and were able to show that several identified mutations are located in close proximity to the active site. Further analysis demonstrated that the

mutations from the screen cause a LOF in human AMDHD2 by: (1) disrupting proper protein folding, mainly due to exchanges of the small amino acid glycine by bigger and bulkier residues; (2) affecting protein activity presumably by disturbing binding of the substrate or co-factor.

Alignments of the mouse and human AMDHD2 amino acid sequence with its bacterial and fungal homologs demonstrated a high degree of conservation (Supplementary Figure 1). For the *E. coli* homolog NagA, a putative catalytic mechanism was described previously (Hall, Xiang, et al. 2007). Conservation of the potential functional residues in the human and murine protein indicates a similar catalytic mechanism. AMDHD2 is composed of a deacetylase domain and a small domain with unknown function (DUF). We identified only one mutation, I38T, within the DUF domain and this mutant showed a reduced solubility, potentially explaining the LOF. Nonetheless, the soluble fraction of AMDHD2 I38T mutant protein was as active as wild type AMDHD2 in activity assays, suggesting that the DUF domain is dispensable for catalysis.

AMDHD2 is an amidohydrolase that plays a potential role in catalyzing the “reverse” direction of the second step in the HBP by deacetylation of GlcNAc6P to generate GlcN6P (White and Pasternak 1967). Nonetheless, so far AMDHD2 is often not integrated into the HBP and most knowledge is based on the fungal and bacterial homolog NagA, which is important for catabolism of cell wall components (Park 2001; Uehara et al. 2005; Plumbridge 2009). For mammalian AMDHD2, a crucial role for degradation of N-glycolylneuraminic acid (Neu5Gc) was previously shown, which is one of the most common sialic acids at the terminal position of glycoconjugates in mammals (Bergfeld et al. 2012). To elucidate if AMDHD2 plays a functional role in HBP regulation in a mammalian system, we compared UDP-HexNAc levels of WT and AMDHD2 K.O. cells. Indeed, we confirmed with our data that, similar to GlcNAc supplementation and the previously identified GOF mutation in GFAT1, loss of AMDHD2 increases UDP-HexNAc levels in AN3-12 and N2a cells by blocking of the HBP reverse flux, thereby mediating TM resistance. Thus, we were able to highlight for the first time the relevance of mammalian AMDHD2 in regulation of the HBP and its final product UDP-GlcNAc. Concluding, we were able to broaden the knowledge about mammalian AMDHD2 and confirmed that LOF mutations in *Amdhd2* confer TM resistance by increasing HBP flux and thus UDP-GlcNAc levels. This novel regulatory function of mammalian AMDHD2 as a modulator of HBP activity and UDP-GlcNAc homeostasis provides a reasonable starting point for many future applications.

3.2 *In vivo* characterization of AMDHD2

After identification of AMDHD2 as a novel regulator of HBP activity, we aimed to further examine its biological relevance. To gain insight into the physiological function of AMDHD2, we performed *in vivo* analyses by generating K.O. mutants in the nematode *C. elegans* and in *M. musculus*.

3.2.1 Loss of the *C. elegans* AMDHD2 homolog *F59B2.3* has no effect on HBP activity

It has been previously shown that elevated UDP-GlcNAc levels, obtained by GlcNAc supplementation and GOF mutations as well as overexpression (OE) of the rate limiting enzyme GFAT-1, can improve protein homeostasis, leading to TM resistance, and an extended lifespan in *C. elegans* (Denzel et al. 2014). As a matter of fact, I could reproduce a drastic increase in TM resistance in the *gfat-1* (*dh784*) GOF worm and highly elevated UDP-GlcNAc levels in the GFAT-1 OE mutant (*gfat-1P::gfat1*) compared to WT control worms (Figure 16C, D). Although this positive control confirmed a properly working experimental setup, none of the two independent K.O. mutants for the putative AMDHD2 homolog *F59B2.3* showed either TM resistance or increased UDP-GlcNAc levels. On a genetic level, insertions/deletions within the *F59B2.3* gene should result in a frameshift, leading to a premature stop codon, and indeed qPCR revealed a decreased mRNA abundance for both mutants compared to WT worms. However, due to the lack of a working antibody for the *C. elegans* homolog *F59B2.3*, remaining functional protein cannot be excluded. Moreover, the *F59B2.3* gene is only a predicted homolog with 50% amino acid identity compared to human AMDHD2 (Supplementary Figure 1). Despite the moderate conservation, another functional role in the worm could explain the lack of impact on the phenotype. Another possible explanation is a cell type-specific effect, which could be masked by analyzing the multicellular organism *C. elegans*. These possibilities could also explain the missing identification of AMDHD2 in the previously performed TM resistance screen in the nematode (Denzel et al. 2014).

3.2.2 AMDHD2 is essential for embryonic development in *M. musculus*

To better understand the physiological relevance of AMDHD2 disruption in a mammalian *in vivo* model, K.O. mice were engineered and analyzed. For disruption of protein functionality exon 4 was targeted, since most of the identified mutations cluster in this locus and our first eukaryotic protein structure displayed this area to encode for the active site of human AMDHD2. Four different founder lines with different deletions within *Amdhd2* were analyzed, in order to exclude phenotypes mediated by off-targets. Although genotyping of dissected prenatal embryos revealed the existence of homozygous pups in the expected mendelian ratio (24%), no viable mice with a homozygous *Amdhd2* mutation could be weaned. Macroscopic analysis of the homozygous K.O. embryos during dissections between E9-E13 revealed smaller size of the embryos with signs of resorption. These data provide strong evidence for an early embryonic lethality upon homozygous deletion of AMDHD2. However, a deeper analysis of the underlying developmental defect and in which embryonic state exactly lethality occurs, is still an open question. Of note, heterozygous mutant mice up to 1 year did not show any obvious phenotype, suggesting that mutations within AMDHD2 are recessive and one allele is sufficient to preserve functionality. Nevertheless, a detailed characterization of heterozygous mice on a physiological and molecular level is still missing. Therefore, detrimental effects starting later in life are still possible. Interestingly, ubiquitous OE of human His₆-N-tagged WT GFAT1 or GFAT1 with the G451E GOF mutation was sufficient to increase UDP-GlcNAc levels significantly in the brain of three-month-old mice, but had no effect on development (Allmeroth 2021). However, His₆-N-tagged GFAT1 was described to have reduced activity (Olchowy et al. 2006). Therefore, one possible explanation for this contradiction could be that the loss of AMDHD2 even exceeds the effect of GFAT1 OE, resulting in a too high and lethal dose of UDP-GlcNAc levels. In accordance with our data, homozygous deletion of GNPDA1, the enzyme catalyzing the reverse reaction of GFAT, is also indispensable for viability in mice and its loss mediates embryonic lethality (IMPC, <http://www.mousephenotype.org/>). *Vice versa*, a whole body K.O. of GFAT1 is neither compatible with life and a muscle-specific deletion causes myasthenia and myopathy in mice (Issop et al. 2018; Pantaleon, Scott, and Kaye 2008). Interestingly, also homozygous deletion of GNA1, the counteractor of AMDHD2, caused embryonic lethality at E7.5 in mice (Boehmelt, Wakeham, et al. 2000). Thus, an optimally balanced UDP-GlcNAc homeostasis seems to be required for proper development with deleterious effects if too high or too low. It is already described that a balanced O-GlcNAc cycle is of high

importance for proper embryogenesis in diverse model organisms. For example, deletion of OGT leads to developmental defects in the fly, zebrafish, and mice (Mariappa, Ferenbach, and van Aalten 2018; O'Donnell et al. 2004; Shafi et al. 2000; Webster et al. 2009; Muha et al. 2021). Moreover, it is possible that AMDHD2 is of special importance in ESCs and in turn during embryonic development. To summarize, homozygous mutations in AMDHD2 result in embryonic lethality in mice, which might be due to altered UDP-GlcNAc homeostasis during early embryogenesis. Therefore, our data provide evidence for a putative role of AMDHD2 as a so far unknown essential factor for embryonic development. To further elucidate this phenomenon, a conditional and tissue-specific AMDHD2 K.O. in mice could be beneficial. Detailed expression analysis of different tissues and at multiple stages could also help to identify when exactly expression is required during development and which tissues specifically rely on AMDHD2 functionality.

3.3 Cell type-specific regulation of the HBP

Comparison of AMDHD2 K.O. AN3-12 cells and N2a cells suggested a different relevance of AMDHD2 in HBP regulation. Indeed, a cell type-specific regulation was already described for other HBP enzymes. While the more prominent paralog GFAT1 is ubiquitously expressed, GFAT2 mainly occurs in the central nervous system (Oki et al. 1999). Furthermore, GNA1, the counterplayer of AMDHD2, was also shown to be differentially regulated in a cell type-specific manner (Boehmelt, Fialka, et al. 2000). Given this information, in the next part of the thesis we aimed to further investigate if and how HBP flux is controlled in a cell type-specific context.

3.3.1 GFAT2 controls metabolite entry into the HBP in mESCs

To unravel a potentially different mode of enzymatic HBP regulation in AN3-12 cells compared to N2a cells, we analyzed the previously described ways of activating the HBP and the newly identified K.O. of AMDHD2 in both cell lines. It was published already, that GlcNAc supplementation and introducing the G451E GOF mutation into murine GFAT1 can upregulate UDP-GlcNAc levels up to 5-fold in N2a cells (Horn et al. 2020; Ruegenberg et al. 2020b). Although I could reproduce these data with both known HBP activators, the K.O. of AMDHD2 was not able to increase UDP-GlcNAc levels significantly in N2a cells. Contrary, AN3-12 cells showed the opposite effect, with deletion of AMDHD2 being the

only activator achieving significant upregulation of UDP-GlcNAc levels. GlcNAc can enter the HBP downstream of GFAT1 upon phosphorylation to GlcNAc6P by the kinase NAGK (Weihofen et al. 2006). Preliminary qPCR data indicated a low expression level of *NagK* in AN3-12 cells, which is 7-fold increased in N2a cells (data not shown). This low abundance of NAGK in the AN3-12 cell line could explain the missing potential of GlcNAc to enter the HBP and thereby elevate its flux. Similarly, the lack of HBP activation or inhibition upon GFAT1 manipulation in AN3-12 cells, either by introducing the GOF mutation or the complete loss of GFAT1, can be explained by low *Gfat1* expression. Additionally, this low expression level of GFAT1 in AN3-12 could be a reason why we were not able to identify the previously described G451E GOF substitution in our screen. Not only the AN3-12 cells, but also E14 mESCs displayed a very low GFAT1 abundance in parallel to a high GFAT2 protein level, indicating the replacement of the more common GFAT1 by GFAT2 as a general mESC-specific feature. In contrast, GFAT1 is highly abundant in more differentiated cell lines like N2a cells and C2C12 myoblasts, while GFAT2 is virtually undetectable. These results explain why manipulation of GFAT1 is sufficient to elevate HBP flux in N2a cells. In accordance, it was already shown that GFAT2 acts as the key regulator for the HBP in intestinal SCs in *D. melanogaster* (Mattila et al. 2018). The same study claimed a potential mechanism, in which the HBP can mediate a metabolic rewiring of intestinal SCs according to nutrient availability.

A recent publication demonstrated a FoxO1-dependent GFAT2 upregulation upon stress in macrophages simultaneously to increased O-GlcNAc levels (Al-Mukh et al. 2020). Interestingly, the transcription factor (TF) FoxO1 is described to have a functional role for expression of developmentally regulated genes and is involved in cell fate decisions. For instance, FoxO1 is downregulated upon neurogenesis and GOF or LOF mutants were able to prevent or promote differentiation of NPCs, respectively (Kim et al. 2015). Moreover, FoxO1 was identified as an essential regulator of pluripotency in human ESCs by mediating OCT4 and SOX2 expression (Zhang, Yalcin, et al. 2011). In accordance, it was previously reported that FoxO1 itself is modified and activated by O-GlcNAc, indicating a positive feedback loop upon upregulation of GFAT2 (Kuo et al. 2008). Together, these data suggest that FoxO1 acts as the TF for GFAT2 expression, thereby mediating increased UDP-GlcNAc levels in an ESC-specific manner.

Concluding, the replacement of GFAT1 by GFAT2 seems to be a so far unknown ESC-specific feature, which may facilitate the metabolic rewiring required for the specialized properties of ESCs, like the high proliferation potential.

3.3.2 AMDHD2 in tandem with GFAT2 results in elevated HBP flux in mESCs

Deeper analysis of AMDHD2 expression in diverse cell lines revealed a high protein abundance in the tested mESC lines, while a reduced level was observed in the more differentiated N2a and C2C12 cell lines. Interestingly, this cell type-specific regulation does not seem to occur on a transcriptional level as the mRNA levels for *Amdhd2* are similar in all tested cell lines. Thus, elevated AMDHD2 availability in mESCs is rather mediated by enhanced translation or an increased protein stability. For a detailed understanding of this adaptation, further experiments are required like ribosome profiling to test changes in translation or proteasome inhibition to examine altered protein turnover by the UPS. The observed co-expression of AMDHD2 in cells that rely on GFAT2 for HBP entry caused higher UDP-GlcNAc concentrations in parallel to higher O-GlcNAc levels in mESCs. It is described that ESCs require high O-GlcNAc levels for their maintenance, since many pluripotency TFs like OCT4 and SOX2 are positively regulated by O-GlcNAcylation (Constable et al. 2017b; Jang et al. 2012). High UDP-GlcNAc levels are moreover associated with pluripotency and ESC maintenance by affecting synthesis of ECM components, functionality of proper PQC mechanism, and chromatin remodelling (Fong et al. 2012; Vigetti et al. 2012). As a sum, the specific enzymatic configuration of the HBP we observed in mESCs, including the combined expression of AMDHD2 and GFAT2, could be required for balancing higher UDP-GlcNAc levels as an adaptive mechanism for pluripotency and SC self-renewal.

3.3.3 Differentiation of ESCs reduces the GFAT2:GFAT1 ratio

ESCs exhibit a unique metabolic rewiring according to their special properties like a high proliferating ability (Figure 7). Therefore, the predominant usage of GFAT2 instead of GFAT1 as key enzyme of the HBP most likely reflects a metabolic adaptation in ESCs. Consequently, we hypothesized an enzymatic reconfiguration of the HBP upon differentiation of ESCs including the upregulation of GFAT1 in combination with a decreased GFAT2 expression, ultimately resulting in a reduced GFAT2:GFAT1 ratio. Depletion of leukemia inhibitory factor (LIF) from the medium is known to initiate SC differentiation (Hocke, Cui, and Fey 1995). Thus, we induced partial differentiation by LIF removal for 5 days and asked if this is sufficient to switch the enzymatic configuration of the HBP from GFAT2 to GFAT1 expression. Significant downregulation of the ESC markers confirmed partial differentiation of AN3-12 mESCs, which was indeed sufficient

to decrease GFAT2 mRNA and protein abundance (Figure 23B). In contrast, neither GFAT1, AMDHD2 nor ultimately UDP-GlcNAc levels were changed upon LIF depletion. These data suggest, that differentiation *per se* is able to rewire the HBP's enzymatic configuration. While the transcriptional downregulation of GFAT2 seems to occur already in early steps of differentiation, 5 days of LIF removal were not sufficient to alter GFAT1 or AMDHD2 levels.

Ample evidence indicated a special importance of the HBP in differentiation into neuronal and cardiac lineages. Elevated HBP flux by GlcN treatment in ESCs was shown to be able to decrease cardiomyocyte differentiation (Kim et al. 2009). *Vice versa*, the same study observed that compound-based inhibition of GFAT1 increases the number of cardiomyocyte precursors. In accordance, C2C12 myoblasts require a decrease in global O-GlcNAc levels for proper myogenesis: Genetic or pharmacological inactivation of OGA prohibits the decrease of O-GlcNAcylation and disturbs myoblast fusion and expression of myogenic regulatory factors (Ogawa et al. 2012). Similarly, OGA inhibition disturbed differentiation of hESCs into neural progenitor cells (NPCs) (Parween et al. 2017). In accordance, chemical inhibition of OGT which reduces O-GlcNAc levels, impaired hESC maintenance and promoted differentiation along the neural lineage (Andres et al. 2017; Parween et al. 2017). Therefore, we focused our research on HBP regulation in the context of neurogenesis and myogenesis. Indeed, by *in silico* analysis of already published datasets we observed a decreased GFAT2:GFAT1 ratio upon differentiation of hESCs along both, cardiac or neural lineages (Saez et al. 2018; Frank et al. 2019; Bartsch et al. 2021). Thus, we could not only confirm our hypothesis of a replacement of GFAT2 by GFAT1 during differentiation, but can also show that this mechanism is conserved in hESCs. Concluding, although incomplete differentiation of AN3-12 cells was only partially able to alter HBP configuration, analysis of already published datasets strengthened our hypothesis of a high GFAT2:GFAT1 ratio as an ESC-specific feature, which decreases with differentiation. Thus, we could prove for the first time an enzymatic reconfiguration of the HBP during differentiation, which might be important to adapt to the specialized metabolic profile of ESCs.

3.3.4 Loss of AMDHD2 delays differentiation and increases ESC maintenance

Given the essential role of O-GlcNAc regulation, and thus HBP activity, for differentiation of human ESCs into neural progenitor cells (NPCs) (Parween et al. 2017), we aimed to investigate how an AMDHD2 K.O. impacts the differentiation potential of AN3-12 mESCs into NPCs. In general, the differentiation protocol was successful since we confirmed decreased expression of ESC markers combined with a drastic upregulation of the neuronal marker gene *Nestin* compared to undifferentiated WT mESCs. Increased *Nestin* levels were also observed in AMDHD2 K.O. cells upon differentiation, indicating a functional differentiation *per se* in these cells, despite the elevated basal UDP-GlcNAc levels. However, the differentiation seemed to be delayed upon loss of AMDHD2 since *Nestin* levels were only 2.8-fold increased in the according NPCs, compared to a 4.8-fold increase in WT NPCs. In compliance with these data, also the decreased expression of SC markers was more pronounced in WT than in AMDHD2 K.O. NPCs. It is worth mentioning, these are only preliminary data and further replicates are required to test statistical significance of this effect. It is known that altered HBP activity, and thus changes in UDP-GlcNAc levels, can influence cell cycling and proliferation. For instance, deletion of GNA1 was shown to diminish the proliferative capacity of MEFs, which could be rescued by GlcNAc supplementation (Boehmelt, Wakeham, et al. 2000). Moreover, tumor suppressors like FOXO3 and p53 can be regulated by O-GlcNAcylation and thereby modify cell growth and apoptosis (Yang et al. 2006; Shin et al. 2018). Differences between WT and AMDHD2 K.O. cells regarding cell cycle progression were not excluded so far, which could explain the delayed differentiation of mutant cells. In addition, increased induction of apoptosis in AMDHD2 K.O. NPCs could enrich for mESCs and thus, might contribute to the observed effect in the qPCR data. Therefore, follow up experiments are required to better understand the underlying mechanism of a potential delayed differentiation upon loss of AMDHD2.

High O-GlcNAcylation levels were shown to be essential for ESCs pluripotency, while increased levels can disturb differentiation (Jang et al. 2012). Moreover, alterations in the UDP-GlcNAc availability, which serves as a direct precursor for O-GlcNAcylation, can modulate O-GlcNAc levels leading to hypo- or hyper-O-GlcNAcylation (Shen et al. 2012; Taylor et al. 2008). Although UDP-GlcNAc levels in AMDHD2 K.O. cells are highly elevated compared to WT AN3-12 cells, O-GlcNAc levels were only slightly but not significantly increased in mutant cells (Figure 12B, C; Figure 25B). It is well described that the O-GlcNAc cycle, driven by the two regulating enzymes OGA and OGT, is tightly

regulated and can adapt rapidly according to substrate availability in order to maintain O-GlcNAc homeostasis in an optimal range. Thus, it is possible that the elevated UDP-GlcNAc levels upon AMDHD2 loss are not sufficient to be reflected by the O-GlcNAc proteome, due to compensatory mechanisms. For example, a decreased OGT or alternatively increased OGA abundance, could result in stable O-GlcNAc levels. Indeed, a recent study could proof that GlcN supplementation is able to decrease OGT levels and at the same time increases OGA expression to balance O-GlcNAc concentrations in lung cancer cells (Lin et al. 2021). Moreover, we measured the O-GlcNAc levels only by WB analysis, which might not be sensitive enough to detect minor differences, while more drastic perturbations induced by OGA inhibition, could be measured. Thus, it would be interesting to perform mass spectrometry-based analysis of the O-GlcNAc proteome in WT and AMDHD2 K.O. cells.

To test and compare the pluripotency capacity of WT and AMDHD2 K.O. cells we performed a CFA followed by staining for alkaline phosphatase, a SC specific marker. Removal of LIF served as a positive control for differentiation. However, even when cells were cultured without LIF, only less than 10% of the cells showed a completely differentiated phenotype. Still, a slightly decreased percentage of ESCs in parallel with a moderate increase in the fraction of intermediate cells upon LIF depletion in WT as well as AMDHD2 K.O. cells confirmed successful partial differentiation and specific staining of ESCs. In accordance with the putatively delayed differentiation potential of AMDHD2 K.O., we observed a significantly increased SC fraction in combination with a reduced percentage of intermediate cells under basal conditions in AMDHD2 K.O. cells compared to control mESCs. Thus, we suggest that the loss of AMDHD2, and the corresponding increase in HBP flux, might increase ESC pluripotency and by this disturbs differentiation. However, the general size of colonies of AMDHD2 K.O. cells was smaller compared to those of WT cells, indicating a reduced cell proliferation promoted either by altered cell cycle regulation or induced apoptosis as discussed above. Summarizing, deletion of AMDHD2 potentially improves ESC maintenance which may impairs differentiation. Thus, our data reveal first indications for the development of novel therapeutic agents targeting AMDHD2 for manipulation of HBP flux and thus SC self-renewal and differentiation.

3.3.5 GFAT2 and GFAT1 differ in their substrate affinity and susceptibility for feedback inhibition

It is described that GFAT1 and GFAT2 are expressed in a tissues-specific manner (Oki et al. 1999). Moreover, the two paralogs seem to be regulated differently by PTMs. For example, just recently it was shown that PKA-mediated phosphorylation of GFAT1 at Ser205 is required for its regulation and can, dependent on the UDP-GlcNAc concentration, activate or inhibit GFAT1 (Ruegenberg et al. 2021). The preserved Ser202 in GFAT2, however, was shown to increase enzyme activity (Hu et al. 2004). GFAT1 additionally contains a second PKA target site at S235, which is not conserved in GFAT2 (Supplementary Figure 2). Moreover, only GFAT1 has a potential ubiquitination site at Lys48 and was shown to interact with diverse E3 ligases, indicating a UPS-based degradation (Akimov et al. 2018; Kristensen, Gsponer, and Foster 2012; Wagner et al. 2011).

Importantly, in this study we performed the first detailed comparison of the kinetic parameters and observed a 3-fold decreased affinity for Frc6P in parallel to a 2-fold increased affinity for L-Gln of GFAT2 compared to GFAT1. These differences regarding substrate affinities raise the possibility of an adaptative mechanism for different cellular substrate availabilities. One metabolic feature of ESCs is the highly elevated glycolytic flux despite the presence of oxygen (Warburg, Wind, and Negelein 1927) (Figure 7). This increased glycolysis results in increased Frc6P levels, which can enter the HBP. Given the fact that GFAT2 is the predominant key enzyme for HBP entry in ESCs, the lower affinity of GFAT2 for Frc6P could be an adaptation for the high availability of Frc6P and thus, could aid balancing final UDP-GlcNAc levels. At the same time, ESCs have a higher dependency on Gln as a carbon source, since TCA cycle activity is diminished (Vander Heiden, Cantley, and Thompson 2009) (Figure 7). Contradictive, especially in highly proliferative cells, like ESCs, the demand for carbons is elevated to guarantee the production of sufficient biomass. Thus, elevated glutaminolysis is required to feed the TCA cycle and is vital for ESC maintenance (Tohyama et al. 2016). It was shown that glutaminolysis and the HBP compete for Gln as substrate and inhibition of glutaminolysis can elevate HBP flux (Araujo et al. 2017). Additionally, nucleotide metabolism is increased in ESCs which also requires Gln availability (Newsholme, Crabtree, and Ardawi 1985) (Figure 7). Together, the higher affinity of GFAT2 for Gln could be an adaptation to the reduced substrate availability due to the increased activity of other Gln-consuming, competing pathways. In accordance, GFAT2 is also upregulated in other rapidly

proliferating cells with similar metabolic profiles, like in some types of cancer cells (Shaul et al. 2014; Zhang et al. 2018; Szymura et al. 2019).

Previously, it was shown that under physiological conditions GFAT1 is strongly feedback inhibited by UDP-GlcNAc (Ruegenberg et al. 2020b). Thus, if GFAT1 is the main regulator of HBP flux, as in N2a cells, loss of the reverse flux by AMDHD2 K.O. has no drastic effect on UDP-GlcNAc levels. For GFAT2, however, we observed a decreased susceptibility to UDP-GlcNAc feedback inhibition compared to GFAT1. We demonstrated that GFAT2 can be fully inhibited by UDP-GlcNAc, but requires approximately 6-fold higher UDP-GlcNAc concentrations to reach a similar extent of inhibition compared to GFAT1. The reduced feedback inhibition when HBP flux is controlled by GFAT2, allows the presence of higher basal UDP-GlcNAc levels as we observed in the tested mESC lines. Moreover, these data suggest that GFAT1 is sufficiently regulated by feedback inhibition to determine HBP flux, whereas cells using GFAT2 in the HBP require another way to adjust product levels and thus utilise AMDHD2 to balance forward and reverse flux in the HBP. Overall, not only the expression pattern and PTMs but also the kinetic properties, and feedback regulation of GFAT1 and GFAT2 differ, which might reflect an adaptation to altered cell type-specific substrate availabilities.

3.3.6 Enzymatic reconfiguration of the HBP as an adaptation to ESC metabolism

In this study, we discovered an ESC-specific regulation of the HBP, including the replacement of the more common GFAT1 by GFAT2. GFAT2 is less susceptible to UDP-GlcNAc feedback inhibition than GFAT1 and therefore requires another way for balancing UDP-HexNAc homeostasis, which is mediated by AMDHD2 activity (Figure 26). The reduced feedback inhibition of GFAT2 results in increased basal UDP-GlcNAc levels in ESCs, which could reflect an adaptation to the specialized metabolism and demands of ESCs. The HBP relies on the consumption of sugar (Glc), amino acids (Gln), nucleotides (UTP), and lipids (acetyl-CoA), facilitating its role as a metabolic sensor, which is interconnected to all major metabolic pathways. Since most of these linked pathways are differentially regulated in ESCs, it is reasonable that also the HBP needs to be rewired according to the changed substrate availabilities. For instance, GFAT2 has a lower affinity to Frc6P compared to GFAT1, which could be an adaptation to the increased glycolytic flux in ESCs. On the other hand, the affinity for L-Gln was higher in GFAT2 compared to GFAT1, potentially reflecting the need to compete with other Gln-consuming pathways,

which are upregulated in ESCs (nucleotide metabolism, glutaminolysis for TCA entry) (Figure 7). Concluding, the discovery of a stem cell-specific HBP regulation obtained by our data can aid to develop novel therapies with regard to development, aging, and disease as discussed in the following paragraph.

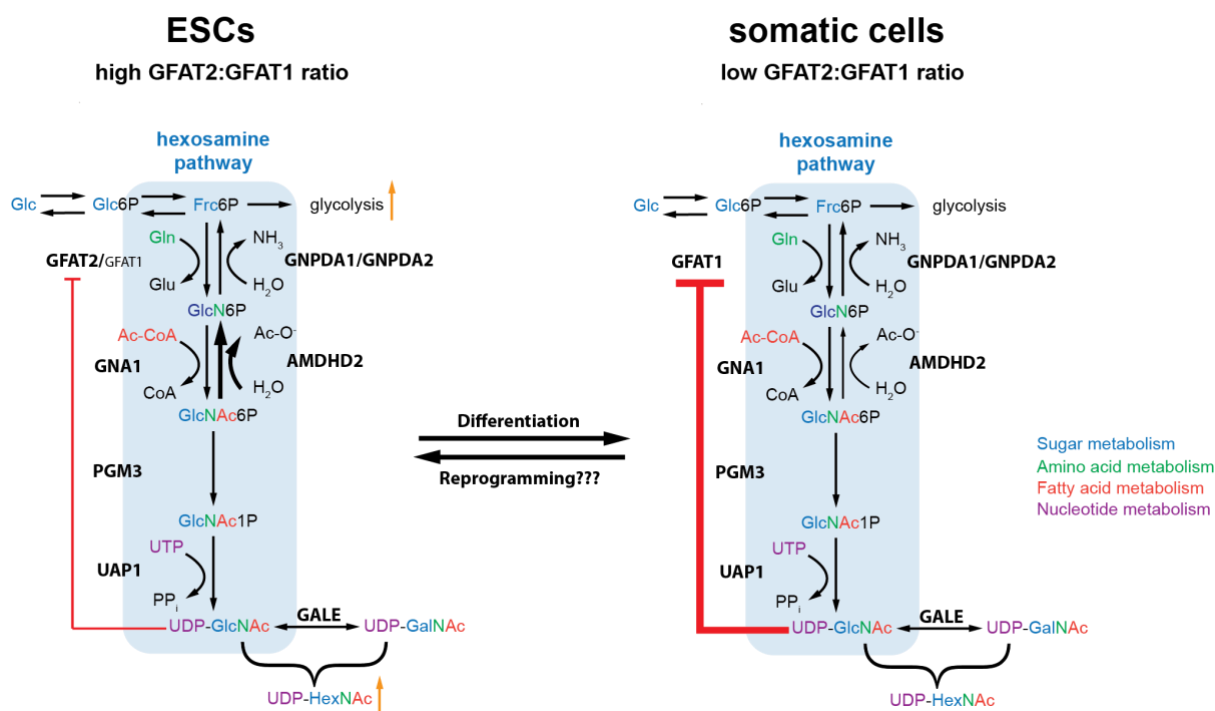


Figure 26: Enzymatic reconfiguration of the HBP in ESCs. The HBP (blue box) generates UDP-HexNAc in multiple enzymatic steps. ESCs have an adapted metabolic profile, including higher glycolysis flux and an elevated demand for UDP-HexNAc (indicated by orange arrows). While ESCs mainly rely on GFAT2, more differentiated cells use GFAT1 for HBP entry. GFAT2 is less susceptible to UDP-GlcNAc inhibition than GFAT1 (indicated by red arrow). As alternative regulatory mechanism ESCs require AMDHD2. Differentiation of ESCs induces an enzymatic shift, resulting in a decreased GFAT2:GFAT1 ratio. If reprogramming of somatic cells into iPSCs is able to reverse this effect, remains an open question. GFAT: glutamine fructose-6-phosphate amidotransferase, GNPDA: D-glucosamine-6-phosphate deaminase, GNA1: D-glucosamine-6-phosphate-Nacetyltransferase, AMDHD2: N-acetylglucosamine-6-phosphatideacetylase, PGM3: phosphoglucomutase, UAP1: UDP-N-acetylglucosamine pyrophosphorylase, GALE: UDP-galactose-4'-epimerase.

3.4 AMDHD2 as a novel target for multifunctional applications

Given the importance of a properly coordinated HBP in ESC-renewal and differentiation, it is not surprising that altered HBP flux can also disturb embryonic development. Multiple lines of evidence already confirmed that manipulation of the HBP and O-GlcNAc cycle can perturb embryogenesis in diverse model organisms. Mutation in the *Ogt* homolog in *D. melanogaster*, *super sex combs (sxc)*, resulted in developmental defects (Gambetta,

Oktaba, and Müller 2009; Sinclair et al. 2009). In the zebrafish OE of OGT disturbed embryonic growth and cell viability (Webster et al. 2009). Accordingly, proper O-GlcNAc cycling is essential for embryonic development and viability in mice (Shafi et al. 2000; Muha et al. 2021; O'Donnell et al. 2004; Keembiyehetty et al. 2015). Together with the fact that homozygous deletion of GFAT1, GNPDA1 and GNA1 also results in embryonic lethality, these data emphasize the essential role of a functional HBP in embryogenesis (Boehmelt, Fialka, et al. 2000; Pantaleon, Scott, and Kaye 2008; Issop et al. 2018; Oikari et al. 2018). Thus, the lethality we observed in this work in the AMDHD2 K.O. mice is consistent with previous literature.

In humans, mutations within *Gfat1* are known to cause a subtype of congenital myasthenic syndrome, resulting in myopathy and muscle weakness (Bauche et al. 2017; Huh et al. 2012). Moreover, just recently disturbed UDP-GlcNAc biosynthesis, by missense mutations in the HBP enzyme UAP1, was shown to cause developmental delay (Chen, Raimi, et al. 2021). In accordance, OGT missense mutations were already shown to be connected to X-linked intellectual disability in humans (Willems et al. 2017; Pravata et al. 2020; Selvan et al. 2018). Thus, a balanced HBP flux is not only essential for embryogenesis in different organisms but also seems to be required for proper development in humans. Furthermore, its deregulation can also result in the manifestation of various diseases. Despite these previous findings, the work of this thesis led to the discovery of an uncharted role of AMDHD2 in HBP regulation in an ESC-specific context. In essence, our data can help to better understand ESC metabolism and give rise to new therapeutic opportunities for SC maintenance in aging and disease.

3.4.1 The HBP as therapeutic target in aging and disease

Besides its substantial role in ESCs and embryonic development, the identification of AMDHD2 provides a novel target for a broad range of therapeutic interventions, especially with focus on the development of anti-aging drugs. Manipulation of the HBP is a promising approach with regard to many characteristics and age-related diseases (Figure 8).

First of all, cancer stem cells (CSCs) are highly proliferative and have a similar metabolic profile as ESCs, including increased metabolism of glucose, glutamine, and fatty acids (Akella, Ciraku, and Reginato 2019; Chiaradonna, Ricciardiello, and Palorini 2018). Based on the described interplay of these metabolic pathways and the HBP, elevated HBP flux in cancer cells is not surprising. Indeed, the HBP was already shown to play a pivotal role in the progression and severeness of different types of cancer. For instance, GFAT

expression is often increased in cancer cells and correlates with a poor prognosis in cancer patients (Vasconcelos-dos-Santos et al. 2015). As for ESCs, elevated HBP flux increases HA production and by this malignancy of cancer cells, while suppression of GFAT was sufficient to diminish CSCs properties (Oikari et al. 2018). In accordance with our findings, Oikari et al. could show highly increased expression of the GFAT2 paralog, accompanied with elevated UDP-GlcNAc levels in breast cancer cells. Moreover, analysis of oncogenic gene expression datasets examined upregulation of other HBP enzymes like GNA1, PGM3 and UAP1 compared to control cells (Itkonen et al. 2015; Chokchaitaweek et al. 2019). However, AMDHD2 was so far not in the focus for HBP modulation and thus, not investigated as a target for cancer therapy to date. Of note, based on the results shown in this study, GFAT2-controlled HBP requires AMDHD2 activity to balance of UDP-GlcNAc levels. Thus, the activation of AMDHD2 might have beneficial effects, especially in cancer types with elevated GFAT2 expression.

Secondly, elevated HBP flux was reported to be connected to diabetes, which is characterized by increased blood glucose levels (hyperglycemia) in parallel to reduced insulin sensitivity of glucose-consuming tissues as muscle, liver, and adipose tissue (Marshall, Bacote, and Traxinger 1991). Pharmacological manipulation of the O-GlcNAc cycle in the insulin-producing pancreatic β -cells confirmed that this PTM can act as a glucose sensor, mediating gene expression accordingly (Durning et al. 2016). Moreover, prolonged elevation of O-GlcNAc levels, like in diabetic conditions, showed deleterious effects on β -cells by inducing apoptosis, which in turn causes dysregulated insulin secretion (Akimoto et al. 2000; Hanover et al. 1999). Consequently, reduction of HBP flux by activation of AMDHD2 might be a promising approach for the treatment of diabetic conditions.

Since O-GlcNAc plays a key role in nutrient sensation and insulin resistance, the insulin-responsive muscle tissue is especially sensitive to altered HBP activity. Indeed, elevated O-GlcNAc levels were already associated with cardiovascular diseases (Marsh, Collins, and Chatham 2014; Dassanayaka and Jones 2014). Interestingly, most studies observed increased functionality of cardiac tissue with reduced chronic O-GlcNAc levels, while acute increased O-GlcNAcylation seems to be protective upon stress-induced injuries (Clark et al. 2003; Ramirez-Correa et al. 2008). Therefore, depending on the context, activation or inhibition of AMDHD2 might be beneficial for cardiac function.

Another well studied phenomenon is the connection of the HBP activity and neurodegenerative diseases including Parkinson's disease (PD) and Alzheimer's disease (AD). Of note, for neurons a critical role of O-GlcNAcylation as a metabolic sensor was

described. The brain is one of the organs with especially high levels of OGA and OGT and reduced O-GlcNAc levels in the brain during aging can promote the development of AD (Liu et al. 2012; Yuzwa and Vocadlo 2014). The best studied connection of altered HBP flux and onset of AD is the modification of tau by O-GlcNAcylation (Arnold et al. 1996). Hyperphosphorylation of tau promotes its aggregation and O-GlcNAcylation was shown to be mutually exclusive with phosphorylation of tau (Li et al. 2006). Thus, pharmacological manipulation of the O-GlcNAc homeostasis was reported to affect tau aggregation and thereby AD progression (Yuzwa et al. 2008; Shen et al. 2012). In addition, increased HBP activity by GFAT1 GOF or OE and manipulation of the O-GlcNAc cycle were shown to be beneficial regarding aggregation of other proteotoxic species as peptides containing polyglutamine (polyQ) stretches or β -amyloid (A β) peptides and could impact longevity in the nematode *C. elegans*, with a conserved function in mouse N2a cells (Denzel et al. 2014; Horn et al. 2020; Wang et al. 2012). Given these results, inhibition of AMDHD2 could serve as a promising treatment of neurodegenerative diseases.

Moreover, mammalian AMDHD2 was displayed as a crucial factor for Neu5Gc catabolism, one of the most abundant sialic acids in glycoconjugates (Bergfeld et al. 2012). Humans are incapable to produce Neu5Gc *de novo* but rely on the uptake of dietary sources (Bardor et al. 2005). Thus, it can be sensed as a “foreign” epitope and an access in uptake or disturbed degradation can induce inflammation (Bergfeld et al. 2012; Dhar, Sasmal, and Varki 2019). Activation of AMDHD2 could reduce this inflammatory phenotype.

Lastly, GlcNAc degradation is of special importance for bacteria and fungi since it is part of their cell wall components chitin and peptidoglycan. Indeed, the HBP is a known target for many pathogenic antifungal agents and antibiotics (Munro and Gow 2001; Swiatek et al. 2012; Yamada-Okabe et al. 2001). Thus, targeting of AMDHD2 could give rise to novel future perspectives in the context of antimicrobial activity.

3.4.2 AMDHD2 as a promising druggable target for manipulation of the HBP flux

Since all these diverse pathological conditions are related to disturbed processes relying on UDP-GlcNAc as substrate, this emphasizes the importance of a fine-tuned regulatory mechanism to balance UDP-GlcNAc homeostasis, while levels outside an optimal range can have deleterious effects. Intriguingly, for all these age-associated diseases with regard to altered HBP flux, most therapeutic interventions focus on the manipulation of OGA and OGT. On the one hand, since these two enzymes are solely responsible for regulating O-GlcNAc cycling, their inhibition has a specific and efficient effect. On the other

hand, however, since O-GlcNAcylation acts as a metabolic sensor and impacts a broad range of essential downstream signaling pathways, these interventions can induce severe side effects and toxic off-targets (Liu et al. 2017). Therefore, regulation of the upstream positioned HBP may serve as a milder way of counteracting altered O-GlcNAc levels. For instance, our data indicate that loss of AMDHD2 could not induce significant changes in the overall O-GlcNAc proteome as measured by WB analysis, but seemed to be sufficient to manipulate SC fate decisions (Figure 25B, H, I). Moreover, by manipulation of HBP activity also other downstream routes emanating from UDP-GlcNAc, which are disturbed during aging or disease, can be targeted as for example N-linked glycosylation, O-linked glycosylation, and production of proteoglycans. GlcN supplementation is already established as a HBP activator and thus, as a multifunctional drug for diverse biomedical applications (Dalirfardouei, Karimi, and Jamialahmadi 2016). GlcN is widely used as an anti-inflammatory drug for treatment of osteoarthritis and rheumatic diseases, although the underlying mechanism and its efficiency is still controversial (Tat et al. 2007). However, GlcN is only poorly absorbed by the gut and glucose transporters show low affinity for import into the cell, limiting its effect (Aghazadeh-Habashi and Jamali 2011). GlcN can enter the HBP upon phosphorylation to GlcN6P, which acts as a moderate inhibitor of GFAT1, further limiting its activating function (Grigorian et al. 2007). Thus, AMDHD2 inhibition could overcome the problem of low bioavailability of GlcN supplementation. In general, influencing HBP flux provides a variety of possibilities for future therapeutic and biomedical approaches. Of note, eukaryotic AMDHD2 was a so far poorly described enzyme and the identification of its critical role in HBP regulation offers novel approaches to tackle age-related diseases, among other potential interventions. Therefore, identification of small-molecules that act as AMDHD2 inhibitors or activators could provide more successful HBP manipulation in the clinics.

4 Future perspective

The results identified in this work extend the understanding of the HBP and its pivotal role in diverse processes in an ESC-specific manner. However, the exact nature of this cell type-dependent regulation and its functional role still requires further experiments. Thus, this last part focuses on some possible follow-up experiments that could help to better understand this newly discovered mechanism.

4.1 What is the role of the HBP in ESC fate decisions?

In this study we demonstrated an ESC-specific configuration of the HBP, with a GFAT2-dependent metabolite entry into to HBP, which requires AMDHD2 activity for regulation of basal UDP-GlcNAc levels. Upon differentiation, we observed a rewiring of this specific enzymatic regulation, characterized by reduced GFAT2:GFAT1 ratios. However, if and how this specialized HBP regulation can affect ESC maintenance and differentiation remains an open question. So far, we only have preliminary data which indicate that HBP activity can influence ESC fate decisions and delays differentiation. To further elucidate this possibility, it is important to first exclude that the observed phenotype is based on differences in cell cycling between WT and AMDHD2 K.O. mESCs, since it was published earlier that ESC maintenance depends on the length of the cell cycle (Stead et al. 2002). To elucidate alterations regarding cell cycle progression we could perform a flow-cytometry-based cell cycle analysis. Besides WT and AMDHD2 K.O. cells it would be interesting to also include cells treated with 6-diazo-5-oxo-L-norleucine (DON), a GFAT inhibitor, that should result in decreased UDP-GlcNAc levels and thus, could help to identify dose-dependent effects. Moreover, it was reported that multiple cell survival factors are extensively O-GlcNAc modified, including p53, NF- κ B, and c-Myc (Yang et al. 2006; Chou, Hart, and Dang 1995; Ma, Chalkley, and Vosseller 2017). Consequently, another possibility could be increased induction of apoptosis upon AMDHD2 K.O., which could be tested by WB analysis for apoptotic markers or annexin V/propidium iodide staining followed by FACS analysis. Interestingly, for the previously generated and published GNA1 K.O. mESCs, which contain reduced UDP-GlcNAc levels, no difference in cell growth or apoptosis was observed (Boehmelt, Wakeham, et al. 2000).

Differences with regard to the pluripotency and differentiation potential between WT, AMDHD2 K.O. and DON treated cells could be further analyzed by EB formation followed by differentiation into all 3 germ layers, which can be measured by corresponding changes

in gene expression. A working protocol for AN3-12 mESC differentiation was already published (Elling et al. 2017). Moreover, it would be interesting to further analyze the enzymatic composition of the HBP upon differentiation along the different lineages with special interest on GFAT1, GFAT2 and AMDHD2. *Vice versa*, it is still unclear if reprogramming of somatic cells into iPSCs has the opposite effect with an increasing GFAT2:GFAT1 ratio. Besides the differentiation capacity it would also be worth knowing how different intracellular UDP-GlcNAc levels affect the SC self-renewal of mESCs. To interrogate this hypothesis, it would be helpful to repeat the CFA in WT, AMDHD2 K.O. and DON treated cells to solidify our preliminary data.

After gaining a functional understanding of the role of HBP activity in ESC fate decisions, it would be important to further narrow down the molecular mechanism, with special focus on O-GlcNAcylation. For this purpose, manipulation of the O-GlcNAc cycle by pharmacological inhibition and a genetic knockdown of OGA and OGT could be helpful. Preliminary data with the potent OGA inhibitor GlcNAcstatin G confirmed increased O-GlcNAc levels in a dose-dependent manner in AN3-12 mESCs (Figure 25A). These results could provide information if the HBP is able to link glucose metabolism in ESCs with cell fate decisions, mediated by changes in O-GlcNAc modification. Besides WB analysis with the O-GlcNAc-specific AB used in this study, LC-MS-based measurements of the O-GlcNAc proteome could serve as a more sensitive method to detect alterations and maybe to identify specific regulators.

In addition, our data suggest a regulatory role of the HBP uncoupled from UDP-GlcNAc synthesis by cross-regulation of other interconnected pathways as the TCA cycle, PPP, glycolysis or glutaminolysis, which are all altered in ESC metabolism. Thus, HBP activity could indirectly influence cell fate by modulation of other essential metabolic pathways. To unravel a potential role of the HBP flux in coordinating other metabolic pathways in a cell type-specific manner, we could perform a flux analysis with labeled glucose, glutamine, and acetate, which are the main molecules shared by the different pathways. Tracing of labeled metabolite incorporation by LC-MS and comparison of mESCs and their differentiated counterparts could clarify the significance of the differently regulated HBP on the metabolic flux of interconnected pathways.

4.2 What is the role of AMDHD2 in embryonic development?

We observed in this study, that AMDHD2 is a novel essential regulator for embryonic development, since homozygous deletion of AMDHD2 caused embryonic lethality. Given the potential role of the HBP in ESC maintenance and differentiation, this could explain its high importance for proper embryogenesis. However, a detailed analysis of the developmental defects in AMDHD2 K.O. mice still needs to be performed in order to gain further information about the connection of altered HBP activity and embryonic lethality. It would be interesting to determine the exact time point of developmental failure in the homozygous AMDHD2 K.O. embryos. We observed a smaller size of homozygous AMDHD2 K.O. embryos with partial resorption by macroscopic analysis during dissections between E9-E13. In accordance, reduced UDP-GlcNAc levels by homozygous deletion of AMDHD2's counteractor GNA1 induced embryonic lethality occurring at E7.5 in mice, indicating an essential role of balanced UDP-GlcNAc levels beyond this stage (Boehmelt, Wakeham, et al. 2000). Serial section of GNA1 K.O. embryos revealed a less organized structure of the three germ layers caused by growth and developmental delay, which would also fit to our hypothesis of a pivotal role of the HBP flux in ESC fate decisions. Since it is not clear which tissues are most affected by altered HBP flux and when its enzymatic reconfiguration becomes substantially, it would be helpful to perform a systematic analysis of the expression pattern of diverse HBP enzymes, with special interest on GFAT1, GFAT2, GNA1, and AMDHD2 in different tissues and different developmental stages. Based on this knowledge, conditional or tissue-specific AMDHD2 K.O. mice can be generated to further investigate the role of the HBP also in aging mice. On the long-term, these mice could not only elucidate to which extent HBP activity is important for ESC properties and development, but also aid to further unravel the underlying process of aging. For instance, the combination of a conditional AMDHD2 K.O. with a mouse model for neurodegeneration could provide new information about the connection of HBP activity and age-related diseases.

5 Material and methods

5.1 Mouse handling

5.1.1 *M. musculus* maintenance

Animals were housed on a 12:12 h light:dark cycle with *ad libitum* access to food (Sniff) under pathogen-free conditions in individually ventilated cages. All animals were kept in C57BL/6J background. Animal care and experimental procedures were in accordance with the institutional and governmental guidelines.

5.1.2 Generation of transgenic mice

5.1.2.1 CRISPR/Cas9-mediated generation of transgenic mice

CRISPR/Cas9-mediated generation of AMDHD2 knockout mice was performed by ribonucleoprotein complex injection in mouse zygotes. Single guide RNAs (sgRNAs) targeting exon 4 of the *Amdhd2* locus were designed online (crispor.org) and purchased from IDT (see Table 3). sgRNA and tracrRNA were resuspended in injection buffer (1 mM Tris-HCl pH 7.5, 0.1 mM EDTA) and annealed at 1:1 molar concentration in a thermocycler (95°C for 5 min, ramp down to 25°C at 5°C/min). To prepare the injection mix (100 µl), two guide RNAs and the Cas9 enzyme (*S. pyogenes*, NEB) were diluted to a final concentration of 20 ng/µl each in injection buffer. The mix was incubated for 10-15 min at room temperature to allow ribonucleoprotein complex assembly. After centrifugation, 80 µl of the supernatant were passed through a filter (Millipore, UFC30VV25). Both centrifugation steps were performed for 5 min at 13.000 rpm at room temperature. The filtered injection mix was used for zygote injections.

Table 3: Primer sequences for sgRNAs for gene editing of transgenic mice.

Primer	Sequence (5'→3')
msAMDHD2_E4_guide1	TACCTTCCGGCCCTTGTGGT
msAMDHD2_E4_guide2	ATCAAGTAGTCCTGGTTGTC
msAMDHD2_E4_guide3	GCTAGAACTACCTCTGTCCC

5.1.2.2 Microinjections of mouse zygotes

3- to 4-week-old C57Bl/6J females were super-ovulated by intraperitoneal injection of Pregnant Mare Serum Gonadotropin followed by intraperitoneal injection of Human Chorionic Gonadotropin hormone (Intervet) 48 h later. Super-ovulated females were mated with 10- to 20-week-old stud males. The mated females were euthanized the next day and zygotes were collected in M2 media (Sigma-Aldrich) supplemented with hyaluronidase (Sigma-Aldrich).

Fertilized oocytes were injected into the pronuclei or cytoplasm with the prepared CRISPR/Cas9 reagents. Injections were performed under an inverted microscope (Zeiss AxioObserver) associated micromanipulator (Eppendorf NK2) and the microinjection apparatus (Eppendorf Femtojet) with in-house pulled glass capillaries. Injected zygotes were incubated at 37°C, 5% CO₂ in KSOM (Merck) until transplantation. 25 zygotes were surgically transferred into one oviduct of pseudo-pregnant CD1 female mice. All procedures have been performed in our specialized facility, followed all relevant animal welfare guidelines and regulations, and were approved by LANUV NRW 84-02.04.2015.A025.

5.2 *C. elegans* handling

5.2.1 *C. elegans* maintenance

All *C. elegans* strains were grown under standard conditions at 20°C on nematode growth medium (NGM: 2.5% bacto-agar, 0.225% bacto-peptone, 0.3% NaCl (all w/v), 1 mM CaCl₂, 1 mM MgSO₄, 25 mM KPO₄, 5 µg/ml cholesterol) seeded with the OP50 strain of *E.coli* bacteria (Brenner 1974). As wild type reference and for genomic engineering the N2 Bristol strain was used.

5.2.2 Generation of transgenic worms

5.2.2.1 CRISPR/Cas9-mediated generation of transgenic worms

CRISPR/Cas9-mediated gene engineering in *C. elegans* was performed using the recombinant Cas9 EnGen nuclease from *S. pyogenes* (NEB). Single guides RNAs (sgRNAs) for the Cas9 enzyme were designed using the CRISPOR.org web tool. sgRNAs and tracrRNA were received from Integrated DNA technologies. As co-injection marker sgRNAs targeting the *dpy-10* gene were used (Paix, Folkmann, and Seydoux 2017).

Injections were performed using the following mix: 1 μl Cas9 (3.2 $\mu\text{g}/\mu\text{l}$), 2.5 μl tracrRNA (4 $\mu\text{g}/\mu\text{l}$), 0.4 μl *dpy-10* sgRNA (8 $\mu\text{g}/\mu\text{L}$), 0.5 μl *F59B2.3* sgRNA (8 $\mu\text{g}/\mu\text{l}$), 0.25 μl KCl (1M), 0.375 μl HEPES pH7.4 (200mM), H₂O up to a total volume of 10 μl . For activation of the Cas9 enzyme the mix was incubated for 10 min at 37°C.

5.2.2.2 Microinjections of *C. elegans*

L4 larvae or young adults were placed on a 2% agarose pad with a 20 μl drop of halocarbon oil (Sigma-Aldrich). Microinjections of the CRISPR/Cas9 mix were performed using a Carl Zeiss Axio Imager Z1 microscope with a manual micromanipulator and a connected microinjector (Femtojet4). When the progeny of injected worms showed a *dpy* phenotype in the F1 generation, siblings of the same parental worm were singled and used for genotyping.

5.2.3 Developmental tunicamycin resistance assay

For developmental tunicamycin resistance assays, NGM plates supplemented with 0-8 $\mu\text{g}/\text{mL}$ tunicamycin (Merck Millipore) and control plates without tunicamycin were used (seeded with OP50 bacteria). Worms were synchronized by egg-lay and 30 eggs per genotype and/or condition were added to the plates. Development to the adult stage was scored after five days at 20°C.

5.3 Cell biological methods

5.3.1 Cell maintenance

AN3-12 mouse embryonic stem cells were cultured as previously described (Elling et al. 2011). In brief, DMEM high glucose (Sigma-Aldrich) was supplemented with glutamine, fetal bovine serum (15%), penicillin/streptomycin, non-essential amino acids, sodium pyruvate (all Thermo Fisher Scientific), β -mercaptoethanol and LIF (both Merck Millipore) and used to culture cells at 37°C in 5% CO₂ on non-coated tissue culture plates. For partial differentiation of diploid AN3-12 cells, cells were seeded at a density of 2000-3000 cells/6-well and incubated for 5 days in medium without LIF.

Neuro2a (N2a) mouse neuroblastoma cells (ATCC) and C2C12 (ATCC) cells were cultured in DMEM containing 4.5 g/l glucose supplemented with 10% fetal bovine serum and penicillin/streptomycin (all Thermo Fisher Scientific) at 37°C in 5% CO₂.

E14 mouse embryonic stem cells were kindly provided by the laboratory of Dr. Hisham Bazzi and cultured as described previously (Ju Lee et al. 2017). In short, cells were cultured on plates coated with 0.1% gelatin in Knockout™ DMEM (ThermoFisher Scientific) supplemented with HyClone™ fetal bovine serum (15%, VWR), L-glutamine, penicillin/streptomycin (Biochrom), sodium pyruvate, non-essential amino acids, β-mercaptoethanol (all from Thermo Fisher Scientific), LIF (Merck), and 2i (1 μM PD0325901 and 3 μM CHIR99021; Miltenyi Biotech).

5.3.2 Cell sorting

To maintain a haploid cell population cells were stained with 10 μg/ml Hoechst33342 (Thermo Fisher Scientific) for 30 min at 37°C, while shaking regularly to avoid cell attachment. To exclude dead cells propidium iodide (Sigma-Aldrich) staining was added. Cells were sorted for DNA content on a FACS Aria Fusion sorter and flow profiles were recorded with the FACSDiva software (BD Franklin Lakes). Cell sorting was performed by Kat Folz-Donahue and Lena Schumacher from the FACS and Imaging Core Facility (Max Planck Institute for Biology of Ageing, Cologne, Germany).

5.3.3 Cell viability assay (XTT)

Relative cell viability was assessed using the XTT cell proliferation Kit II (Roche) according to the manufacturer's instructions. Treatments with 0.5 μg/ml tunicamycin (Merck Millipore) were performed for 48h, starting 24h after cell seeding. XTT turnover was normalized to corresponding untreated control cells.

5.3.4 Insertional mutagenesis screening

5.3.4.1 Retroviral-based insertional mutagenesis and drug selection

The generation of a comprehensive cell bank of haploid AN3-12 cells, containing insertions in 16.970 mouse genes, was already created and described elsewhere (www.haplobank.at, (Elling et al. 2019)). In short, for retroviral library generation enhanced gene-trap (EGT) viruses carrying a neomycin-resistance cassette were packaged in PlatinumE (Cell Biolabs) cells. The virus was concentrated by centrifugation (25,000 r.p.m., 4°C, 4h) and haploid mESCs were infected for 8 h in the presence of 2 μg/ml polybrene. Upon infection for 30h, cells were treated with 0.2 mg/ml G418 (Gibco) for selection of gene-trap insertions. To estimate numbers of integrations 500.000 cells were plated on 15 cm dishes, selected for integrations using G418 selection and colonies

counted after 10 days. For comparison, 5.000 cells were plated without selection. From the barcoded AN3-12 Retro Library, 3 million cells were plated on 15 cm plates and drug selection was performed for 21 days starting 24h post mutagenesis using 0.5 $\mu\text{g/ml}$ tunicamycin (Merck Millipore).

5.3.4.2 Inverse PCR

Inverse PCR was performed for mapping of the genomic integration site upon insertional mutagenesis. The restriction enzyme NlaIII (or in a second parallel approach MseI) (NEB, R0525L and R0125L) were used for digestion of genomic DNA and fragments were purified using the QIAquick PCR Purification Kit (28106, Qiagen) (Figure 27).

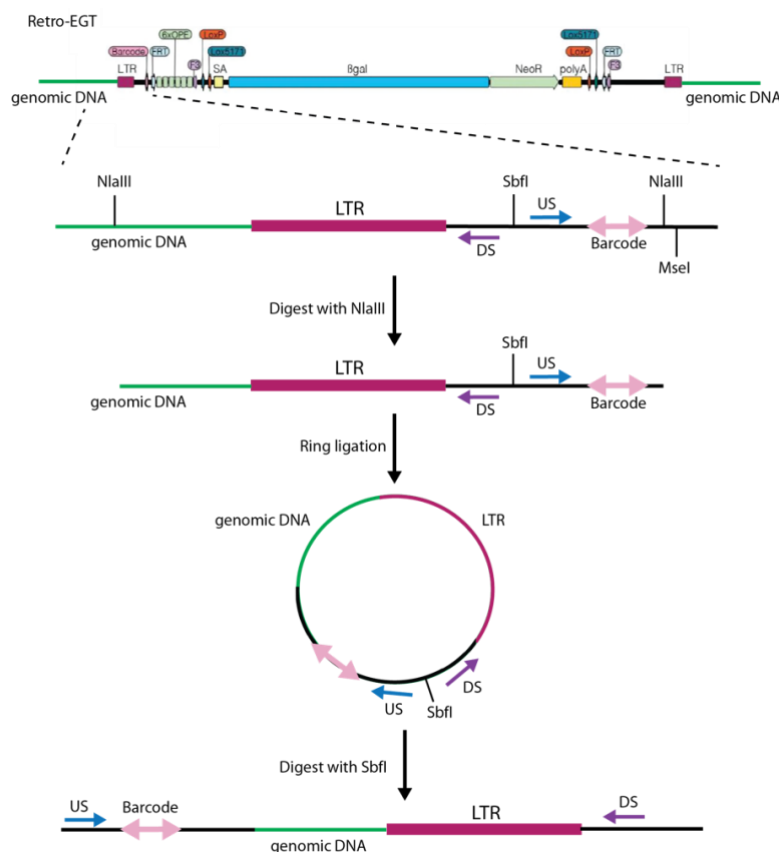


Figure 27: Schematic representation of library preparation for retroviral enhanced gene trap (Retro-EGT) vector integration sites. Detailed information and sequences are available on the Haplobank website (www.haplobank.at). Following random integration, the genomic DNA is fragmented by the E1 enzyme NlaIII. The gene trap start that contains the barcode and which is flanked by part of the genomic DNA is circularized (ring ligation). Prior to PCR amplification the plasmid is linearized by digestion with SbfI. Each integration site is mapped by a second E1 enzyme, which is MseI. The genomic region is then amplified by PCR using US and DS primers. (Modified from Elling et al., 2019)

The gene trap start containing the barcode and part of the flanking genomic DNA was circularized (T4 DNA ligase and buffer, Roche, 10716359001) at 16°C over night.

The ring ligate was re-linearized using SbfI (NEB, R0642L) and the genomic region was amplified using the primers “DS” (GAGCCAGAACCAGAAGGAACTTGAC) and “US” (GTGACTGGAGTTCAGACGTGTGCTCTTC). The PCR reaction was analyzed on an agarose gel, purified and used for Sanger Sequencing with primer “DS”. Sequences were analyzed manually with the USCS Genome Browser.

5.3.5 Chemical mutagenesis screening

5.3.5.1 Chemical-based mutagenesis and drug selection

For chemical mutagenesis cells were singled with trypsin (Thermo Fisher Scientific) and transferred to a 15 ml tube. Mutagenesis was performed in full medium for 2h at RT with 0.01 mg/ml Ethylnitrosourea (ENU). Then cells were washed five times with medium without LIF 5 before being transferred to a culture dish. Drug selection was performed for 21 days starting 24h post mutagenesis using 0.5 µg/ml tunicamycin (Merck Millipore).

5.3.5.2 Exome sequencing and analysis

The screening procedure and the data analysis were extensively described previously (Horn et al. 2018). After drug selection upon chemical mutagenesis, resistant clones were isolated and subjected to tunicamycin cytotoxicity assays. The genomic DNA was extracted using the Genra Puregene Tissue Kit (Qiagen). Paired end, 150 bp whole exome sequencing was performed on an Illumina Novaseq 6000 instrument after precapture-barcoding and exome capture with the Agilent SureSelect Mouse All Exon kit. For data analysis, raw reads were aligned to the reference genome mm9. Variants were identified and annotated using GATK (v.3.4.46) and snpEff (v.4.2). Tunicamycin resistance causing alterations were identified by allelism only considering variants with moderate or high effect on protein and a read coverage > 20.

5.3.6 Differentiation into neural progenitor cells (NPCs)

Diploid AN3-12 mESCs were used for embryoid body (EB) formation, induced using the hanging drop technique (13.500 cells per 27 µl drop) in ESCM without LIF for 48h. The EBs were transferred to untreated Petri dishes for further differentiation for 4 days in ESCM lacking LIF and the addition of 1 µM retinoic acid (Sigma-Aldrich, R2625), with exchange of the medium after 72h. On day 4 EBs were collected, trypsinized and plated for further experiments.

5.3.7 Colony formation assay (CFA)

Diploid AN3-12 mESCs were seeded at low density on uncoated 6-well tissue culture plates (2.500 cells/well for WT, 3.750 cells/well for AMDHD2 K.O. cells). The cells were grown at 37°C in 5% CO₂ in ESCM and in ESCM without LIF to force differentiation as control for reduced stem cell maintenance. The medium was replaced every other day and cells were grown for 5 days until colonies were formed. Colonies were collected for WB analysis or qPCR at this point or used for alkaline phosphatase staining. For staining colonies were washed with PBS and fixed with 2% PFA (in PBS, Sigma-Aldrich) for 2 min at RT. The cells were washed with PBS twice and colonies were stained using the Alkaline Phosphatase Detection Kit (SCR004, Sigma-Aldrich) according to manufacturer's instructions for 15 min in the dark. The wells were washed with PBS, air dried and scanned. 100 random colonies per genotype and condition were analyzed manually by grouping into "stem cell", "intermediate cell" or "differentiated cell" dependent on the staining intensity.

5.4 Molecular biological methods

5.4.1 Mouse genotyping

5.4.1.1 Isolation of mouse genomic DNA from ear clips

Ear clips were taken by the Comparative Biology Facility at the Max Planck Institute for Biology of Ageing (Cologne, Germany) at weaning age (3-4 weeks of age) and stored at -20°C until use. 150 µl ddH₂O and 150 µl directPCR Tail Lysis reagent (Peqlab) were mixed with 3 µl proteinase K (20 mg/ml in 25 mM Tris-HCl, 5 mM Ca₂Cl, pH 8.0, Sigma-Aldrich). This mixture was applied to the ear clips, which were then incubated at 56°C overnight (maximum 16 h) shaking at 300 rpm. Proteinase K was inactivated at 85°C for 45 min without shaking. The lysis reaction (2 µl) was used for genotyping PCR without further processing. For genotyping of mouse genomic DNA DreamTaq DNA polymerase (ThermoFisher Scientific) was used.

5.4.1.2 Genotyping PCR for the *Amdhd2* locus

For genotyping of mouse genomic DNA DreamTaq DNA polymerase (ThermoFisher Scientific) was used. PCR reactions were set up as follows:

Table 4: Composition of a DreamTaq PCR reaction mix.

Reagent	Volume (μ l)	Stock concentration
Template DNA	2	
Colored buffer	2.5	10x
dNTPs	0.6-1	10 mM each nt
Primer	1.25	20 μ M
DreamTaq	0.125	5 U/ μ l
ddH ₂ O	ad. 25	

Table 5: Cycling and temperature profiles of a mouse genotyping PCR.

Temperature ($^{\circ}$ C)	Time (s)	Action	Number of cycles
95	120	denaturation	1
95	30	denaturation	
64	30	annealing (T_A)	35
72	60	elongation	
72	600	final elongation	1

For amplification of the *Amdhd2* locus, the primers E4_fwd (TCTAGCTGTTTGGCCAAAGC) and E4_rev (AGAGACACACGGATGCCTTG) were used. These primers bind in the genomic region flanking the CRISPR/Cas9-mediated deletion. Therefore, the primers can be used to amplify the *Amdhd2* wildtype (675 bp) and the knockout allele (around 300 bp).

5.4.2 Worm genotyping

5.4.2.1 Single worm lysis

To obtain template DNA for genotyping, single worms were lysed in 10 μ l single worm lysis buffer containing: 10 mM Tris pH 8.3, 50mM KCl, 2.5 mM MgCl₂, 0.45% Tween 20, 0.45% Triton X-100 (all v/v), 1 mg/ml proteinase K (NEB). The worms were heated up for 60 min at 65 $^{\circ}$ C and subsequently 15 min at 95 $^{\circ}$ C for inactivation of the enzyme.

5.4.2.2 Genotyping PCR for the F59B2.3 locus

For genotyping of *C. elegans* genomic DNA Phusion DNA polymerase (ThermoFisher Scientific) was used. PCR reactions were set up as follows:

Table 6: Composition of a Phusion PCR reaction mix.

Reagent	Volume (μ l)	Stock concentration
Template DNA	5	
Colored HF buffer	2.5	10x
dNTPs	0.25	10 mM each nt
Primer	1.25	10 μ M
Phusion	0.5	5 U/ μ l
ddH ₂ O	ad. 25	

Table 7: Cycling and temperature profiles of a worm genotyping PCR for F59B2.3.

Temperature ($^{\circ}$ C)	Time (s)	Action	Number of cycles
95	120	denaturation	1
95	30	denaturation	
60	30	annealing (T _A)	35
72	60	elongation	
72	600	final elongation	1

For amplification of the exon 1 within the *F59B2.3* locus, the primers E1_fwd (CGTAGCTAAATAATATCTTGTGTG) and E1_rev (ACCTGAAATCCTAGCTTTAATAG) were used. These primers bind in the genomic region flanking the CRISPR/Cas9-mediated deletion. Therefore, the primers can be used to amplify the *F59B2.3* wildtype (549 bp) and the knockout allele (shorter product).

5.4.3 Gel electrophoresis

DNA fragments were separated in agarose gels (1-1.5% agarose in 1x TAE buffer: 40 mM Tris Base, 1 mM EDTA, 1.1 ml acetic acid, pH 8.0) using horizontal gel electrophoresis at 120 V and visualized with Roti®-GelStain (Carl Roth). The Quick-Load® 100 bp or 1 kb DNA Ladder (New England Biolabs) was used as a marker.

5.4.4 Gene editing and genotyping by Sanger sequencing

The specific GFAT1 G451E substitution as well as the K.O. of GFAT1 and AMDHD2 was engineered in AN3-12 cells (for the AMDHD2 K.O. also in N2a cells) using the CRISPR/Cas9 technology as described previously (Ran et al. 2013). Sequences for sgRNAs were designed online (<http://crispor.org>, Table 8), purchased from Sigma-Aldrich, and cloned into the Cas9-GFP expressing plasmid PX458 (Addgene #48138). Corresponding guide and Cas9 expressing plasmids were transfected for generation of gene knock outs or co-transfected with a single stranded DNA repair template (Integrated

DNA technologies) for SNV integration, using Lipofectamine 3000 (Thermo Fisher Scientific) according to manufacturer's instructions. GFP positive cells were singled using FACS Aria Fusion sorter and subjected to genotyping. DNA was extracted (DNA extraction solution, Epicentre Biotechnologies) and edited regions were specifically amplified by genotyping PCR (Table 8). Sanger sequencing was performed at Eurofins Genomics GmbH.

Table 8: Primer sequences for gene editing and genotyping of cells.

Primer	Sequence (5'→ 3')
msGFAT1_G451E_guide 1	GAGTCGGCAGTTCTATATCA
msGFAT1_G451E_guide 2	GGTGGGGATCACAAATACAGT
msAMDHD2_guide1	GTTTCATCAGCCGGGAAAAGCG
msAMDHD2_guide2	GCATTGGCTTCAAAGGAGCGG
msAMDHD2_guide3	GAGGAGCGGAGGTAGGCCTCG
msAMDHD2_guide4	GCTTTTCCCGGCTGATGAAT
msAMDHD2_guide5	GCCCTCCAAGTGCACCCCTGA
msGFAT1_G451E_repair template	GGCGAGACAGCTGACACCCTGATGGGACTTCGTT ACTGTAAGGAGAGAGGAGCCTTAACTGTGGGCAT CACTAATACAGTCGAAAAGTTCCATATCAAGAGAGA CAGATTGCGGGGTTTCATATTAATGCTGGTCCTGAG ATTGGCGTGGCCAGTACAAAG
msGFAT1_G451E_geno_fwd	AGTCGGTTGGTTTTTCGTGT
msGFAT1_G451E_geno_fev	ACTGCCCCACAGATCAGAGT
msAMDHD2_geno_fwd	GGCCTTCATCTTCAGCTCCT
msAMDHD2_geno_rev	TGAGATCAGTTTCTGCAGCAG

5.4.5 RNA isolation

Cells were collected in QIAzol (Qiagen) and snap frozen in liquid nitrogen. Samples were subjected to three freeze/thaw cycles (liquid nitrogen/ 37°C water bath) before addition of another half of the total QIAzol volume. After incubation for 5 min at RT, 200 µl chloroform were added per 1 ml QIAzol. Samples were vortexed, incubated for 2 min at RT, and centrifuged at 10.000 rpm and 4°C for 15 min. The aqueous phase was mixed with an equal volume of 70% ethanol and transferred to a RNeasy Mini spin column (Qiagen). The total RNA was isolated using the RNeasy Mini Kit (Qiagen).

5.4.6 Quantitative PCR (qPCR)

cDNA was generated using the iScript cDNA Synthesis Kit (Bio-Rad Laboratories). Quantitative PCR was performed using Power SYBR Green master mix (Applied Biosystems) on a ViiA 7 Real-Time PCR System (Applied Biosystems). GAPDH expression functioned as internal control. All used primers for qPCR analysis are listed in Table 9 below.

Table 9: Primer sequences for quantitative PCR.

Primer	Sequence (5'→ 3')
msGAPDH_fwd	GGCATGGACTGTGGTCATGAG
msGAPDH_rev	TGCACCACCAACTGCTTAGC
msGfat1_fwd	AAAGGAAGCTGCGGTCTTTCCC
msGfat1_rev	GTGTGCTCTATCACGGCACTTG
msGfat2_fwd	CTACAGAACAGGAGACAAGAGATC
msGfat2_rev	GTTATATCCCCGTCCCATCAC
msAmdhd2_fwd	CTTGCGCCCAAAGCTTG
msAmdhd2_rev	ACCCACAGATCCTCCCTG
msNanog_fwd	ATGAAGTGCAAGCGGTGGCAGAAA
msNanog_rev	CCTGGTGGAGTCACAGAGTAGTTC
msKlf4_fwd	ACAGGCGAGAAACCTTACCACTGT
msKlf4_rev	GCCTCTTCATGTGTAAGGCAAGGT
msSox2_fwd	AAAAACCACCAATCCCATCCA
msSox2_rev	CGAAGCGCCTAACGTACCAC
msOct4_fwd	CCTACAGCAGATCACTCACATCGCC
msOct4_rev	CCTGTAGCCTCATACTCTTCTCGTTGG
msNestin_fwd	GCCTATAGTTCAACGCCCCC
msNestin_rev	AGACAGGCAGGGCTAGCAAG
ceF59B2.3_fwd	CGAAACTTGATGGGACAAATACG
ceF59B2.3_rev	CATCACTAACACCGAGCAGG
ceCdc-42_fwd	CTGCTGGACAGGAAGATTACG
ceCdc-42_rev	CTCGGACATTCTCGAATGAAG

5.5 Biochemical methods

5.5.1 Immunoblot analysis

Protein concentration of cell lysates was determined using the Pierce™ BCA protein assay kit according to manufacturer's instructions (ThermoFisher Scientific). Samples were adjusted in 5x LDS sample buffer containing 50 mM DTT. After boiling and a sonication step, equal protein amounts were subjected to SDS-PAGE and blotted on a nitrocellulose membrane using the Trans-Blot Turbo Transfer system (BioRad). All antibodies were used in 5% low-fat milk or 5% BSA in TBS-Tween. After incubation with HRP-conjugated secondary antibody, the blot was developed using ECL solution (Merck Millipore) on a ChemiDoc MP Imaging System (BioRad).

The following antibodies were used in this study: GFAT1 (rb, EPR4854, Abcam ab125069, 1:1000), GFAT2 (rb, Abcam, ab190966, 1:5000), O-Linked N-Acetylglucosamine Antibody (ms, clone RL2, MABS157, Merck, 1:1000), AMDHD2 (ms, S6 clone, in-house produced, 1:500), α -TUBULIN (ms, clone B-5-1-2, Sigma-Aldrich T9026, 1:5000), rabbit IgG (gt, HRP-conjugated, G21234, Thermo Fisher, 1:5000), and mouse IgG (gt, HRP-conjugated, G21040, Thermo Fisher, 1:5000).

5.5.2 LC-MS/MS and IC-MS/MS analysis

Two different approaches were applied for the analysis of UDP-HexNAc levels (5.5.2.1) or separated measurements of UDP-GlcNAc and UDP-GalNAc (5.5.2.2).

5.5.2.1 Determination of UDP-HexNAc levels

For measurement of UDP-HexNAc levels, cells were trypsinized and collected. The pellet was washed once with PBS and snap frozen in liquid nitrogen. 250 μ l ddH₂O were added to the pellet and the samples were vortexed for 30 s. The samples were subjected to four freeze/ thaw cycles (liquid nitrogen/ 37 °C water bath). Next, the protein concentration was measured using the Pierce™ BCA protein assay kit (ThermoFisher Scientific). 200 μ l with a protein concentration of 1 μ g/ μ l were mixed with 1 ml chloroform:methanol (1:2) and incubated on a nutator mixer for 1 h at RT. After centrifugation for 5 min at full speed, the supernatant was transferred to a glass vial. The liquid was evaporated in an EZ-2 Plus Genevac centrifuge evaporator (SP Scientific) with the following settings: time to final stage 15 min, final stage time 4 h, low boiling point mixture. After evaporation, the samples were stored at -20°C until further use. Absolute UDP-HexNAc levels were determined

using an Acquity UPLC connected to a Xevo TQ Mass Spectrometer (both Waters) and normalized to total protein content. The measurements and subsequent analysis were performed by Yvonne Hinze from the Metabolomics Core Facility at the Max Planck Institute for Biology of Ageing (Cologne, Germany) as previously described (Denzel et al. 2014).

5.5.2.2 Determination of UDP-GlcNAc and UDP-GalNAc levels

Separated measurement of UDP-GlcNAc and UDP-GalNAc was performed by anion exchange chromatography mass spectrometry (IC-MS) analysis. Cells were subjected to methanol:acetonitrile:mili-Q ultrapure water (40:40:20 [v:v:v]) extraction. UDP-GlcNAc and UDP-GalNAc concentrations were measured using IC-MS analysis. Extracted metabolites were re-suspended in 500 μ l of Optima LC/MS grade water (Thermo Fisher Scientific) of which 100 μ l were transferred to polypropylene autosampler vials (Chromatography Accessories Trott, Germany). The samples were analyzed using a Dionex ionchromatography system (ICS5000, Thermo Fisher Scientific) connected to a triple quadrupole MS (Waters, TQ). In brief, 10 μ l of the metabolite extract were injected in full loop mode using an overfill factor of 3, onto a Dionex IonPac AS11-HC column (2 mm \times 250 mm, 4 μ m particle size, Thermo Scientific) equipped with a Dionex IonPac AG11-HC guard column (2 mm \times 50 mm, 4 μ m, Thermo Scientific). The column temperature was held at 30°C, while the auto sampler was set to 6°C. The metabolite separation was carried using a KOH gradient at a flow rate of 380 μ l/min, applying the following gradient conditions: 0-8 min, 30-35 mM KOH; 8-12 min, 35-100 mM KOH; 12-15 min, 100 mM KOH, 15-15.1 min, 10 mM KOH. The column was re-equilibrated at 10 mM for 4 min. UDP-HexNAcs were detected using multiple reaction monitoring (MRM) mode with the following settings: capillary voltage 2.7 kV, desolvation temperature 550°C, desolvation gas flow 800 l/h, collision cell gas flow 0.15 ml/min. The transitions for UDP-GalNAc, as well as for UDP-GlcNAc were m/z 606 [M-H⁺]⁺ for the precursor mass and m/z 385 [M-H⁺]⁺ for the first and m/z 282 [M-H⁺]⁺ for the second transition mass. The cone voltage was set to 46V and the collision energy was set to 22V. UDP-GalNAc eluted at 10.48 min and UDP-GlcNAc eluted at 11.05 min. MS data analysis was performed using the TargetLynx Software (Version 4.1, Waters). Absolute compound concentrations were calculated from response curves of differently diluted authentic standards treated and extracted as the samples.

5.5.3 Protein expression and purification

5.5.3.1 Expression and purification of human AMDHD2

A pET28a(+)-AMDHD2 plasmid was purchased from BioCat (Heidelberg, Germany), where human AMDHD2 isoform 1 was integrated in pET28a(+) using NdeI and HindIII restriction sites. This vector was used to recombinantly express human AMDHD2 isoform 1 with N-terminal His₆ tag and a thrombin cleavage site under the control of the T7 promoter in BL21 (DE3) *E. coli*. LB cultures were incubated at 37°C and 180 rpm until an OD₆₀₀ of 0.4-0.6 was reached. Then, protein expression was induced by addition of 0.5 mM isopropyl-β-D-1-thiogalactopyranosid (IPTG) and incubated for 20-22 h at 20°C and 180 rpm. Cultures were harvested and pellets stored at -80°C. The purification buffers were modified from Bergfeld *et al.* (Bergfeld *et al.* 2012). *E. coli* were lysed in 50 mM Tris/HCl pH 7.5, 100 mM NaCl, 20 mM imidazole, 1 mM Tris(2-carboxyethyl) phosphin (TCEP) with complete EDTA-free protease inhibitor cocktail (Roche) and 10 µg/ml DNaseI (Sigma-Aldrich) by sonication. The lysate was clarified by centrifugation and the supernatant loaded on Ni-NTA Superflow affinity resin (Qiagen). The resin was washed with wash buffer (50 mM Tris-HCl, 100 mM NaCl, 50 mM imidazole, 1 mM TCEP; pH 7.5) and the protein was eluted with wash buffer containing 250 mM imidazole. The His₆-tag was proteolytically removed using 5 Units of thrombin (Sigma-Aldrich) per mg protein overnight at 4°C. AMDHD2 was further purified according to its size on a HiLoad™ 16/60 Superdex™ 200 prep grade preppacked column (GE Healthcare) using an ÄKTAprime chromatography system at 4°C with a SEC buffer containing 50 mM Tris-HCl, 100 mM NaCl, 1 mM TCEP, 5 % glycerol; pH 7.5.

5.5.3.2 Expression and purification of human GFAT1 and GFAT2

Sf21 (DSMZ, ACC 119) insect cells were used for hGFAT1 and hGFAT2 expression. Suspension cultures were maintained in SFM4Insect™ HyClone™ medium with glutamine (GE Lifesciences) in shaker flasks at 27°C and 90 rpm in an orbital shaker. GFAT1 and GFAT2 were expressed in *Sf21* cells using the MultiBac baculovirus expression system (Berger, Fitzgerald, and Richmond 2004). In short, GFAT was integrated into the baculovirus genome via Tn7 transposition and maintained as bacterial artificial chromosome in DH10EMBacY *E. coli* cells. Recombinant baculoviruses were generated by transfection of *Sf21* with bacmid DNA. The generated baculoviruses were used for protein expression in *Sf21* cells.

Sf21 cells were lysed by sonication in lysis buffer (50 mM Tris/HCl pH 7.5, 200 mM NaCl, 10 mM Imidazole, 2 mM TCEP, 0.5 mM Na₂Frc6P, 10% (v/v) glycerol) supplemented with complete EDTA-free protease inhibitor cocktail (Roche) and 10 µg/ml DNaseI (Sigma-Aldrich). Upon removal of cell debris and protein aggregates by centrifugation, the supernatant was loaded on a Ni-NTA Superflow affinity resin (Qiagen). The resin was washed with lysis buffer and the protein eluted with lysis buffer containing 200 mM imidazole. The proteins were further purified according to their size on a HiLoad™ 16/60 Superdex™ 200 prep grade preppacked column (GE Healthcare) using an ÄKTAprime chromatography system at 4°C with a SEC buffer containing 50 mM Tris/HCl, pH 7.5, 2 mM TCEP, 0.5 mM Na₂Frc6P, and 10% (v/v) glycerol.

5.5.3.3 Expression and purification of human GNA1

The expression plasmid for human N-terminally His₆-tagged GNA1 was cloned as described previously (Ruegenberg et al. 2020b). In short, human GNA1 was expressed in Rosetta (DE3) *E. coli* cells. LB cultures were incubated at 37°C and 180 rpm until an OD₆₀₀ of 0.4-0.6 was reached. Upon induction of protein expression by addition of 0.5 mM IPTG and incubation for 3 h at 37°C and 180 rpm, cultures were harvested and pellets stored at -80°C until further processing. Human GNA1 purification protocol was based on the protocol of Hurtado-Guerrero et al. (Hurtado-Guerrero et al. 2008) with small modifications. *E. coli* were lysed by sonication in 50 mM HEPES/NaOH pH 7.2, 500 mM NaCl, 10 mM imidazole, 2 mM 2-mercaptoethanol, 5% (v/v) glycerol with complete EDTA-free protease inhibitor cocktail (Roche) and 10 µg/ml DNaseI (Sigma-Aldrich). The lysate was clarified by centrifugation and the supernatant loaded on Ni-NTA Superflow affinity resin (Qiagen). The resin was washed with wash buffer (50 mM HEPES/NaOH pH 7.2, 500 mM NaCl, 50 mM imidazole, 5% (v/v) glycerol) and the protein was eluted with wash buffer containing 250 mM imidazole. Eluted protein was dialyzed against storage buffer (20 mM HEPES/NaOH pH 7.2, 500 mM NaCl, 5% (v/v) glycerol).

5.5.4 Site-directed mutagenesis

The AMDHD2 mutations were introduced into the pET28a(+)-AMDHD2 plasmid by site-directed mutagenesis as described previously (Zheng, Baumann, and Reymond 2004) (mutagenesis primers are listed in Table 10). The same protocol was used to integrate an internal His₆-tag between Ser300 and Asp301 in human GFAT2 in the plasmid FLAG-HA-hGFAT2-pcDNA3.1 (pcDNA™3.1(+), ThermoFisher Scientific

#V79020). This position is equivalent to the internal His₆-tag in human GFAT1, which does not interfere with GFAT kinetic properties (Richez et al. 2007). The GFAT2 gene with internal His₆-tag was subsequently subcloned into the pFL vector for the generation of baculoviruses using XbaI and HindIII entry sites.

Table 10: Primer sequences used for site-directed mutagenesis. Mutation sites are indicated by big letters.

Primer	Sequence (5'→ 3')
hAMDHD2_I38T_fwd	ggccgca CT tggaccagagaagc
hAMDHD2_I38T_rev	gggtccaaagtg CG gcctccgcgca
hAMDHD2_G102D_fwd	tgcacg Ac gtcacctcctctgcc
hAMDHD2_G102D_rev	gaggtgacgt CG tgacaggatcc
hAMDHD2_G130R_fwd	aagagt CG tggtcccatggggcag
hAMDHD2_G130R_rev	tggggaccacgact CT tacagggga
hAMDHD2_L142F_fwd	ctgcac Tt Cgagggcccctcatca
hAMDHD2_L142F_rev	gggccctcgaag GC agcccgagga
hAMDHD2_F146L_fwd	ggcccct Gat cagccgggagaagc
hAMDHD2_F146L_rev	cggctgatcaagggg CC ctccaggt
hAMDHD2_A154P_fwd	gggc Cc Acaccccgaggcccacct
hAMDHD2_A154P_rev	tcgggg Tg tgggccccgcttctccc
hAMDHD2_T185A_fwd	atcgt Gc Tctggcccagagttgg
hAMDHD2_T185A_rev	ggggccagagccac GC gatgcggacat
hAMDHD2_S208T_fwd	tgcgt Ac Tctagggcactcagtgg
hAMDHD2_S208T_rev	tgcc ct agagtcacgcagatgccac
hAMDHD2_G226E_fwd	tggag CG Aagccacctcatcacc
hAMDHD2_G226E_rev	aaggtgg ct cgctccacacagcat
hAMDHD2_G265V_for	ttctat GC atgattgcagatggcacgc
hAMDHD2_G265V_rev	gcaatcatgacatagaagatgcagcggc
hAMDHD2_G265R_fwd	ttctat Cg Tatgattgcagatggcacgc
hAMDHD2_G265R_rev	gcaatc at acgatagaagatgcagcggc
hAMDHD2_D294A_fwd	gtcacc gC tgccatccctgcc
hAMDHD2_D294A_rev	ggca Gc ggtgaccagcaccag
hGFAT2-300-His6_SDM	cgctcggccag TCAT CACCATCACCATCACgatgacc catctc gag ccatccagacctgcagatggaac

5.5.5 Enzyme activity assays

5.5.5.1 GlcN6P production of AMDHD2

The deacetylase activity of AMDHD2 was determined by following the cleavage of the amide/peptide bond of GlcNAc6P at 205 nm in UV transparent 96-well microplates (F-bottom, Brand #781614). The assay mix contained 1 mM GlcNAc6P in 50 mM Tris-HCl pH 7.5 and was pre-warmed for 10 min at 37 °C in the plate reader. The reaction was started by adding 20 pmol AMDHD2 and was monitored several minutes at 37°C. The initial reaction rates (0-1 min) were determined by Excel (Microsoft) and the amount of consumed GlcNAc6P was calculated from a GlcNAc6P standard curve. All measurements were performed in duplicates. For the analysis of the impact of several divalent metal ions on the activity of AMDHD2, the protein was incubated for 10 min with 0.1 μM EDTA and afterwards 10 μM divalent was added to potentially restore activity.

5.5.5.2 GNA1 and GNA1-coupled activity assays

The activity of human GNA1 was measured in 96-well standard microplates (F-bottom, BRAND #781602) as described previously (Li, Lopez, et al. 2007). For kinetic measurements, a buffer containing 0.5 mM Ac-CoA, 0.5 mM DTNB, 1 mM EDTA, 50 mM Tris/HCl pH 7.5 and varying concentrations of D-GlcN6P was used. Plates were pre-warmed at 37°C before reactions were initiated by addition of GNA1. The absorbance was measured continuously at 412 nm at 37°C in a microplate reader. The amount of produced TNB, matches with the CoA production and was calculated with $\epsilon_{(412 \text{ nm, TNB})} = 13800 \text{ l} \cdot \text{mol}^{-1} \cdot \text{cm}^{-1}$. Typically, GNA1 preparations showed a K_m of 0.2 ± 0.1 mM and a k_{cat} of $41 \pm 8 \text{ sec}^{-1}$.

GFAT's D-GlcN6P production was measured by a GNA1-coupled activity assay following the consumption of AcCoA at 230 nm in UV transparent 96-well microplates (F-bottom, Brand #781614) as described by Li et al. (Li, Lopez, et al. 2007). In brief, the used buffer contains 10 mM L-Gln, 0.1 mM AcCoA, 50 mM Tris/HCl pH 7.5, 2 μg hGNA1 and varying concentrations of Frc6P. The plates were pre-warmed at 37°C for 4 min and reactions were induced by adding L-Gln. Activity was monitored continuously at 230 nm and 37°C in a microplate reader. The amount of consumed AcCoA was calculated with $\epsilon_{(230 \text{ nm, AcCoA})} = 6436 \text{ l} \cdot \text{mol}^{-1} \cdot \text{cm}^{-1}$. As UDP-GlcNAc absorbs light at 230 nm, the GNA1-coupled assay cannot be used to analyze UDP-GlcNAc effects on activity.

5.5.5.3 GDH-coupled activity assay and UDP-GlcNAc inhibition

For measurement of GFAT's amidohydrolysis activity a coupled enzymatic assay using bovine glutamate dehydrogenase (GDH, Sigma-Aldrich G2626) in 96-well microplates (F-bottom, BRAND #781602) was used as previously described (Richez et al. 2007) with small modifications. In brief, the reaction buffer contained 6 mM Frc6P, 1 mM APAD, 1 mM EDTA, 50 mM KCl, 100 mM potassium-phosphate buffer pH 7.5, 6.5 U GDH per 96 well and for L-Gln kinetics varying concentrations of L-Gln. For UDP-GlcNAc inhibition assays the L-Gln concentration was kept at 10 mM. After pre-warming of plates at 37°C for 10 min, the reaction was started by enzyme addition and the absorbance monitored continuously at 363 nm in a microplate reader. The amount of formed APADH was calculated with $\epsilon_{(363 \text{ nm, APADH})} = 9100 \text{ l} \cdot \text{mol}^{-1} \cdot \text{cm}^{-1}$. Reaction rates were calculated with Excel (Microsoft) and K_m , v_{max} , and IC_{50} were obtained from Michaelis Menten or dose response curves, which were fitted by Prism 8 software (Graphpad).

5.5.6 Generation of anti-AMDHD2 antibody

To generate monoclonal antibodies directed against AMDHD2, His-tagged human AMDHD2 was expressed in *Escherichia coli*, affinity purified, and used for immunization of eight-week-old male Balb/cJRj mice. The first immunization with 80 μg of recombinant protein was enhanced by Freund's complete adjuvant; subsequent injections used 40 μg protein with Freund's incomplete adjuvant. After multiple immunizations, the serum of the mice was tested for immunoreaction by enzyme-linked immunosorbent assay (ELISA) with the recombinant His-hAMDHD2 protein. In addition, the serum was used to stain immunoblots with lysates of HEK293T cells overexpressing FLAG-HA-hAMDHD2. After this positive testing, cells from the popliteal lymph node were fused with mouse myeloma SP2/0 cells by a standard fusion protocol. Monoclonal hybridoma lines were characterized, expanded, and subcloned according to standard procedures (Köhler and Milstein 1975). Initial screening of clones was performed by ELISA with recombinant His-AMDHD2 protein and immunoblots using FLAG-HA-hAMDHD2 overexpressed in HEK293T cells. Isotyping of selected clones was performed with Pierce Rapid Isotyping Kit (Thermo Scientific, #26179). Final validation of antibody specificity was done by immunoblots of WT N2a cells compared to cells overexpressing FLAG-HA-hAMDHD2 and AMDHD2 K.O. cells.

5.5.7 Human AMDHD2 crystallization and crystal soaking

Human AMDHD2 was co-crystallized with a 1.25x ratio (molar) of ZnCl₂ at a concentration of 9 mg/ml in sitting-drops by vapor diffusion at 20°C. Intergrown crystal plates formed in the PACT *premier*[™] HT-96 (Molecular Dimensions) screen in condition H5 with a reservoir solution containing 0.1 M bis-tris propane pH 8.5, 0.2 M sodium nitrate, and 20% (w/v) PEG3350. In an optimization screen, the concentration of PEG3350 was constant at 20 % (w/v), while the pH value of bis-tris propane and the concentration of sodium nitrate were varied. The drops were set up in 1.5 µl protein solution to 1.5 µl precipitant solution and 2 µl protein solution to 1 µl precipitant solution. Best crystals were obtained with a drop ratio of 2 µl protein solution to 1 µl precipitant solution at 0.1 M bis tris propane pH 8.25, 0.25 M sodium nitrate, and 20% (w/v) PEG3350. 5 mM GlcN6P in reservoir solution was soaked into the crystals for 2 to 24h. For crystal harvesting, the intergrown plates were separated with a needle and 15% glycerol was used as cryoprotectant.

5.6 Data collection and refinement

X-ray diffraction measurements were performed at beamline P13 at PETRA III, DESY, Hamburg (Germany) and beamline X06SA at the Swiss Light Source, Paul Scherrer Institute, Villigen (Switzerland). The diffraction images were processed by XDS (Kabsch 2010). The structure of human AMDHD2 was determined by molecular replacement (Hoppe 1957; Huber 1965) with phenix.phaser (McCoy 2007; Adams et al. 2010) using the models of *B. subtilis* AMDHD2 (PDB 2VHL) as search model. The structures were further manually built using COOT (Emsley et al. 2010) and iterative refinement rounds were performed using phenix.refine (Adams et al. 2010). The structure of GlcN6P soaked crystals was solved by molecular replacement using our human AMDHD2 structure as search model. Geometry restraints for GlcN6P was generated with phenix.elbow software (Adams et al. 2010). Structures were visualized using PyMOL (Schrödinger) and 2D ligand-protein interaction diagrams were generated using LigPlot+ (Laskowski and Swindells 2011).

5.7 Data availability

Structural data reported in this study have been deposited in the Protein Data Bank with the accession codes 7NUT [<https://doi.org/10.2210/pdb7NUT/pdb>] and 7NUU [<https://doi.org/10.2210/pdb7NUU/pdb>].

5.8 Alignments

Following UniProt IDs were used for the protein sequence alignment of AMDHD2: *Homo sapiens* isoform 1: Q9Y303-1, *Mus musculus*: Q8JZV7, *Caenorhabditis elegans*: P34480, *Candida albicans*: Q9C0N5, *Escherichia coli*: P0AF18, *Bacillus subtilis*: O34450. Following UniProt IDs were used for the protein sequence alignment of hGFAT1 and hGFAT2: *Homo sapiens* GFAT1 isoform 2: Q06210-2 and *Homo sapiens* GFAT2 isoform 1: O94808-1.

ClustalOmega (<https://www.ebi.ac.uk/Tools/msa/clustalo/>) was used to perform sequence alignments of GFAT and AMDHD2 (Sievers et al. 2011). These alignments were formatted with the ESPript3 server (esript.ibcp.fr/) (Robert and Gouet 2014) and further modified.

5.9 Statistical analysis

Data are presented as mean \pm SEM or mean \pm SD. Biological replicates represent different passages of the cells that were seeded on independent days. Statistical significance was calculated using GraphPad Prism 9 (GraphPad Software). The statistical tests that were used are specified in the respective figure legend. Significance levels are * $p < 0.05$, ** $p < 0.01$, *** $p < 0.001$ versus the respective control.

5.10 Software

Most graphs were generated using the program GraphPad Prism 9 (GraphPad Software). For Western blot analysis, the intensity of the bands was quantified using the Image Lab 6 software (BioRad). Flow profiles were recorded and exported with the FACSDiva™ software (BD Biosciences).

References

- Abdel Rahman, Anas M, Michael Ryczko, Judy Pawling, and James W Dennis. 2013. 'Probing the hexosamine biosynthetic pathway in human tumor cells by multitargeted tandem mass spectrometry', *ACS chemical biology*, 8: 2053-62.
- Adams, P. D., P. V. Afonine, G. Bunkoczi, V. B. Chen, I. W. Davis, N. Echols, J. J. Headd, L. W. Hung, G. J. Kapral, R. W. Grosse-Kunstleve, A. J. McCoy, N. W. Moriarty, R. Oeffner, R. J. Read, D. C. Richardson, J. S. Richardson, T. C. Terwilliger, and P. H. Zwart. 2010. 'PHENIX: a comprehensive Python-based system for macromolecular structure solution', *Acta Crystallogr D Biol Crystallogr*, 66: 213-21.
- Aghazadeh-Habashi, Ali, and Fakhreddin Jamali. 2011. 'The glucosamine controversy; a pharmacokinetic issue', *Journal of Pharmacy & Pharmaceutical Sciences*, 14: 264-73.
- Ahangar, M. S., C. M. Furze, C. S. Guy, C. Cooper, K. S. Maskew, B. Graham, A. D. Cameron, and E. Fullam. 2018. 'Structural and functional determination of homologs of the Mycobacterium tuberculosis N-acetylglucosamine-6-phosphate deacetylase (NagA)', *J Biol Chem*, 293: 9770-83.
- Akella, Neha M., Lorela Ciraku, and Mauricio J. Reginato. 2019. 'Fueling the fire: emerging role of the hexosamine biosynthetic pathway in cancer', *BMC Biol*, 17: 52.
- Akimoto, Y, LK Kreppel, H Hirano, and Gerald Warren Hart. 2000. 'Increased O-GlcNAc transferase in pancreas of rats with streptozotocin-induced diabetes', *Diabetologia*, 43: 1239-47.
- Akimov, V., I. Barrio-Hernandez, S. V. F. Hansen, P. Hallenborg, A. K. Pedersen, D. B. Bekker-Jensen, M. Puglia, S. D. K. Christensen, J. T. Vanselow, M. M. Nielsen, I. Kratchmarova, C. D. Kelstrup, J. V. Olsen, and B. Blagoev. 2018. 'UbiSite approach for comprehensive mapping of lysine and N-terminal ubiquitination sites', *Nat Struct Mol Biol*, 25: 631-40.
- Al-Mukh, H., L. Baudoin, A. Bouaboud, J. L. Sanchez-Salgado, N. Maraqa, M. Khair, P. Pagesy, G. Bismuth, F. Niedergang, and T. Issad. 2020. 'Lipopolysaccharide Induces GFAT2 Expression to Promote O-Linked β -N-Acetylglucosaminylation and Attenuate Inflammation in Macrophages', *J Immunol*, 205: 2499-510.
- Allmeroth, K., M. Horn, V. Kroef, S. Mieth, R. U. Müller, and M. S. Denzel. 2020. 'Bortezomib resistance mutations in PSMB5 determine response to second-generation proteasome inhibitors in multiple myeloma', *Leukemia*.
- Allmeroth, Kira. 2021. 'Metabolic control of hair follicle stem cell fate decisions', University of Cologne.
- Álvarez-Añorve, Laura I., Diego A. Alonzo, Rodrigo Mora-Lugo, Samuel Lara-González, Ismael Bustos-Jaimes, Jacqueline Plumbridge, and Mario L. Calcagno. 2011. 'Allosteric kinetics of the isoform 1 of human glucosamine-6-phosphate deaminase', *Biochimica et Biophysica Acta (BBA) - Proteins and Proteomics*, 1814: 1846-53.
- Andres, Lissette M., Ian W. Blong, Angela C. Evans, Neil G. Rumachik, Teppei Yamaguchi, Nam D. Pham, Pamela Thompson, Jennifer J. Kohler, and Carolyn R. Bertozzi. 2017. 'Chemical Modulation of Protein O-GlcNAcylation via OGT Inhibition Promotes Human Neural Cell Differentiation', *ACS chemical biology*, 12: 2030-39.
- Apweiler, Rolf, Henning Hermjakob, and Nathan Sharon. 1999. 'On the frequency of protein glycosylation, as deduced from analysis of the SWISS-PROT database', *Biochimica et Biophysica Acta (BBA)-General Subjects*, 1473: 4-8.
- Araujo, Lindsey, Phillip Khim, Haik Mkhikian, Christie-Lynn Mortales, and Michael Demetriou. 2017. 'Glycolysis and glutaminolysis cooperatively control T cell function by limiting metabolite supply to N-glycosylation', *eLife*, 6: e21330.
- Arnold, C. S., G. V. Johnson, R. N. Cole, D. L. Dong, M. Lee, and G. W. Hart. 1996. 'The microtubule-associated protein tau is extensively modified with O-linked N-acetylglucosamine', *J Biol Chem*, 271: 28741-4.

- Arnold, Carrie N, Michael J Barnes, Michael Berger, Amanda L Blasius, Katharina Brandl, Ben Croker, Karine Crozat, Xin Du, Celine Eidschenk, and Philippe Georgel. 2012. 'ENU-induced phenovariance in mice: inferences from 587 mutations', *BMC research notes*, 5: 1-14.
- Arreola, R., B. Valderrama, M. L. Morante, and E. Horjales. 2003. 'Two mammalian glucosamine-6-phosphate deaminases: a structural and genetic study', *FEBS Lett*, 551: 63-70.
- Azuara, Véronique, Pascale Perry, Stephan Sauer, Mikhail Spivakov, Helle F Jørgensen, Rosalind M John, Mina Gouti, Miguel Casanova, Gary Warnes, and Matthias Merkenschlager. 2006. 'Chromatin signatures of pluripotent cell lines', *Nature Cell Biology*, 8: 532-38.
- Bacigalupa, Zachary A., Chaitali H. Bhadiadra, and Mauricio J. Reginato. 2018. 'O-GlcNAcylation: key regulator of glycolytic pathways', *Journal of Bioenergetics and Biomembranes*, 50: 189-98.
- Banner, D. W., A. C. Bloomer, G. A. Petsko, D. C. Phillips, C. I. Pogson, I. A. Wilson, P. H. Corran, A. J. Furth, J. D. Milman, R. E. Offord, J. D. Priddle, and S. G. Waley. 1975. 'Structure of chicken muscle triose phosphate isomerase determined crystallographically at 2.5Å resolution: using amino acid sequence data', *Nature*, 255: 609-14.
- Bardor, M., D. H. Nguyen, S. Diaz, and A. Varki. 2005. 'Mechanism of uptake and incorporation of the non-human sialic acid N-glycolylneuraminic acid into human cells', *J Biol Chem*, 280: 4228-37.
- Bartsch, Deniz, Kaustubh Kalamkar, Gaurav Ahuja, Hisham Bazzi, Argyris Papantonis, and Leo Kurian. 2021. 'Translational specialization in pluripotency by RBPMS poises future lineage-decisions', *bioRxiv*: 2021.04.12.439420.
- Bauche, S., G. Vellieux, D. Sternberg, M. J. Fontenille, E. De Bruyckere, C. S. Davoine, G. Brochier, J. Messeant, L. Wolf, M. Fardeau, E. Lacene, N. Romero, J. Koenig, E. Fournier, D. Hantai, N. Streichenberger, V. Manel, A. Lacour, A. Nadaj-Pakleza, S. Sukno, F. Bouhour, P. Laforet, B. Fontaine, L. Strohlic, B. Eymard, F. Chevessier, T. Stojkovic, and S. Nicole. 2017. 'Mutations in GFPT1-related congenital myasthenic syndromes are associated with synaptic morphological defects and underlie a tubular aggregate myopathy with synaptopathy', *J Neurol*, 264: 1791-803.
- Behrens, Nicolás H., and Luis F. Leloir. 1970. 'Dolichol Monophosphate Glucose: An Intermediate in Glucose Transfer in Liver', *Proceedings of the National Academy of Sciences of the United States of America*, 66: 153-59.
- Bennett, Eric P, Ulla Mandel, Henrik Clausen, Thomas A Gerken, Timothy A Fritz, and Lawrence A Tabak. 2012. 'Control of mucin-type O-glycosylation: a classification of the polypeptide GalNAc-transferase gene family', *Glycobiology*, 22: 736-56.
- Berger, I., D. J. Fitzgerald, and T. J. Richmond. 2004. 'Baculovirus expression system for heterologous multiprotein complexes', *Nat Biotechnol*, 22: 1583-7.
- Bergfeld, A. K., O. M. Pearce, S. L. Diaz, T. Pham, and A. Varki. 2012. 'Metabolism of vertebrate amino sugars with N-glycolyl groups: elucidating the intracellular fate of the non-human sialic acid N-glycolylneuraminic acid', *J Biol Chem*, 287: 28865-81.
- Birsoy, K., T. Wang, R. Possemato, O. H. Yilmaz, C. E. Koch, W. W. Chen, A. W. Hutchins, Y. Gultekin, T. R. Peterson, J. E. Carette, T. R. Brummelkamp, C. B. Clish, and D. M. Sabatini. 2013. 'MCT1-mediated transport of a toxic molecule is an effective strategy for targeting glycolytic tumors', *Nat Genet*, 45: 104-8.
- Blair, Kathryn, Jason Wray, and Austin Smith. 2011. 'The liberation of embryonic stem cells', *PLoS Genet*, 7: e1002019.
- Boehmelt, G., I. Fialka, G. Brothers, M. D. McGinley, S. D. Patterson, R. Mo, C. C. Hui, S. Chung, L. A. Huber, T. W. Mak, and N. N. Iscove. 2000. 'Cloning and characterization of the murine glucosamine-6-phosphate acetyltransferase EMeg32. Differential expression and intracellular membrane association', *J Biol Chem*, 275: 12821-32.

- Boehmelt, G., A. Wakeham, A. Elia, T. Sasaki, S. Plyte, J. Potter, Y. Yang, E. Tsang, J. Ruland, N. N. Iscove, J. W. Dennis, and T. W. Mak. 2000. 'Decreased UDP-GlcNAc levels abrogate proliferation control in EMeg32-deficient cells', *Embo j*, 19: 5092-104.
- Bond, M. R., and J. A. Hanover. 2015. 'A little sugar goes a long way: the cell biology of O-GlcNAc', *J Cell Biol*, 208: 869-80.
- Braidman, I., M. Carroll, N. Dance, D. Robinson, L. Poenaru, A. Weber, J. C. Dreyfus, B. Overdijk, and G. J. Hoogwinkel. 1974. 'Characterisation of human N-acetyl-beta-hexosaminidase C', *FEBS Lett*, 41: 181-4.
- Brenner, S. 1974. 'The genetics of *Caenorhabditis elegans*', *Genetics*, 77: 71-94.
- Brockhausen, Inka. 2006. 'Mucin-type O-glycans in human colon and breast cancer: glycodynamics and functions', *EMBO Rep*, 7: 599-604.
- Broschat, K. O., C. Gorka, J. D. Page, C. L. Martin-Berger, M. S. Davies, H. C. Huang Hc, E. A. Gulve, W. J. Salsgiver, and T. P. Kasten. 2002. 'Kinetic characterization of human glutamine-fructose-6-phosphate amidotransferase I: potent feedback inhibition by glucosamine 6-phosphate', *J Biol Chem*, 277: 14764-70.
- Bullen, John W, Jeremy L Balsbaugh, Dipanjan Chanda, Jeffrey Shabanowitz, Donald F Hunt, Dietbert Neumann, and Gerald W Hart. 2014. 'Cross-talk between two essential nutrient-sensitive enzymes: O-GlcNAc transferase (OGT) and AMP-activated protein kinase (AMPK)', *Journal of Biological Chemistry*, 289: 10592-606.
- Burla, Romina, Mattia La Torre, Chiara Merigliano, Fiammetta Verni, and Isabella Saggio. 2018. 'Genomic instability and DNA replication defects in progeroid syndromes', *Nucleus*, 9: 368-79.
- Campbell, P., T. C. Laurent, and L. Roden. 1987. 'Assay and properties of N-acetylglucosamine-6-phosphate deacetylase from rat liver', *Anal Biochem*, 166: 134-41.
- Campbell, P., J. N. Thompson, J. R. Fraser, T. C. Laurent, H. Pertoft, and L. Roden. 1990. 'N-acetylglucosamine-6-phosphate deacetylase in hepatocytes, Kupffer cells and sinusoidal endothelial cells from rat liver', *Hepatology*, 11: 199-204.
- Carette, J. E., C. P. Guimaraes, M. Varadarajan, A. S. Park, I. Wuethrich, A. Godarova, M. Kotecki, B. H. Cochran, E. Spooner, H. L. Ploegh, and T. R. Brummelkamp. 2009. 'Haploid genetic screens in human cells identify host factors used by pathogens', *Science*, 326: 1231-5.
- Carey, B. W., L. W. Finley, J. R. Cross, C. D. Allis, and C. B. Thompson. 2015. 'Intracellular α -ketoglutarate maintains the pluripotency of embryonic stem cells', *Nature*, 518: 413-6.
- Chaiyawat, Parunya, Daranee Chokchaichamnankit, Kriengsak Lirdprapamongkol, Chantragan Srisomsap, Jisnuson Svasti, and Voraratt Champattanachai. 2015. 'Alteration of O-GlcNAcylation affects serine phosphorylation and regulates gene expression and activity of pyruvate kinase M2 in colorectal cancer cells', *Oncology reports*, 34: 1933-42.
- Chang, Q., K. Su, J. R. Baker, X. Yang, A. J. Paterson, and J. E. Kudlow. 2000. 'Phosphorylation of human glutamine:fructose-6-phosphate amidotransferase by cAMP-dependent protein kinase at serine 205 blocks the enzyme activity', *J Biol Chem*, 275: 21981-7.
- Chen, J., X. Dong, X. Cheng, Q. Zhu, J. Zhang, Q. Li, X. Huang, M. Wang, L. Li, W. Guo, B. Sun, Q. Shu, W. Yi, and X. Li. 2021. 'Ogt controls neural stem/progenitor cell pool and adult neurogenesis through modulating Notch signaling', *Cell Rep*, 34: 108905.
- Chen, Q., and X. Yu. 2016. 'OGT restrains the expansion of DNA damage signaling', *Nucleic Acids Res*, 44: 9266-78.
- Chen, X., O. G. Raimi, A. T. Ferenbach, and D. M. F. van Aalten. 2021. 'A missense mutation in a patient with developmental delay affects the activity and structure of the hexosamine biosynthetic pathway enzyme AGX1', *FEBS Lett*, 595: 110-22.
- Cheung, Win D, and Gerald W Hart. 2008. 'AMP-activated protein kinase and p38 MAPK activate O-GlcNAcylation of neuronal proteins during glucose deprivation', *Journal of Biological Chemistry*, 283: 13009-20.

- Chiaradonna, F., F. Ricciardiello, and R. Palorini. 2018. 'The Nutrient-Sensing Hexosamine Biosynthetic Pathway as the Hub of Cancer Metabolic Rewiring', *Cells*, 7.
- Cho, Young Min, Sujin Kwon, Youngmi Kim Pak, Hye Won Seol, Young Min Choi, Do Joon Park, Kyong Soo Park, and Hong Kyu Lee. 2006. 'Dynamic changes in mitochondrial biogenesis and antioxidant enzymes during the spontaneous differentiation of human embryonic stem cells', *Biochemical and Biophysical Research Communications*, 348: 1472-78.
- Choi, C. W., H. Y. An, Y. J. Lee, Y. G. Lee, S. H. Yun, E. C. Park, Y. Hong, G. H. Kim, J. E. Park, S. J. Baek, H. S. Kim, and S. I. Kim. 2013. 'Characterization of *Streptococcus pneumoniae* N-acetylglucosamine-6-phosphate deacetylase as a novel diagnostic marker', *J Microbiol*, 51: 659-64.
- Chokchaitaweek, Chatchadawalai, Takashi Kobayashi, Tomomi Izumikawa, and Naoki Itano. 2019. 'Enhanced hexosamine metabolism drives metabolic and signaling networks involving hyaluronan production and O-GlcNAcylation to exacerbate breast cancer', *Cell Death & Disease*, 10: 803.
- Chou, T. Y., G. W. Hart, and C. V. Dang. 1995. 'c-Myc is glycosylated at threonine 58, a known phosphorylation site and a mutational hot spot in lymphomas', *J Biol Chem*, 270: 18961-5.
- Christensen, K., M. Thinggaard, A. Oksuzyan, T. Steenstrup, K. Andersen-Ranberg, B. Jeune, M. McGue, and J. W. Vaupel. 2013. 'Physical and cognitive functioning of people older than 90 years: a comparison of two Danish cohorts born 10 years apart', *Lancet*, 382: 1507-13.
- Clark, Raymond J, Patrick M McDonough, Eric Swanson, Susanne U Trost, Misa Suzuki, Minoru Fukuda, and Wolfgang H Dillmann. 2003. 'Diabetes and the accompanying hyperglycemia impairs cardiomyocyte calcium cycling through increased nuclear O-GlcNAcylation', *Journal of Biological Chemistry*, 278: 44230-37.
- Constable, S., J. M. Lim, K. Vaidyanathan, and L. Wells. 2017a. 'O-GlcNAc transferase regulates transcriptional activity of human Oct4', *Glycobiology*, 27: 927-37.
- Constable, Sandii, Jae-Min Lim, Krithika Vaidyanathan, and Lance Wells. 2017b. 'O-GlcNAc transferase regulates transcriptional activity of human Oct4', *Glycobiology*, 27: 927-37.
- Cork, Gentry K., Jeffrey Thompson, and Chad Slawson. 2018. 'Real Talk: The Inter-play Between the mTOR, AMPK, and Hexosamine Biosynthetic Pathways in Cell Signaling', *Frontiers in endocrinology*, 9.
- Coskun, Ü, M. Grzybek, D. Drechsel, and K. Simons. 2011. 'Regulation of human EGF receptor by lipids', *Proc Natl Acad Sci U S A*, 108: 9044-8.
- Crimmins, E. M. 2015. 'Lifespan and Healthspan: Past, Present, and Promise', *Gerontologist*, 55: 901-11.
- Dalirfardouei, Razieh, Gholamreza Karimi, and Khadijeh Jamialahmadi. 2016. 'Molecular mechanisms and biomedical applications of glucosamine as a potential multifunctional therapeutic agent', *Life Sciences*, 152: 21-29.
- Dassanayaka, Sujith, and Steven P Jones. 2014. 'O-GlcNAc and the cardiovascular system', *Pharmacology & therapeutics*, 142: 62-71.
- Dehennaut, Vanessa, Dominique Leprince, and Tony Lefebvre. 2014. 'O-GlcNAcylation, an Epigenetic Mark. Focus on the Histone Code, TET Family Proteins, and Polycomb Group Proteins', *Frontiers in endocrinology*, 5: 155-55.
- Denzel, M. S., N. J. Storm, A. Gutschmidt, R. Baddi, Y. Hinze, E. Jarosch, T. Sommer, T. Hoppe, and A. Antebi. 2014. 'Hexosamine pathway metabolites enhance protein quality control and prolong life', *Cell*, 156: 1167-78.
- Dhar, C., A. Sasmal, and A. Varki. 2019. 'From "Serum Sickness" to "Xenosialitis": Past, Present, and Future Significance of the Non-human Sialic Acid Neu5Gc', *Front Immunol*, 10: 807.
- Discher, D. E., D. J. Mooney, and P. W. Zandstra. 2009. 'Growth factors, matrices, and forces combine and control stem cells', *Science*, 324: 1673-7.
- Dorfmueller, Helge C., Vladimir S. Borodkin, Marianne Schimpl, Xiaowei Zheng, Robert Kime, Kevin D. Read, and Daan M. F. van Aalten. 2010. 'Cell-penetrant, nanomolar O-

- GlcNAcase inhibitors selective against lysosomal hexosaminidases', *Chemistry & biology*, 17: 1250-55.
- Doudna, J. A., and E. Charpentier. 2014. 'Genome editing. The new frontier of genome engineering with CRISPR-Cas9', *Science*, 346: 1258096.
- Durning, Sean P., Heather Flanagan-Steet, Nripesh Prasad, and Lance Wells. 2016. 'O-Linked β -N-acetylglucosamine (O-GlcNAc) Acts as a Glucose Sensor to Epigenetically Regulate the Insulin Gene in Pancreatic Beta Cells*', *Journal of Biological Chemistry*, 291: 2107-18.
- Dwek, R. A. 1996. 'Glycobiology: Toward Understanding the Function of Sugars', *Chem Rev*, 96: 683-720.
- Echeverri, Christophe J, Philip A Beachy, Buzz Baum, Michael Boutros, Frank Buchholz, Sumit K Chanda, Julian Downward, Jan Ellenberg, Andrew G Fraser, and Nir Hacohen. 2006. 'Minimizing the risk of reporting false positives in large-scale RNAi screens', *Nature methods*, 3: 777-79.
- Efimova, E. V., O. K. Appelbe, N. Ricco, S. S. Lee, Y. Liu, D. J. Wolfgeher, T. N. Collins, A. C. Flor, A. Ramamurthy, S. Warrington, V. P. Bindokas, and S. J. Kron. 2019. 'O-GlcNAcylation Enhances Double-Strand Break Repair, Promotes Cancer Cell Proliferation, and Prevents Therapy-Induced Senescence in Irradiated Tumors', *Mol Cancer Res*, 17: 1338-50.
- Eguchi, S., N. Oshiro, T. Miyamoto, K. Yoshino, S. Okamoto, T. Ono, U. Kikkawa, and K. Yonezawa. 2009. 'AMP-activated protein kinase phosphorylates glutamine : fructose-6-phosphate amidotransferase 1 at Ser243 to modulate its enzymatic activity', *Genes Cells*, 14: 179-89.
- Elling, U., J. Taubenschmid, G. Wirmsberger, R. O'Malley, S. P. Demers, Q. Vanhaelen, A. I. Shukalyuk, G. Schmauss, D. Schramek, F. Schnuetgen, H. von Melchner, J. R. Ecker, W. L. Stanford, J. Zuber, A. Stark, and J. M. Penninger. 2011. 'Forward and reverse genetics through derivation of haploid mouse embryonic stem cells', *Cell Stem Cell*, 9: 563-74.
- Elling, U., M. Woods, J. V. Forment, B. Fu, F. Yang, B. L. Ng, J. R. Vicente, D. J. Adams, B. Doe, S. P. Jackson, J. M. Penninger, and G. Balmus. 2019. 'Derivation and maintenance of mouse haploid embryonic stem cells', *Nat Protoc*.
- Elling, Ulrich, and Josef M. Penninger. 2014. 'Genome wide functional genetics in haploid cells', *FEBS letters*, 588: 2415-21.
- Elling, Ulrich, Reiner A. Wimmer, Andreas Leibbrandt, Thomas Burkard, Georg Michlits, Alexandra Leopoldi, Thomas Micheler, Dana Abdeen, Sergei Zhuk, Irene M. Aspalter, Cornelia Handl, Julia Liebergesell, Maria Hubmann, Anna-Maria Husa, Manuela Kinzer, Nicole Schuller, Ellen Wetzl, Nina van de Loo, Jorge Arturo Zepeda Martinez, David Estoppey, Ralph Riedl, Fengtang Yang, Beiyuan Fu, Thomas Dechat, Zoltán Ivics, Chukwuma A. Agu, Oliver Bell, Dieter Blaas, Holger Gerhardt, Dominic Hoepfner, Alexander Stark, and Josef M. Penninger. 2017. 'A reversible haploid mouse embryonic stem cell biobank resource for functional genomics', *Nature*, 550: 114-18.
- Emsley, P., B. Lohkamp, W. G. Scott, and K. Cowtan. 2010. 'Features and development of Coot', *Acta Crystallogr D Biol Crystallogr*, 66: 486-501.
- Engler, Adam J, Shamik Sen, H Lee Sweeney, and Dennis E Discher. 2006. 'Matrix elasticity directs stem cell lineage specification', *Cell*, 126: 677-89.
- Essletzbichler, Patrick, Tomasz Konopka, Federica Santoro, Doris Chen, Bianca V Gapp, Robert Kralovics, Thijn R Brummelkamp, Sebastian MB Nijman, and Tilmann Bürckstümmer. 2014. 'Megabase-scale deletion using CRISPR/Cas9 to generate a fully haploid human cell line', *Genome research*, 24: 2059-65.
- Ferreira, F. M., G. Mendoza-Hernandez, M. Castañeda-Bueno, R. Aparicio, H. Fischer, M. L. Calcagno, and G. Oliva. 2006. 'Structural analysis of N-acetylglucosamine-6-phosphate deacetylase apoenzyme from Escherichia coli', *J Mol Biol*, 359: 308-21.
- Ferrer, Christina M, Thomas P Lynch, Valerie L Sodi, John N Falcone, Luciana P Schwab, Danielle L Peacock, David J Vocado, Tiffany N Seagroves, and Mauricio J Reginato.

2014. 'O-GlcNAcylation regulates cancer metabolism and survival stress signaling via regulation of the HIF-1 pathway', *Molecular cell*, 54: 820-31.
- Folmes, Clifford DL, Timothy J Nelson, Almudena Martinez-Fernandez, D Kent Arrell, Jelena Zlatkovic Lindor, Petras P Dzeja, Yasuhiro Ikeda, Carmen Perez-Terzic, and Andre Terzic. 2011. 'Somatic oxidative bioenergetics transitions into pluripotency-dependent glycolysis to facilitate nuclear reprogramming', *Cell metabolism*, 14: 264-71.
- Fong, Jerry J., Brenda L. Nguyen, Robert Bridger, Estela E. Medrano, Lance Wells, Shujuan Pan, and Richard N. Sifers. 2012. ' β -N-Acetylglucosamine (O-GlcNAc) Is a Novel Regulator of Mitosis-specific Phosphorylations on Histone H3*', *Journal of Biological Chemistry*, 287: 12195-203.
- Forment, Josep V., Mareike Herzog, Julia Coates, Tomasz Konopka, Bianca V. Gapp, Sebastian M. Nijman, David J. Adams, Thomas M. Keane, and Stephen P. Jackson. 2017. 'Genome-wide genetic screening with chemically-mutagenized haploid embryonic stem cells', *Nature chemical biology*, 13: 12-14.
- Frank, S., G. Ahuja, D. Bartsch, N. Russ, W. Yao, J. C. Kuo, J. P. Derks, V. S. Akhade, Y. Kargapolova, T. Georgomanolis, J. E. Messling, M. Gramm, L. Brant, R. Rehimi, N. E. Vargas, A. Kuroczik, T. P. Yang, R. G. A. Sahito, J. Franzen, J. Hescheler, A. Sachinidis, M. Peifer, A. Rada-Iglesias, M. Kanduri, I. G. Costa, C. Kanduri, A. Papantonis, and L. Kurian. 2019. 'yylncT Defines a Class of Divergently Transcribed lncRNAs and Safeguards the T-mediated Mesodermal Commitment of Human PSCs', *Cell Stem Cell*, 24: 318-27.e8.
- Fujiki, Ryoji, Waka Hashiba, Hiroki Sekine, Atsushi Yokoyama, Toshihiro Chikanishi, Saya Ito, Yuuki Imai, Jaehoon Kim, Housheng Hansen He, Katsuhide Igarashi, Jun Kanno, Fumiaki Ohtake, Hirochika Kitagawa, Robert G. Roeder, Myles Brown, and Shigeaki Kato. 2011. 'GlcNAcylation of histone H2B facilitates its monoubiquitination', *Nature*, 480: 557-60.
- Gambetta, M. C., K. Oktaba, and J. Müller. 2009. 'Essential role of the glycosyltransferase *sxc/Ogt* in polycomb repression', *Science*, 325: 93-6.
- Gao, Yuan, Lance Wells, Frank I Comer, Glendon J Parker, and Gerald W Hart. 2001. 'Dynamic O-glycosylation of nuclear and cytosolic proteins: cloning and characterization of a neutral, cytosolic β -N-acetylglucosaminidase from human brain', *Journal of Biological Chemistry*, 276: 9838-45.
- Gaspar-Maia, Alexandre, Adi Alajem, Eran Meshorer, and Miguel Ramalho-Santos. 2011. 'Open chromatin in pluripotency and reprogramming', *Nature Reviews Molecular Cell Biology*, 12: 36-47.
- Ghosh, S., H. J. Blumenthal, E. Davidson, and S. Roseman. 1960. 'Glucosamine metabolism. V. Enzymatic synthesis of glucosamine 6-phosphate', *J Biol Chem*, 235: 1265-73.
- Giaever, Guri, Angela M Chu, Li Ni, Carla Connelly, Linda Riles, Steeve Véronneau, Sally Dow, Ankuta Lucau-Danila, Keith Anderson, and Bruno Andre. 2002. 'Functional profiling of the *Saccharomyces cerevisiae* genome', *Nature*, 418: 387-91.
- Gilbert, Luke A, Max A Horlbeck, Britt Adamson, Jacqueline E Villalta, Yuwen Chen, Evan H Whitehead, Carla Guimaraes, Barbara Panning, Hidde L Ploegh, and Michael C Bassik. 2014. 'Genome-scale CRISPR-mediated control of gene repression and activation', *Cell*, 159: 647-61.
- Gill, D. J., H. Clausen, and F. Bard. 2011. 'Location, location, location: new insights into O-GalNAc protein glycosylation', *Trends Cell Biol*, 21: 149-58.
- Goldblatt, Harry, and Gladys Cameron. 1953. 'Induced malignancy in cells from rat myocardium subjected to intermittent anaerobiosis during long propagation in vitro', *The Journal of experimental medicine*, 97: 525-52.
- Grigorian, A., S. U. Lee, W. Tian, I. J. Chen, G. Gao, R. Mendelsohn, J. W. Dennis, and M. Demetriou. 2007. 'Control of T Cell-mediated autoimmunity by metabolite flux to N-glycan biosynthesis', *J Biol Chem*, 282: 20027-35.
- Guinez, Céline, Jérôme Lemoine, Jean-Claude Michalski, and Tony Lefebvre. 2004. '70-kDa heat shock protein presents an adjustable lectinic activity towards O-linked N-

- acetylglucosamine', *Biochemical and Biophysical Research Communications*, 319: 21-26.
- Hall, R. S., S. Brown, A. A. Fedorov, E. V. Fedorov, C. Xu, P. C. Babbitt, S. C. Almo, and F. M. Raushel. 2007. 'Structural diversity within the mononuclear and binuclear active sites of N-acetyl-D-glucosamine-6-phosphate deacetylase', *Biochemistry*, 46: 7953-62.
- Hall, R. S., D. F. Xiang, C. Xu, and F. M. Raushel. 2007. 'N-Acetyl-D-glucosamine-6-phosphate deacetylase: substrate activation via a single divalent metal ion', *Biochemistry*, 46: 7942-52.
- Haltiwanger, R. S., G. D. Holt, and G. W. Hart. 1990. 'Enzymatic addition of O-GlcNAc to nuclear and cytoplasmic proteins. Identification of a uridine diphospho-N-acetylglucosamine:peptide beta-N-acetylglucosaminyltransferase', *Journal of Biological Chemistry*, 265: 2563-68.
- Hanai, N., G. A. Nores, C. MacLeod, C. R. Torres-Mendez, and S. Hakomori. 1988. 'Ganglioside-mediated modulation of cell growth. Specific effects of GM3 and lyso-GM3 in tyrosine phosphorylation of the epidermal growth factor receptor', *J Biol Chem*, 263: 10915-21.
- Hanover, John A, Zhennan Lai, George Lee, William A Lubas, and Sheryl M Sato. 1999. 'Elevated O-Linked N-Acetylglucosamine Metabolism in Pancreatic β -Cells', *Arch Biochem Biophys*, 362: 38-45.
- Harper, Sarah, and George Leeson. 2008. 'Introducing the journal of population ageing', *Journal of Population Ageing*, 1: 1-5.
- Hart, G. W. 1997. 'Dynamic O-linked glycosylation of nuclear and cytoskeletal proteins', *Annu Rev Biochem*, 66: 315-35.
- Hartwell, L. H., J. Culotti, J. R. Pringle, and B. J. Reid. 1974. 'Genetic control of the cell division cycle in yeast', *Science*, 183: 46-51.
- Hay, D. C., L. Sutherland, J. Clark, and T. Burdon. 2004. 'Oct-4 knockdown induces similar patterns of endoderm and trophoblast differentiation markers in human and mouse embryonic stem cells', *Stem Cells*, 22: 225-35.
- Heifetz, A., R. W. Keenan, and A. D. Elbein. 1979. 'Mechanism of action of tunicamycin on the UDP-GlcNAc:dolichyl-phosphate Glc-NAC-1-phosphate transferase', *Biochemistry*, 18: 2186-92.
- Helenius, A., and M. Aebi. 2004. 'Roles of N-linked glycans in the endoplasmic reticulum', *Annu Rev Biochem*, 73: 1019-49.
- Helenius, Ari, Aebi, and Markus. 2001. 'Intracellular Functions of N-Linked Glycans', *Science*, 291: 2364.
- Hetz, Claudio. 2012. 'The unfolded protein response: controlling cell fate decisions under ER stress and beyond', *Nat Rev Mol Cell Biol*, 13: 89-102.
- Hipp, Mark S., Prasad Kasturi, and F. Ulrich Hartl. 2019. 'The proteostasis network and its decline in ageing', *Nature Reviews Molecular Cell Biology*, 20: 421-35.
- Hocke, G. M., M. Z. Cui, and G. H. Fey. 1995. 'The LIF response element of the alpha 2 macroglobulin gene confers LIF-induced transcriptional activation in embryonal stem cells', *Cytokine*, 7: 491-502.
- Hoppe, W. 1957. 'Die Faltmolekülmethode: Eine neue Methode zur Bestimmung der Kristallstruktur bei ganz oder teilweise bekannten Molekülstrukturen', *Acta Crystallogr A*, 10: 750-51.
- Horn, M., S. I. Denzel, B. Srinivasan, K. Allmeroth, I. Schiffer, V. Karthikaisamy, S. Miethé, P. Breuer, A. Antebi, and M. S. Denzel. 2020. 'Hexosamine Pathway Activation Improves Protein Homeostasis through the Integrated Stress Response', *iScience*, 23: 100887.
- Horn, Moritz, Virginia Kroef, Kira Allmeroth, Nicole Schuller, Stephan Miethé, Martin Peifer, Josef M. Penninger, Ulrich Elling, and Martin S. Denzel. 2018. *Unbiased compound-protein interface mapping and prediction of chemoresistance loci through forward genetics in haploid stem cells*.
- Hounsell, Elizabeth F., Michael J. Davies, and David V. Renouf. 1996. 'O-linked protein glycosylation structure and function', *Glycoconjugate Journal*, 13: 19-26.

- Hu, Y., L. Riesland, A. J. Paterson, and J. E. Kudlow. 2004. 'Phosphorylation of mouse glutamine-fructose-6-phosphate amidotransferase 2 (GFAT2) by cAMP-dependent protein kinase increases the enzyme activity', *J Biol Chem*, 279: 29988-93.
- Huber, R. 1965. 'Die automatisierte Falzmolekülmethode', *Acta Crystallogr A*, 19: 353–56.
- Huh, S. Y., H. S. Kim, H. J. Jang, Y. E. Park, and D. S. Kim. 2012. 'Limb-girdle myasthenia with tubular aggregates associated with novel GFPT1 mutations', *Muscle Nerve*, 46: 600-4.
- Hurtado-Guerrero, R., O. G. Raimi, J. Min, H. Zeng, L. Vallius, S. Shepherd, A. F. Ibrahim, H. Wu, A. N. Plotnikov, and D. M. van Aalten. 2008. 'Structural and kinetic differences between human and *Aspergillus fumigatus* D-glucosamine-6-phosphate N-acetyltransferase', *Biochem J*, 415: 217-23.
- Huttlin, E. L., L. Ting, R. J. Bruckner, F. Gebreab, M. P. Gygi, J. Szpyt, S. Tam, G. Zarraga, G. Colby, K. Baltier, R. Dong, V. Guarani, L. P. Vaites, A. Ordureau, R. Rad, B. K. Erickson, M. Wühr, J. Chick, B. Zhai, D. Kolippakkam, J. Mintseris, R. A. Obar, T. Harris, S. Artavanis-Tsakonas, M. E. Sowa, P. De Camilli, J. A. Paulo, J. W. Harper, and S. P. Gygi. 2015. 'The BioPlex Network: A Systematic Exploration of the Human Interactome', *Cell*, 162: 425-40.
- Hynes, R. O., and A. Naba. 2012. 'Overview of the matrisome--an inventory of extracellular matrix constituents and functions', *Cold Spring Harb Perspect Biol*, 4: a004903.
- Issop, Yasmin, Denisa Hathazi, Muzamil Majid Khan, Rüdiger Rudolf, Joachim Weis, Sally Spendiff, Clarke R. Slater, Andreas Roos, and Hanns Lochmüller. 2018. 'GFPT1 deficiency in muscle leads to myasthenia and myopathy in mice', *Human Molecular Genetics*, 27: 3218-32.
- Itkonen, HM, N Engedal, E Babaie, M Luhr, IJ Guldvik, S Minner, J Hohloch, MC Tsourlakis, T Schlomm, and IG Mills. 2015. 'UAP1 is overexpressed in prostate cancer and is protective against inhibitors of N-linked glycosylation', *Oncogene*, 34: 3744-50.
- Jagger, C., C. Gillies, F. Moscone, E. Cambois, H. Van Oyen, W. Nusselder, and J. M. Robine. 2008. 'Inequalities in healthy life years in the 25 countries of the European Union in 2005: a cross-national meta-regression analysis', *Lancet*, 372: 2124-31.
- Jang, H., T. W. Kim, S. Yoon, S. Y. Choi, T. W. Kang, S. Y. Kim, Y. W. Kwon, E. J. Cho, and H. D. Youn. 2012. 'O-GlcNAc regulates pluripotency and reprogramming by directly acting on core components of the pluripotency network', *Cell Stem Cell*, 11: 62-74.
- Jokela, Tiina A., Katri M. Makkonen, Sanna Oikari, Riikka Kärnä, Elina Koli, Gerald W. Hart, Raija H. Tammi, Carsten Carlberg, and Markku I. Tammi. 2011. 'Cellular content of UDP-N-acetylhexosamines controls hyaluronan synthase 2 expression and correlates with O-linked N-acetylglucosamine modification of transcription factors YY1 and SP1', *The Journal of biological chemistry*, 286: 33632-40.
- Ju Lee, Hyun, Deniz Bartsch, Cally Xiao, Santiago Guerrero, Gaurav Ahuja, Christina Schindler, James J. Moresco, John R. Yates, Fátima Gebauer, Hisham Bazzi, Christoph Dieterich, Leo Kurian, and David Vilchez. 2017. 'A post-transcriptional program coordinated by CSDE1 prevents intrinsic neural differentiation of human embryonic stem cells', *Nature Communications*, 8: 1456.
- Kabsch, W. 2010. 'Xds', *Acta Crystallogr D Biol Crystallogr*, 66: 125-32.
- Kaeberlein, Matt. 2013. 'Longevity and aging', *F1000prime reports*, 5: 5-5.
- Kaelin, William G. 2012. 'Use and abuse of RNAi to study mammalian gene function', *Science*, 337: 421-22.
- Kaplanis, J., A. Gordon, T. Shor, O. Weissbrod, D. Geiger, M. Wahl, M. Gershovits, B. Markus, M. Sheikh, M. Gymrek, G. Bhatia, D. G. MacArthur, A. L. Price, and Y. Erlich. 2018. 'Quantitative analysis of population-scale family trees with millions of relatives', *Science*, 360: 171-75.
- Kasahara, Atsuko, Sara Cipolat, Yun Chen, Gerald W Dorn, and Luca Scorrano. 2013. 'Mitochondrial fusion directs cardiomyocyte differentiation via calcineurin and Notch signaling', *Science*, 342: 734-37.

- Kaufman, M. H., E. J. Robertson, A. H. Handyside, and M. J. Evans. 1983. 'Establishment of pluripotential cell lines from haploid mouse embryos', *J Embryol Exp Morphol*, 73: 249-61.
- Kazemi, Zahra, Hana Chang, Sarah Haserodt, Cathrine McKen, and Natasha E Zachara. 2010. 'O-linked β -N-acetylglucosamine (O-GlcNAc) regulates stress-induced heat shock protein expression in a GSK-3 β -dependent manner', *Journal of Biological Chemistry*, 285: 39096-107.
- Keembiyehetty, Chithra. 2015. 'Disruption of O-GlcNAc cycling by deletion of O-GlcNAcase (Oga/Mgea5) changed gene expression pattern in mouse embryonic fibroblast (MEF) cells', *Genomics data*, 5: 30-33.
- Keembiyehetty, Chithra, Dona C. Love, Katryn R. Harwood, Oksana Gavrilova, Marcella E. Comly, and John A. Hanover. 2015. 'Conditional knock-out reveals a requirement for O-linked N-Acetylglucosaminase (O-GlcNAcase) in metabolic homeostasis', *The Journal of biological chemistry*, 290: 7097-113.
- Kenyon, C. 2005. 'The plasticity of aging: insights from long-lived mutants', *Cell*, 120: 449-60.
- Khidekel, Nelly, Scott B Ficarro, Peter M Clark, Marian C Bryan, Danielle L Swaney, Jessica E Rexach, Yi E Sun, Joshua J Coon, Eric C Peters, and Linda C Hsieh-Wilson. 2007. 'Probing the dynamics of O-GlcNAc glycosylation in the brain using quantitative proteomics', *Nat Chem Biol*, 3: 339-48.
- Kim, D. Y., I. Hwang, F. L. Muller, and J. H. Paik. 2015. 'Functional regulation of FoxO1 in neural stem cell differentiation', *Cell death and differentiation*, 22: 2034-45.
- Kim, Hoe-Suk, Sang Yoon Park, Yu Rim Choi, Jeong Gu Kang, Hyun Jung Joo, Woo Kyung Moon, and Jin Won Cho. 2009. 'Excessive O-GlcNAcylation of proteins suppresses spontaneous cardiogenesis in ES cells', *FEBS letters*, 583: 2474-78.
- Klass, M. R. 1983. 'A method for the isolation of longevity mutants in the nematode *Caenorhabditis elegans* and initial results', *Mech Ageing Dev*, 22: 279-86.
- Köhler, G., and C. Milstein. 1975. 'Continuous cultures of fused cells secreting antibody of predefined specificity', *Nature*, 256: 495-97.
- Kondoh, H., M. E. Leonart, Y. Nakashima, M. Yokode, M. Tanaka, D. Bernard, J. Gil, and D. Beach. 2007. 'A high glycolytic flux supports the proliferative potential of murine embryonic stem cells', *Antioxid Redox Signal*, 9: 293-9.
- Kotecki, Maciej, P Sanjeeva Reddy, and Brent H Cochran. 1999. 'Isolation and characterization of a near-haploid human cell line', *Experimental cell research*, 252: 273-80.
- Kozarsky, K., D. Kingsley, and M. Krieger. 1988. 'Use of a mutant cell line to study the kinetics and function of O-linked glycosylation of low density lipoprotein receptors', *Proc Natl Acad Sci U S A*, 85: 4335-9.
- Kozutsumi, Yasunori, Mark Segal, Karl Normington, Mary-Jane Gething, and Joe Sambrook. 1988. 'The presence of malfolded proteins in the endoplasmic reticulum signals the induction of glucose-regulated proteins', *Nature*, 332: 462-64.
- Kristensen, A. R., J. Gsponer, and L. J. Foster. 2012. 'A high-throughput approach for measuring temporal changes in the interactome', *Nat Methods*, 9: 907-9.
- Kuo, MeiShiue, Vladimir Zilberfarb, Nicolas Gangneux, Névéna Christeff, and Tarik Issad. 2008. 'O-glycosylation of FoxO1 increases its transcriptional activity towards the glucose 6-phosphatase gene', *FEBS letters*, 582: 829-34.
- Larsson, Jessica M. Holmn, Hasse Karlsson, Jessica Gråberg Crespo, Malin E. V. Johansson, Lisbeth Eklund, Henrik Sjövall, and Gunnar C. Hansson. 2011. 'Altered O-glycosylation profile of MUC2 mucin occurs in active ulcerative colitis and is associated with increased inflammation', *Inflammatory Bowel Diseases*, 17: 2299-307.
- Laskowski, R. A., and M. B. Swindells. 2011. 'LigPlot+: multiple ligand-protein interaction diagrams for drug discovery', *J Chem Inf Model*, 51: 2778-86.
- Latham, K. E., H. Akutsu, B. Patel, and R. Yanagimachi. 2002. 'Comparison of gene expression during preimplantation development between diploid and haploid mouse embryos', *Biol Reprod*, 67: 386-92.

- Lazarus, Michael B, Jiaoyang Jiang, Vaibhav Kapuria, Tanja Bhuiyan, John Janetzko, Wesley F Zandberg, David J Vocadlo, Winship Herr, and Suzanne Walker. 2013. 'HCF-1 is cleaved in the active site of O-GlcNAc transferase', *Science*, 342: 1235-39.
- Lazarus, Michael B, Yunsun Nam, Jiaoyang Jiang, Piotr Sliz, and Suzanne Walker. 2011. 'Structure of human O-GlcNAc transferase and its complex with a peptide substrate', *Nature*, 469: 564-67.
- Lee, J. S., and Z. Zhang. 2016. 'O-linked N-acetylglucosamine transferase (OGT) interacts with the histone chaperone HIRA complex and regulates nucleosome assembly and cellular senescence', *Proc Natl Acad Sci U S A*, 113: E3213-20.
- Leeb, Martin, and Anton Wutz. 2011. 'Derivation of haploid embryonic stem cells from mouse embryos', *Nature*, 479: 131-34.
- Lewis, Brian A, and John A Hanover. 2014. 'O-GlcNAc and the epigenetic regulation of gene expression', *Journal of Biological Chemistry*, 289: 34440-48.
- Li, Xu, Fen Lu, Jian-Zhi Wang, and Cheng-Xin Gong. 2006. 'Concurrent alterations of O-GlcNAcylation and phosphorylation of tau in mouse brains during fasting', *European Journal of Neuroscience*, 23: 2078-86.
- Li, Y., P. Lopez, P. Durand, J. Ouazzani, B. Badet, and M. A. Badet-Denisot. 2007. 'An enzyme-coupled assay for amidotransferase activity of glucosamine-6-phosphate synthase', *Anal Biochem*, 370: 142-6.
- Li, Y., C. Roux, S. Lazereg, J. P. LeCaer, O. Lapr evote, B. Badet, and M. A. Badet-Denisot. 2007. 'Identification of a novel serine phosphorylation site in human glutamine:fructose-6-phosphate amidotransferase isoform 1', *Biochemistry*, 46: 13163-9.
- Lin, Chia-Hung, Chen-Chung Liao, Mei-Yu Chen, and Teh-Ying Chou. 2021. 'Feedback Regulation of O-GlcNAc Transferase through Translation Control to Maintain Intracellular O-GlcNAc Homeostasis', *International Journal of Molecular Sciences*, 22.
- Lindahl, U. 2014. 'A personal voyage through the proteoglycan field', *Matrix Biol*, 35: 3-7.
- Lis, H., and N. Sharon. 1993. 'Protein glycosylation. Structural and functional aspects', *Eur J Biochem*, 218: 1-27.
- Liu, F., K. Iqbal, I. Grundke-Iqbal, G. W. Hart, and C. X. Gong. 2004. 'O-GlcNAcylation regulates phosphorylation of tau: a mechanism involved in Alzheimer's disease', *Proc Natl Acad Sci U S A*, 101: 10804-9.
- Liu, Ying, Xiaojing Li, Yang Yu, Jianhua Shi, Zhihou Liang, Xiaoqin Run, Yi Li, Chun-ling Dai, Inge Grundke-Iqbal, and Khalid Iqbal. 2012. 'Developmental regulation of protein O-GlcNAcylation, O-GlcNAc transferase, and O-GlcNAcase in mammalian brain', *PLoS One*, 7: e43724.
- Liu, Yubo, Yang Ren, Yu Cao, Huang Huang, Qiong Wu, Wenli Li, Sijin Wu, and Jianing Zhang. 2017. 'Discovery of a Low Toxicity O-GlcNAc Transferase (OGT) Inhibitor by Structure-based Virtual Screening of Natural Products', *Sci Rep*, 7: 12334-34.
- Loh, Y. H., Q. Wu, J. L. Chew, V. B. Vega, W. Zhang, X. Chen, G. Bourque, J. George, B. Leong, J. Liu, K. Y. Wong, K. W. Sung, C. W. Lee, X. D. Zhao, K. P. Chiu, L. Lipovich, V. A. Kuznetsov, P. Robson, L. W. Stanton, C. L. Wei, Y. Ruan, B. Lim, and H. H. Ng. 2006. 'The Oct4 and Nanog transcription network regulates pluripotency in mouse embryonic stem cells', *Nat Genet*, 38: 431-40.
- L pez-Ot n, Carlos, Maria A. Blasco, Linda Partridge, Manuel Serrano, and Guido Kroemer. 2013. 'The hallmarks of aging', *Cell*, 153: 1194-217.
- Love, Dona C, Salil Ghosh, Michelle A Mondoux, Tetsunari Fukushige, Peng Wang, Mark A Wilson, Wendy B Iser, Catherine A Wolkow, Michael W Krause, and John A Hanover. 2010. 'Dynamic O-GlcNAc cycling at promoters of *Caenorhabditis elegans* genes regulating longevity, stress, and immunity', *Proceedings of the National Academy of Sciences*, 107: 7413-18.
- Love, Dona C, Jarema Kochran, R Lamont Cathey, Sang-Hoon Shin, and John A Hanover. 2003. 'Mitochondrial and nucleocytoplasmic targeting of O-linked GlcNAc transferase', *Journal of cell science*, 116: 647-54.

- Lu, P., K. Takai, V. M. Weaver, and Z. Werb. 2011. 'Extracellular matrix degradation and remodeling in development and disease', *Cold Spring Harb Perspect Biol*, 3.
- Lubas, W. A., D. W. Frank, M. Krause, and J. A. Hanover. 1997. 'O-Linked GlcNAc transferase is a conserved nucleocytoplasmic protein containing tetratricopeptide repeats', *J Biol Chem*, 272: 9316-24.
- Lunt, S. Y., and M. G. Vander Heiden. 2011. 'Aerobic glycolysis: meeting the metabolic requirements of cell proliferation', *Annu Rev Cell Dev Biol*, 27: 441-64.
- Ma, Z., R. J. Chalkley, and K. Vosseller. 2017. 'Hyper-O-GlcNAcylation activates nuclear factor κ -light-chain-enhancer of activated B cells (NF- κ B) signaling through interplay with phosphorylation and acetylation', *J Biol Chem*, 292: 9150-63.
- Mali, Prashant, Bin-Kuan Chou, Jonathan Yen, Zhaohui Ye, Jizhong Zou, Sarah Dowe, Robert A Brodsky, Joyce E Ohm, Wayne Yu, and Stephen B Baylin. 2010. 'Butyrate greatly enhances derivation of human induced pluripotent stem cells by promoting epigenetic remodeling and the expression of pluripotency-associated genes', *Stem Cells*, 28: 713-20.
- Marahrens, York, Barbara Panning, Jessica Dausman, William Strauss, and Rudolf Jaenisch. 1997. 'Xist-deficient mice are defective in dosage compensation but not spermatogenesis', *Genes & development*, 11: 156-66.
- Mariappa, Daniel, Andrew T. Ferenbach, and Daan M. F. van Aalten. 2018. 'Effects of hypo-O-GlcNAcylation on Drosophila development', *Journal of Biological Chemistry*, 293: 7209-21.
- Mariappa, Daniel, Xiaowei Zheng, Marianne Schimpl, Olawale Raimi, Andrew T. Ferenbach, H. Arno J. Müller, and Daan M. F. van Aalten. 2015. 'Dual functionality of O-GlcNAc transferase is required for Drosophila development', *Open biology*, 5: 150234-34.
- Marsboom, Glenn, Guo-Fang Zhang, Nicole Pohl-Avila, Yanmin Zhang, Yang Yuan, Hojin Kang, Bo Hao, Henri Brunengraber, Asrar B Malik, and Jalees Rehman. 2016. 'Glutamine metabolism regulates the pluripotency transcription factor OCT4', *Cell Reports*, 16: 323-32.
- Marsh, Susan A, Helen E Collins, and John C Chatham. 2014. 'Protein O-GlcNAcylation and cardiovascular (patho) physiology', *Journal of Biological Chemistry*, 289: 34449-56.
- Marshall, S., V. Bacote, and R. R. Traxinger. 1991. 'Discovery of a metabolic pathway mediating glucose-induced desensitization of the glucose transport system. Role of hexosamine biosynthesis in the induction of insulin resistance', *J Biol Chem*, 266: 4706-12.
- Marshall, S., O. Nadeau, and K. Yamasaki. 2004. 'Dynamic actions of glucose and glucosamine on hexosamine biosynthesis in isolated adipocytes: differential effects on glucosamine 6-phosphate, UDP-N-acetylglucosamine, and ATP levels', *J Biol Chem*, 279: 35313-9.
- Martin, George M, and Junko Oshima. 2000. 'Lessons from human progeroid syndromes', *Nature*, 408: 263-66.
- Mattila, J., K. Kokki, V. Hietakangas, and M. Boutros. 2018. 'Stem Cell Intrinsic Hexosamine Metabolism Regulates Intestinal Adaptation to Nutrient Content', *Dev Cell*, 47: 112-21.e3.
- McClain, D. A., and E. D. Crook. 1996. 'Hexosamines and insulin resistance', *Diabetes*, 45: 1003-9.
- McCoy, A. J. 2007. 'Solving structures of protein complexes by molecular replacement with Phaser', *Acta Crystallogr D Biol Crystallogr*, 63: 32-41.
- Merrill, A. H., Jr. 2011. 'Sphingolipid and glycosphingolipid metabolic pathways in the era of sphingolipidomics', *Chem Rev*, 111: 6387-422.
- Metallo, Christian M., Paulo A. Gameiro, Eric L. Bell, Katherine R. Mattaini, Juanjuan Yang, Karsten Hiller, Christopher M. Jewell, Zachary R. Johnson, Darrell J. Irvine, Leonard Guarente, Joanne K. Kelleher, Matthew G. Vander Heiden, Othon Iliopoulos, and Gregory Stephanopoulos. 2012. 'Reductive glutamine metabolism by IDH1 mediates lipogenesis under hypoxia', *Nature*, 481: 380-84.

- Mio, T., T. Yabe, M. Arisawa, and H. Yamada-Okabe. 1998. 'The eukaryotic UDP-N-acetylglucosamine pyrophosphorylases. Gene cloning, protein expression, and catalytic mechanism', *J Biol Chem*, 273: 14392-7.
- Mitrečić, D., D. J. Petrović, P. Stančin, J. Isaković, B. Zavan, G. Tricarico, M. Kujundžić Tiljak, and M. Di Luca. 2020. 'How to face the aging world - lessons from dementia research', *Croat Med J*, 61: 139-46.
- Moussaieff, Arieh, Matthieu Rouleau, Daniel Kitsberg, Merav Cohen, Gahl Levy, Dinorah Barasch, Alina Nemirovski, Shai Shen-Orr, Ilana Laevsky, and Michal Amit. 2015. 'Glycolysis-mediated changes in acetyl-CoA and histone acetylation control the early differentiation of embryonic stem cells', *Cell metabolism*, 21: 392-402.
- Muha, V., F. Authier, Z. Szoke-Kovacs, S. Johnson, J. Gallagher, A. McNeilly, R. J. McCrimmon, L. Teboul, and D. M. F. van Aalten. 2021. 'Loss of O-GlcNAcase catalytic activity leads to defects in mouse embryogenesis', *J Biol Chem*: 100439.
- Munro, C. A., and N. A. Gow. 2001. 'Chitin synthesis in human pathogenic fungi', *Med Mycol*, 39 Suppl 1: 41-53.
- Myers, S. A., S. Peddada, N. Chatterjee, T. Friedrich, K. Tomoda, G. Krings, S. Thomas, J. Maynard, M. Broeker, M. Thomson, K. Pollard, S. Yamanaka, A. L. Burlingame, and B. Panning. 2016. 'SOX2 O-GlcNAcylation alters its protein-protein interactions and genomic occupancy to modulate gene expression in pluripotent cells', *eLife*, 5: e10647.
- Nakajima, K., S. Kitazume, T. Angata, R. Fujinawa, K. Ohtsubo, E. Miyoshi, and N. Taniguchi. 2010. 'Simultaneous determination of nucleotide sugars with ion-pair reversed-phase HPLC', *Glycobiology*, 20: 865-71.
- Nallanthighal, Sameera, James Patrick Heiserman, and Dong-Joo Cheon. 2019. 'The role of the extracellular matrix in cancer stemness', *Frontiers in Cell and Developmental Biology*, 7: 86.
- Newsholme, EA, B Crabtree, and MSM Ardawi. 1985. 'The role of high rates of glycolysis and glutamine utilization in rapidly dividing cells', *Bioscience reports*, 5: 393-400.
- Niccoli, Teresa, and Linda Partridge. 2012. 'Ageing as a Risk Factor for Disease', *Current biology : CB*, 22: R741-52.
- Nichols, J., B. Zevnik, K. Anastasiadis, H. Niwa, D. Klewe-Nebenius, I. Chambers, H. Schöler, and A. Smith. 1998. 'Formation of pluripotent stem cells in the mammalian embryo depends on the POU transcription factor Oct4', *Cell*, 95: 379-91.
- O'Connor, E., A. Topf, R. P. Zahedi, S. Spendiff, D. Cox, A. Roos, and H. Lochmuller. 2018. 'Clinical and research strategies for limb-girdle congenital myasthenic syndromes', *Ann N Y Acad Sci*, 1412: 102-12.
- O'Donnell, Niall, Natasha E Zachara, Gerald W Hart, and Jamey D Marth. 2004. 'Ogt-dependent X-chromosome-linked protein glycosylation is a requisite modification in somatic cell function and embryo viability', *Molecular and cellular biology*, 24: 1680-90.
- Oeppen, J., and J. W. Vaupel. 2002. 'Demography. Broken limits to life expectancy', *Science*, 296: 1029-31.
- Ogawa, Mitsutaka, Hidenori Mizofuchi, Yuki Kobayashi, Genta Tsuzuki, Mayumi Yamamoto, Shuichi Wada, and Kazuo Kamemura. 2012. 'Terminal differentiation program of skeletal myogenesis is negatively regulated by O-GlcNAc glycosylation', *Biochimica et biophysica acta*, 1820: 24-32.
- Oikari, S., K. Makkonen, A. J. Deen, I. Tyni, R. Karna, R. H. Tammi, and M. I. Tammi. 2016. 'Hexosamine biosynthesis in keratinocytes: roles of GFAT and GNPDA enzymes in the maintenance of UDP-GlcNAc content and hyaluronan synthesis', *Glycobiology*, 26: 710-22.
- Oikari, Sanna, Tiia Kettunen, Satu Tiainen, Jukka Häyrynen, Amro Masarwah, Mazen Sudah, Anna Sutela, Ritva Vanninen, Markku Tammi, and Päivi Auvinen. 2018. 'UDP-sugar accumulation drives hyaluronan synthesis in breast cancer', *Matrix Biology*, 67: 63-74.
- Oki, T., K. Yamazaki, J. Kuromitsu, M. Okada, and I. Tanaka. 1999. 'cDNA cloning and mapping of a novel subtype of glutamine:fructose-6-phosphate amidotransferase (GFAT2) in human and mouse', *Genomics*, 57: 227-34.

- Olchoway, J., K. Kur, P. Sachadyn, and S. Milewski. 2006. 'Construction, purification, and functional characterization of His-tagged *Candida albicans* glucosamine-6-phosphate synthase expressed in *Escherichia coli*', *Protein Expr Purif*, 46: 309-15.
- Olivier-Van Stichelen, S., P. Wang, M. Comly, D. C. Love, and J. A. Hanover. 2017. 'Nutrient-driven O-linked N-acetylglucosamine (O-GlcNAc) cycling impacts neurodevelopmental timing and metabolism', *J Biol Chem*, 292: 6076-85.
- Ong, Qunxiang, Weiping Han, and Xiaoyong Yang. 2018. 'O-GlcNAc as an Integrator of Signaling Pathways', *Frontiers in endocrinology*, 9.
- Paix, A., A. Folkmann, and G. Seydoux. 2017. 'Precision genome editing using CRISPR-Cas9 and linear repair templates in *C. elegans*', *Methods*, 121-122: 86-93.
- Panopoulos, Athanasia D, Oscar Yanes, Sergio Ruiz, Yasuyuki S Kida, Dinh Diep, Ralf Tautenhahn, Aída Herrerías, Erika M Batchelder, Nongluk Plongthongkum, and Margaret Lutz. 2012. 'The metabolome of induced pluripotent stem cells reveals metabolic changes occurring in somatic cell reprogramming', *Cell research*, 22: 168-77.
- Pantaleon, Marie, Jeanie Scott, and Peter L. Kaye. 2008. 'Nutrient Sensing by the Early Mouse Embryo: Hexosamine Biosynthesis and Glucose Signaling During Preimplantation Development¹', *Biology of Reproduction*, 78: 595-600.
- Park, J. T. 2001. 'Identification of a dedicated recycling pathway for anhydro-N-acetylmuramic acid and N-acetylglucosamine derived from *Escherichia coli* cell wall murein', *J Bacteriol*, 183: 3842-7.
- Park, Seung Yoon, Jiwon Ryu, and Wan Lee. 2005. 'O-GlcNAc modification on IRS-1 and Akt2 by PUGNAc inhibits their phosphorylation and induces insulin resistance in rat primary adipocytes', *Experimental & molecular medicine*, 37: 220-29.
- Park, Sung-Kyun, Xiaorong Zhou, Kathryn E. Pendleton, Olga V. Hunter, Jennifer J. Kohler, Kathryn A. O'Donnell, and Nicholas K. Conrad. 2017. 'A Conserved Splicing Silencer Dynamically Regulates O-GlcNAc Transferase Intron Retention and O-GlcNAc Homeostasis', *Cell Reports*, 20: 1088-99.
- Parodi, A. J. 2000. 'Role of N-oligosaccharide endoplasmic reticulum processing reactions in glycoprotein folding and degradation', *Biochem J*, 348 Pt 1: 1-13.
- Partridge, L., J. Deelen, and P. E. Slagboom. 2018. 'Facing up to the global challenges of ageing', *Nature*, 561: 45-56.
- Parween, Shama, Divya S. Varghese, Mustafa T. Ardah, Ashok D. Prabakaran, Eric Mensah-Brown, Bright Starling Emerald, and Suraiya A. Ansari. 2017. 'Higher O-GlcNAc Levels Are Associated with Defects in Progenitor Proliferation and Premature Neuronal Differentiation during in-Vitro Human Embryonic Cortical Neurogenesis', *Frontiers in cellular neuroscience*, 11: 415-15.
- Pathak, Shalini, Jana Alonso, Marianne Schimpl, Karim Rafie, David E Blair, Vladimir S Borodkin, Alexander W Schüttelkopf, Osama Albarbarawi, and Daan MF Van Aalten. 2015. 'The active site of O-GlcNAc transferase imposes constraints on substrate sequence', *Nature structural & molecular biology*, 22: 744.
- Petersen, J., A. W. Purcell, and J. Rossjohn. 2009. 'Post-translationally modified T cell epitopes: immune recognition and immunotherapy', *J Mol Med (Berl)*, 87: 1045-51.
- Plumbridge, J. 2009. 'An alternative route for recycling of N-acetylglucosamine from peptidoglycan involves the N-acetylglucosamine phosphotransferase system in *Escherichia coli*', *J Bacteriol*, 191: 5641-7.
- Pravata, V. M., M. Gundogdu, S. G. Bartual, A. T. Ferenbach, M. Stavridis, K. Öunap, S. Pajusalu, R. Žordania, M. H. Wojcik, and D. M. F. van Aalten. 2020. 'A missense mutation in the catalytic domain of O-GlcNAc transferase links perturbations in protein O-GlcNAcylation to X-linked intellectual disability', *FEBS Lett*, 594: 717-27.
- Prigione, Alessandro, Nadine Rohwer, Sheila Hoffmann, Barbara Mlody, Katharina Drews, Raul Bukowiecki, Katharina Blümlein, Erich E Wanker, Markus Ralser, and Thorsten Cramer. 2014. 'HIF1 α modulates cell fate reprogramming through early glycolytic shift and upregulation of PDK1–3 and PKM2', *Stem Cells*, 32: 364-76.

- Qian, Kevin, Simeng Wang, Minnie Fu, Jinfeng Zhou, Jay Prakash Singh, Min-Dian Li, Yunfan Yang, Kaisi Zhang, Jing Wu, Yongzhan Nie, Hai-Bin Ruan, and Xiaoyong Yang. 2018. 'Transcriptional regulation of O-GlcNAc homeostasis is disrupted in pancreatic cancer', *The Journal of biological chemistry*, 293: 13989-4000.
- Qiu, Tao, Hongyi Wang, Yang Wang, Yu Zhang, Qiang Hui, and Kai Tao. 2015. 'Identification of genes associated with melanoma metastasis', *The Kaohsiung Journal of Medical Sciences*, 31: 553-61.
- Ramirez-Correa, Genaro A, Wenhai Jin, Zihao Wang, Xin Zhong, Wei Dong Gao, Wagner B Dias, Cecilia Vecoli, Gerald W Hart, and Anne M Murphy. 2008. 'O-linked GlcNAc modification of cardiac myofilament proteins: a novel regulator of myocardial contractile function', *Circulation research*, 103: 1354-58.
- Ran, F. A., P. D. Hsu, J. Wright, V. Agarwala, D. A. Scott, and F. Zhang. 2013. 'Genome engineering using the CRISPR-Cas9 system', *Nat Protoc*, 8: 2281-308.
- Ranuncolo, Stella M, Salil Ghosh, John A Hanover, Gerald W Hart, and Brian A Lewis. 2012. 'Evidence of the involvement of O-GlcNAc-modified human RNA polymerase II CTD in transcription in vitro and in vivo', *Journal of Biological Chemistry*, 287: 23549-61.
- Rao, Xiongjian, Xiaotao Duan, Weimin Mao, Xuexia Li, Zhonghua Li, Qian Li, Zhiguo Zheng, Haimiao Xu, Min Chen, and Peng G Wang. 2015. 'O-GlcNAcylation of G6PD promotes the pentose phosphate pathway and tumor growth', *Nature Communications*, 6: 1-10.
- Ricciardiello, F., G. Votta, R. Palorini, I. Raccagni, L. Brunelli, A. Paiotta, F. Tinelli, G. D'Orazio, S. Valtorta, L. De Gioia, R. Pastorelli, R. M. Moresco, B. La Ferla, and F. Chiaradonna. 2018. 'Inhibition of the Hexosamine Biosynthetic Pathway by targeting PGM3 causes breast cancer growth arrest and apoptosis', *Cell Death Dis*, 9: 377.
- Richez, C., J. Boetzel, N. Floquet, K. Koteshwar, J. Stevens, B. Badet, and M. A. Badet-Denisot. 2007. 'Expression and purification of active human internal His(6)-tagged L-glutamine: D-Fructose-6P amidotransferase I', *Protein Expr Purif*, 54: 45-53.
- Robert, X., and P. Gouet. 2014. 'Deciphering key features in protein structures with the new ENDscript server', *Nucleic Acids Res*, 42: W320-4.
- Rolland, T., M. Taşan, B. Charlotiaux, S. J. Pevzner, Q. Zhong, N. Sahni, S. Yi, I. Lemmens, C. Fontanillo, R. Mosca, A. Kamburov, S. D. Ghiassian, X. Yang, L. Ghamsari, D. Balcha, B. E. Begg, P. Braun, M. Brehme, M. P. Broly, A. R. Carvunis, D. Convery-Zupan, R. Corominas, J. Coulombe-Huntington, E. Dann, M. Dreze, A. Dricot, C. Fan, E. Franzosa, F. Gebreab, B. J. Gutierrez, M. F. Hardy, M. Jin, S. Kang, R. Kiros, G. N. Lin, K. Luck, A. MacWilliams, J. Menche, R. R. Murray, A. Palagi, M. M. Poulin, X. Rambout, J. Rasla, P. Reichert, V. Romero, E. Ruysinck, J. M. Sahalie, A. Scholz, A. A. Shah, A. Sharma, Y. Shen, K. Spirohn, S. Tam, A. O. Tejada, S. A. Trigg, J. C. Twizere, K. Vega, J. Walsh, M. E. Cusick, Y. Xia, A. L. Barabási, L. M. Iakoucheva, P. Aloy, J. De Las Rivas, J. Tavernier, M. A. Calderwood, D. E. Hill, T. Hao, F. P. Roth, and M. Vidal. 2014. 'A proteome-scale map of the human interactome network', *Cell*, 159: 1212-26.
- Ruan, Hai-Bin, Xuemei Han, Min-Dian Li, Jay Prakash Singh, Kevin Qian, Sascha Azarhoush, Lin Zhao, Anton M Bennett, Varman T Samuel, and Jing Wu. 2012. 'O-GlcNAc transferase/host cell factor C1 complex regulates gluconeogenesis by modulating PGC-1 α stability', *Cell metabolism*, 16: 226-37.
- Ruan, Hai-Bin, Yongzhan Nie, and Xiaoyong Yang. 2013. 'Regulation of protein degradation by O-GlcNAcylation: crosstalk with ubiquitination', *Molecular & cellular proteomics : MCP*, 12: 3489-97.
- Ruegenberg, S., M. Horn, C. Pichlo, K. Allmeroth, U. Baumann, and M. S. Denzel. 2020b. 'Loss of GFAT-1 feedback regulation activates the hexosamine pathway that modulates protein homeostasis', *Nat Commun*, 11: 687.
- Ruegenberg, Sabine. 2020a. 'Structural and Functional Analyses of Hexosamine Pathway Enzymes.', University of Cologne.
- Ruegenberg, Sabine, Felix A. M. C. Mayr, Ilian Atanassov, Ulrich Baumann, and Martin S. Denzel. 2021. 'Protein kinase A controls the hexosamine pathway by tuning the feedback inhibition of GFAT-1', *Nature Communications*, 12: 2176.

- Russell, W. L., E. M. Kelly, P. R. Hunsicker, J. W. Bangham, S. C. Maddux, and E. L. Phipps. 1979. 'Specific-locus test shows ethylnitrosourea to be the most potent mutagen in the mouse', *Proceedings of the National Academy of Sciences of the United States of America*, 76: 5818-19.
- Saez, Isabel, Seda Koyuncu, Ricardo Gutierrez-Garcia, Christoph Dieterich, and David Vilchez. 2018. 'Insights into the ubiquitin-proteasome system of human embryonic stem cells', *Sci Rep*, 8: 4092.
- Sagi, I., G. Chia, T. Golan-Lev, M. Peretz, U. Weissbein, L. Sui, M. V. Sauer, O. Yanuka, D. Egli, and N. Benvenisty. 2016. 'Derivation and differentiation of haploid human embryonic stem cells', *Nature*, 532: 107-11.
- Sakabe, K., Z. Wang, and G. W. Hart. 2010. 'Beta-N-acetylglucosamine (O-GlcNAc) is part of the histone code', *Proc Natl Acad Sci U S A*, 107: 19915-20.
- Saxon, Eliana, and Carolyn R Bertozzi. 2001. 'Chemical and biological strategies for engineering cell surface glycosylation', *Annual review of cell and developmental biology*, 17: 1-23.
- Sayeski, Peter P, Andrew J Paterson, and Jeffrey E Kudlow. 1994. 'The murine glutamine: fructose-6-phosphate amidotransferase-encoding cDNA sequence', *Gene*, 140: 289-90.
- Schachter, Harry. 1978. '2 - Glycoprotein Biosynthesis.' in Martin I. Horowitz and Ward Pigman (eds.), *The Glycoconjugates* (Academic Press).
- Schimpl, M., V. S. Borodkin, L. J. Gray, and D. M. van Aalten. 2012. 'Synergy of peptide and sugar in O-GlcNAcase substrate recognition', *Chem Biol*, 19: 173-8.
- Schnütgen, Frank, Jens Hansen, Silke De-Zolt, Carsten Horn, Marcus Lutz, Thomas Floss, Wolfgang Wurst, Patricia Ruiz Noppinger, and Harald von Melchner. 2008. 'Enhanced gene trapping in mouse embryonic stem cells', *Nucleic Acids Research*, 36: e133-e33.
- Schroder, M., and R. J. Kaufman. 2005. 'The mammalian unfolded protein response', *Annu Rev Biochem*, 74: 739-89.
- Sekine, H., K. Okazaki, K. Kato, M. M. Alam, H. Shima, F. Katsuoka, T. Tsujita, N. Suzuki, A. Kobayashi, K. Igarashi, M. Yamamoto, and H. Motohashi. 2018. 'O-GlcNAcylation Signal Mediates Proteasome Inhibitor Resistance in Cancer Cells by Stabilizing NRF1', *Mol Cell Biol*, 38.
- Selvan, N., S. George, F. J. Serajee, M. Shaw, L. Hobson, V. Kalscheuer, N. Prasad, S. E. Levy, J. Taylor, S. Aftimos, C. E. Schwartz, A. M. Huq, J. Gecz, and L. Wells. 2018. 'O-GlcNAc transferase missense mutations linked to X-linked intellectual disability deregulate genes involved in cell fate determination and signaling', *J Biol Chem*, 293: 10810-24.
- Senderek, J., J. S. Muller, M. Dusl, T. M. Strom, V. Guergueltcheva, I. Diepolder, S. H. Laval, S. Maxwell, J. Cossins, S. Krause, N. Muelas, J. J. Vilchez, J. Colomer, C. J. Mallebrera, A. Nascimento, S. Nafissi, A. Kariminejad, Y. Nilipour, B. Bozorgmehr, H. Najmabadi, C. Rodolico, J. P. Sieb, O. K. Steinlein, B. Schlotter, B. Schoser, J. Kirschner, R. Herrmann, T. Voit, A. Oldfors, C. Lindbergh, A. Urtizberea, M. von der Hagen, A. Hubner, J. Palace, K. Bushby, V. Straub, D. Beeson, A. Abicht, and H. Lochmuller. 2011. 'Hexosamine biosynthetic pathway mutations cause neuromuscular transmission defect', *Am J Hum Genet*, 88: 162-72.
- Shafi, R., S. P. Iyer, L. G. Ellies, N. O'Donnell, K. W. Marek, D. Chui, G. W. Hart, and J. D. Marth. 2000. 'The O-GlcNAc transferase gene resides on the X chromosome and is essential for embryonic stem cell viability and mouse ontogeny', *Proc Natl Acad Sci U S A*, 97: 5735-9.
- Shalem, O., N. E. Sanjana, and F. Zhang. 2015. 'High-throughput functional genomics using CRISPR-Cas9', *Nat Rev Genet*, 16: 299-311.
- Sharp, Phillip A. 1999. 'RNAi and double-strand RNA', *Genes & development*, 13: 139-41.
- Shaul, Yoav D, Elizaveta Freinkman, William C Comb, Jason R Cantor, Wai Leong Tam, Prathapan Thiru, Dohoon Kim, Naama Kanarek, Michael E Pacold, and Walter W Chen. 2014. 'Dihydropyrimidine accumulation is required for the epithelial-mesenchymal transition', *Cell*, 158: 1094-109.

- Sheikh, K. A., J. Sun, Y. Liu, H. Kawai, T. O. Crawford, R. L. Proia, J. W. Griffin, and R. L. Schnaar. 1999. 'Mice lacking complex gangliosides develop Wallerian degeneration and myelination defects', *Proc Natl Acad Sci U S A*, 96: 7532-7.
- Shen, David L, Tracey M Gloster, Scott A Yuzwa, and David J Vocadlo. 2012. 'Insights into O-linked N-acetylglucosamine ([0-9] O-GlcNAc) processing and dynamics through kinetic analysis of O-GlcNAc transferase and O-GlcNAcase activity on protein substrates', *Journal of Biological Chemistry*, 287: 15395-408.
- Shi, F. T., H. Kim, W. Lu, Q. He, D. Liu, M. A. Goodell, M. Wan, and Z. Songyang. 2013. 'Ten-eleven translocation 1 (Tet1) is regulated by O-linked N-acetylglucosamine transferase (Ogt) for target gene repression in mouse embryonic stem cells', *J Biol Chem*, 288: 20776-84.
- Shin, H., H. J. Cha, K. Na, M. J. Lee, J. Y. Cho, C. Y. Kim, E. K. Kim, C. M. Kang, H. Kim, and Y. K. Paik. 2018. 'O-GlcNAcylation of the Tumor Suppressor FOXO3 Triggers Aberrant Cancer Cell Growth', *Cancer Res*, 78: 1214-24.
- Shyh-Chang, Ng, and Huck-Hui Ng. 2017. 'The metabolic programming of stem cells', *Genes & development*, 31: 336-46.
- Sievers, F., A. Wilm, D. Dineen, T. J. Gibson, K. Karplus, W. Li, R. Lopez, H. McWilliam, M. Remmert, J. Soding, J. D. Thompson, and D. G. Higgins. 2011. 'Fast, scalable generation of high-quality protein multiple sequence alignments using Clustal Omega', *Mol Syst Biol*, 7: 539.
- Silberstein, S., and R. Gilmore. 1996. 'Biochemistry, molecular biology, and genetics of the oligosaccharyltransferase', *Faseb j*, 10: 849-58.
- Sinclair, D. A., M. Syrzycka, M. S. Macauley, T. Rastgardani, I. Komljenovic, D. J. Vocadlo, H. W. Brock, and B. M. Honda. 2009. 'Drosophila O-GlcNAc transferase (OGT) is encoded by the Polycomb group (PcG) gene, super sex combs (sxc)', *Proc Natl Acad Sci U S A*, 106: 13427-32.
- Singh, U., R. H. Quintanilla, S. Grecian, K. R. Gee, M. S. Rao, and U. Lakshmiopathy. 2012. 'Novel live alkaline phosphatase substrate for identification of pluripotent stem cells', *Stem Cell Rev Rep*, 8: 1021-9.
- Song, Sun-Hwa, Kyungjong Kim, Jeong Joo Park, Kyung Hoon Min, and Wonhee Suh. 2014. 'Reactive oxygen species regulate the quiescence of CD34-positive cells derived from human embryonic stem cells', *Cardiovascular research*, 103: 147-55.
- Speakman, C. M., T. C. Domke, W. Wongpaiboonwattana, K. Sanders, M. Mudaliar, D. M. van Aalten, G. J. Barton, and M. P. Stavridis. 2014. 'Elevated O-GlcNAc levels activate epigenetically repressed genes and delay mouse ESC differentiation without affecting naïve to primed cell transition', *Stem Cells*, 32: 2605-15.
- Stead, Elaine, Josephine White, Renate Faast, Simon Conn, Sherilyn Goldstone, Joy Rathjen, Urvashi Dhingra, Peter Rathjen, Duncan Walker, and Stephen Dalton. 2002. 'Pluripotent cell division cycles are driven by ectopic Cdk2, cyclin A/E and E2F activities', *Oncogene*, 21: 8320-33.
- Sun, C., J. Shang, Y. Yao, X. Yin, M. Liu, H. Liu, and Y. Zhou. 2016. 'O-GlcNAcylation: a bridge between glucose and cell differentiation', *J Cell Mol Med*, 20: 769-81.
- Swiatek, M. A., E. Tenconi, S. Rigali, and G. P. van Wezel. 2012. 'Functional analysis of the N-acetylglucosamine metabolic genes of *Streptomyces coelicolor* and role in control of development and antibiotic production', *J Bacteriol*, 194: 1136-44.
- Szymura, Szymon J., Jacob P. Zaemes, David F. Allison, Sheena H. Clift, Jaclyn M. D'Innocenzi, Lisa G. Gray, Brian D. McKenna, Benjamin B. Morris, Stefan Bekiranov, Robin D. LeGallo, David R. Jones, and Marty W. Mayo. 2019. 'NF- κ B upregulates glutamine-fructose-6-phosphate transaminase 2 to promote migration in non-small cell lung cancer', *Cell Communication and Signaling*, 17: 24.
- Takahasi, K Ryo, Yoshiyuki Sakuraba, and Yoichi Gondo. 2007. 'Mutational pattern and frequency of induced nucleotide changes in mouse ENU mutagenesis', *BMC molecular biology*, 8: 1-10.
- Takatsuki, A., K. Arima, and G. Tamura. 1971. 'Tunicamycin, a new antibiotic. I. Isolation and characterization of tunicamycin', *J Antibiot (Tokyo)*, 24: 215-23.

- Tan, Ee Phie, Steven R. McGreal, Stefan Graw, Robert Tessman, Scott J. Koppel, Pramod Dhakal, Zhen Zhang, Miranda Machacek, Natasha E. Zachara, Devin C. Koestler, Kenneth R. Peterson, John P. Thyfault, Russell H. Swerdlow, Partha Krishnamurthy, Luciano DiTacchio, Udayan Apte, and Chad Slawson. 2017. 'Sustained O-GlcNAcylation reprograms mitochondrial function to regulate energy metabolism', *Journal of Biological Chemistry*, 292: 14940-62.
- Tan, Ee Phie, Maria T. Villar, Lezi E, Jianghua Lu, J. Eva Selfridge, Antonio Artigues, Russell H. Swerdlow, and Chad Slawson. 2014. 'Altering O-Linked β -N-Acetylglucosamine Cycling Disrupts Mitochondrial Function*', *Journal of Biological Chemistry*, 289: 14719-30.
- Tan, Z. W., G. Fei, J. A. Paulo, S. Bellaousov, S. E. S. Martin, D. Y. Duveau, C. J. Thomas, S. P. Gygi, P. L. Boutz, and S. Walker. 2020. 'O-GlcNAc regulates gene expression by controlling detained intron splicing', *Nucleic Acids Res*, 48: 5656-69.
- Tat, S. K., J. P. Pelletier, J. Vergés, D. Lajeunesse, E. Montell, H. Fahmi, M. Lavigne, and J. Martel-Pelletier. 2007. 'Chondroitin and glucosamine sulfate in combination decrease the pro-resorptive properties of human osteoarthritis subchondral bone osteoblasts: a basic science study', *Arthritis Res Ther*, 9: R117.
- Taylor, Rodrick P, Taylor S Geisler, Jefferson H Chambers, and Donald A McClain. 2009. 'Up-regulation of O-GlcNAc transferase with glucose deprivation in HepG2 cells is mediated by decreased hexosamine pathway flux', *Journal of Biological Chemistry*, 284: 3425-32.
- Taylor, Rodrick P, Glendon J Parker, Mark W Hazel, Yudi Soesanto, William Fuller, Marla J Yazzie, and Donald A McClain. 2008. 'Glucose deprivation stimulates O-GlcNAc modification of proteins through up-regulation of O-linked N-acetylglucosaminyltransferase', *Journal of Biological Chemistry*, 283: 6050-57.
- Tharanathan, Rudrapatnam N., and Farooqahmed S. Kittur. 2003. 'Chitin — The Undisputed Biomolecule of Great Potential', *Critical Reviews in Food Science and Nutrition*, 43: 61-87.
- Thoden, J. B., T. M. Wohlers, J. L. Fridovich-Keil, and H. M. Holden. 2001. 'Human UDP-galactose 4-epimerase. Accommodation of UDP-N-acetylglucosamine within the active site', *J Biol Chem*, 276: 15131-6.
- Tian, E., M. P. Hoffman, and K. G. Ten Hagen. 2012. 'O-glycosylation modulates integrin and FGF signalling by influencing the secretion of basement membrane components', *Nat Commun*, 3: 869.
- Tkacz, J. S., and O. Lampen. 1975. 'Tunicamycin inhibition of polyisoprenyl N-acetylglucosaminyl pyrophosphate formation in calf-liver microsomes', *Biochem Biophys Res Commun*, 65: 248-57.
- Tohyama, Shugo, Jun Fujita, Takako Hishiki, Tomomi Matsuura, Fumiyuki Hattori, Rei Ohno, Hideaki Kanazawa, Tomohisa Seki, Kazuaki Nakajima, and Yoshikazu Kishino. 2016. 'Glutamine oxidation is indispensable for survival of human pluripotent stem cells', *Cell metabolism*, 23: 663-74.
- Uehara, T., K. Suefuji, N. Valbuena, B. Meehan, M. Donegan, and J. T. Park. 2005. 'Recycling of the anhydro-N-acetylmuramic acid derived from cell wall murein involves a two-step conversion to N-acetylglucosamine-phosphate', *J Bacteriol*, 187: 3643-9.
- van den Berg, N., M. Beekman, K. R. Smith, A. Janssens, and P. E. Slagboom. 2017. 'Historical demography and longevity genetics: Back to the future', *Ageing Res Rev*, 38: 28-39.
- van der Laarse, S. A. M., A. C. Leney, and A. J. R. Heck. 2018. 'Crosstalk between phosphorylation and O-GlcNAcylation: friend or foe', *Febs j*, 285: 3152-67.
- Vander Heiden, M. G., L. C. Cantley, and C. B. Thompson. 2009. 'Understanding the Warburg effect: the metabolic requirements of cell proliferation', *Science*, 324: 1029-33.
- Varum, Sandra, Ana S Rodrigues, Michelle B Moura, Olga Momcilovic, Charles A Easley IV, João Ramalho-Santos, Bennett Van Houten, and Gerald Schatten. 2011. 'Energy metabolism in human pluripotent stem cells and their differentiated counterparts', *PLoS One*, 6: e20914.

- Vasconcelos-dos-Santos, Andréia, Isadora A Oliveira, Miguel Clodomiro Lucena, Natalia Rodrigues Mantuano, Stephen A Whelan, Wagner Barbosa Dias, and Adriane Regina Todeschini. 2015. 'Biosynthetic machinery involved in aberrant glycosylation: promising targets for developing of drugs against cancer', *Frontiers in oncology*, 5: 138.
- Vaupel, J. W., J. R. Carey, K. Christensen, T. E. Johnson, A. I. Yashin, N. V. Holm, I. A. Iachine, V. Kannisto, A. A. Khazaeli, P. Liedo, V. D. Longo, Y. Zeng, K. G. Manton, and J. W. Curtsinger. 1998. 'Biodemographic trajectories of longevity', *Science*, 280: 855-60.
- Vazquez-Martin, Alejandro, Bruna Corominas-Faja, Sílvia Cufí, Luciano Vellon, Cristina Oliveras-Ferraros, Octavio J Menendez, Jorge Joven, Ruth Lupu, and Javier A Menendez. 2013. 'The mitochondrial H⁺-ATP synthase and the lipogenic switch: new core components of metabolic reprogramming in induced pluripotent stem (iPS) cells', *Cell cycle*, 12: 207-18.
- Vazquez-Martin, Alejandro, Sílvia Cufí, Bruna Corominas-Faja, Cristina Oliveras-Ferraros, Luciano Vellon, and Javier A Menendez. 2012. 'Mitochondrial fusion by pharmacological manipulation impedes somatic cell reprogramming to pluripotency: new insight into the role of mitophagy in cell stemness', *Aging (Albany NY)*, 4: 393.
- Vella, P., A. Scelfo, S. Jammula, F. Chiacchiera, K. Williams, A. Cuomo, A. Roberto, J. Christensen, T. Bonaldi, K. Helin, and D. Pasini. 2013. 'Tet proteins connect the O-linked N-acetylglucosamine transferase Ogt to chromatin in embryonic stem cells', *Mol Cell*, 49: 645-56.
- Vigetti, D., S. Deleonibus, P. Moretto, E. Karousou, M. Viola, B. Bartolini, V. C. Hascall, M. Tammi, G. De Luca, and A. Passi. 2012. 'Role of UDP-N-acetylglucosamine (GlcNAc) and O-GlcNAcylation of hyaluronan synthase 2 in the control of chondroitin sulfate and hyaluronan synthesis', *J Biol Chem*, 287: 35544-55.
- Vijg, J., and J. Campisi. 2008. 'Puzzles, promises and a cure for ageing', *Nature*, 454: 1065-71.
- Vilchez, David, Milos S. Simic, and Andrew Dillin. 2014. 'Proteostasis and aging of stem cells', *Trends in Cell Biology*, 24: 161-70.
- Vincent, F., D. Yates, E. Garman, G. J. Davies, and J. A. Brannigan. 2004. 'The three-dimensional structure of the N-acetylglucosamine-6-phosphate deacetylase, NagA, from *Bacillus subtilis*: a member of the urease superfamily', *J Biol Chem*, 279: 2809-16.
- Wagner, S. A., P. Beli, B. T. Weinert, M. L. Nielsen, J. Cox, M. Mann, and C. Choudhary. 2011. 'A proteome-wide, quantitative survey of in vivo ubiquitylation sites reveals widespread regulatory roles', *Mol Cell Proteomics*, 10: M111.013284.
- Wamelink, MMC, EA Struys, and CAJM Jakobs. 2008. 'The biochemistry, metabolism and inherited defects of the pentose phosphate pathway: a review', *Journal of Inherited Metabolic Disease: Official Journal of the Society for the Study of Inborn Errors of Metabolism*, 31: 703-17.
- Wan, Cuihong, Blake Borgeson, Sadhna Phanse, Fan Tu, Kevin Drew, Greg Clark, Xuejian Xiong, Olga Kagan, Julian Kwan, Alexandr Bezginov, Kyle Chessman, Swati Pal, Graham Cromar, Ophelia Papoulas, Zuyao Ni, Daniel R. Boutz, Snejana Stoilova, Pierre C. Havugimana, Xinghua Guo, Ramy H. Malty, Mihail Sarov, Jack Greenblatt, Mohan Babu, W. Brent Derry, Elisabeth R. Tillier, John B. Wallingford, John Parkinson, Edward M. Marcotte, and Andrew Emili. 2015. 'Panorama of ancient metazoan macromolecular complexes', *Nature*, 525: 339-44.
- Wang, J., R. Liu, M. Hawkins, N. Barzilai, and L. Rossetti. 1998. 'A nutrient-sensing pathway regulates leptin gene expression in muscle and fat', *Nature*, 393: 684-8.
- Wang, J., X. Liu, Y. H. Liang, L. F. Li, and X. D. Su. 2008. 'Acceptor substrate binding revealed by crystal structure of human glucosamine-6-phosphate N-acetyltransferase 1', *FEBS Lett*, 582: 2973-8.
- Wang, Peng, Brooke D. Lazarus, Michele E. Forsythe, Dona C. Love, Michael W. Krause, and John A. Hanover. 2012. 'O-GlcNAc cycling mutants modulate proteotoxicity in

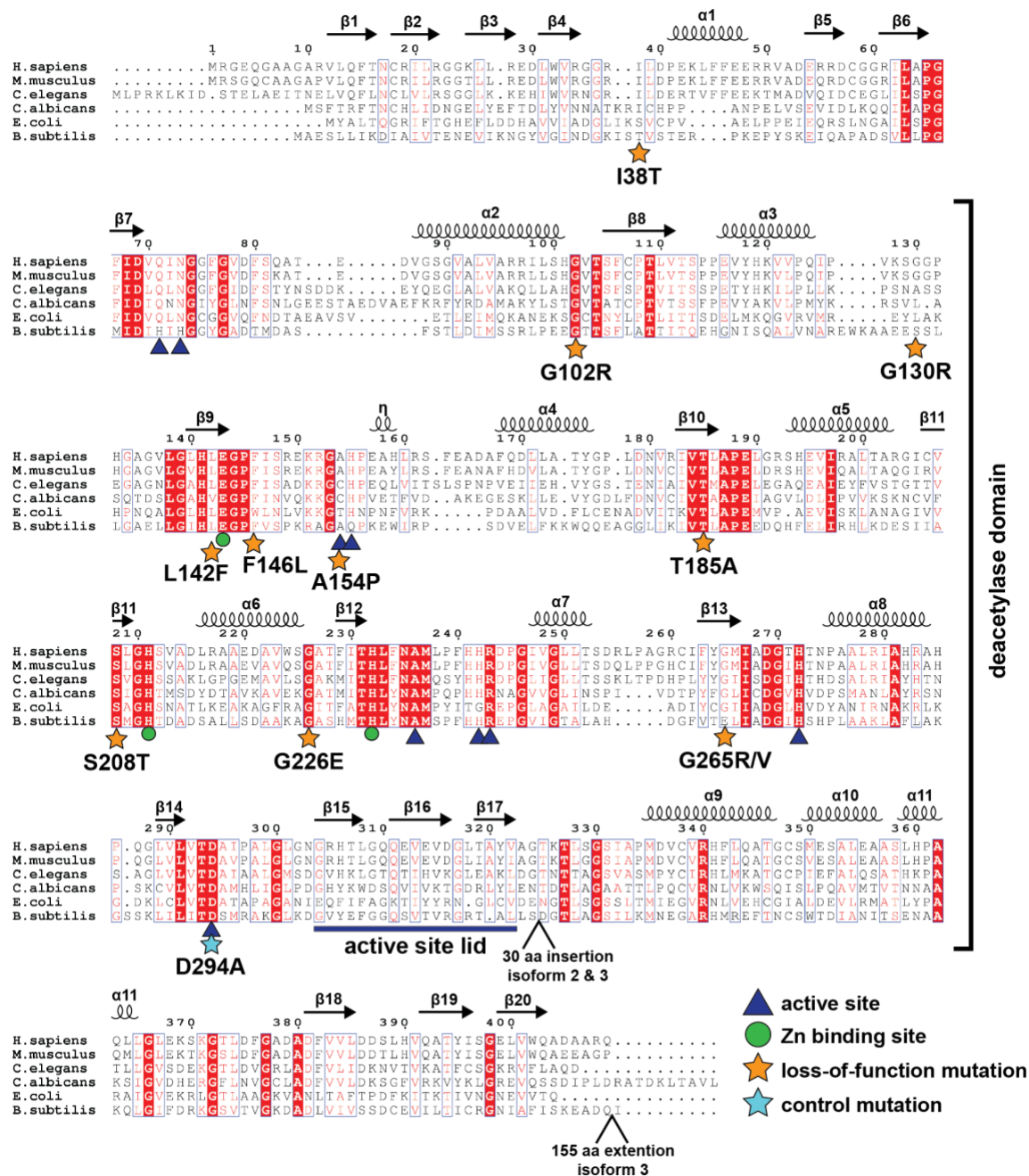
- Caenorhabditis elegans models of human neurodegenerative diseases', *Proceedings of the National Academy of Sciences*, 109: 17669.
- Wang, Zhao V, Yingfeng Deng, Ningguo Gao, Zully Pedrozo, Dan L Li, Cyndi R Morales, Alfredo Criollo, Xiang Luo, Wei Tan, and Nan Jiang. 2014. 'Spliced X-box binding protein 1 couples the unfolded protein response to hexosamine biosynthetic pathway', *Cell*, 156: 1179-92.
- Warburg, O., F. Wind, and E. Negelein. 1927. 'THE METABOLISM OF TUMORS IN THE BODY', *J Gen Physiol*, 8: 519-30.
- Watson, L. J., B. W. Long, A. M. DeMartino, K. R. Brittan, R. D. Readnow, R. E. Brainard, T. D. Cummins, L. Annamalai, B. G. Hill, and S. P. Jones. 2014. 'Cardiomyocyte Ogt is essential for postnatal viability', *Am J Physiol Heart Circ Physiol*, 306: H142-53.
- Webster, Danielle M, Chin Fen Teo, Yuhua Sun, Dorota Wloga, Steven Gay, Kimberly D Klonowski, Lance Wells, and Scott T Dougan. 2009. 'O-GlcNAc modifications regulate cell survival and epiboly during zebrafish development', *BMC developmental biology*, 9: 1-24.
- Weidanz, J. A., P. Campbell, D. Moore, L. J. DeLucas, L. Roden, J. N. Thompson, and A. C. Vezza. 1996. 'N-acetylglucosamine kinase and N-acetylglucosamine 6-phosphate deacetylase in normal human erythrocytes and Plasmodium falciparum', *Br J Haematol*, 95: 645-53.
- Weigert, C., K. Brodbeck, R. Lehmann, H. U. Häring, and E. D. Schleicher. 2001. 'Overexpression of glutamine:fructose-6-phosphate-amidotransferase induces transforming growth factor-beta1 synthesis in NIH-3T3 fibroblasts', *FEBS Lett*, 488: 95-9.
- Weihofen, W. A., M. Berger, H. Chen, W. Saenger, and S. Hinderlich. 2006. 'Structures of human N-Acetylglucosamine kinase in two complexes with N-Acetylglucosamine and with ADP/glucose: insights into substrate specificity and regulation', *J Mol Biol*, 364: 388-99.
- Weissmann, B., and D. F. Hinrichsen. 1969. 'Mammalian alpha-acetylgalactosaminidase. Occurrence, partial purification, and action on linkages in submaxillary mucins', *Biochemistry*, 8: 2034-43.
- Wen, Jessica H., Ludovic G. Vincent, Alexander Fuhrmann, Yu Suk Choi, Kolin C. Hribar, Hermes Taylor-Weiner, Shaochen Chen, and Adam J. Engler. 2014. 'Interplay of matrix stiffness and protein tethering in stem cell differentiation', *Nature Materials*, 13: 979-87.
- Werdelin, Ole, Morten Meldal, and Teis Jensen. 2002. 'Processing of glycans on glycoprotein and glycopeptide antigens in antigen-presenting cells', *Proceedings of the National Academy of Sciences*, 99: 9611.
- White, C. W., 3rd, X. Fan, J. C. Maynard, E. G. Wheatley, G. Bieri, J. Couthouis, A. L. Burlingame, and S. A. Villeda. 2020. 'Age-related loss of neural stem cell O-GlcNAc promotes a glial fate switch through STAT3 activation', *Proc Natl Acad Sci U S A*, 117: 22214-24.
- White, R. J., and C. A. Pasternak. 1967. 'The purification and properties of N-acetylglucosamine 6-phosphate deacetylase from Escherichia coli', *Biochem J*, 105: 121-5.
- Wijdeven, Ruud H, Baoxu Pang, Sabina Y van der Zanden, Xiaohang Qiao, Vincent Blomen, Marlous Hoogstraat, Esther H Lips, Lennert Janssen, Lodewyk Wessels, and Thijn R Brummelkamp. 2015. 'Genome-wide identification and characterization of novel factors conferring resistance to topoisomerase II poisons in cancer', *Cancer research*, 75: 4176-87.
- Willems, A. P., M. Gundogdu, M. J. E. Kempers, J. C. Giltay, R. Pfundt, M. Elferink, B. F. Loza, J. Fuijkschot, A. T. Ferenbach, K. L. I. van Gassen, D. M. F. van Aalten, and D. J. Lefeber. 2017. 'Mutations in N-acetylglucosamine (O-GlcNAc) transferase in patients with X-linked intellectual disability', *J Biol Chem*, 292: 12621-31.
- Winzeler, Elizabeth A, Daniel D Shoemaker, Anna Astromoff, Hong Liang, Keith Anderson, Bruno Andre, Rhonda Bangham, Rocio Benito, Jef D Boeke, and Howard Bussey.

1999. 'Functional characterization of the *S. cerevisiae* genome by gene deletion and parallel analysis', *Science*, 285: 901-06.
- Wyss, D. F., J. S. Choi, J. Li, M. H. Knoppers, K. J. Willis, A. R. Arulanandam, A. Smolyar, E. L. Reinherz, and G. Wagner. 1995. 'Conformation and function of the N-linked glycan in the adhesion domain of human CD2', *Science*, 269: 1273-8.
- Yamada-Okabe, T., Y. Sakamori, T. Mio, and H. Yamada-Okabe. 2001. 'Identification and characterization of the genes for N-acetylglucosamine kinase and N-acetylglucosamine-phosphate deacetylase in the pathogenic fungus *Candida albicans*', *Eur J Biochem*, 268: 2498-505.
- Yamashita, T., R. Wada, T. Sasaki, C. Deng, U. Bierfreund, K. Sandhoff, and R. L. Proia. 1999. 'A vital role for glycosphingolipid synthesis during development and differentiation', *Proc Natl Acad Sci U S A*, 96: 9142-7.
- Yan, Pengze, Jie Ren, Weiqi Zhang, Jing Qu, and Guang-Hui Liu. 2020. 'Protein quality control of cell stemness', *Cell regeneration (London, England)*, 9: 22-22.
- Yang, Won Ho, Ji Eun Kim, Hyung Wook Nam, Jung Won Ju, Hoe Suk Kim, Yu Sam Kim, and Jin Won Cho. 2006. 'Modification of p53 with O-linked N-acetylglucosamine regulates p53 activity and stability', *Nature Cell Biology*, 8: 1074-83.
- Yang, Xiaoyong, and Kevin Qian. 2017. 'Protein O-GlcNAcylation: emerging mechanisms and functions', *Nature Reviews Molecular Cell Biology*, 18: 452-65.
- Yang, Xiaoyong, Fengxue Zhang, and Jeffrey E Kudlow. 2002. 'Recruitment of O-GlcNAc transferase to promoters by corepressor mSin3A: coupling protein O-GlcNAcylation to transcriptional repression', *Cell*, 110: 69-80.
- Yang, Yong Ryoul, Minseok Song, Ho Lee, Yoon Jeon, Eun-Jeong Choi, Hyun-Jun Jang, Hyo Youl Moon, Ha-Young Byun, Eung-Kyun Kim, and Dae Hyun Kim. 2012. 'O-GlcNAcase is essential for embryonic development and maintenance of genomic stability', *Aging cell*, 11: 439-48.
- Yi, Meisheng, Ni Hong, and Yunhan Hong. 2009. 'Generation of Medaka Fish Haploid Embryonic Stem Cells', *Science*, 326: 430.
- Yi, Wen, Peter M Clark, Daniel E Mason, Marie C Keenan, Collin Hill, William A Goddard, Eric C Peters, Edward M Driggers, and Linda C Hsieh-Wilson. 2012. 'Phosphofructokinase 1 glycosylation regulates cell growth and metabolism', *Science*, 337: 975-80.
- Yuzwa, S. A., M. S. Macauley, J. E. Heinonen, X. Shan, R. J. Dennis, Y. He, G. E. Whitworth, K. A. Stubbs, E. J. McEachern, G. J. Davies, and D. J. Vocadlo. 2008. 'A potent mechanism-inspired O-GlcNAcase inhibitor that blocks phosphorylation of tau in vivo', *Nat Chem Biol*, 4: 483-90.
- Yuzwa, S. A., and D. J. Vocadlo. 2014. 'O-GlcNAc and neurodegeneration: biochemical mechanisms and potential roles in Alzheimer's disease and beyond', *Chem Soc Rev*, 43: 6839-58.
- Zachara, Natasha E, Henrik Molina, Ker Yi Wong, Akhilesh Pandey, and Gerald W Hart. 2011. 'The dynamic stress-induced "O-GlcNAc-ome" highlights functions for O-GlcNAc in regulating DNA damage/repair and other cellular pathways', *Amino acids*, 40: 793-808.
- Zeng, Y., Q. Feng, T. Hesketh, K. Christensen, and J. W. Vaupel. 2017. 'Survival, disabilities in activities of daily living, and physical and cognitive functioning among the oldest-old in China: a cohort study', *Lancet*, 389: 1619-29.
- Zhang, F., K. Su, X. Yang, D. B. Bowe, A. J. Paterson, and J. E. Kudlow. 2003. 'O-GlcNAc modification is an endogenous inhibitor of the proteasome', *Cell*, 115: 715-25.
- Zhang, J., I. Khvorostov, J. S. Hong, Y. Oktay, L. Vergnes, E. Nuebel, P. N. Wahjudi, K. Setoguchi, G. Wang, A. Do, H. J. Jung, J. M. McCaffery, I. J. Kurland, K. Reue, W. N. Lee, C. M. Koehler, and M. A. Teitell. 2011. 'UCP2 regulates energy metabolism and differentiation potential of human pluripotent stem cells', *Embo j*, 30: 4860-73.
- Zhang, L., D. T. Tran, and K. G. Ten Hagen. 2010. 'An O-glycosyltransferase promotes cell adhesion during development by influencing secretion of an extracellular matrix integrin ligand', *J Biol Chem*, 285: 19491-501.
- Zhang, Suisheng, Kevin Roche, Heinz-Peter Nasheuer, and Noel Francis Lowndes. 2011. 'Modification of Histones by Sugar β -N-Acetylglucosamine (GlcNAc) Occurs on

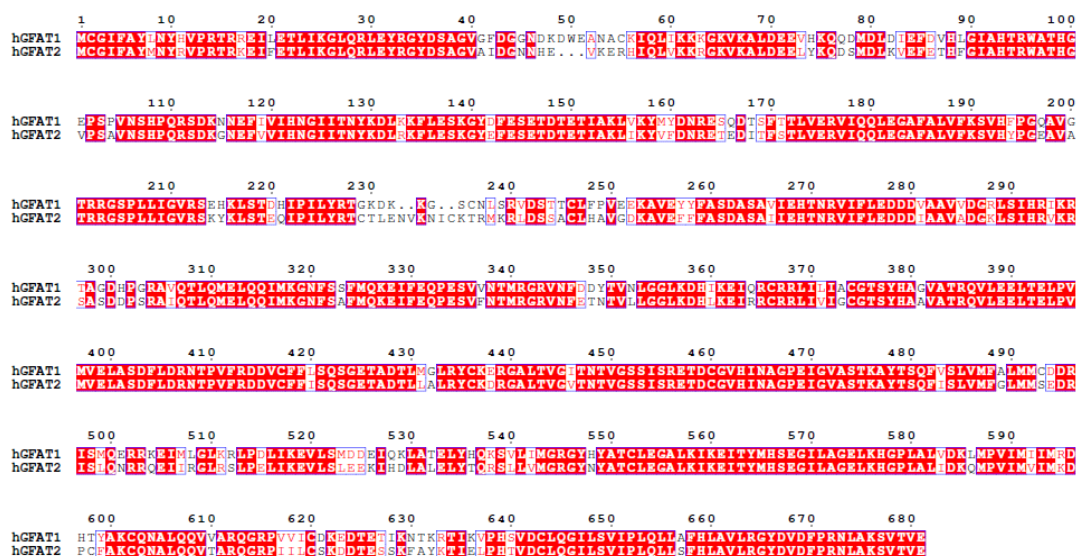
- Multiple Residues, Including Histone H3 Serine 10, and Is Cell Cycle-regulated*', *Journal of Biological Chemistry*, 286: 37483-95.
- Zhang, W., G. Bouchard, A. Yu, M. Shafiq, M. Jamali, J. B. Shrager, K. Ayers, S. Bakr, A. J. Gentles, M. Diehn, A. Quon, R. B. West, V. Nair, M. van de Rijn, S. Napel, and S. K. Plevritis. 2018. 'GFPT2-Expressing Cancer-Associated Fibroblasts Mediate Metabolic Reprogramming in Human Lung Adenocarcinoma', *Cancer Res*, 78: 3445-57.
- Zhang, Xin, Safak Yalcin, Dung-Fang Lee, Tsung-Yin J. Yeh, Seung-Min Lee, Jie Su, Sathish Kumar Mungamuri, Pauline Rimmelé, Marion Kennedy, Rani Sellers, Markus Landthaler, Thomas Tuschl, Nai-Wen Chi, Ihor Lemischka, Gordon Keller, and Saghi Ghaffari. 2011. 'FOXO1 is an essential regulator of pluripotency in human embryonic stem cells', *Nature Cell Biology*, 13: 1092-99.
- Zhang, Z., E. P. Tan, N. J. VandenHull, K. R. Peterson, and C. Slawson. 2014. 'O-GlcNAcase Expression is Sensitive to Changes in O-GlcNAc Homeostasis', *Front Endocrinol (Lausanne)*, 5: 206.
- Zheng, L., U. Baumann, and J. L. Reymond. 2004. 'An efficient one-step site-directed and site-saturation mutagenesis protocol', *Nucleic Acids Res*, 32: e115.
- Zhong, X., P. Cui, Y. Cai, L. Wang, X. He, P. Long, K. Lu, R. Yan, Y. Zhang, X. Pan, X. Zhao, W. Li, H. Zhang, Q. Zhou, and P. Gao. 2019. 'Mitochondrial Dynamics Is Critical for the Full Pluripotency and Embryonic Developmental Potential of Pluripotent Stem Cells', *Cell Metab*, 29: 979-92.e4.
- Zhou, J., J. L. Neidigh, R. Espinosa, 3rd, M. M. LeBeau, and D. A. McClain. 1995. 'Human glutamine: fructose-6-phosphate amidotransferase: characterization of mRNA and chromosomal assignment to 2p13', *Hum Genet*, 96: 99-101.
- Zhu, Saiyong, Wenlin Li, Hongyan Zhou, Wanguo Wei, Rajesh Ambasudhan, Tongxiang Lin, Janghwan Kim, Kang Zhang, and Sheng Ding. 2010. 'Reprogramming of human primary somatic cells by OCT4 and chemical compounds', *Cell Stem Cell*, 7: 651-55.
- Zhu, Yanping, Ta-Wei Liu, Samy Cecioni, Razieh Eskandari, Wesley F Zandberg, and David J Vocadlo. 2015. 'O-GlcNAc occurs cotranslationally to stabilize nascent polypeptide chains', *Nat Chem Biol*, 11: 319-25.
- Zibrova, D., F. Vandermoere, O. Göransson, M. Peggie, K. V. Mariño, A. Knierim, K. Spengler, C. Weigert, B. Viollet, N. A. Morrice, K. Sakamoto, and R. Heller. 2017. 'GFAT1 phosphorylation by AMPK promotes VEGF-induced angiogenesis', *Biochem J*, 474: 983-1001.
- Zoltowska, K., R. Webster, S. Finlayson, S. Maxwell, J. Cossins, J. Muller, H. Lochmuller, and D. Beeson. 2013. 'Mutations in GFPT1 that underlie limb-girdle congenital myasthenic syndrome result in reduced cell-surface expression of muscle AChR', *Hum Mol Genet*, 22: 2905-13.

Appendix

Supplementary data



Supplementary Figure 1: Protein sequence alignment of AMDHD2. Identical residues are depicted by red boxes and similar residues are depicted by red letters. The deacetylase domain and secondary structure motifs are annotated as well as insertions and extensions occurring in AMDHD2 isoform 2 and isoform 3. Residues involved in binding of the product, co-factor, and for catalysis are highlighted. The putative active site lid is marked. The identified loss-of-function mutations and the control mutation are labeled by stars. (Data was already described in: Ruegenberg, 2020a).



Supplementary Figure 2: Protein sequence alignment of human GFAT1 and GFAT2. Identical residues are depicted by red boxes and similar residues are depicted by red letters. (Data was already described in: Ruegenberg, 2020a).

List of figures

Figure 1: The universal hallmarks of aging.....	13
Figure 2: The hexosamine biosynthetic pathway.	14
Figure 3: Schematic representation of N-linked glycosylation.	21
Figure 4: Schematic representation of O-GlcNAcylation and its functional outputs..	22
Figure 5: The hexosamine biosynthetic pathway and its multiple functional outputs.	26
Figure 6: The HBP and its interconnection with other metabolic pathways.	28
Figure 7: Stem cell maintenance requires metabolic rewiring and the accompanying HBP outputs.....	34
Figure 8: The HBP has a putative central role for the manifestation of the hallmarks of aging.....	37
Figure 9: Schematic workflow of haploid mESC generation.	41
Figure 10: Chemical mutagenesis screen for tunicamycin resistance in mESCs identifies AMDHD2..	46
Figure 11: Confirmation of <i>Amdhd2</i> as tunicamycin resistance-conferring gene.	47
Figure 12: Loss of AMDHD2 leads to hexosamine pathway activation.....	48
Figure 13: Insertional mutagenesis screen confirms the loss of AMDHD2 as hexosamine pathway activator.....	49
Figure 14: Structural analysis of human AMDHD2..	51
Figure 15: <i>In vitro</i> characterization of identified loss-of-function mutations in AMDHD2.....	53
Figure 16: Loss of the <i>C. elegans</i> AMDHD2 homologue <i>F59B2.3</i> has no effect on HBP activity.....	55
Figure 17: Loss of AMDHD2 in <i>M. musculus</i> leads to embryonic lethality.....	56
Figure 18: Loss of AMDHD2 in N2a cells leads to hexosamine pathway activation.	58
Figure 19: GFAT2 controls metabolite entry into the hexosamine pathway in mESCs. .	60
Figure 20: GFAT2 has a lower sensitivity to UDP-GlcNAc feedback inhibition than GFAT1.....	61
Figure 21: GFAT2 in tandem with AMDHD2 result in elevated hexosamine pathway flux in mESCs.....	63
Figure 22: Differentiation of human ESCs results in a decreased GFAT2:GFAT1 ratio.	64
Figure 23: Partial differentiation of AN3-12 cells by LIF removal reduces GFAT2 abundance.....	65
Figure 24: Differentiation of AN3-12 cells into NPCs is delayed upon AMDHD2 K.O... ..	66
Figure 25: The loss of AMDHD2 increases stem cell maintenance under basal conditions.	69
Figure 26: Enzymatic reconfiguration of the HBP in ESCs.....	84
Figure 27: Schematic representation of library preparation for retroviral enhanced gene trap (Retro-EGT) vector integration sites	96
Supplementary Figure 1: Protein sequence alignment of AMDHD2.....	133
Supplementary Figure 2: Protein sequence alignment of human GFAT1 and GFAT2.....	134

List of tables

Table 1: Kinetic measurements of human GFAT1 and GFAT2 enzyme.....	62
Table 2: UDP-GlcNAc inhibition of human GFAT1 and GFAT2 enzyme.	62
Table 3: Primer sequences for sgRNAs for gene editing of transgenic mice.	92
Table 4: Composition of a DreamTaq PCR reaction mix.....	99
Table 5: Cycling and temperature profiles of a mouse genotyping PCR.	99
Table 6: Composition of a Phusion PCR reaction mix.	100
Table 7: Cycling and temperature profiles of a worm genotyping PCR for F59B2.3. ...	100
Table 8: Primer sequences for gene editing and genotyping of cells.....	101
Table 9: Primer sequences for quantitative PCR.	102
Table 10: Primer sequences used for site-directed mutagenesis.	107

Work contributions

I performed all experiments described in this work independently, except for:

Dr. Sabine Ruegenberg from Martin Denzel's laboratory (Max Planck Institute for Biology of Ageing, Cologne, Germany) performed all biochemical experiments, including crystallization and biochemical analysis of hAMDHD2, *in vitro* analysis of AMDHD2 loss-of-function mutants and kinetic measurements of GFAT1 and GFAT2 (Figure 14, Figure 15, Figure 20). Activity assays for GFAT1 and GFAT2 were performed with the help of her Master student Seyma Bozkus.

Dr. Moritz Horn from Martin Denzel's laboratory (Max Planck Institute for Biology of Ageing, Cologne, Germany) supervised and helped with the initial screen for tunicamycin resistance (Figure 10) and designed the sgRNAs for the G451E GFAT1 substitution (Figure 19B).

Dr. Kira Allmeroth from Martin Denzel's laboratory (Max Planck Institute for Biology of Ageing, Cologne, Germany) designed and performed all work in *M. musculus* (Figure 17), helped collecting/preparing some samples for LC-MS measurements (Figure 19A), and generated the G451E GFAT1 mutant in the N2a cells line (Figure 19B).

Dr. Bernhard Schermer and Lena Ebert from the Nephrolab (Kidney research Center Cologne, Germany) generated the AMDHD2 antibody.

Dr. Maxime Derisbourg from Martin Denzel's laboratory (Max Planck Institute for Biology of Ageing, Cologne, Germany) performed injections of *C. elegans* for the generation of F59B2.3 CRISPR/Cas9 lines (Figure 16).

Dr. Ulrich Elling (Institute of Molecular Biotechnology, Vienna, Austria) performed virus transfection of AN3-12 cells for the insertional mutagenesis screen (Figure 13).

Marta Grzonka from Hisham Bazzi's laboratory (Cluster of Excellence at the University of Cologne, Germany) cultivated and plated E14 mESCs for further sample preparation (Figure 19E; Figure 21B, C, D).

Cell sorting was performed by Kat Folz-Donahue and Lena Schumacher from the FACS and Imaging Core Facility (Max Planck Institute for Biology of Ageing, Cologne, Germany).

UDP-HexNAc levels were analyzed by Yvonne Hinze from the Metabolomics Core Facility (Max Planck Institute for Biology of Ageing, Cologne, Germany)

UDP-GlcNAc and UDP-GalNAc levels were determined by Silvina Perin from the Metabolomics Core Facility (Max Planck Institute for Biology of Ageing, Cologne, Germany).

I thank all these people for their essential contributions.

Curriculum Vitae

Persönliche Informationen

Virginia Kroef
Gleueler Str. 67
50931 Köln

geboren am 08.06.1992 in Köln
Nationalität: deutsch
E-Mail: Virginia.Kroef@gmx.de
Telefon: +49 177 388 9338

Ausbildung

- | | |
|------------------|---|
| Seit 08/2017 | Promotion in Genetik
Max-Planck-Institut für Biologie des Alterns, Köln, Deutschland
Arbeitsgruppe von Dr. Martin Denzel
Titel der Dissertation: |
| 4/2015 - 07/2017 | Master of Science in Biological Sciences
Universität zu Köln
Masterarbeit in der Arbeitsgruppe von Dr. Martin Denzel
am Max-Planck-Institut für Biologie des Alterns, Köln, Deutschland |
| 10/2011 - 3/2015 | Bachelor of Science in Biologie
Universität zu Köln
Bachelorarbeit in der Arbeitsgruppe von Prof. Dr. Thorsten Hoppe
am CECAD, Köln, Deutschland |
| 06/2011 | Allgemeine Hochschulreife
Elisabeth-von-Thüringen Gymnasium, Köln, Deutschland |

Relevante Publikationen

Publizierte Artikel:

Horn, M., Kroef, V., Allmeroth, K., Schuller, N., Miethe, S., Peifer, M., M. Penninger, J., Elling, U., and S. Denzel, M. (2018). Unbiased compound-protein interface mapping and prediction of chemoresistance loci through forward genetics in haploid stem cells.

Saez, I., Gerbracht, J.V., Koyuncu, S., Lee, H.J., Horn, M., Kroef, V., Denzel, M.S., Dieterich, C., Gehring, N.H., and Vilchez, D. (2020). The E3 ubiquitin ligase UBR 5 interacts with the H/ACA ribonucleoprotein complex and regulates ribosomal RNA biogenesis in embryonic stem cells. *FEBS letters* 594, 175-188.

Allmeroth, K., Horn, M., Kroef, V., Miethe, S., Müller, R.U., and Denzel, M.S. (2020). Bortezomib resistance mutations in PSMB5 determine response to second-generation proteasome inhibitors in multiple myeloma. *Leukemia*.

Artikel in Bearbeitung:

Kroef, V., Ruegenberg, S., Horn, M., Allmeroth, K., Eberg, L., Bozkus, S., Miethe, S., Schermer, B., Baumann, U., and Denzel, M.S. (2021). GFAT2 and AMDHD2 act in tandem to control the hexosamine biosynthetic pathway. *bioRxiv*

Erklärung zur Dissertation

Hiermit versichere ich an Eides statt, dass ich die vorliegende Dissertation selbstständig und ohne die Benutzung anderer als der angegebenen Hilfsmittel und Literatur angefertigt habe. Alle Stellen, die wörtlich oder sinngemäß aus veröffentlichten und nicht veröffentlichten Werken dem Wortlaut oder dem Sinn nach entnommen wurden, sind als solche kenntlich gemacht. Ich versichere an Eides statt, dass diese Dissertation noch keiner anderen Fakultät oder Universität zur Prüfung vorgelegen hat; dass sie - abgesehen von unten angegebenen Teilpublikationen und eingebundenen Artikeln und Manuskripten - noch nicht veröffentlicht worden ist sowie, dass ich eine Veröffentlichung der Dissertation vor Abschluss der Promotion nicht ohne Genehmigung des Promotionsausschusses vornehmen werde. Die Bestimmungen dieser Ordnung sind mir bekannt. Darüber hinaus erkläre ich hiermit, dass ich die Ordnung zur Sicherung guter wissenschaftlicher Praxis und zum Umgang mit wissenschaftlichem Fehlverhalten der Universität zu Köln gelesen und sie bei der Durchführung der Dissertation zugrundeliegenden Arbeiten und der schriftlich verfassten Dissertation beachtet habe und verpflichte mich hiermit, die dort genannten Vorgaben bei allen wissenschaftlichen Tätigkeiten zu beachten und umzusetzen. Ich versichere, dass die eingereichte elektronische Fassung der eingereichten Druckfassung vollständig entspricht.

Teilpublikationen:

Kroef, V., Ruegenberg, S., Horn, M., Allmeroth, K., Eberg, L., Bozkus, S., Miethe, S., Schermer, B., Baumann, U., and Denzel, M.S. (2021). GFAT2 and AMDHD2 act in tandem to control the hexosamine biosynthetic pathway. bioRxiv

Köln, 01.07.2021

Ort, Datum

V. Kroef

Unterschrift